9605

A COLLABORATIVE STUDY: MARINE GEOPHYSICAL INVESTIGATION OF THE PUERTO RICO TRENCH

A COLLABORATIVE STUDY: MARINE GEOPHYSICAL INVESTIGATION OF THE PUERTO RICO TRENCH

EW96-05 CRUISE REPORT

SAN JUAN -SAN JUAN, PR JUNE 15-JULY 8, 1996

CHIEF SCIENTISTS:

NANCY GRINDLAY, UNIVERSITY OF PUERTO RICO
PAUL MANN, INSTITUTE FOR GEOPHYSICS, UNIVERSITY OF TEXAS AT AUSTIN
JAMES DOLAN, UNIVERSITY OF SOUTHERN CALIFORNIA

PRELIMINARY SHIPBOARD SCIENTIFIC RESULTS
(PLEASE RESTRICT DISTRIBUTION TO UPR, UTIG , IEO, SOEST AND USC PARTICIPANTS)

TABLE OF CONTENTS

CHAPTER 1. INTRODUCTION AND HISTORY OF EW96-05 PROJECT....3
CHAPTER 2. COMPARISON OF PROPOSED OBJECTIVES OF EW96-05 WITH A PRELIMINARY ANALYSIS OF THE DATA....7
CHAPTER 3. SINGLE-CHANNEL SEISMIC REFLECTION OPERATIONS....30
CHAPTER 4. AIRGUN CONFIGURATION....39
CHAPTER 5. ONBOARD PROCESSING AND PRELIMINARY INTERPRETATION OF SEISMIC DATA....43
CHAPTER 6. PROCESSING PLAN AT UTIG FOR THE SCS DATA....60
CHAPTER 7. HYDROSWEEP SYSTEM....61
CHAPTER 8. HYDROSWEEP DATA PROCESSING....66
CHAPTER 9. MR1 SYSTEM....73
CHAPTER 10. MR1 DATA PROCESSING....81
CHAPTER 11. 3.5 kHz SONAR SYSTEM AND SODAR PROGRAM....82
CHAPTER 12. SEA WATER TEMPERATURE....84
CHAPTER 13. WEATHER STATION....91
CHAPTER 14. COMPUTER SYSTEM....92
CHAPTER 15. NAVIGATION....94
CHAPTER 16. GRAVITY MEASUREMENTS....96
CHAPTER 17. MAGNETIC DATA ACQUISITION....103
CHAPTER 18. REVIEW OF EXISTING LITERATURE....111
18.1 REVIEW OF CRUSTAL STRUCTURE IN STUDY AREA....111
18.2 REVIEW OF SHALLOW STRUCTURES IN STUDY AREA....134
18.3 REVIEW OF CURRENTS AND DEPOSITION IN STUDY AREA....142
BIBLIOGRAPHY....145
APPENDICES....151
APPENDIX I - CRUISE EW96-05 DAILY JOURNAL....152
APPENDIX II - GEOMAG PROGRAM....161
APPENDIX III - CORE AND DREDGE LOCATIONS....169
APPENDIX IV - EW96-05 LOGGED DATA FORMAT....174
APPENDIX V - ADDRESSES OF SCIENCE PARTY....186

CHAPTER 1. INTRODUCTION AND HISTORY OF EW96-05 PROJECT

This report describes the methods and preliminary results of a marine geophysical (HMR1, single-channel seismic, gravity and magnetics) cruise EW96-05 aboard the R/V MAURICE EWING to the Puerto Rico trench during June 15, 1996 to July 8, 1996. This report is accompanied by the UNOLS Research Vessel Cruise Assessment Form and the UNOLS Cruise Report/Ship Utilization Data Report.

The Puerto Rico trench and northern margin of the island of Puerto Rico occupy a zone of tectonic transition between subduction tectonics of the Lesser Antilles island arc and strike-slip tectonics of the Septentrional-Cayman trough left-lateral strike-slip fault system to the west (Fig. 1, inset). Obliquely colliding high-standing bathymetric features on the downgoing North America plate beneath the Caribbean plate make this region a promising area to investigate the time-transgressive deformational effects of fracture zone and aseismic ridge collisional events at margins of highly oblique convergence. (Fig. 1.1).

The project was initiated by Grindlay, Mann and Dolan with a proposal submitted to the Marine Geology and Geophysics program of the National Science Foundation's Ocean Sciences Division in the Spring of 1994. Ship time and use of a magnetometer, single-channel seismic system and gravimeter were requested on the R/V ENDEAVOR through a subcontract with the University of Rhode Island. Use of the HMR1 system was requested through a subcontract with the Hawaii Mapping Research Group at the University of Hawaii. The NSF proposal and accompanying subcontracts were initially turned down.

A revised version of the NSF proposal submitted by UPR-UTIG-USC and accompanying subcontracts from URI and HMRG were submitted in fall of 1994 and approved for funding pending availability of ship time. In spring of 1995 due to UNOLS ship scheduling logistics the program was scheduled for June 1996 on the R/V MAURICE EWING and a subcontract from LDEO replaced the URI subcontract. Funding to start the UPR-UTIG-USC program and LDEO and HMRG subcontracts became available on April 15, 1996 and extends through 1999.

Science Party

The science party of EW96-05 consisted of 19 individuals from seven different institutions (for an alphabetical listing of names and addresses of UPR, UT, USC, IEO, WVWC and SOEST participants see Appendix V):

University of Puerto Rico (UPR), USA
Dr. Nancy Grindlay, Co-Chief-scientist
Ms. Frances Delano, Undergraduate student
Mr. Wilfredo Rosado, Undergraduate student

University of Texas at Austin, Institue for Geophysics (UTIG) and Department of Geological Sciences (DOGS), USA
Dr. Paul Mann, Co-Chief scientist, UTIG
Mr. Steve Muszala, Graduate research assistant, DOGS, PhD aspirant
Mr. Jean-Paul van Gestel, Graduate research assistant, DOGS, PhD aspirant

University of Southern California (USC), USA
Dr. James Dolan, Co-Chief scientist

Spanish Institute of Oceanography (IEO), Madrid, Spain
Dr. Araceli Munoz, Participating scientist

West Virginia Weslyan College, USA
Mr. John Charles, III, Undergraduate student

SOEST - University of Hawaii, USA
Dr. Bruce Appelgate, MR1 Chief of operations
Mr. Steve Tottori, MR1 Engineer
Ms. Karen Sender, MR1 Data processor
Ms. Tina Mueller, MR1 Data processor

Lamont Doherty Earth Observatory of Columbia University, USA
Mr. Chris Leidhold, Science Officer
Mr. John DiBernardo, Technician (airguns)
Mr. Carlos Alvarez, Technician (airguns)
Mr. Paul Osgard, Technician (electrical)
Mr. William Robinson, Computer systems manager
Mr. Michael Wittreich, Technician (airguns)

Crew

Captain James O'Laughlin
Mr. Stan Ziegler, Chief mate
Mr. Mark Landow, Second mate
Mr. Jeff Sylvia, Third mate
Mr. Larry Barros, Boatswain
Mr. John Shank, A/B
Mr. Dermot Taaffe, A/B
Mr. David Wolford, A/B
Mr. Robert Hagg, O/S
Mr. Rickey Wyatt, O/S
Mr. Albert Karlyn, Chief Engineer
Mr. Sport Moran, 1st Engr.
Mr. Todd Soper, 2nd Engr.
Mr. Paul Morric, 3rd Engr.
Mr. Edward Shimel, Oiler
Mr. Guillermo Uribe, Oiler
Mr. William Osborn, Oiler
Mr. John Schwartz, Electrician
Mr. Tim Hummel, Steward
Mr. Richard Craig, Cook
Mr. Joseph LoPrinzi, Utility

Research Vessel Specifications and Equipment Used for Science Operations

The R/V MAURICE EWING is a 72.750 meter long oceanographic research vessel with a gross tonnage of 1978. It is owned and operated by Lamont Doherty Earth Observatory, Columbia University. The R/V EWING was built by Marine Industrie Ltde of Quebec Canada in 1983 and was converted to oceanographic research use in 1990. It can reach and maintain underway speeds of 12 kts, and it has a berthing capacity for up to 50 persons.

The R/V EWING is equiped with a Bell Aerospace BGM-3 gravimeter, Varion proton precession magnetomer, DMS 2000 SCS seismic system and Hydrosweep multibeam bathyetric system. In this study the MR1 sidescan sonar system including launching/recovery system and tow winch were shipped from Hawaii and bolted into the back deck. The SCS streamer and air-gun array, magnetometer, and MR1 were all deployed and recovered from the fantail.

The Main Science Lab on Deck C was used for watchstanding and as a general work area. The wet staging area on Deck C was used to as an electronics workshop for testing and repairing the MR1 system and as the primarly location of MR1 data processing.

Acknowledgements

The dedication and hard work of Captain O'Loughlin, the crew, science officer and technicians aboard the R/V EWING during cruise EW96-05 are gratefully acknowledged. The professional ship handling and seamanship were instrumental to the scientific research conducted during the cruise.

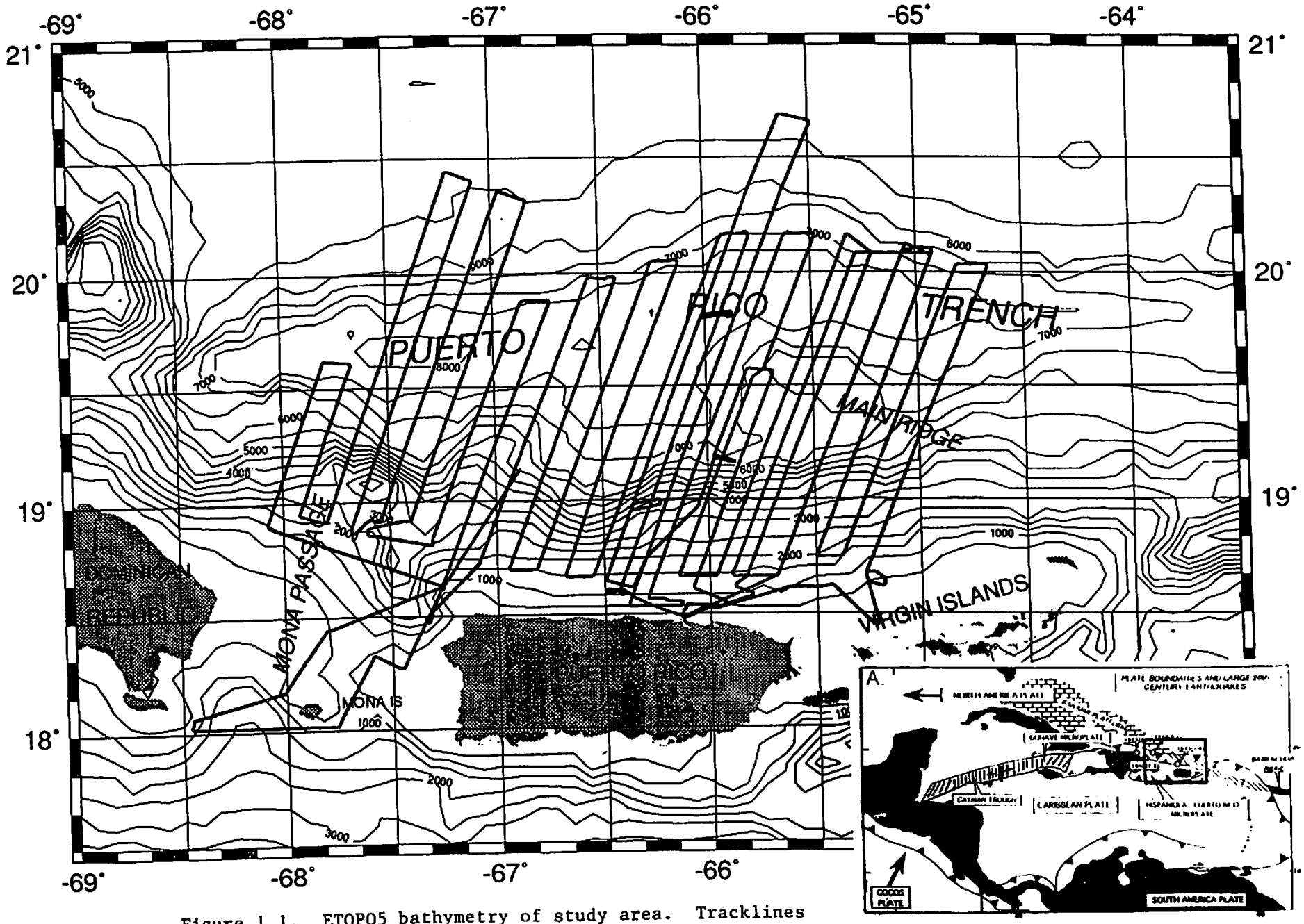

Figure 1.1. ETOPO5 bathymetry of study area. Tracklines for JD 167-188 shown as thick black lines. Inset shows regional setting of study area.

CHAPTER 2. COMPARISON OF PROPOSED OBJECTIVES OF EW96-05 WITH A PRELIMINARY ANALYSIS OF THE DATA

by Paul Mann, Nancy Grindlay and James Dolan

The major objective of this high-resolution sidescan/bathymetric (MR1) and geophysical (magnetic, gravity and SCS data) investigation of the Puerto Rico trench and northern slope of the island of Puerto Rico is to systematically map the zone of active collision between obliquely subducting aseismic ridges and a plate boundary margin. The Main Ridge area of the Puerto Rico trench is selected as the focus of this study because this area appears to represent the zone of active collision along this segment of the North American-Caribbean plate boundary (McCann and Sykes, 1984) (Fig. 2.2A). The character of this collision zone is critical for understanding patterns of ancient deformation in a postulated post-collisional zone from the Main Ridge to the Lesser Antilles Islands as well as understanding the present-day zone of deformation and related seismicity. Our survey area includes a postulated pre-collisional area to the west of the Main Ridge in order to better understand transpressional and strike-slip deformation unrelated to collision.

An added complexity to the understanding of this area involves the post-collisional effects of the passage of the southeastern extension of the Bahama platform. The active collision of the Bahama platform is presently occurring along the northeastern margin of Hispaniola (Dolan and Wald, in press) so it is reasonable to assume that this zone of left-lateral oblique slip that the Puerto Rico margin experienced this collisional event in the late Neogene and is now in a state of post-collisional adjustment.

Below we list verbatim our proposed objectives followed by an evaluation of these objectives based on the preliminary results of EW96-05.

Proposed Objective 1: Does the Main Ridge in the Puerto Rico Area Demarcate a Zone of More Deformed Seafloor to the East From a Zone of Less Deformed or Undeformed Seafloor to the West?

Studies of obliquely subducting ridges and seamounts along the Tonga Trench (Ballance et al., 1989), and orthogonally subducted seamounts and ridges at the Japan and Peru convergent margins (von Huene and Lallemand, 1990) show accelerated tectonic erosion of the forearc due to the fracturing and shearing of arc substrate rocks as they are lifted up by the colliding bathymetric high, and then left to collapse as the ridge moves away. This wave of vertical tectonism travels along the landward trench slope lifting it and then letting it subside again leaving an extended or collapsed terrain in its "wake". von Huene et al. (1995) have recently shown spectacular examples using Hydrosweep bathymetry of furrows up to 55 km long in the Costa Rica accretionary prism that mark the collapsing paths of subducting seamounts.

A time-transgressive zone of deformation caused by the oblique subduction of the Barracuda Ridge has been proposed by McCann and Sykes (1984) mainly on the basis of teleseismic data and widely spaced SCS lines. Figure 2.2A and B summarizes the relationship of obliquely subducting ridges to the proposed forearc basins of McCann and Sykes (1984). According to their model, the forearc basins west of the Main Ridge have not been affected by shallow subduction of Barracuda-Main Ridge and therefore contain undisturbed sedimentary rocks deposited in an arcuate but discontinuous "forearc basin" inferred from the central part of the Lesser Antilles to the Puerto Rico trench area. Main Ridge lies oblique to the ridges and basins that make up the forearc of the inner wall of the Puerto Rico trench. The Main Ridge interrupts these features and they are not observed east of where it intersects the arc. According to McCann and Sykes (1984) as the Main Ridge passed beneath the sediments on the inner wall of the trench, where it disrupted "well developed structures and left a chaotic terrain in its wake".

To illustrate this hypothesis, they presented two SCS lines collected by the R/V CONRAD in the early 1970s. Line A-A' in Figure 2.2B is a north-south line which according to McCann and Sykes (1984) is a "classical ridge basin sequence in the forearc region" that has not yet been affected by the oblique subduction of the Main-Barracuda Ridge. The "classic forearc structure" they refer to includes: 1) the Puerto Rico trench; 2) the "Main Ridge", which was first named by Ewing et al. (1965)(Fig. 2.1); 2) an "Outer Arc Ridge", called the "Median Ridge" by Ewing et al. (1965), and lying to the west of the Main Ridge; and 3) a "Forearc Basin" called the "Elevated Plain" by Ewing et al. (1965) because it forms a turbidite-filled basin south of the Main Plain of the Puerto Rico trench but a shallower depth.

The Forearc basin/Elevated Plain is filled with about 0.5 seconds of highly reflective turbidites tilted to the southwest away from the Median Ridge. This basin acts as a channel for turbidites derived from the Puerto Rican shelf margin. These turbidites flow from the Elevated Plain into the Main Plain of the Puerto Rico trench through an "Abyssal Gap" identified by Ewing et al. (1965) at the western end of the Median Ridge.

In a second line, B-B', McCann and Sykes emphasized a "ridge-trough topography" between the Main Ridge and the trench whose troughs are inferred to be young in age because they do not contain young turbidites. This area is inferred to be the chaotic area formed in the wake of the obliquely subducting Main Ridge.

We proposed to collect higher resolution and synoptic sidescan imagery and seismic profiles at 14 km spacing across a zone east of the Main Ridge (after deformation), on the Main Ridge (zone of active collision) and west of the Main Ridge (zone as yet undeformed by the collision event). The higher resolution MR1 sidescan images and bathymetry combined with SCS profiles could potentially allow us to map convergent structures at the front of the ridge and extended or collapse structures in the "wake" of the ridge along with furrows marking the path of the bathymetric high along the base of the accretionary wedge.

Evaluation of Objective 1 Based on Preliminary EW96-05 Results:

Our closely spaced SCS lines reveal the distribution of turbiditic sediments and the along-strike continuity of the Main and Median Ridges and can therefore be used to evaluated the McCann and Sykes (1984) model that is shown in Figure 2.2A and B.

Landward projection of the Main Ridge. The Main Ridge is first seen as a rise on the slope of the Virgin Islands platform on Line 14 at the eastern limit of the study area. As predicted in the McCann and Sykes (1984) model, this ridge projects towards Anegada, the easternmost island in the Virgin Islands, which they interpreted as a surficial bulge above the bathymetric high of the subducted Main-Barracuda ridge (Fig. 2.2A). This island is the only island in the Virgin Islands exhibiting evidence for late Quaternary uplift (McCann and Sykes, 1984).

Post-collisional area. On Line 14 on Figure 2.4A, a "ridge trough topography" with no turbidite fill is present north of this rise on the slope and leads to the Puerto Rico trench, a narrow zone also lacking a turbidite fill. The crest of the Main Ridge reaches maximum elevation on Line 9 and progressively plunges in elevation to the west on Lines 8 through 4 (Fig. 2.4B). On Line 19, the Main Ridge disappears as a discrete topographic high and the Median Ridge appears with the strongly southwestwardly tilted turbidites of the Forearc basin/Elevated plain along its southwestern flank (Fig. 2.4B). The uplift of the Median Ridge and the strong tilting seen in the adjacent Elevated Plain suggests that this deformation may be linked to the disappearance and oblique subduction of the Main Ridge at this location on the Puerto Rico trench presumably by oblique subduction.

However, the argument by McCann and Sykes (1984) that the Median Ridge-Elevated Plain represents a "classic forearc basin" may be flawed for three reasons:

• the Median Ridge-Elevated Plain is highly oblique to the Puerto Rico trench and cannot be traced more than 30 km along strike. If these features formed as "classic forearc features" they would be expected to extend for greater distances along the strike of the Puerto Rico trench, particularly if the direction of plate convergence is as large (S70°W) as predicted by McCann and Sykes (1984). A more likely explanation based on the seismic lines shown in Figure 2.4 is that the Median Ridge is a highly localized response to oblique subduction of the Main Ridge.

• the turbidite fill of the Elevated Plain is dependent on the location of this area downslope from the Puerto Rico shelf (Ewing et al., 1965). The Median Ridge shields the area along its northeastern flank from turbidite sedimentation. While its possible that this northeastern flank lacks sediment because of its post-collisional setting, it is also possible that these differences are related only to the blockage of turbidite sedimentation by the Median Ridge itself.

• Masson and Scanlon (1991) show from GLORIA data that almost all of the tectonic elements of the basin and ridge province to the east and west of the Main Ridge are distinctly oblique to the trench, a situation not seen in other forearcs, even in areas of highly oblique convergence such as off the western Aleutians.

Proposed Objective 2: What is the Nature of the Main Ridge?

MR1 data and seismic profiles may reveal that Main Ridge represents the deformation produced by a subducted fracture zone on the downgoing North America plate that is continuous with fracture zones of the southeastern Bahama Platform mapped in 1989 by Dolan et al. using the SeaMARC II sidescan system. We favor this interpretation and its corollary - a regional decollement separating the top of the downgoing bathymetric high from a thin flap of the overriding Caribbean plate. Alternatively, the Main Ridge could be a localized zone of uplift in the overriding Caribbean plate between en echelon stepping strike-slip faults as proposed by Masson and Scanlon (1991) (cf. fig. 3B) or a fragment of the metamorphic basement rocks of the Caribbean that has been uplifted along a reverse or thrust fault. At the time of the proposal, we preferred the first interpretation mainly because the gravity anomaly of the Main Ridge aligns so well with fracture zone trends on the downgoing plate in both the Bahamas and Lesser Antilles (Fig. 2.2A).

Bathymetric data in combination with gravity data will provide information about the subsurface density structure in the region to further constrain the nature of the Main Ridge. Magnetic anomalies have been observed in association with aseismic ridges and fracture zones traces in the region (Geddes and Dennis, 1964; Griscom and Geddes, 1966). If the Main Ridge is indeed continuous with the southeastern Bahama Platform, a magnetic lineament may be traced between these features (Fig. 2.2A). Many of the existing MCS lines in the region have had very limited processing. We propose to migrate some existing MCS lines to help define the upper plate from the lower plate and examine deeper structures in the vicinity of the Main Ridge.

Evaluation of Objective 2 Based on Preliminary EW96-05 Results:

Figure 18.1.10 compares the position of a fracture zone mapped by Treadgold (1985) using reflection and refraction data and a topographic high mapped by Leonardi (1981, unpublished data) using Seabeam? bathymetric mapped (map published by McCann and Sykes, 1984). On EW96-05, we surveyed this ridge using SCS (Lines 26, 27 and 28) and MR1 sidescan and confirmed its location and dimensions of about 15 km wide and with about 600 m of bathymetric relief above the surrounding seafloor (Figure 18.1. 3A and B).

As pointed out by McCann and Sykes (1984), the later bathymetric high and the Main Ridge are collinear across the Puerto Rico trench. The fracture zone mapped by Treadgold (1985) is about 30 km north of the bathymetric high and projects into the ridge-trough topography northeast of the Main Ridge (cf. Lines 5, 6, 7 on Figure 3). The inference that the Main Ridge is formed by a subducted fracture zone that presumably underlies the bathymetric high mapped by Leonardi (1981) therefore is consistent with the data collected on this cruise.

The presence of the eastern fracture zone may explain the abrupt change in strike of normal faults in Atlantic seafloor at 65°45'W. As noted by Masson and Scanlon (1991) this change mirrors a change in the trend of the trench which occurs just outside the eastern edge of their Gloria study area. The zone of normal faulting on the bending Atlantic plate also changes character at this point. To the west its made up of two major fault scarps, but to the east it is much broader and is made up of a complex horst and graben province. Detailed sections across the turbidite fill of the Puerto Rico trench reveal what appear to be strike-slip faults nucleating on the faults separating the downbending basement highs of Atlantic crust. The long straight, ENE-striking faults in the Atlantic crust of the western trench may therefore be in the process of being reactivated as strike-slip faults.

Proposed Objective 3: What is the Relation of Thrust Faults and Strike-Slip Faults in the area of the Main Ridge?

Do strike-slip faults including the main trace of the North America-Caribbean plate boundary (Septentrional/Escarpment fault system) terminate at the Main Ridge or do they extend eastwards across the zone of active collision? In the former case the collision would have a greater effect in transforming the character of the plate boundary than in the latter case.

The GLORIA sidescan data collected over the northern margin of Puerto Rico was incomplete and of insufficient resolution to image the East Septentrional/Escarpment fault system. The proposed survey will provide complete coverage of the fault system from landfall in Hispaniola, through the Mona Passage, north of Puerto Rico and the Virgin Islands to its intersection with the Puerto Rico trench/Lesser Antilles subduction zone around 63°W. In addition, we will be able to determine the relation between the active fault systems and areas of submarine slump scars (e.g. Schwab et al., 1991) and identify areas of potential instabilities along the north coast of Puerto Rico and the Virgin Islands. One possibility is that these type of slumps are triggered by major earthquakes like the one that occurred between A.D. 1150-1230 in Hispaniola (Prentice et al, 1993) The seismic reflection data will provide a depth perspective of the faults imaged with the sidescan data to make it possible to define fault geometries and characterize the style of recent faulting along the length of the fault system.

Evaluation of Objective 3 Based on Preliminary EW96-05 Results:

Our last line of the cruise followed what appears to be the eastward continuation of the Septentrional fault zone along the base of the scarp formed by the subsided carbonate margin. A sketch map based on a preliminary MR1 mosaic is provided in Figure 2.5.

Three distinct segments of the fault all display characteristics of an active left-lateral fault zone. Fine scale alternation of releasing and restraining bends on the central segment of the fault establishes its left-slip character along with the orientation of the larger transtensional segments bounding it to the east and west. Only a small part (~10 km) of this fault system was recognized on the Gloria mosaic of Masson and Scanlon (1991).

The western and eastern segments strike 070 to 080 and exhibit a transtensional character. The central segment strikes 080 to 090 and exhibits a pure strike-slip character. The ENE-striking western and eastern segments may control similarly trending segments of the Puerto Rico shelf margin to the south. For example, the western transtensional fault is north of

the ENE-trending eastern edge of the megaslump area described in detail by Schwab et al. (1991). The eastern transtensional fault trends parallel to the more ENE edge of the Virgin Islands Platform.

The eastern transtensional fault segment clearly crosscuts the Main Ridge. The point of intersection corresponds to a bathymetric saddle crossing Main Ridge in an ENE orientation that is visible on maps as crude as the ETOPO-5 bathymetric map with 200 m contours. The apparent lack of offset of the bathymetric trend of the Main Ridge at this saddle suggests that: 1) either the fault is young and offset has not been significant; or 2) that the Main Ridge is a topographic reflection of a topographic feature (fracture zone?) on the underthrust plate that is largely unaffected by strike-slip displacements on the overriding Puerto Rico margin.

Proposed Objective 4: Which Tectonic Model Best Explains the Origin of the Puerto Rico Trench?

We propose sidescan mapping, SCS profiling and migration of existing MCS lines to "test" or at least show the agreement or disagreement of these data with a dizzying array of tectonic models for the formation of the Puerto Rico trench". The main ideas and implications of the models are summarized below and compared with the types of data previously collected and proposed in this study. We emphasize that the origin of the Puerto Rico trench remains enigmatic because previous studies have not been systematic but relied on a hodgepodge of previous and often non-systematic studies.

Model One: The Puerto Rico trench formed in an island arc setting by southwestward subduction of the North America plate beneath the Caribbean plate (McCann and Sykes, 1984; McCann and Pennington, 1990). This model invokes oblique convergence to explain what appears to be a continuous Benioff zone traceable from the Lesser Antilles to eastern Hispaniola. If this hypothesis is correct, we would expect to see structures common in accretionary prisms striking about N135° in young sediments of the Puerto Rico trench. Heubeck and Mann (1991) point out onland geologic inconsistencies in the greater amount of convergence required by this model along the length of the entire plate boundary while Dillon and Coleman (in review) note that this model does not explain the abrupt westward termination of the Benioff zone in eastern Hispaniola. Previous GLORIA studies are instructive but not conclusive on the orientations of active folds and faults in the Puerto Rico trench Earthquake focal mechanisms suggest a range of oblique convergence from N50°-85° (Dolan and Wald, in press) but this results from strain partitioning of strike-slip motion.

Model Two: The Puerto Rico trench formed by transtension (Larue et al., 1990; Larue and Ryan, 1990; Speed and Larue, 1991). This model attributes the depth of the trench, the large reentrant in the plate boundary, the gravity anomaly, and the 4 km of late Neogene subsidence of the southern margin of the Puerto Rico trench to transtension along the plate boundary.

Masson and Scanlon (1991) and Larue (in press) identified faults along the western part of the Main Ridge and the south slope of the Puerto Rico trench but not at the base of the Puerto Rico island slope. The results of this survey suggests faults at the base of the slope. A simple model for the formation of the Puerto Rico trench would consist of a large extensional stepover zone developed between the two overlapping and active strike-slip faults. The lack of compressive deformation in the central and eastern parts of the turbidite-filled Main Plain of the Puerto Rico trench suggests that this feature may be transtensional. Transpressional folding is only present in the western Puerto Rico trench at the foot of the Mona block, a possible restraining bend along the Septentrional fault zone (see below). Masson and Scanlon (1991) point out that the best evidence for subduction is the seismicity and presence of a subducted slab. Most other lines of geological and geophysical evidence, including those collected during this cruise, favor a strike-slip origin.

Model Three: The Puerto Rico trench and associated Benioff zone formed in an island arc setting to the east in the Lesser Antilles area and was rafted westward to its present position on east-west strike-slip faults (Schell and Tarr, 1978; Calais and Mercier de Lepinay, 1991). Transported subducted lithosphere of the North America plate survives to the west in their words because it is "above the critical melting depth". If this model is correct, we would expect to see remnant accretionary wedge structures crosscut by younger east-west strike-slip faults and the downgoing plate "disconnected" by vertical strike-slip faults from the adjacent Benioff zone. A previous SeaMARC II investigation has identified strike-slip faults on the south slope of the Puerto Rico trench that appear to be continuous with known strike-slip faults in Hispaniola.

Model Four and preferred model at the time of the proposal submission: The Puerto Rico trench formed by the oblique collision of an obliquely subducting Atlantic fracture zone. Dolan and Wald (1994) recently proposed that the 4 km of late Neogene subsidence and the reentrant in the northern Puerto Rico slope occurred in response to removal of topographic support for the Puerto Rico shelf provided by underthrusting fracture zones and overlying carbonate banks as the colliding ridges swept westward through time. This model would predict localized and time transgressive subsidence tied to specific fracture zones shown in Figure 2.3A.

Model Five. The Puerto Rico trench formed in response to "deep plate collision" or mantle interaction between south-dipping North America slab depressed by a north-dipping Caribbean slab as shown by serial profiles of seismicity through Puerto Rico (Dillon and Coleman, in review). Depression of the North America plate caused regional subsidence of the Puerto Rico slope that would contrast to the more localized subsidence predicted in Model Four above.

Evaluation of Objective 5 Based on Preliminary EW96-05 Results:

The uplift, subsidence and deformation history of the Oligocene-Early Pliocene carbonate platform of the Virgin Islands, Puerto Rico and the eastern Dominican Republic provides an excellent test of the timing and origin for the formation of the Puerto Rico trench. Previous workers like Moussa et al. (1987)(See chapter 18 for review of Moussa et al.) and Birch (1986) have pointed this out but have failed to provide a regionally consistent model because their data is limited to the margin in central and northwestern Puerto Rico.

New SCS data from EW96-05 has increased this coverage over an along strike distance of 200 km. Four representative SCS lines covering an along-strike distance of 200 km and crossing the platform at a high angle (020) are interpreted on Figure 2.7. It should be emphasized that these interpretations and correlations were done quickly and are subject to revision. Below is a brief summary of new interpretations of this margin based on these data:

1. The carbonate platform may be much thicker and younger beneath the offshore area than assumed by Moussa et al. (1987). The middle unit of Moussa et al. (1987) has somewhat regular internal reflectors and some reflectors have apparent landward dips suggesting listric faulting (Fig. 2.6A). Ages and compositions are poorly constrained because they interpreted this unit as pinching out in a data gap less than 35 km from the CPR-4 well (Fig. 2.6A). They interpret the top of this unit to be the base of the San Sebastian Formation, a Middle Oligocene transgressive deposit found onland to be above folded rocks of Eocene age. By a process of elimination they suggest an age of late Middle Eocene to Middle Oligocene for the middle unit. This unit would therefore have no onshore correlatives.

An alternative interpretation is that the base of the San Sebastian Formation is at the base, not the top, of their middle unit. This would mean that the middle unit is a seaward-thickening offshore part of the late Oligocene to early Pliocene carbonate margin. This interpretation is consistent with the similar seismic character and dip of the middle and upper

units. The geometry of the middle unit suggests that the thicker part of the platform is a greatly expanded section present only in condensed form in the CPR-4 well.

Another argument for this revised interpretation is the fact that the middle unit is unfolded. Onland studies in Puerto Rico have established that rocks of Eocene to Early Oligocene age beneath the Middle Oligocene San Sebastian Formation are folded and thrusted (cf. Dolan et al., 1991, for a review). The lack of a significant discordance at the contact between the upper and middle units indicates that no major folding event occurred at this time.

Larue and Berrong (1991) have emphasized that the unfolded nature of the middle unit is not consistent with Pindell and Barrett's (1990) model for fold-thrust deformation of the Puerto Rico arc during its collision with the Bahama platform. They argue that a Bahama collision event would produce progressively deformed offshore sections rather than the undeformed but tilted section seen on their line. However, if the deposition of their middle unit postdates collision then the fold-thrust model could still be viable.

In their MCS line tied to the Toa Baja well they infer a down-to-the south-vertical fault offsetting Eocene basement near the coast. This fault effectively raises the level of their Eocene basement in the offshore area. This inferred fault throw may have led to a miscorrelation between Eocene rocks that are present at much deeper levels in the offshore areas. The down-to-the-north fault interpretation in the Moussa et al. (1987) line seems a much more likely explanation for the greatly expanded thickness of the middle unit. More work is needed to correlate the Moussa et al. fault with the fault seen on these data.

2. The carbonate margin contains a major, coast parallel but offshore barrier reef complex that is poorly known because it lies at great depth beneath the previously studied area of central and northwest Puerto Rico. The interpretation of Moussa et al. (1987) and Larue and Berrong (1991) is that the carbonate margin is a planar ramp that dips offshore and exhibits no major vertical relief. There is a suggestion of a reefal buildup at about 2.5 seconds on the Moussa et al. (1987) line. Results from this study supporting this claim are given below.

Along strike changes in margin morphology. Figure 2.7 compares four lines that include from east to west: Line 22 off the northwest coast of Puerto Rico, Line 6 off the east-central coast of Puerto Rico in the area of the Toa Baja well and Line 2 of Larue and Berrong (1991), Line 9 off of eastern Puerto Rico, and Line 14 off the Virgin Islands shelf. Enlargements of critical areas on these lines are provided in Figure 2.8.

The margin exhibits progressive erosion and collapse from west to east. In the east the margin appears to represent a complete section including a 70 m thick cap of early Pliocene Quebradillas limestone. The total thickness of the margin is about 1 km. Heezen et al. (1985) report a 1200 m thickness of the carbonate margin overlying Eocene metavolcanic rocks based on their Alvin dives in the east wall of the Mona Canyon.

On Line 14 near the Virgin Islands platform, south-dipping reflectors are similar to those imaged and drilled by Larue and Berrong (1991) on Line 2 and in the Toa Baja well (Figs. 2.6 and 2.7). This suggests that the carbonate platform has been reduced erosion or slumping to a thickness as small as about 0.5 km.

Margin morphology compared to predictive models. The preferred model on beginning this study was that the Puerto Rico trench formed by the collision of an obliquely subducting Atlantic fracture zone. Elaborating on the tectonic erosion hypothesis of Birch (1986), Dolan and Wald (1994) proposed that the 4 km of late Neogene subsidence and the reentrant in the northern Puerto Rico slope occurred in response to removal of topographic support for the Puerto Rico shelf provided by underthrusting fracture zones and overlying carbonate banks as the

colliding ridges swept westward through time. This model would predict localized and time transgressive subsidence tied to specific fracture zones and the southeastern extension of the Bahama platform.

More detailed correlations between closer spaced SCS lines from EW96-05 are needed to test this idea of diachronous deformation along the margin. It is clear that deformation did not involve any post-middle Oligocene (San Sebastian Formation) compressive deformation of the carbonate cap (Figs. 2.6 and 2.7) and that the cap subsided at a uniform rate that resulted in a uniform along-strike northward dip of about 4° (Moussa et al., 1987; Birch, 1986).

Barrier reef complex. The existence of a barrier reef complex well imaged on Line 9 and suggested on Lines 22 and 6 (Fig. 2.8) is proposed here for the first time based on these SCS data. Because the reef appears to plunge to greater depths (or at least be less exhumed) in northwest and east-central Puerto Rico, previous studies in this area may have confused its constructional profile and reflection-free character with underlying Eocene arc basement (Larue and Berrong, 1991). In the less well studied western area for which we have seen no previous seismic data, the top of the reef lies within 0.5 seconds of the seafloor. Line 9 reveals that the reef complex is bounded to the south by a recently active fault exhibiting a "flower structure" of possible strike-slip origin. Down-to-the-south motion on this fault may have created a high upon which initial reef growth occurred. Detailed correlation between these sections and the Toa Baja and CPR-4 wells is needed to confirm the age of reef growth and drowning as well as its along strike continuity. Assuming the reef formed as a continuous barrier-type reef along the north coast, its drowning may be also related to the northward tilting of the Puerto Rico shelf that caused it to subside at a greater rate than could be matched by its upward growth. Reef growth may correlate with several Oligocene-Pliocene transgressive-regressive cycles outlined by Seiglie and Moussa (1985).

Other Hypotheses Addressed During This Study

1. Uplift mechanism for the Mona block and the Aguadilla arch of northwest Puerto Rico: An effect of oblique subduction of the southeastern end of the Bahama platform or restraining bend tectonics? Dolan and Wald (in press) propose that the Mona Block may be the surface expression of the subducted southeastern margin of the Bahama platform. Dredge hauls indicate that the Mona block is composed of blueschist rocks of Cretaceous age and similar to those exposed on the Samana Peninsula of the eastern Dominican Republic. This uplift mechanism is similar to that proposed by McCann and Sykes (1984) for the uplift of the Main Ridge. The topographic effects of such a model could also be explored for the Quaternary uplift of the island of Puerto Rico. Gardner et al. (1981) point out the highest Quaternary shoreline features are located on the Aguadilla Peninsula which is on the landward projection of the Mona block high.

An alternative model is that the Mona block is uplifted at a gentle restraining bend formed along the west-northwesterly striking Septentrional fault zone. The eastern limit of the bend is marked by the abrupt transition from EW to ENE-striking strike-slip faults to WNW faults in the Mona Canyon area. This bend similar in dimensions, style, and bedrock geology to the gentle bend exposing rocks of the Samana Peninsula. The occurrence of localized folding at the base of the Mona block in turbidites of the Puerto Rico trench may also be explained by a bend in this area. Evaluation of this model awaits the availability of processed MR1 sidescan and bathymetric data from this complex area.

2. Tectonic origin of the Mona Canyon and Mona Passage extensional zone and its relationship to Caribbean-North America strike-slip faults Speed and Larue (1991) argue that late Neogene extension in a north-south direction affected Puerto Rico, the Puerto Rico trench, the Mona Passage, and the Anegada Passage. The main zone of extensional detachment was

assumed to be a south-dipping Puerto Rico trench. The hanging wall was assumed to be the drowned island slope of Puerto Rico largely on the basis of its slight anticlinal arching.

MR1 sidescan data from the Mona Passage support the idea of regional extension but in an east-west rather than north-south direction. X-shaped conjugate fault pairs affecting the submerged early Pliocene carbonate cap. The orientation of these fault pairs is particularly well expressed in the area west and southwest of Mona Canyon indicate post-Early Pliocene? extension in an east-west direction. The northwest-striking fault in this pair are thought to be right-lateral oblique-slip faults while the northeast fault is assumed to be a left-lateral oblique-slip fault. North-south-trending rifts such as the Mona Canyon and the Yuma basin are also present and drop the carbonate platform down to depths of 1 km in full and half grabens beneath the adjacent seafloor (Figs. 2.9 A, B, C and D). Diffuse extension probably forms the western margin of the Puerto Rico microplate first postulated by Byrne et al. (1987). GPS studies support such a model because the rate of eastward motion of the Puerto Rico microplate is twice that of the adjacent microplate in Hispaniola (Farina et al., 1995). The interplay between north-south rifts like the Mona Canyon and the east-west striking Septentrional fault zone is complex and will require detailed study.

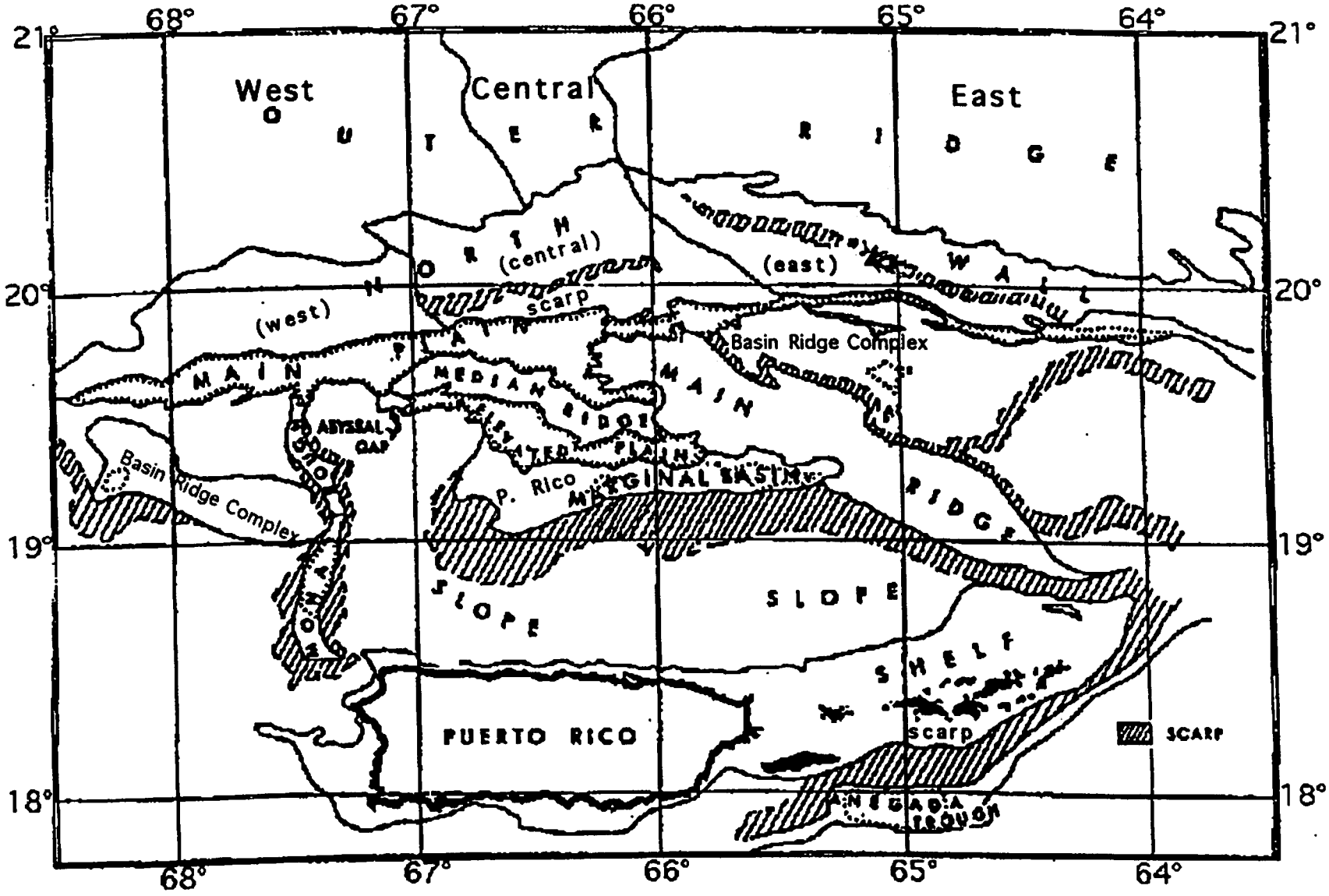

Figure2.1 General physiography and geomorphological features of the Puerto Rico Trench (Modified from Ewing, Lonardi, and Ewing et al. 1966).

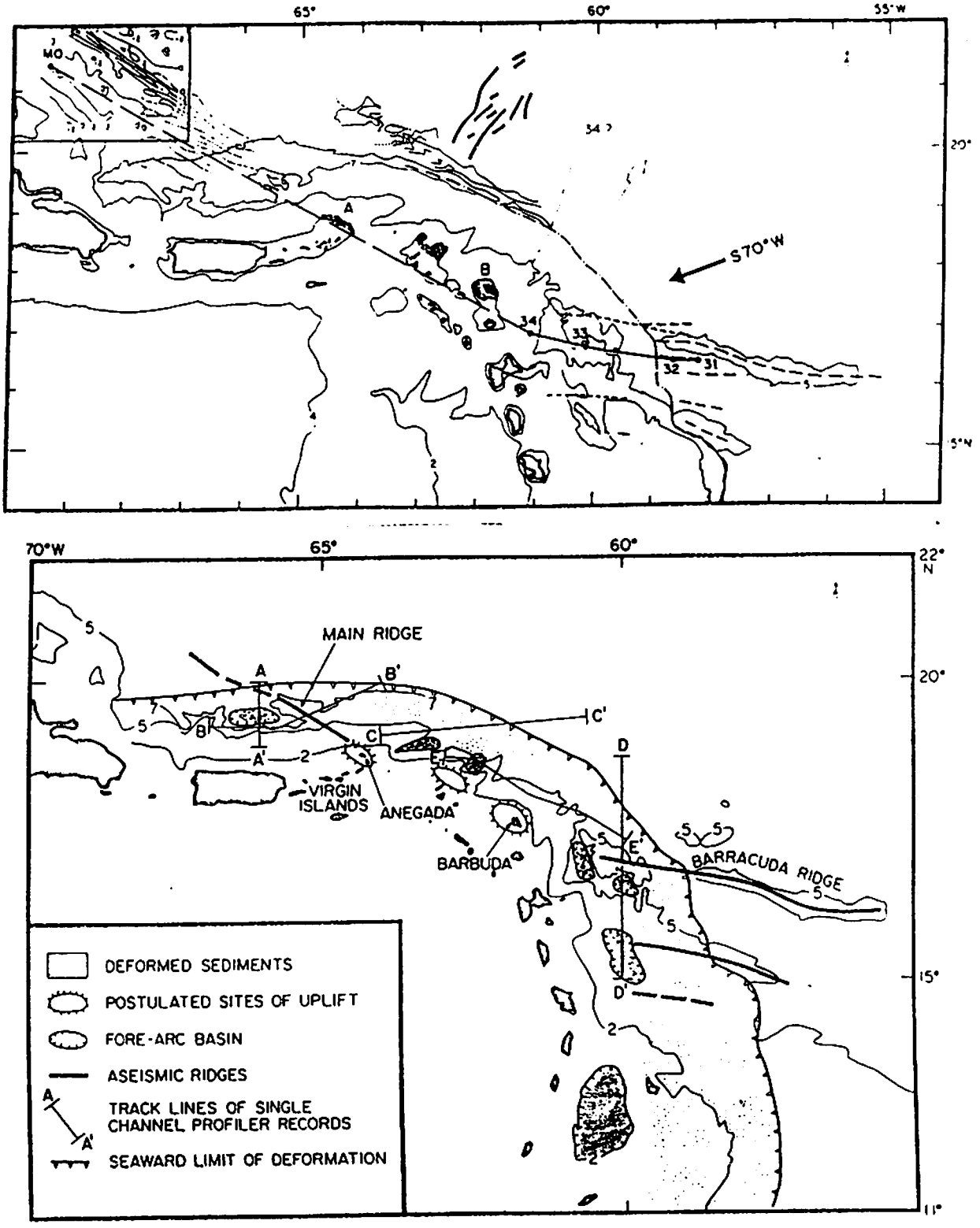

Figure 2.2A. Fracture zone and oceanic spreading fabric at the northeastern margin of the Caribbean plate from McCann and Sykes (1984). The dashed line shows the postulated extent of the subducted Main Ridge-Barracuda Ridge beneath the Caribbean plate. **B.** Geologic effects of the subduction of the Barracuda-Main Ridge according to McCann and Sykes (1984). Note the presence of a semi-continuous "classic" forearc basin along the leading edge of the Caribbean plate. A-A' and B-B' give the locations of seismic lines shown in Figure 2.

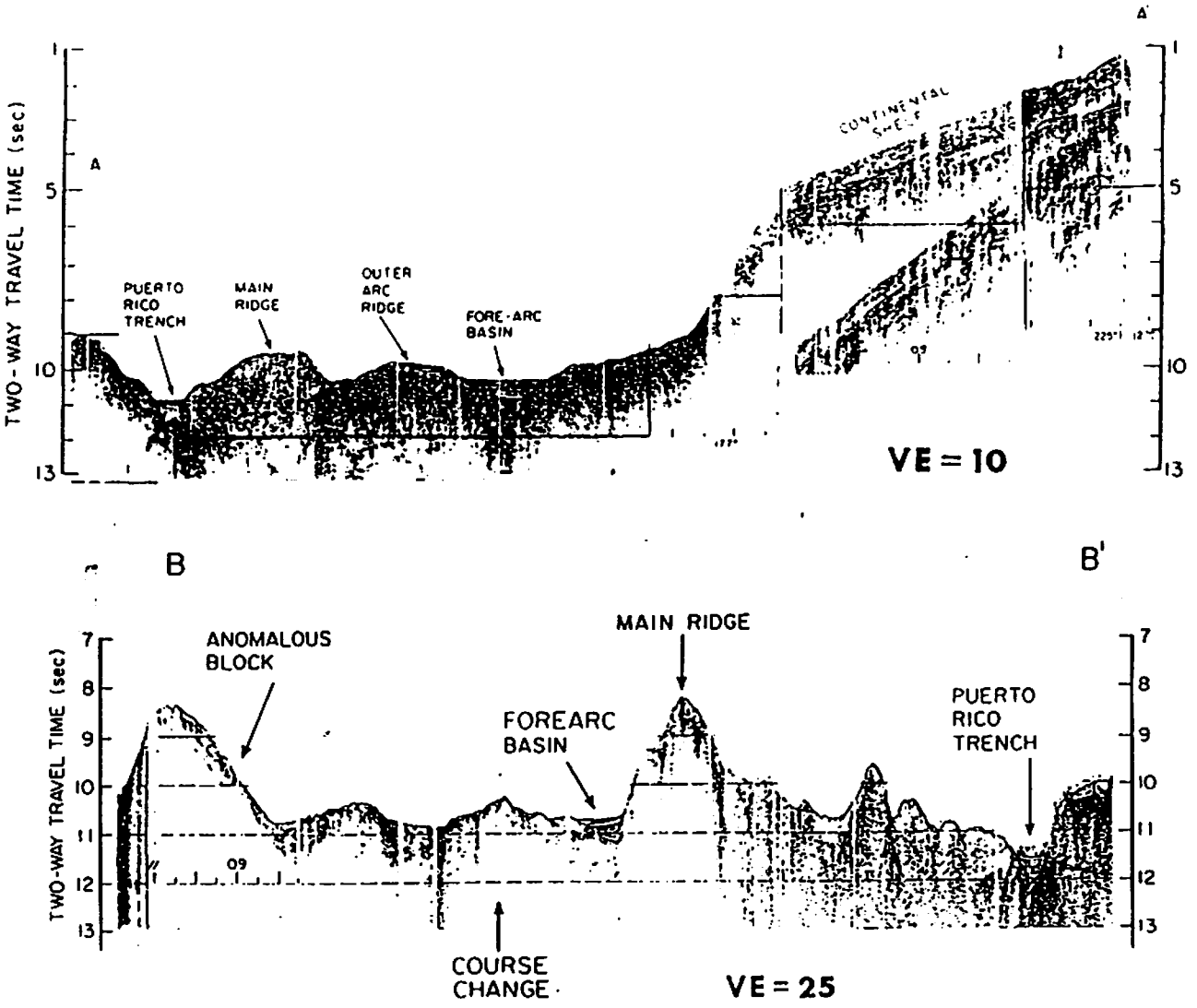

Figure 2.3A. Line A-A' from McCann and Sykes (1984) in the EW96-05 survey area. See text for discussion. **B.** Line B-B' from McCann and Sykes (1984) east of the EW96-05 survey area. See text for discussion.

DOUBLE-WIDTH

PAGES

NOT

SCANNED

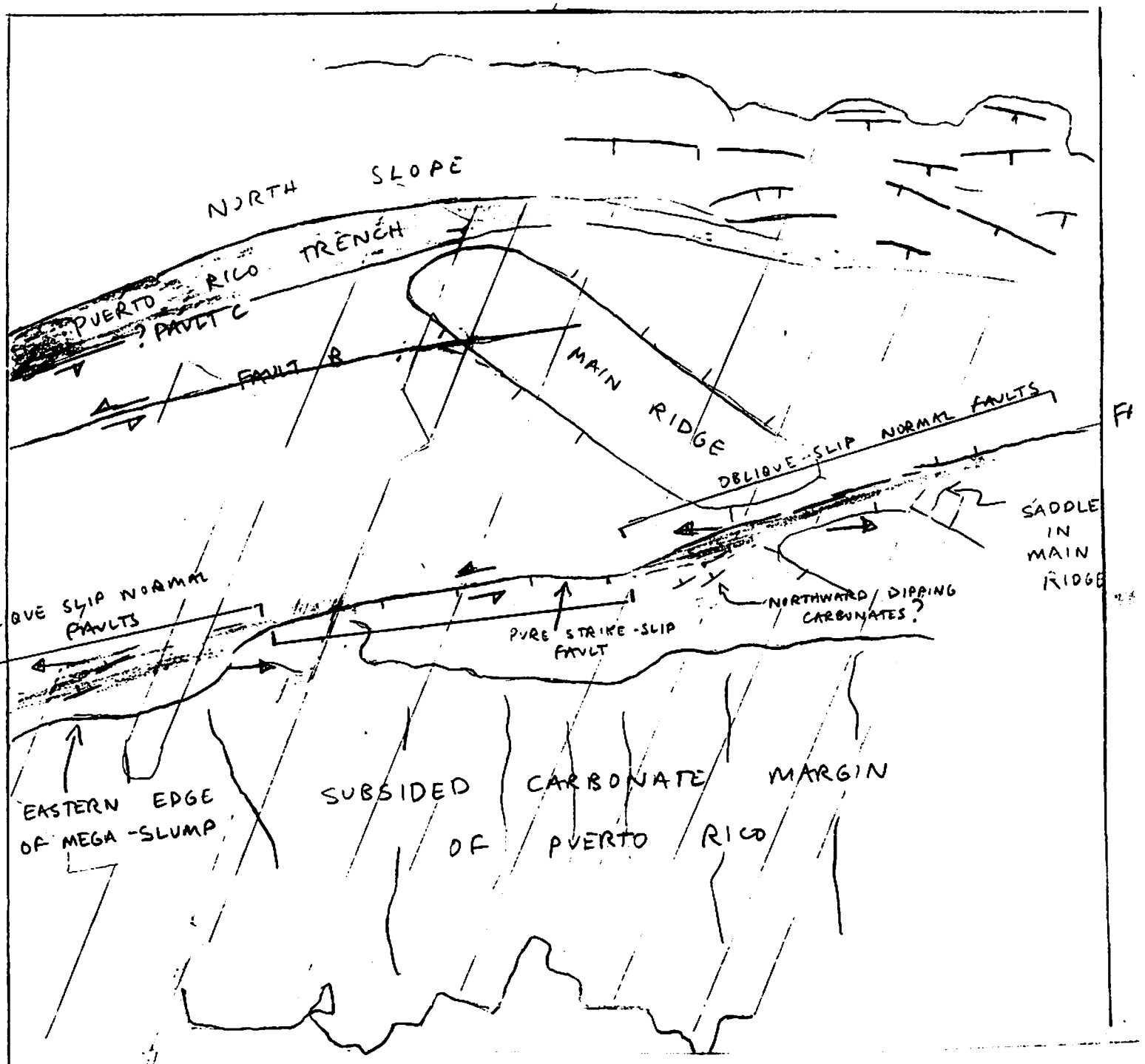

Figure 2.5. Tectonic sketch map based on MR1 sidescan image of the north slope of the Puerto Rico trench collected during EW96-05.

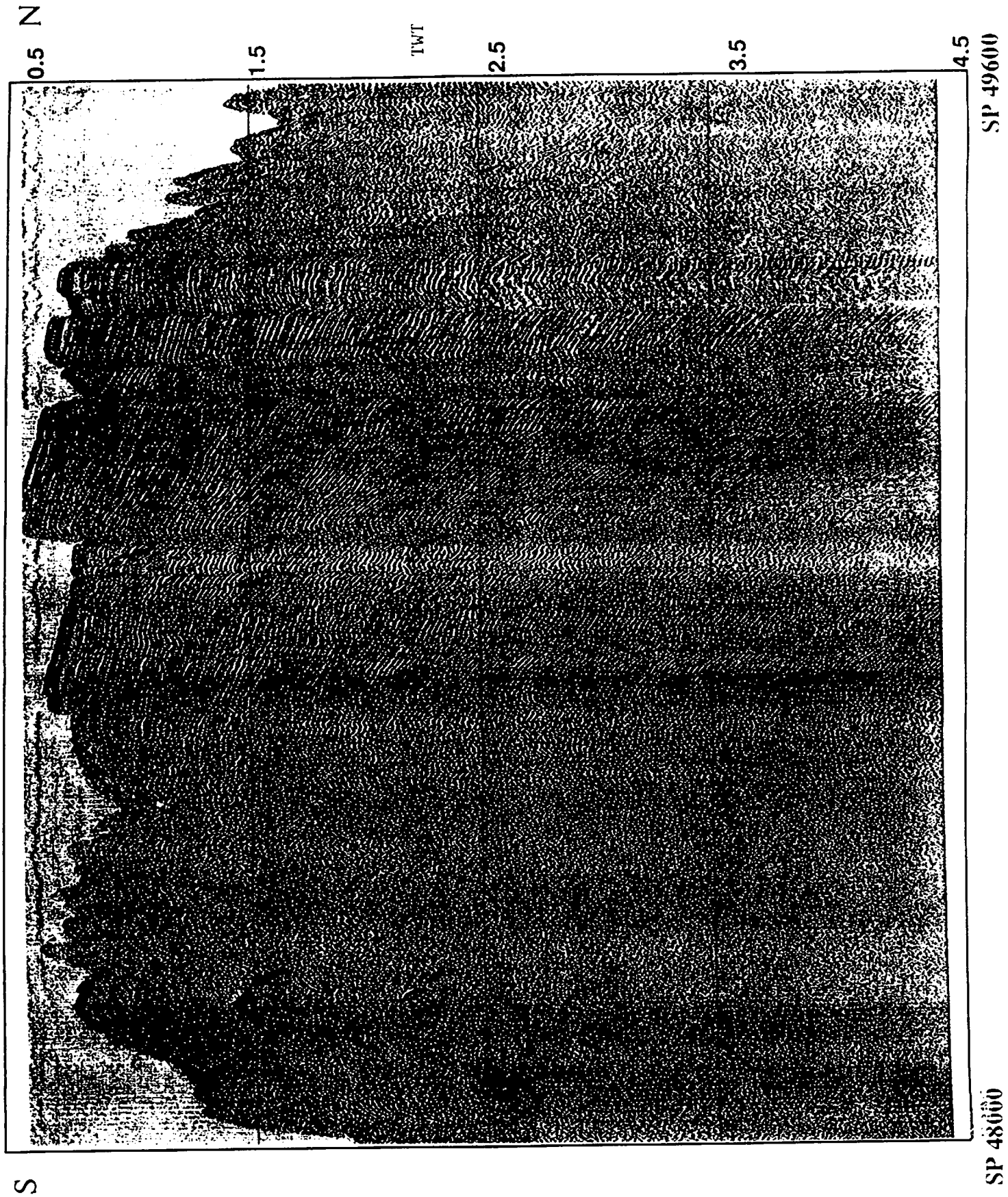

Figure 2.9 Line 35 Mona Passage.

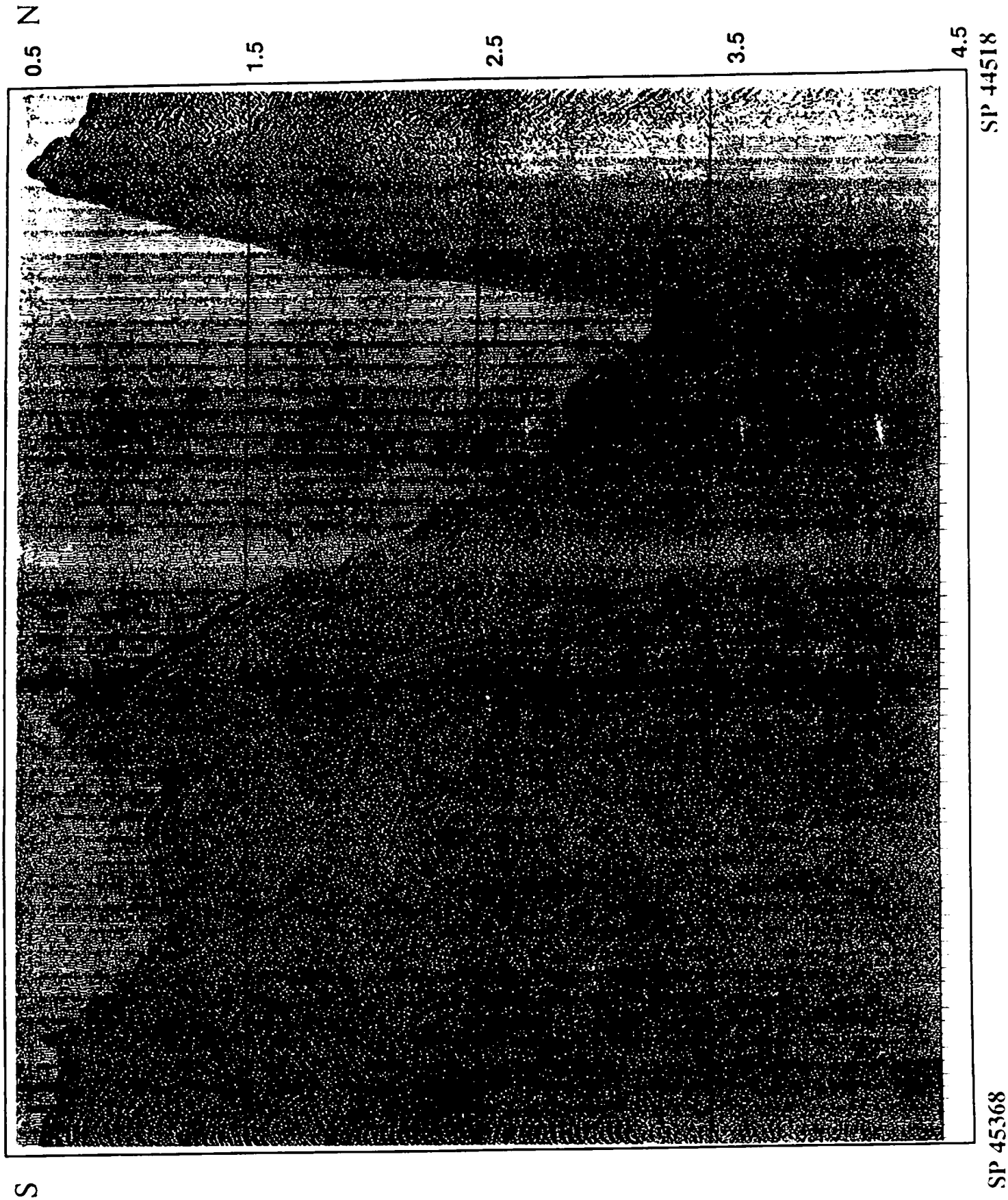

Figure 2.9B: Line 32 Desecheo Ridge.

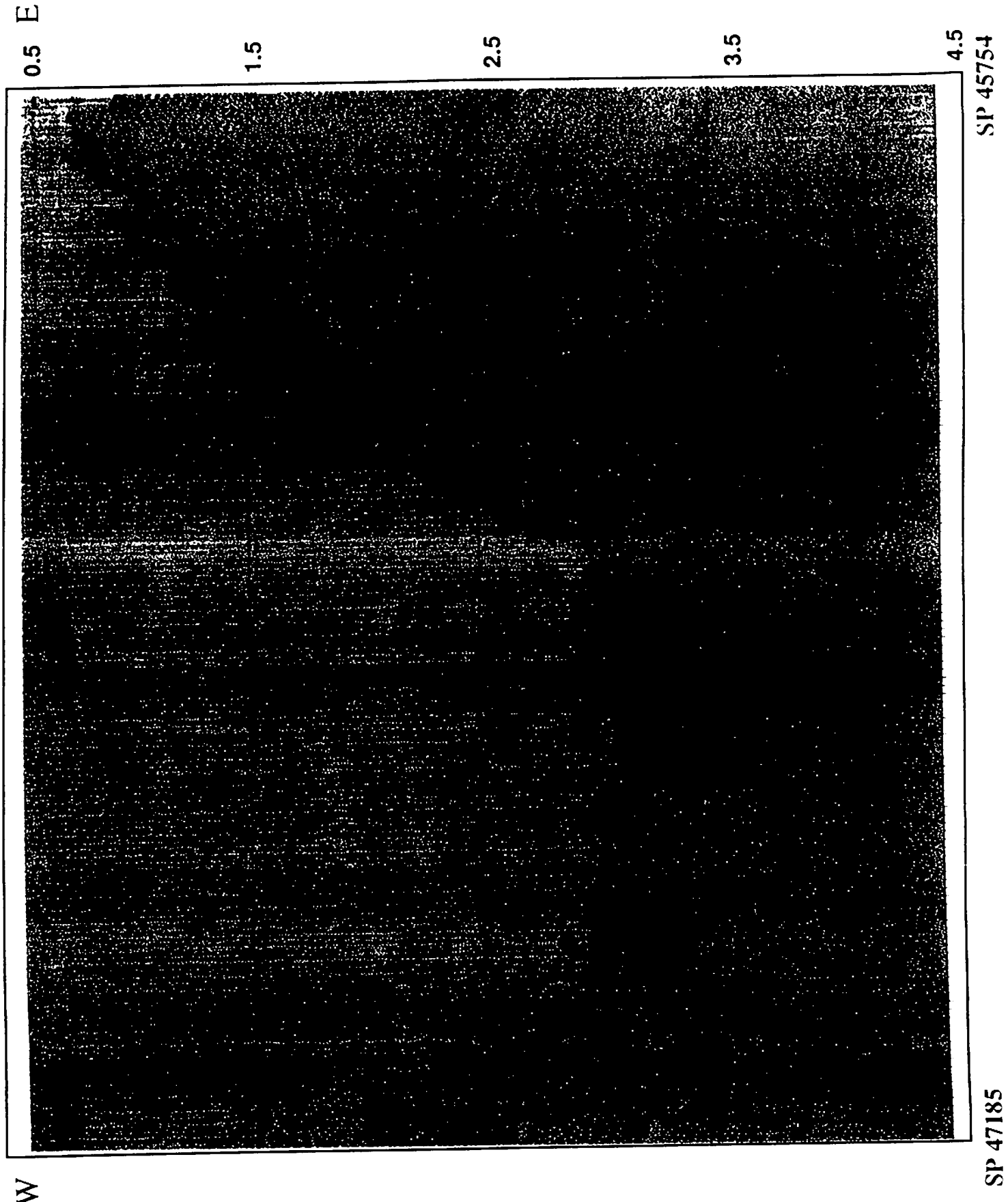

Figure 2.9C: Line 34 Yuma Basin.

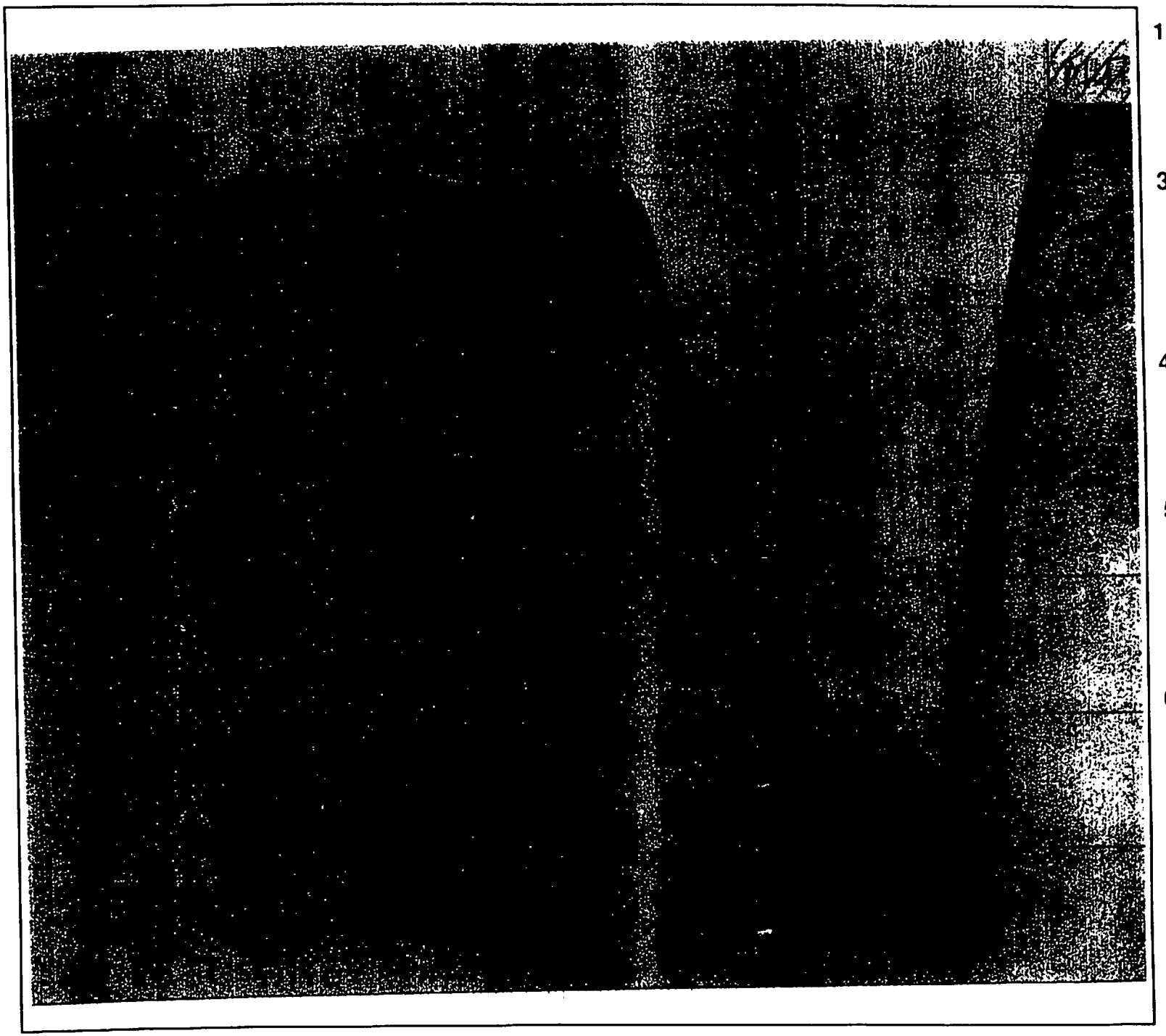

Figure 2.9D Line 31 Mona Canyon.

CHAPTER 3. SINGLE-CHANNEL SEISMIC REFLECTION OPERATIONS

by Jean-Paul van Gestel

Streamer

The "Single-Channel Streamer" (SCS) is a multi-channel streamer that usually consists of 4 to 8 channels (Figs. 3.1 & 3.2). During the EW96-05 cruise, only four of the channels were utilized. The SCS preamplifier is can handle up to 8 channels of data. Streamer had carried the preamplifier itself up until around 1988, and had provided both amplification and a low impedance, single ended output. After this time, commercially built transformer-coupled streamers introduced the problem of having to deal with low-impedance, low-level, differential signal. This problem was overcome with the building of a transformer-coupled preamplifier by Harry Van Santford. This preamplifier provides amplification of the streamer channels for digitization purposes and allows the merging of the individual channels into one channel. This in turn allows the data to be displayed on the line-scan recorders.

The differential analog signal from each of the steamer channels is amplified and converted to a single-ended signal by the transformer-coupled amplifier. The signals are then sent to a 4-channel digitizer and to the buffer-amplifiers. The buffer-amplifiers then send their signal to the front panel (which is kept in the wet-staging area) on the as a test and then to the 8-channel adder. The adder permits any of the channels to be combined to form a single analog signal. This single analog signal is then sent through a variable-gain amplifier and then to the line scan recorders. The gain of the variable-gain amplifier is usually set at 10 dB while the total gain at the preamplifier is around 70 dB.

The streamer used during this cruise consisted of 7 components. They will be described in order from the fantail of the ship to the end of the streamer. The first component was the 156.75 m kevlar tow leader. The next is a 25 m stretch section followed by a 25 m non-stretch rope. After this there follow the 4 channels. The first is 12.5 m long, the second 25 m while the remaining two channels are each 50 m apart. The total active streamer length for the EW96-05 cruise was 137.5 m(Fig. 3.2).

The optimal depth for a streamer in SCS studies is approximately 6m. This depth was maintained during the EW96-05 cruise through two items. The first is an oil filling in the streamer itself, which provides a neutral buoyancy. The second is the 156.75 meter kevlar tow leader, which provides the weight to keep the SCS streamer at its operating depth.

Recording system

The recording system that was aboard the R/V EWING during the EW96-05 cruise was the DSS-240 system. This system consists of a network of processors that make up subsystems that are each responsible for an aspect of recording the SCS data (Fig. 3.3). The recording process begins with the initiation of the shot cycle and ends with the writing of the SCS data to a storage tape.

Radio Data Link 3 (RDL3) is a multi-boat system controller in which the shot cycle originates (Fig. 3.4). RDL3 has the capability to control the shots of up to three seismic vessels. The firing rate during EW96-05 was controlled by a specified time interval. In order to so this, the RDL3 kept track of the time interval plus randomization and the Radio Event Synchronization System 2 (REVS2) within RDL3, initiated the shot cycle by sending the NAV Clock Prime (NCP) closure through the System Interface Board (SIB) to the Serial Line Interface Controller (SLIC). This occurs 312 ms after REVS2 has received closure from RDL3. The SLIC monitors such asynchronous serial devices as the air pressure monitor and streamer cable tension. This information is then sent to the RDL3.

After the SIB receives the NCP signal, the SIB conveys the signal to the Timing Analysis for Gun Synchronization (TAGS) engine (Fig. 3.5). The purpose of TAGS is to control the firing of the airgun array as well as to log the quality control information for each shot. When TAGS receives the signal from NCP, TAGS provides RDL3 with its setup and the source enable status. TAGS further gives source and array information to the Class Loop Automatic Source Synchronizer (CLASS) about when to fire the guns. Essentially, CLASS's responsibility is to fire the guns at precisely the correct time.

When RDL3 receives the source enable code from TAGS, it 'decides' on whether the guns should be fired. This is dependent on if the conditions for shooting have been met. If they have, then REVS2 sends a BLAST command to the CLASS. As soon as the guns have fired, CLASS generates a Time Break closure, sends it to the SIB and sends the measured firing times to TAGS. Tags in turn calculates which guns fired early or late and no fires. This data are sent to three places. The first is a monitor that displays the gun status. The second is the Control Executive Overseer (CEO), where a text-line printout shows that the shot times have been recorded. The third is the Ethernet Line Interface Controller (ELIC), which directs the information to the Cable Supervisor and Recording Unit (SCRU) in order that the data may be recorded on tape. The CEO is the user interface that is used in the real-time acquisition lab to program the CSRU.

If the SIB receives a Time Break closure, it generates a Time Break Echo (TBE), which is sent to RDL3. If this signal is not received by RDL3 within a certain time frame after receiving the Nav Clock signal, then the data for that particular shot are not recorded and an error is reported. RDL3 then receives the shot number, GPS recorded shot time and the ship location from SPECTRA. If the TBE receives its signal on time, the previous information is sent through the ELIC to the CSRU to be recorded in Trace 0 on the 3480 tape. In addition to this, the gun status for each shot is also recorded by the CSRU.

The seismic data is then digitized and sent to the Cable Subsystems (CSS) from the telemetry cans. It is then transferred to through the Hydrophone Array Sampling and Telemetry Electronics (HASTE) Personality module to the GPCC interface board where it is demultiplexed (Fig. 3.6). From the GPCC, the data are transferred by a VME bus to the PC Cable Data Display (PCDD) memory buffers. The VME is a high performance 32 but bus with a data through put bandwidth of 10 megabits/second. The high transfer rate is a function of the amount of data that are sent to the buffers with every shot. The most recent seismic data is then displayed by PCDD after the signal has been demultiplexed. The data are then displayed at a sample rate of 125 Hz. This is without an anti-aliasing filter, so aliasing is inevitable.

The PCDD contains 16 megabytes of memory, which is broken down into three buffers. One buffer consists of two six megabyte blocks and is used by the CSRU to stage the seismic data. While this is occurring, the PCDD is displaying the data and a SCSI splitter is copying the data from the VME side of the memory and recording it in SEG-D format on 3480 tapes. This is also occurring at the same time that the non-seismic data is entering the CSRU through a smaller GPIB bus (0.1 Mbit/second data throughput). This non-seismic data was the above mentioned data sent to the CSRU from the SLIC, ELIC, and CEO. The brute stack plots and near trace display require another copy of the seismic data, and these are plotted on two flatbed plotters.

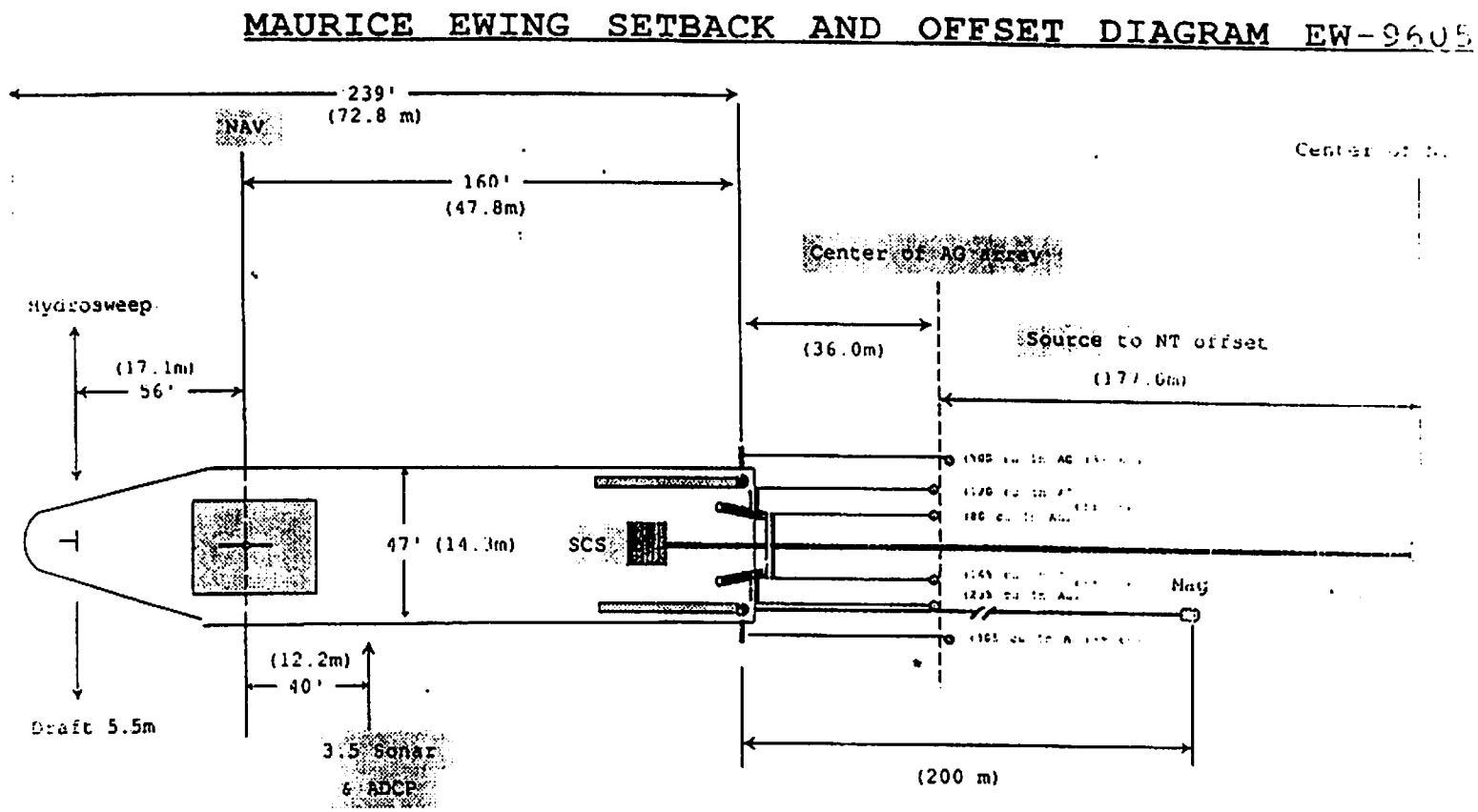

Figure 3.1. Setback and offset diagram for SCS reflection operations for MW96-05. Diagram also shows MR1 fish location and Magnetometer location.

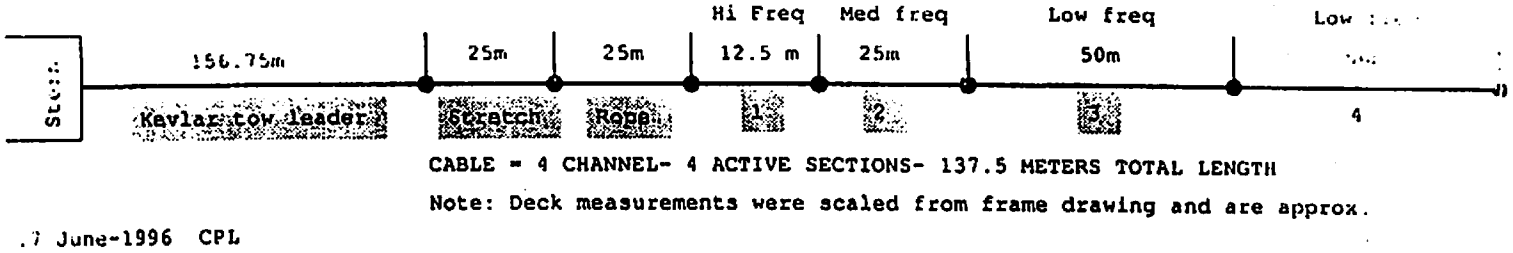

Figure 3.2 Sreamer configuration for SCS operations during MW96-05.

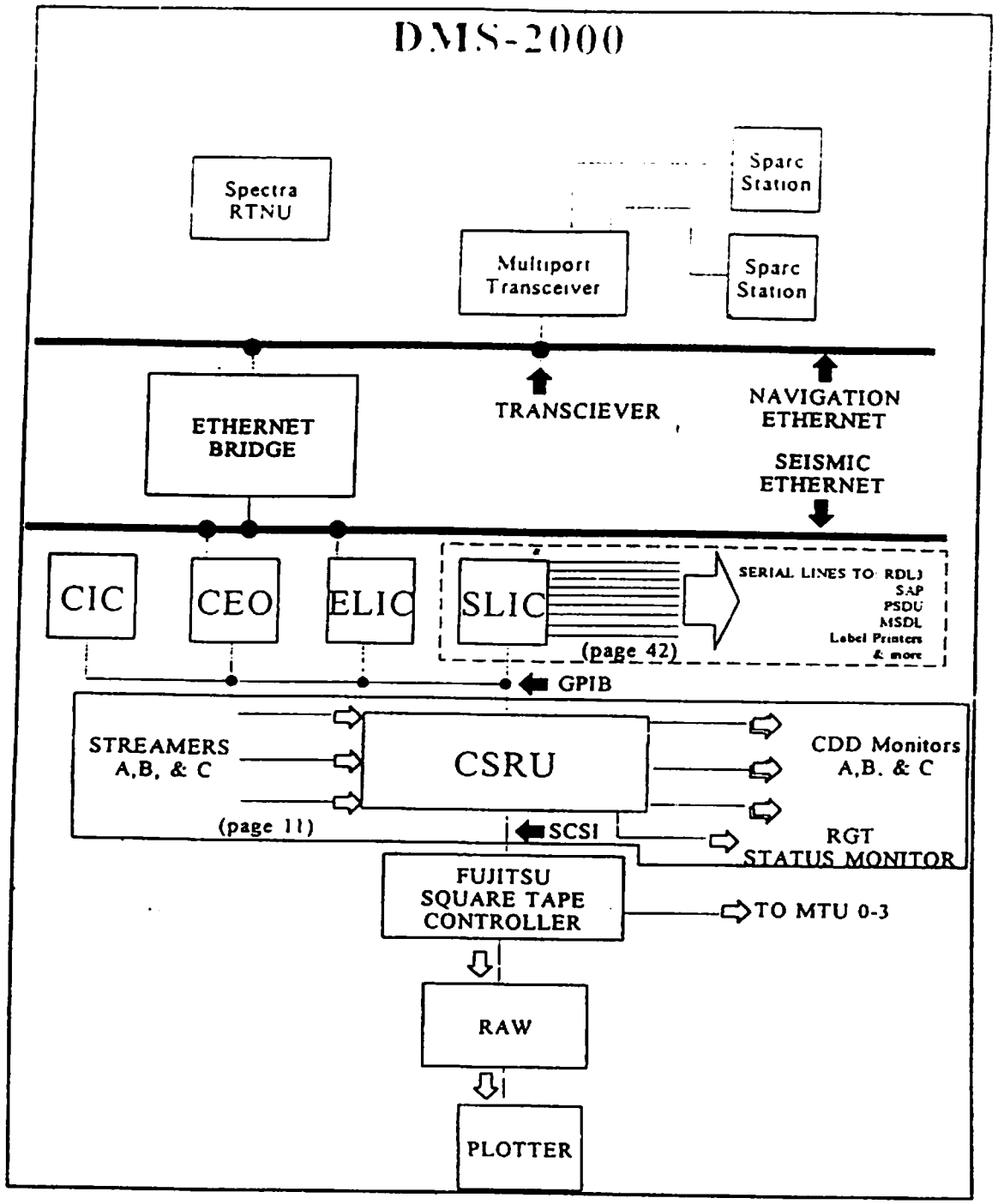

Figure 3.3. Schematic of DMS-2000 recording system. Although the *Ewing* is equipped with the newer DSS-240 system, overall similarities between the two systems allows the use of this diagram to explain the DSS-240.

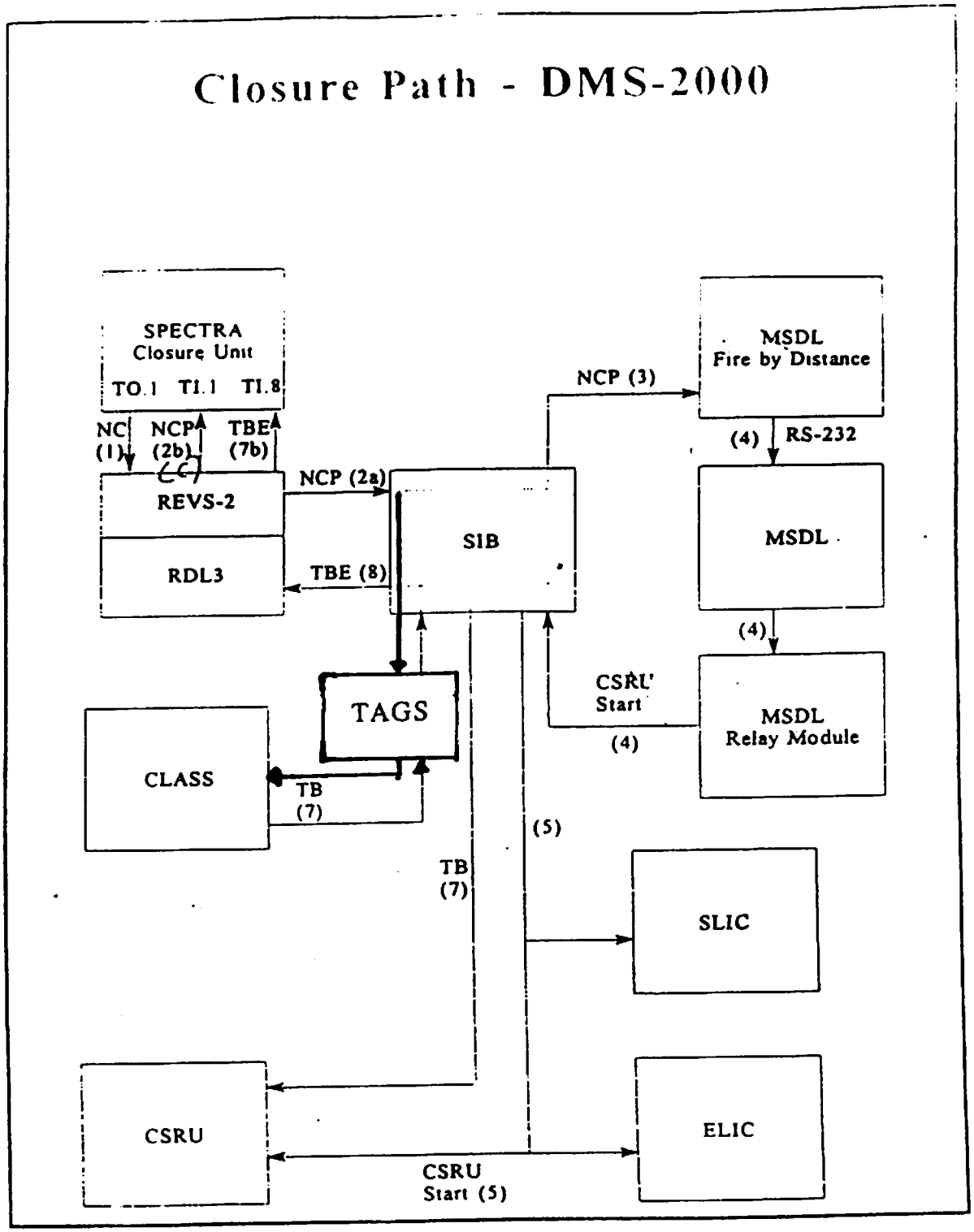

Figure 3.4. Shot cycle for DMS-2000 recording system. The DSS-240 system utilizes the TAGS subsystem in lieu of the MSDL, which was used in the older DMS-2000 system.

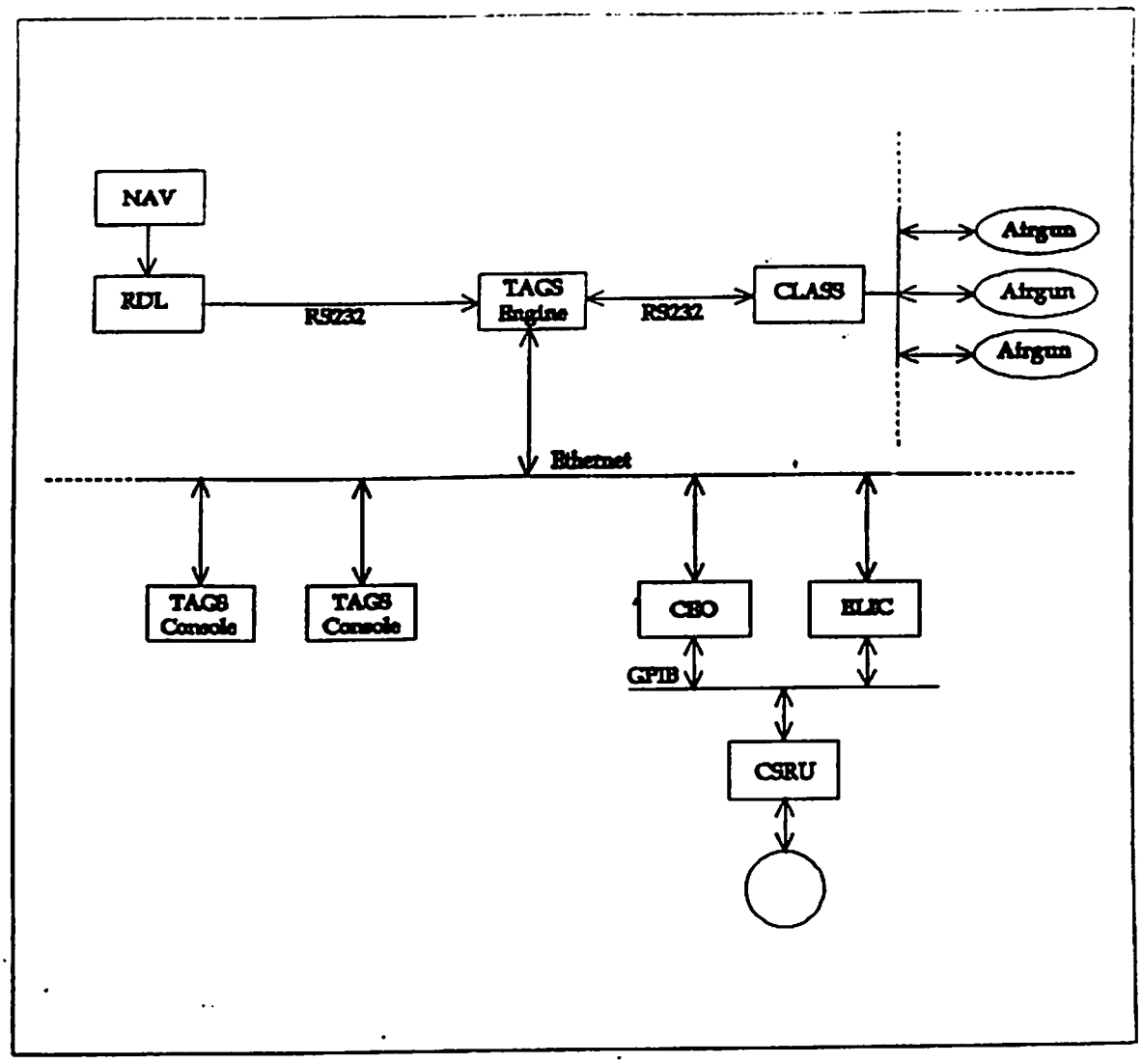

Figure 3.5. TAGS system integration and data flow for the DMS-2000. The DSS-240 has a similar data flow except that it does not receive the NC closure from navigation.

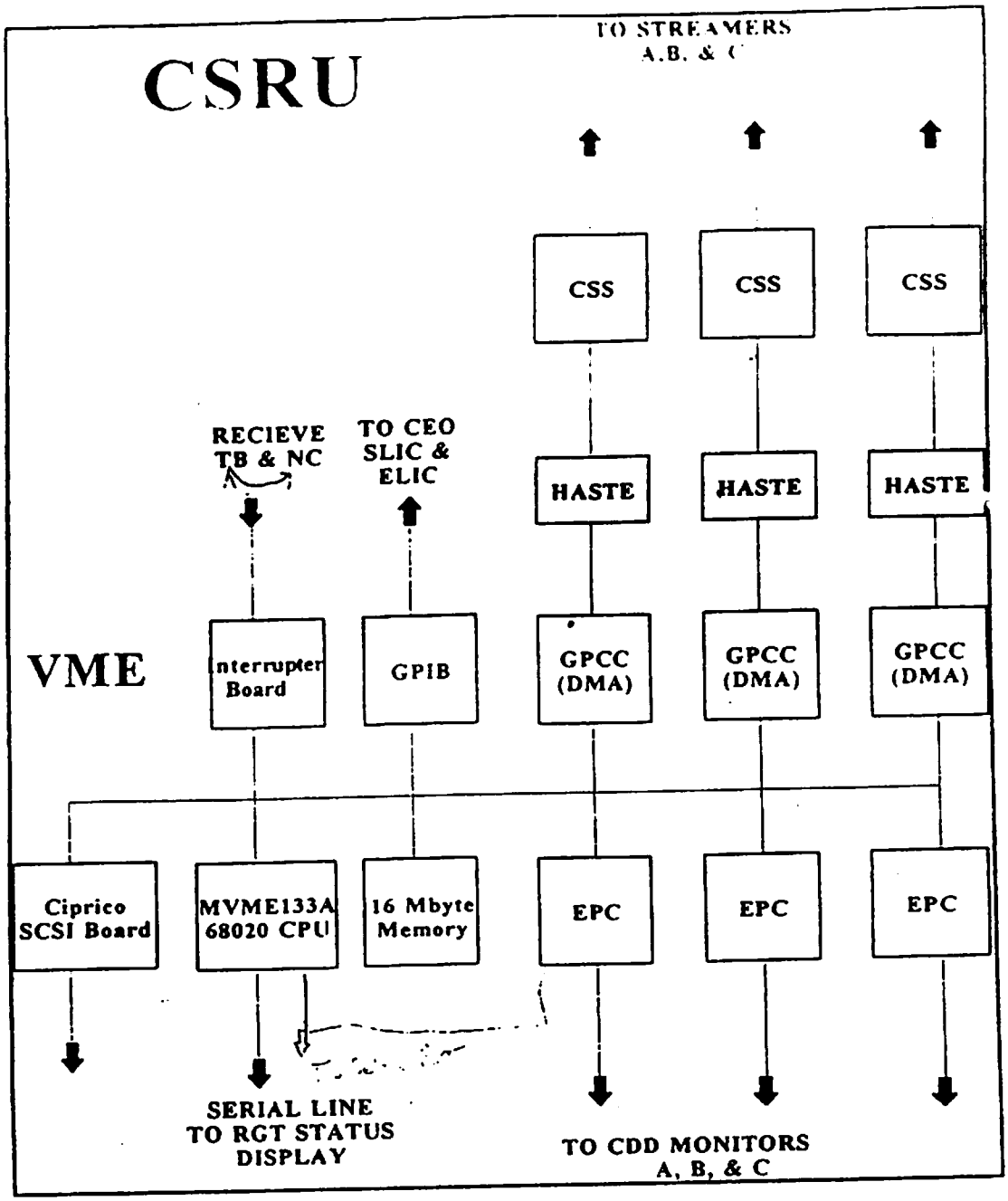

Figure 3.6 CSRU system for the older DMS-2000 system. DSS-240 has a comparable configuration.

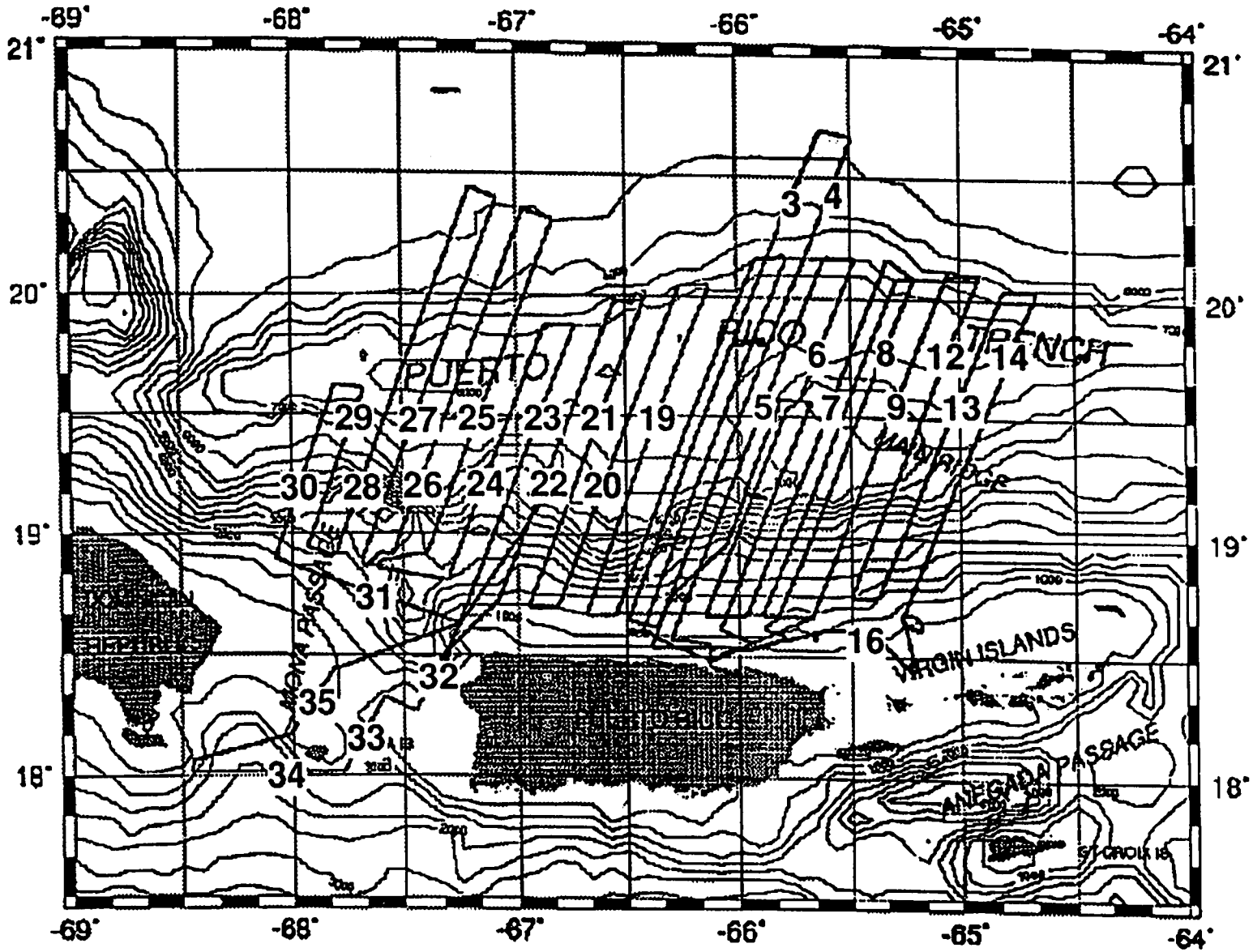

Figure 3.7 - SCS track lines for cruise EW96-05. MR1-only lines are unlabled

CHAPTER 4. AIRGUN CONFIGURATION

by John Charles III and Stefan Muszala

The air guns work by releasing pressurized air into the water creating a wave that travels through the water and bounce off interface changes in the sea floor. These waves bounce up and are received by the seismic streamer. Each gun contains a different amount of air that is released. This variation in size reduces the size of destructive interference or "bubble pulse" created by the air bubbles when the gun are fired. The gun works by filling a compartment with pressurized air then releasing the air suddenly by sending an electrical signal down a cord that is attached to the solenoid. The solenoid controls a small firing pin that releases the air (Figure 4.1).

During this survey we used a six gun array. One gun was mounted to a short boom attachment on the port and starboard booms and four guns where attached to the A-frame. The six guns used on this cruise where the 500, 305, 235, 145, 120, and 80 cubic inch air gun array. These numbers represent the cubic inches of air that the gun holds at 2000 psi. The entire array produces 1385 cubic inches of pressurized air at 2000 psi (Figure 4.2 & 4.3).

After the System Interface Board (SIB) receives the NAV Clock Prime (NCP) signal, the SIB conveys the signal to the Timing Analysis for Gun Synchronization (TAGS) engine (Figure 3.5). The purpose of TAGS is to control the firing of the airgun array as well as to log the quality control information for each shot, such as the depth of the airgun. This, for example, is supplied by a transducer mounted on each individual airgun. When TAGS receives the signal from NCP, TAGS provides Radio Data Link 3 (RDL3) with its setup and the source enable status. TAGS further gives source and array information to the Class Loop Automatic Source Synchronizer (CLASS) about when to fire the guns. Essentially, CLASS's responsibility is to fire the guns at precisely the correct time. When RDL3 receives the source enable code from TAGS, it 'decides' on whether the guns should be fired. If all of the conditions for shooting are met, then a signal is sent to the guns, and they are fired.

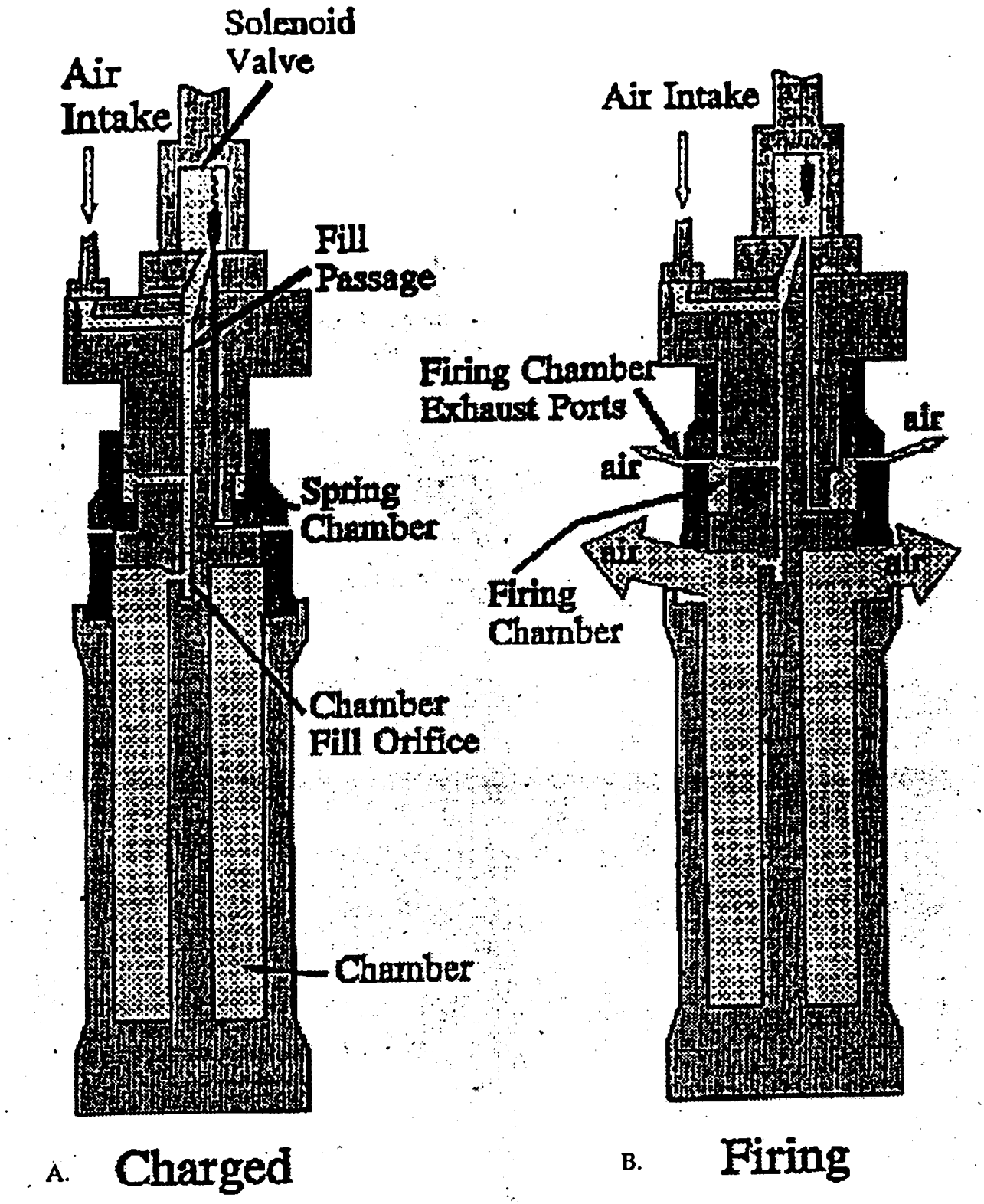

Figure 4.1 A. Is diagram of a charged air gun that is filled with air and at 2000 psi. B. Is a diagram of an air gun firing and releasing air into the water.

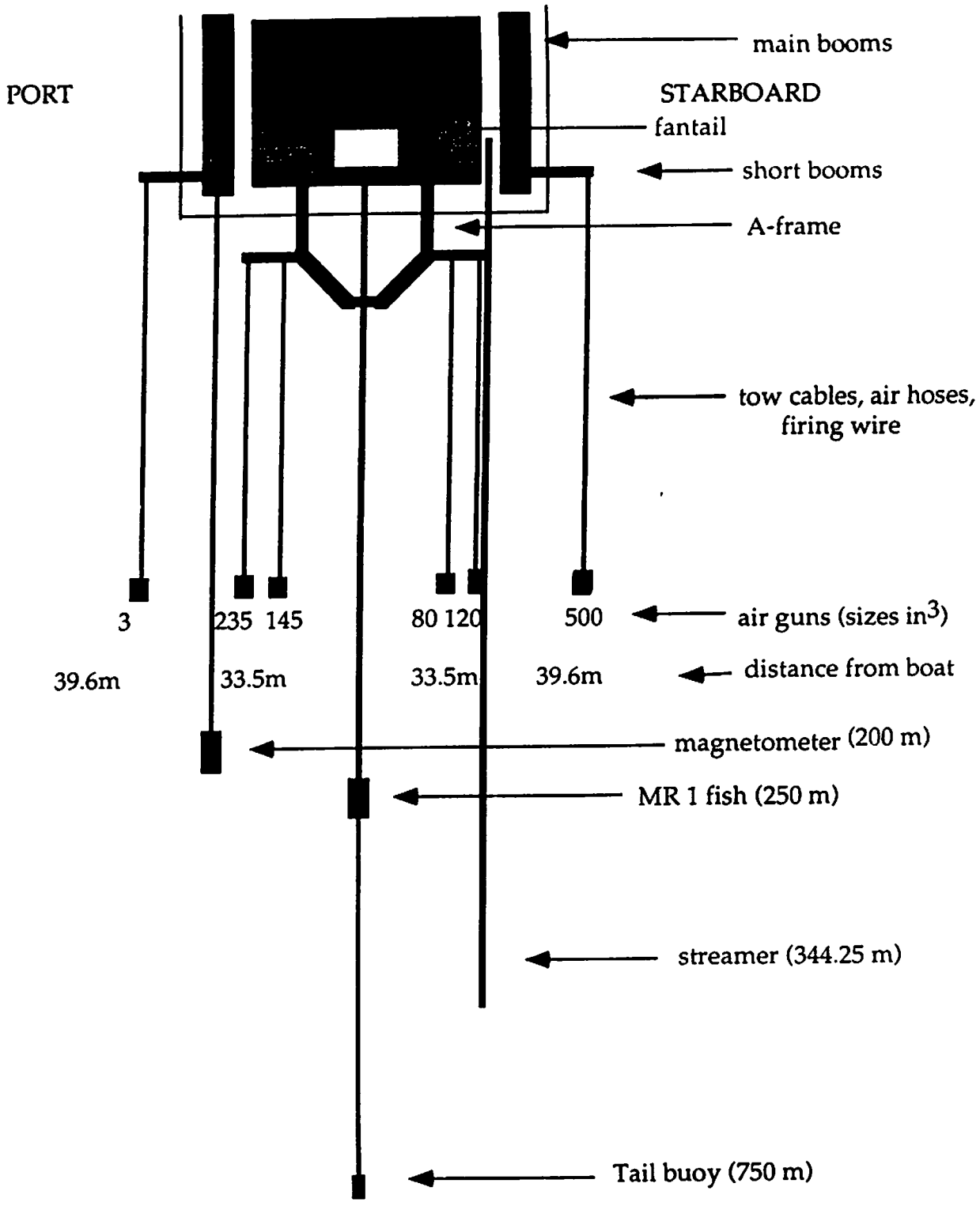

Figure 4. 2 The air gun array showing the six different air guns and where they are mounted. Diagram not drawn to scale.

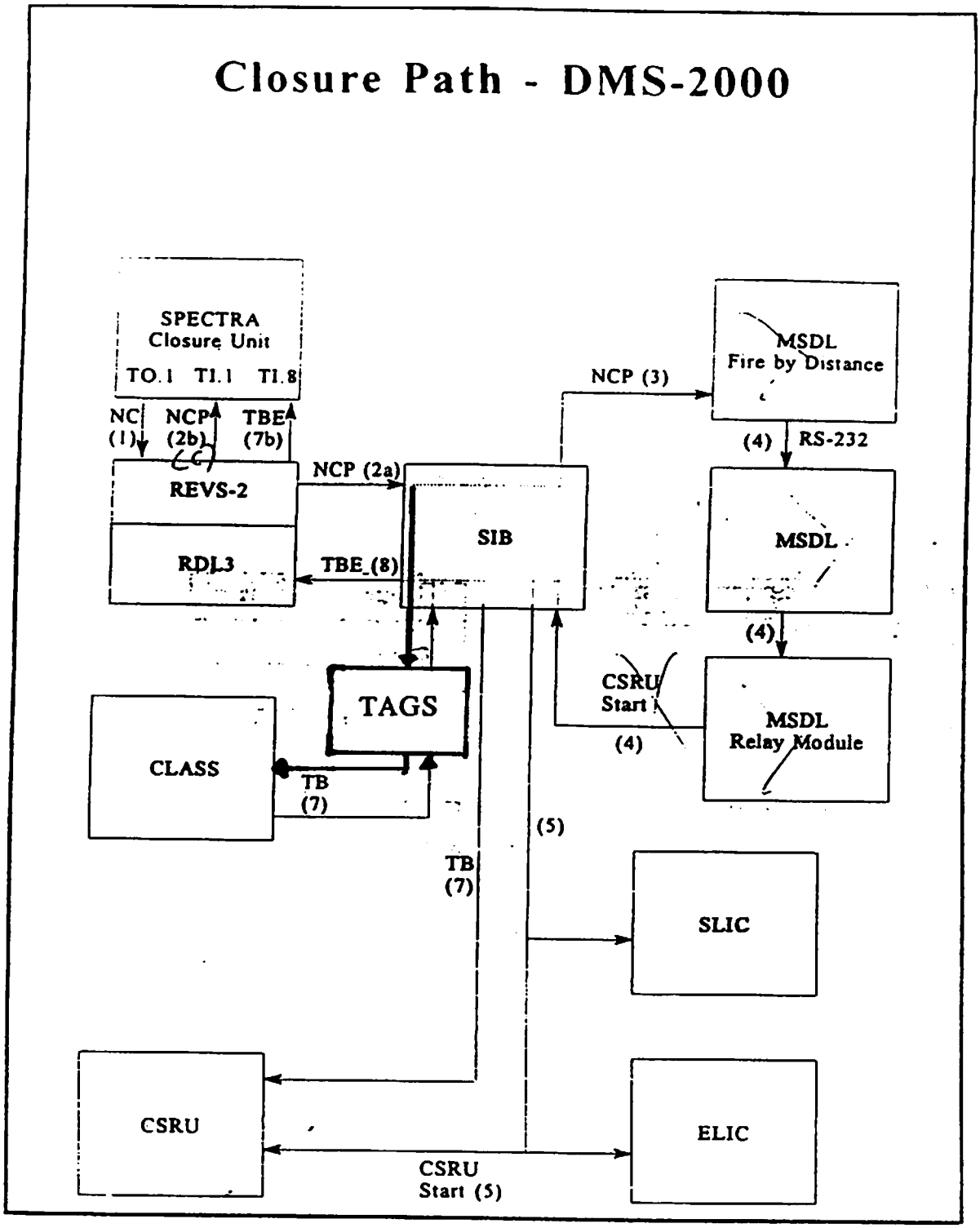

Figure 4.3 - Shematic of shot time recording system used for SCS operations during EW96-05

CHAPTER 5. ONBOARD PROCESSING AND PRELIMINARY INTERPRETATION OF SEISMIC DATA

by Jean Paul van Gestel

With the use of a Sun-workstation and the 3480 tape-driver, all four-channel seismic lines collected on EW96-05 could be read in and processed during the cruise. Up to four seconds of seismic data was plotted with maximum resolution using a Novajet II plotter available in the science lab. The inability of the memory of the Novajet II plotter to hold more than four seconds of seismic data prevented the plotting of the entire twelve second seismic records. Examples of these plots are included in the seismic data interpretation section of this report.

The processing on the ship was carried out in two steps on all lines collected: 1) quality control; and 2) reading in, stacking of data from the 3480 field tapes onto a backup 3480 tape, and plotting of all data. Subsequent to these basic steps applied to all lines, a complete processing sequence through the migration stage was carried out on line seven and all the special features which were printed out for the seismic interpretation chapter.

Step One: Quality control

To check the quality of each line collected, a stack of the line was plotted soon after it was collected. As the data quality remained high throughout the cruise, only a few quality control problems with 3480 data tapes were detected during this stage. These problems included:

Channel 4 noise problem. We noticed that on the beginning of Line 12 that the noise level was considerably higher than on previous lines. Line 12 was started after a 27 hour gap in the collection of seismic data because of problems with the MR1 system. The sudden increase in noise was traced to a local problem with channel 4 of the seismic system which decreased several hours into the collection of Line 4.

Low frequency noise problem. While the channel 4 noise problem abated, we noticed that there was a general increase of low frequency noise in the range of 4 Hz. The source of this noise was possibly related to the R/V EWING's propulsion system. Noise in this low frequency range can easily be filtered out during processing. This low frequency noise started in line 12 and continued during the cruise.

In order to establish the low frequency noise signal generated by the ship's engines and any other related ship-related noise (e.g., cyclical oil pumps, bilge pumps), we recorded ambient noise without guns on JD 184 from 15 hrs. 51 min. to 16 hrs. 01 min. as part of Line 25 (between shot points 29147 through 29216). I was unable to plot out the noise frequencies using Matlab but will attempt to do this again at UTIG.

These noise data could be compared to the frequency spectrum generated by the six gun airgun array (Fig. 5.1). The spectrum shown in figure 5.1 was made by John Diebold of LDEO on a previous cruise but the gun array shown matches that used during EW96-05. The signature is almost a perfect delta pulse with all frequencies between 5 and 125 Hz.

Step Two: Reading in data from 3480 field tapes, stacking them, writing them to a more compact format onto 3480 backup tapes and plotting them

During the EW96-05, all data were read in from the 3480 field tapes, stacked, and backed up on another 3480 tape. The more condensed, backup tapes will be hand carried to UTIG while the more expanded field tapes will be shipped from San Juan to Austin at the end of the cruise along with the plotter roles (seismic and 3.5 kHz data).

Due to the stacking, which decreases the number of channels from eight to one, the amount of data is decreased by the same number, which makes it possible to write all data from one line onto one 3480 backup tape. All the lines were plotted out onto 8 by 10 inch paper (A4 format) to insure that the data was recorded properly and to help locate key tectonic features that were printed out at a more detailed scale for seismic interpretation.

Step Three: Complete processing sequence carried out on selected lines

The SIOSEIS program, available as freeware from Scripp's Institution of Oceanography, was used for initial processing of seismic data collected during EW96-05. The program allowed each line to be processed through the seven steps discussed below and summarized on Figure 5.2. A time consuming disadvantage of the SIOSEIS program as available on this cruise was lack of a view program to preview processed data prior to plotting on the Novajet II plotter.

Processing of marine single-channel seismic data is much simpler than the processing of multichannel seismic data or land seismic data for the following reasons:

• Although the EW96-05 seismic system was collecting four channels of data with different offsets, the distance between these four channels on the 177 m long streamer is very limited compared to the depth to the seafloor which had an average depth of 5 km. The distance between channels 1 and 4 at the two ends of the streamer is 106.25 m making the distance in the arrival time between these two channels on the order of 2 ms which is equal to the sampling rate and is therefore insignificant. Because the data is being recorded along the streamer at virtually the same time, processing of these data does not require steps used in multichannel data processing such as sorting the data to common depth points, correcting arrivals at these points with normal moveout, and stacking them. The processing of the single channel data only requires the stacking of the four channels with no moveout corrections.

• The direct wave does not interfere with the recorded data because the direct wave arrives in the first half second and the reflected waves only arrive after one and a half second. For this reason, fk-filtering of the direct wave is not required as it is for MCS and land seismic data.

• The multiple is recorded after the last reflected wave and has been attenuated to the point that it can be easily removed by applying a mute. The multiple interferes with reflected waves during this survey only in waters shallower than 1500 m. As only a little more than 2% of our cruise was in such shallow water we didn't anything about it.

Processing steps used on the selected lines listed above include the following. Figure 5.2 shows a schematic view of this seismic processing sequence:

1. **Conversion of data from SEGD to SEG - Y format.** The data is read in from the 3480 tapes and saved onto the 3480 backup tape in SEG-Y format. The stacked data on the 3480 tapes is also saved in SEG-Y format.

2. **Stack.** We assumed that the distance between the channels was negligible to the depth of the target zone, so we simple added the four channels to stack the data. Figure 5.3 shows a brute stack of a piece of seismic line number seven right above the trench. This piece was chosen because it imaged both sediment layers and rough Atlantic oceanic crust, where many diffractions formed.

3. **Filter.** We applied a low cut filter of 26 Hz and a high cut filter of 130 Hz on the data. This removes all the mainly low frequency noise such as that produced by the ship.

4. Mute. The direct wave can be removed by application of a mute on the first half second of the data. To insure the removal of all direct waves, a mute of one and a half seconds was applied that changes data values beneath the mute value to zero. In water depths less than 1500 m mutes were adjusted in order that no data was clipped, but these changes in mutes were only necessary for the shallow water parts of Lines 4, 5, 16, 27 and 31 till 34, which as mentioned above is only a very small part of the recorded data.

5. Deconvolution. This step reduces periodic events such as bubble pulses, ringing or even multiples. Deconvolution changes the source pulse into an ideal delta pulse through the use of correlation.

6. Automatic Gain Control (AGC). AGC is a type of amplitude normalization that results more uniform amplitudes that result in more continuous sub-seafloor reflectors. Figure 5.4 shows the effects of applying processing steps 3 through 6 applied to seismic line 7. The net effect of these steps is an improvement in the resolution of reflectors and the reduction of the noise level.

7. FK-Migration. Diffraction hyperbola are common in the raw data particularly where strong reflectors are located to the side of the streamer or along steep seafloor scarps. FK migration attempts to move seismic energy in the seismic record back along the hyperbola to collapse the hyperbola. Because migration requires a lot of CPU time, the line needs to be cut into small windows for migration of smaller data segments. Two mutes are applied before migration: one removes all noise prior to the recording of data while the other removes all noise following the recording of data. The result is a collapse of hyperbola and an improvement in the resolution of data quality. This can be seen in Figure 5.5.

EW96-05 seismic Data Table

In Table 1, all relevant data for future processing is listed. The location and time of the start-point is where the line started recording. The finished turn-point is location and time where the ship turned through the way point and was on the line. The end-point is the location and time where the line stopped recording. When there is no finished turn or change course-point given on Table 1, it means that the there was no turn at all in the line.

Some lines do not start or end at the beginning or end of a straight line segment. This is because that problems with the start up and ending of lines on the seismic control system led to data gaps at the beginnings or end of important areas. For this reason, only the latitude and longitude of the straight line segment was noted and the line continued through the turn.

The numbers of the 3480 tapes, which are also called "reels", for each line are given with starting shot point, end shot point and number of shot points on the reel. The number of shot points on the reel is useful to check to see if the reel is completely filled with data (about 856 shot points) or if there has been a line change. The lines might be divided in sublines (e.g., Line 35, 35a, 35b), after a change of the recording time, which is also listed on Table 1. During a change of lines some data is lost (data gaps related to this average 8 minutes), because data is not being recorded during the line changes. Times of these data gaps is also listed in Table 1. Sometimes a shot point is missing because of a bad reel or a change of lines. These missing shot points are given below. In some cases, a 3480 tape was ejected after only one or two shot points were rejected. In these cases, the label for this tape was attached to a piece of cardboard and the tape was not kept. These reels are indicated as to have no shot point recorded on them.

used abbreviations:

JD	Julian Day
SP	Shot Point
WP	Way Point
CC	Course Change

Interpretation of the seismic profiles over the Puerto Rico Trench from EW96-05

During the survey the trench was crossed 20 times. For the interpretation of the trench six lines were used, starting from the west these lines are 28, 25, 21, 3, 7 and 14. The spacing between these lines is comparable and these lines cover the whole survey, including the most western line (28) and the most eastern line (14). These lines are shown in figure 5.6 A and B.

The trench can roughly be divided in two parts, the western and the eastern part. The border is lain at about 66° W. It is probably not a coincidence that this is the place where the extended Main Ridge would cross the trench, as will be explained below. The main difference between the west and the east side of the trench is the amount of sediment present. In the west the sediments can be seen to have a depth of about one and a half seconds but can go up to two seconds. This would mean a depth of 1150 meter going up to 1500 meter, when taken a velocity of 2000 m/s. On the east side of the trench the sediment layer has a depth of only half a second, which means a depth of just 400 m, taken the same velocity.

The major sediment source is most likely terrigenous material from the islands which is transported as turbidity currents via the Mona Canyon and smaller canyons cut into the submerged carbonate platform directly north of Puerto Rico and the Virgin Island. The Main Ridge which appears to continue across the trench and extend to the Fourth of July Ridge on the outer rise forms a barrier preventing sedimentation in the eastern part of the trench.

The northern side of the trench seems to be covered by a small layer of sediment, turbidites. This layer has a depth of about 0.2 seconds which is about 200 m thickness. Judging by the relatively small amount of deformation of the turbidites, the tectonic processes that created the trench have been quiescent during the deposition of the turbidites. More north this layer even becomes thicker, with up to half a second of sediment.

The northern side of the trench looks less steep than the southern side. The oceanic crust can be followed all the way down underneath the sediments, including the turbidite cover. This can especially be clearly seen in line 25 (Fig. 5.6 B). Although not shown in these profiles, which only cover the part of the trench were the oceanic crust subducts, block faulting has been an important part of the tectonic development of the northern slope of the trench. In the area surveyed, only the western part of the wall is without numerous steep scarps or other indication of normal faulting. Many of the down-faulted blocks, at levels ranging from near the top to near the bottom of the trench wall are covered by the turbidites. If there had been an appreciable amount of sediment deposited on the trench wall since the deformation, one would expect that a different pattern would have been produced as a result of material slumping off the steep slopes and collecting on the steps and in the perched valleys. The observed pattern indicates either an exceedingly slow rate of sedimentation or a recent date for the deformation. Similar observations in other trenches and the additional fact that many have no turbidites at all, strongly indicate a recent date of formation.

Now we take a better look at the sediments in the trench. We will focus on the western part of the trench because the described features are best displayed in these profiles. A first observation is that the sediments show top-lap on both sides of the trench (Fig. 5.6 B). You can also see normal faults coming from the bottom of the basin going up to the seafloor dipping south. Maybe these faults can be interpret as strike slip faults, cause there is not a clear reflecting sediment layer which can be seen on both sides of the faults.

The south side of the slope is much steeper, and there is no clear interface between the sediment layers in the trench and the oceanic crust. Although it looks like the change from clearly visible sediments at 1.5-2 seconds depth to oceanic crust without any reflectors should be almost vertical. South of this feature there is still a little layer of sediments. In these

sediments are a lot of little normal faults dipping northwards, so into the trench, and in the most western layers there is even some folding in these layers.

In conclusion, the little folds in the sediments on the south-slope of the trench are the only real evidence of compression. The top-lap in the sediments and the normal faults which occur on the south side of the slope indicate subsidence in the trench. This together with the block faulting in the north side of the trench which is not covered by recent sediment could be explained by the theory of subducting northern slope underneath the Caribbean plate.

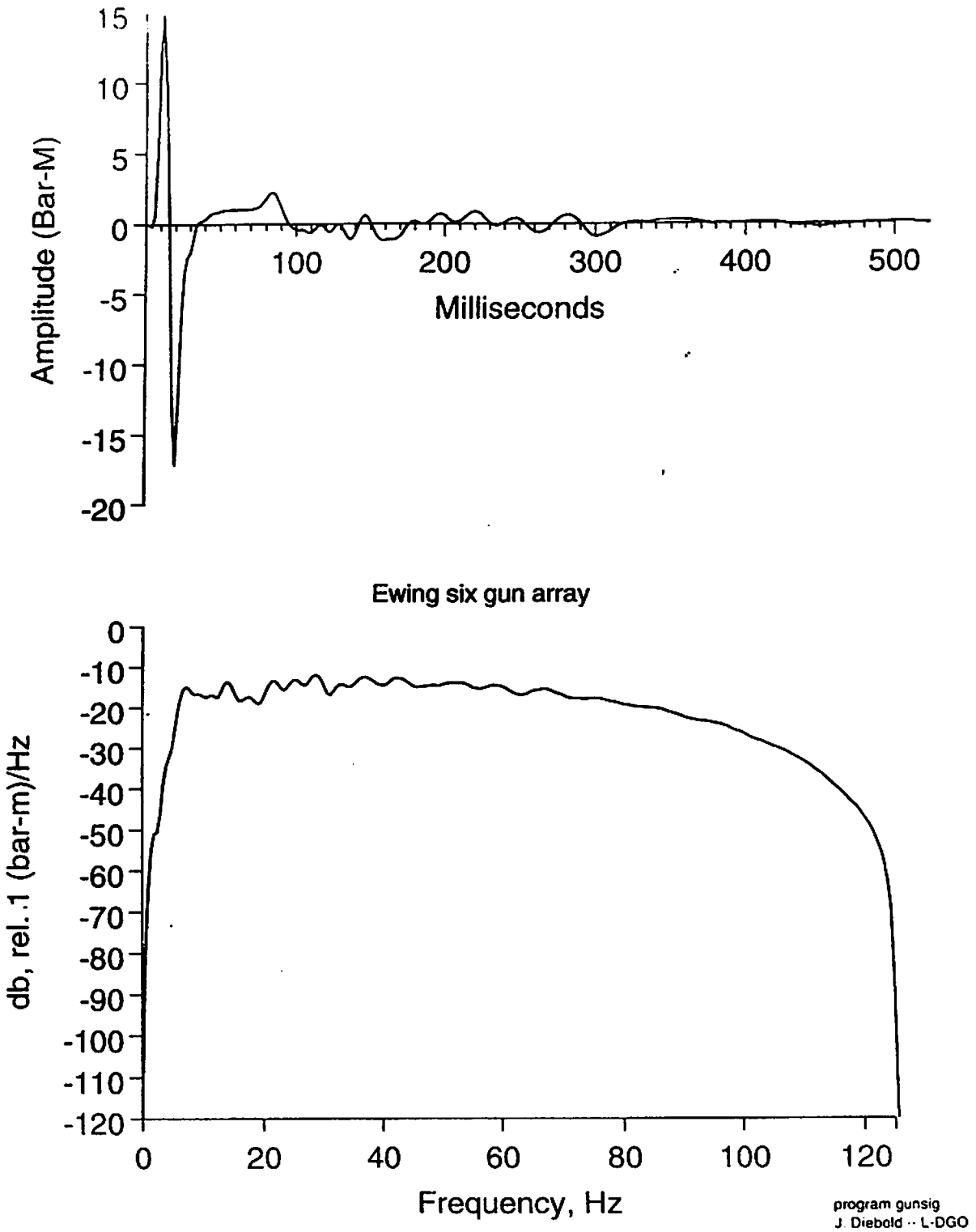

Figure 5.1 : Time picture and frequency spectrum of the airgun array.

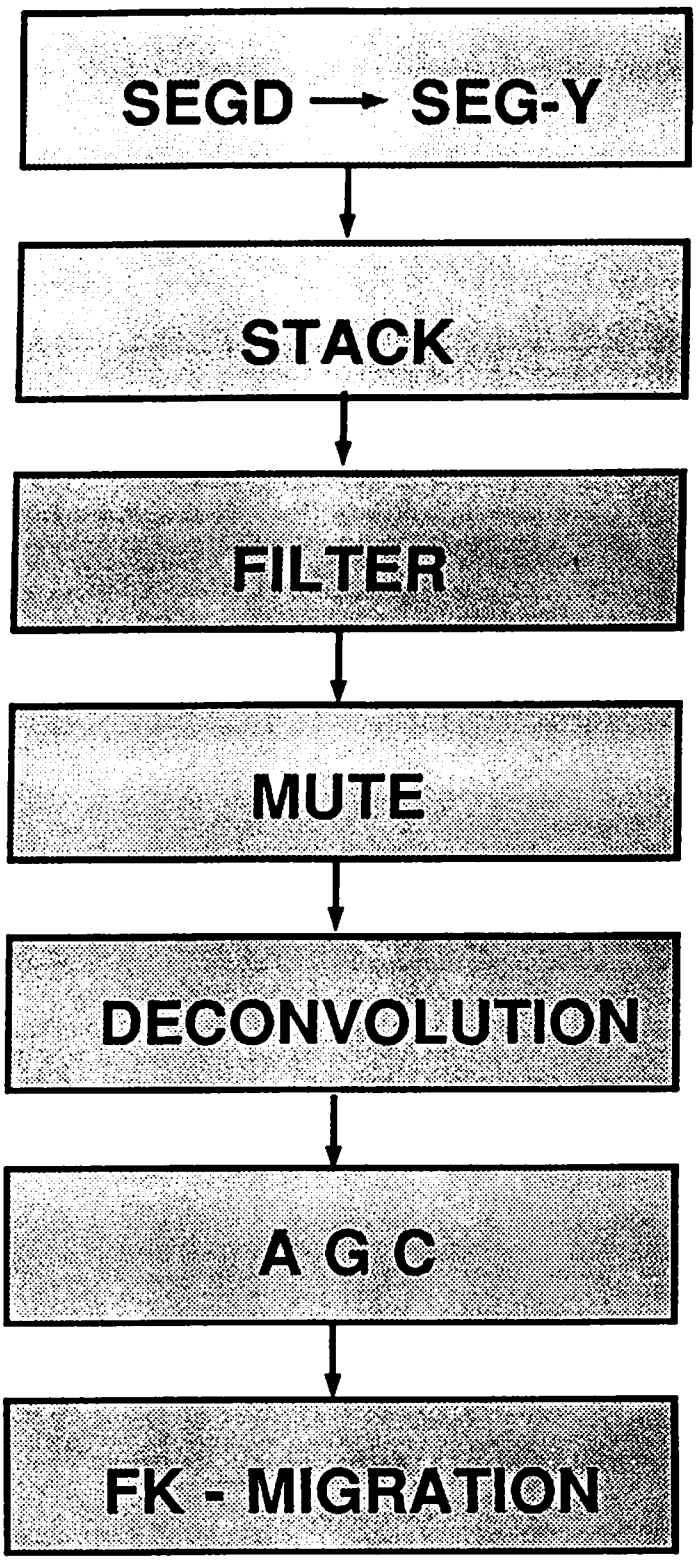

Figure 5.2 : Schematic picture of the processing sequence.

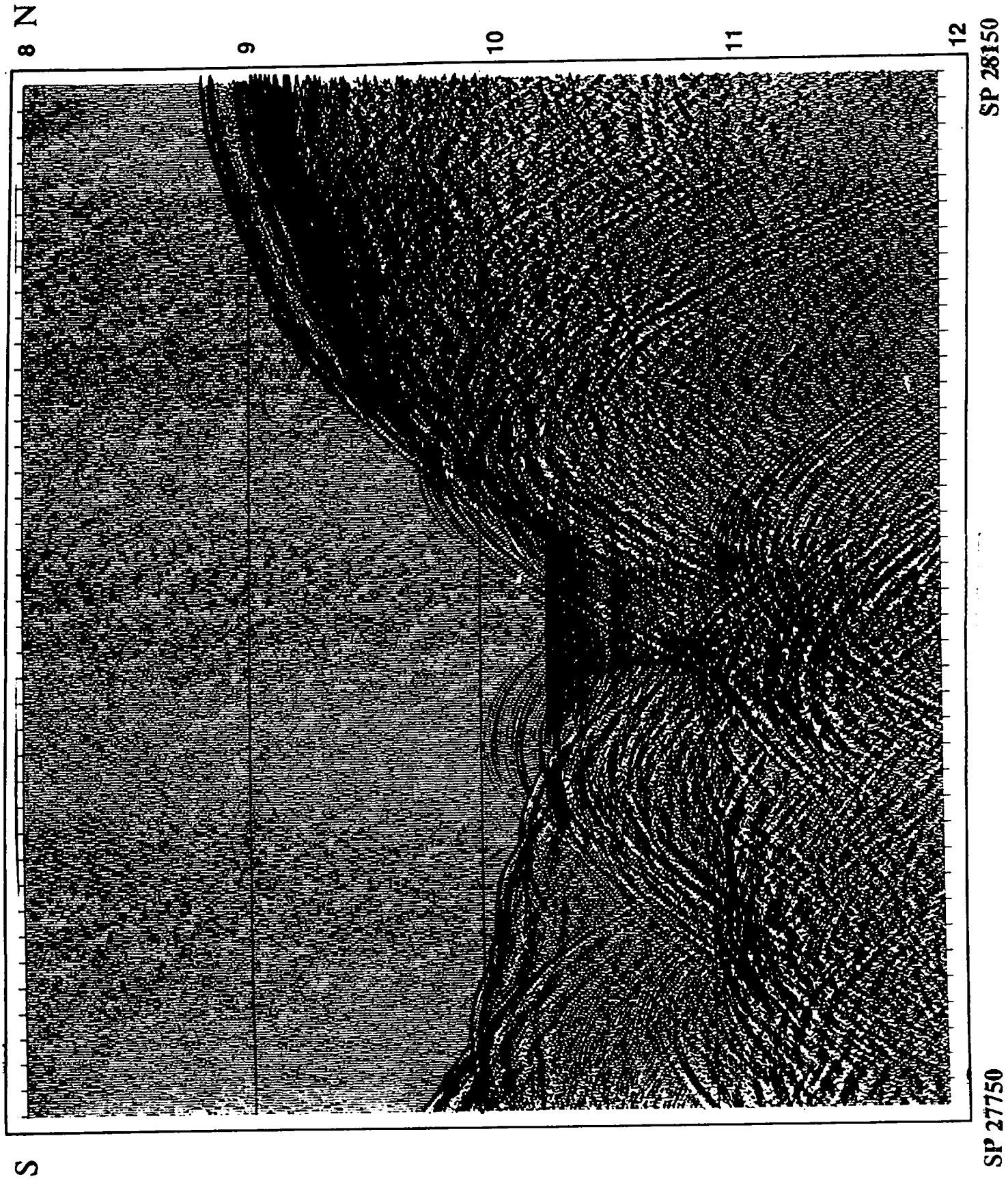

Figure 5.3: Brute stack of line 7.

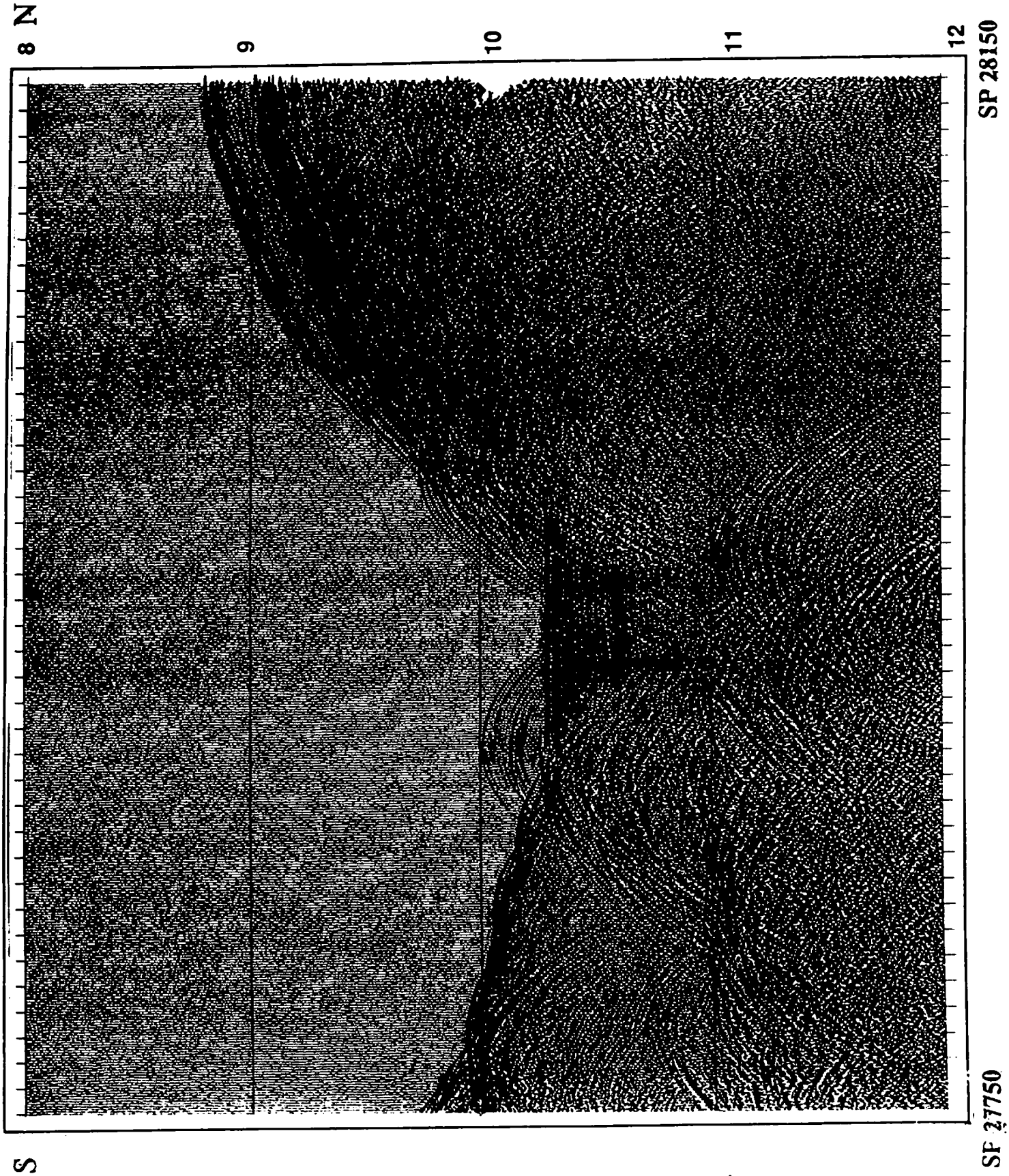

Figure 5.4: Line 7 after applying filter, mute, and deconvolution.

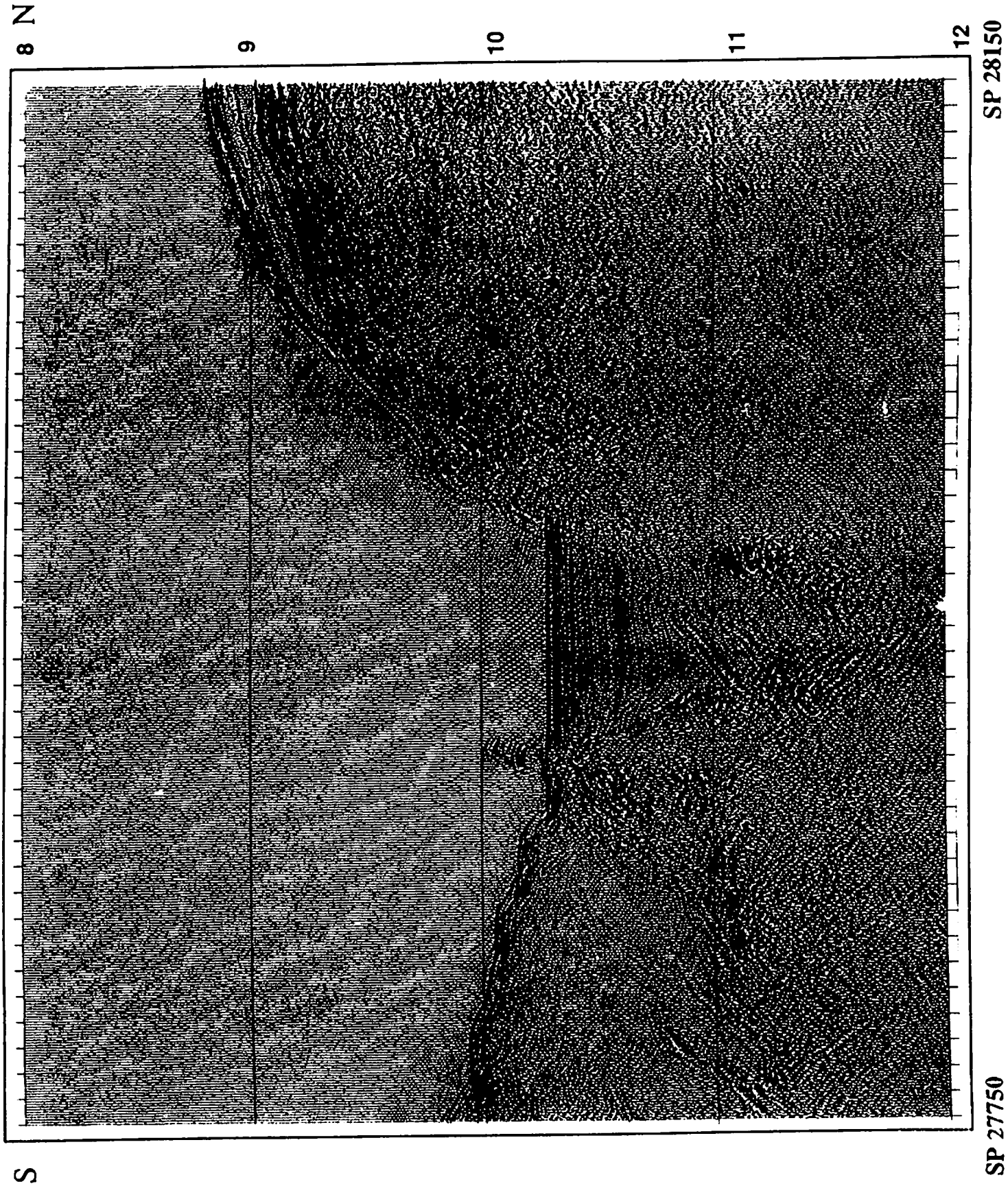

Figure 5.5: Line 7 after applying migration.

CHAPTER 9. MR1 SYSTEM

by Frances Delano and Nancy Grindlay

Introduction

During this survey we used a sonar mapping system, known as the MR1, developed by the Hawaii Mapping Research Group (HMRG) at the University of Hawaii. The name Hawaii MR1 derives from (HIG Acoustic Wide Angle Imaging Instrument, Mapping Researcher 1). The Hawaii MR1 replaces the SeaMARC II system which was lost at sea in early 1991. The MR1 represents a mapping system with an increased dynamic range from its predecessor and provides digital instead of analog data. The HMRG provided staff for service support and data processing during the cruise.

Hardware

The MR1 is a wide-swath, shallow-towed, side-scanning instrument which acquires digital data for the calculation of sea floor backscatter properties and bathymetry. It has been designed for all water depths, however, the MR1 is better suited for depths greater than 500 meters. The depth in which the "fish" is towed ranges from near-surface to 500 meters safely; the normal depth range is of 50 to 150 meters. During the cruise we maintained an average towing depth of 100 meters. Normal swath coverage of the sonar is approximately 20 km; bathymetric swaths extend to the first multiple return (3.4 times towing altitude) (Fig. 9.1, A) . Operational speeds can range from 8 to 10 kts, our average speed has been of 6 kts due to seismic recording specifications. However, higher speeds may be possible with some data degradation. The compatibility of this system with seismic reflection and multi-narrow beam echosounders allows simultaneous recording of many different types of data.

The system has two forms of data: backscatter and bathymetry, which is a result of the calculated difference in phase shift between the rows on each side and converting it to from an acoustic angle to angle/angle datum. Transducer arrays are divided into two rows, A and B, which receive and quantify the phase shift between rows. Backscatter energy provides images of acoustic targets on the sea floor. The sonar system is divided in port and starboard sides, each of which operates in a different frequency so neither can hear the other signal. The port transmits and receives signals of 11 kHz and the starboard of 12 kHz (Fig, 9.1 B). The transmitter emits sound waves downward into the water column, and the receiver detects the reflected acoustic energy. The return signal depends on the angle of incidence and in the interaction between sound wave front and seafloor surface. This angle is directly affected by bottom slope and the position of the "fish". Steep scarps on the sea-floor will show up as shadow features. Hard rocks of high backscatter result in dark colors, whereas smoother sediments (pelagic) appear as lighter colors on the sidescan image.

Pulse length ranges from 1 to 10 msec, which allows extended range in regions of weak backscatter and higher resolution in areas of strong returns. The ping or pulse rate is of 14 sec until 5000 meters, at greater water depths we used 16 seconds. The digital recordings are immediately after transmit until 0.5 seconds prior to the next transmit. The received signals, which are displayed into two separate information windows, show the raw bathymetric and backscattering data. Later processing will result in the final image.

There are an array of safety devices surrounding the MR1 (Fig 9.1 A). The tail buoy serves as a stabilizer and as a radio beam with strobe lights for localization in case it is lost. Within the fish there are two safety systems; first, a depth transponder that responds to shallow water activating the 500 m safety pressure release and second, a radio beam. The depth transponder will release the MR1 from the ship if reaches the 500 m depth limit. On the other hand, with the supervision of the HMRG, we had reach depths shallower than the 500 m without any problems. The radio beam will send signals to be received by the HMRG staff.

Inside the MR1 has syntactic glass foam that would not shrink provides for positive buoyancy. An extra stabilizer is localized between the umbilical cord and the safety pressure release.

The MR1 coverage during the extent of this cruise is summarized in Tables 9.1 and 9.2

Problems with the MR1 System During Cruise EW96-05

The MR1 system was fully deployed by 1900 GMT on June 15, 1996 and data initially looked good. Starboard bathymetry was rough on the outer portions of the swath, but we had been forewarned about this problem. When the R/V EWING passed over the shelf and into water depths >5000m about six hours into the first deployment a severe problem with both starboard sidescan and bathymetry became apparent. The majority of the starboard side-scan swath became uniformly gray, showing little to no evidence that data was actually being collected in this region. Data collection stopped at 1345 GMT on June 16 and the tow fish recovered.

One of the starboard transducer arrays had failed, but there was no obvious reason why this had occurred. One possibility discussed was wet connectors in fish(?). Multiple tests were run on various components within the fish. The MR1 tow fish was re-deployed by 0445 GMT on June 17. Once again sidescan data initially looked good in shallow water but soon after deployment began to get telemetry errors indicating lack of communication between ship and fish, as well as overall background noise interference. The first telemetry error occurred at 1008 GMT and within the next few hours the rate of telemetry errors increased. Complete loss of data occurred at 1330 GMT. The MR1 fish recovery began at approximately 1500 GMT on June 17.

While recovering the tow fish it was discovered that the coaxial cable to the fish had been damaged and would need to be re-terminated (6-7 hr job). Upon opening the fish onboard it became apparent that several pieces of hardware had been damaged (including an array of transducers on starboard side) and would need to be replaced and tested. The possibility of flying in an engineer from Hawaii to meet ship in San Juan was discussed. Several calls were made by the HMRG to the engineer in Hawaii to discuss possible cause of problems and means to isolate and trouble-shoot them. The decision was made to replace parts, re-terminate cable, run tests, redeploy and see results before flying in the engineer.

After over 16 hours of analysis the HMRG decided that the starboard sidescan and bathymetry had a series of problems. The starboard transducer array had blown again for unknown reasons. This meant that there was not enough signal to generate bathymetry data at any depth, and sidescan at depths greater than 4500-5000m. At this point the decision was made to have the Hawaii engineer fly to San Juan and get a launch out to the R/V EWING as soon as possible. The MR1 fish was fully redeployed and collecting data at 0555 on June 20.

Continued to get complete sidescan coverage in water depths <4500m, only port side in water depths >4500m. Bathymetry appeared to be okay on port side at all depths, but bogus on starboard at all water depths. The MR1 fish was recovered at 0615 GMT on June 22. Hawaii engineer, Mark Rognstadt, was picked up at ~0730 local time at sea buoy outside the San Juan harbor on June 22. By 1600 GMT the MR1 group had isolated two problems, both apparently fixable. The first, and the cause for the starboard transmitter to be damaged on both previous deployments, was a shorted tuning inductor. This was repaired and the starboard receiver hardware checked out to make sure it was operating properly. The second problem was time varying gain. The instrument's ability to correctly implement the varying in the gain on the outer part of the swath seem to be impaired. The problem was also linked to the tuning inductor and disappeared once the inductor was fixed. The HMRG worked for the remainder of day and the fish was redeployed and collecting data at 0830 GMT June 23.

The MR1 data looked pretty good, certainly much better than before. Full sidescan coverage on both starboard and port was being collected, and bathymetry seemed realistic, but noisier than what was desirable. Two lines were run at 9 kts without the guns, basically filling in between lines where a data gap existed. On the turn between profiles put the fish on receive-only to diagnose noise interference. Also throttled the engines back to zero, i.e. reducing the screw turns to zero, to assess engine noise in the MR1 signal.

The system was picking up a strong component of 60 cycle noise. This was attributed to the diesel electric motors. The R/V EWING is diesel electric engine which produces AC power. It has a single fixed prop. To speed up/slow down the amount of AC wave that is sampled is changed. The noise is generated when the engine converts change AC power to DC power(?) In an attempt to lessen engine noise interference, the fish was towed at deeper depths, 200m rather than 100m, so the fish was further away from the ship. No obvious improvement was seem in the signal at the deeper water depths. It was proposed that the tow fish be recovered in an attempt made to shield the electronics on the starboard side which might reduce the noise problem. Also the unshielded cable of starboard side would be replaced with a shielded cable . Apparently this shielded cable was removed after the last cruise (due to a short and heat damage to the connector(?)). Mark had brought a used shielded cable with him and would also replace the deck connector.

On June 26 at 0654 GMT, the MR1 was recovered to shield electronics and check grounds. Mark was dropped off outside San Juan Harbor around 1900 GMT. The R/V EWING was underway by 1930 GMT and the MR1 tow fish was fully deployed by 2215 GMT. For the first time during the cruise, the data, both bathymetric and side scan, were of high quality. However, there still was a minor component of low frequency noise in the signal. A dramatic difference in the amount and type of noise in the MR1 data was observed with varying Rpms. A careful watch was maintained on the data and the bridge was asked to call down any Rpm changes. Rpms were varied between 88 and 93 Rpm to maintain a 6 kt speed-made-good.

On July 2 the MR1 starboard array failed at 1742 GMT. Real-time diagnostics indicated that one row of transducers on the starboard array was not operating, resulting in the loss of bathymetry and degradation of sidescan data. The system was recovered for repairs at 1845 GMT. The tow fish was on deck by 1910 GMT and the starboard electronics were removed for testing in the electronics laboratory.

The immediate cause of the starboard array failure was determined to result from short circuits in the row B power amplifier and row B parallel tuning inductor. Testing of row A showed that it was operating properly. The power amplifier and tuning inductor were repaired, and the new components passed subsequent tests on the bench.

A set of additional tests were then conducted to investigate the high levels of noise that had been present in the starboard data during the previous tow. During the course of this investigation and testing the parts associated with tuning inductors were replaces, as was the entire preamplifier circuit board. These changes did not reduce the high noise level. Next the digitizer board was tested, and a short between the preamplifier board ground and the digitizer board ground was detected. The short was traced to the input lead of the input transformer on the digitizer board, which was shorted to the board's analog ground. This condition did not exist during any of the system's previous bench tests. The digitizer board was replaced, and the starboard noise level was observed to be greatly educed when tested on the bench. The starboard electronics were then replaced in the tow fish, and tests involving the entire system on deck showed that the noise level remained low, and the repair was judged to be complete.

Following redeployment at 0306 GMT on July 3, the in-water noise level of the starboard side was found to be approximately equal to the port side. This was almost an order of magnitude improvement relative to the previous tow's starboard noise level. We infer that the shorted input transformer on the digitizer board was the probable cause of the starboard noise that had been present throughout the survey to this point -- with the short, the starboard side was extremely sensitive to noise generated by the ship's electrical system. The intermittent nature of the failure was pernicious because it had not failed on the bench during previous tests. Once the failure occurred on the bench it was relatively simple to diagnose and replace.

TABLE 9.1 Summary of MR1 coverage				
LINE	LATITUDE	LONGITUDE	GMT start	GMT end
prline1	18° 32.2	66° 1.0	167/ 19:32	168/ 9:30
prline1a	19° 33.1	65° 49.0	168/ 9:30	168/ 13:45
prline3a	18° 59.4	66° 14.0	169/ 5:00	169/ 13:30
prline4	18° 32.2	66° 9.4	171/ 5:55	171/ 8:00
prline5	18° 34.1	66° 17.0	171/ 8:00	171/ 13:27
prline5a	19° 4.3	66° 5.1	171/ 13:30	172/ 1:43
prline6	20° 10.0	65° 32.4	172/ 1:43	172/ 14:40
prline6a	19° 4.4	65° 59.0	172/ 14:40	172/ 19:04
prline7	18° 40.0	66° 8.0	172/ 19:04	173/ 00.0
prline7a	18° 60.0	65° 50.0	173/ 00.0	173/ 12:45
prline8	20° 5.0	65° 19.0	173/ 12:45	174/ 00.0
prline8a	19° 5.1	65° 39.0	174/ 00.0	174/ 6:00
prline10	20° 7.0	65° 00.5	175/ 8:05	175/ 9:19
prline11	18° 40.2	65° 40.0	175/ 9:19	176/ 9:30
prline12	20° 4.46	64° 56.0	176/ 9:30	176/ 23:40
prline13	18° 45.2	65° 30.0	176/ 23:40	177/ 4:30
prline13a	19° 5.0	65° 14.0	177/ 4:30	177/ 14:41
prline14	20° 2.0	64° 49.0	177/ 14:41	178/ 00:42
prline14a	19° 14.3	65° 9.0	178/ 00:42	178/ 00:45
prline14b	19° 14.0	65° 1.0	178/ 00:45	178/ 6:54
prline17	18° 40.0	66° 20.0	178/ 23:00	179/ 10:12
prline18	20° 9.2	65° 47.2	179/ 10:12	179/ 22:30
prline19	18° 40.0	66° 36.3	179/ 22:30	180/ 1:40
prline19a	18° 54.1	66° 36.0	180/ 1:40	180/ 14:11
prline20	20° 3.2	66° 8.0	180/ 14:11	180/ 15:21
prline20a	20° 3.0	66° 15.0	180/ 15:21	181/ 3:15
prline20b	18° 57.0	66° 43.0	181/ 3:15	181/ 6:09
prline21	18° 42.0	66° 51.0	181/ 6:09	181/ 10:45
prline21a	19° 3.0	66° 48.4	181/ 10:45	181/ 20:56
prline22	19° 59.0	66° 26.0	181/ 20:56	182/ 8:03
prline22b	19° 3.0	66° 57.0	182/ 8:03	182/ 16:00
prline23a	18° 29.0	67° 19.0	182/ 16:00	182/ 23:46
prline23b	19° 13.0	67° 1.1	182/ 23:46	183/ 7:12
prline24a	19° 53.0	66° 46.0	183/ 7:12	183/ 15:16
prline24b	19° 14.0	67° 8.1	183/ 15:16	183/ 22:44
prline25	18° 52.0	67° 36.0	183/ 22:44	184/ 2:34
prline25a	19° 4.1	67° 20.3	184/ 2:34	184/ 16:09
prline26	20° 20.0	66° 53.2	184/ 16:09	184/ 18:55
prline26c	19° 22.36	67° 21.74	185/ 3:06	185/ 7:48
prline27a	18° 55.230	67° 34.22	185/7:48	186/ 0:55
prline28	20° 24.2	67° 5.1	186/ 0:55	186/ 17:44

TABLE 9.1 Continuation				
prline29	18° 55.1	67° 47.9	186/ 17:44	187/ 1:42
prline30	19° 36.0	67° 40.4	187/ 1:42	187/ 10:15
prline31a	18° 53.2	68° 2.3	187/ 10 :15	187/ 17:30
prline32a	18° 37.6	67° 15.7	187/ 17:30	188/ 00:07
prline33	18° 10.2	67° 47.0	188/ 00:07	188/ 1:45
prline34	18° 1.0	67° 46.2	188/ 1:45	189/ 13:30

Table 9.2 MR1 DATA GAPS			
GMT start	GMT end	Status	Explanations
168/ 13:45	169/ 4:45	out of water	noise on starboard
169/ 13:30	171/ 5:55	out of water	telemetry error
174/ 6:15	175/ 8:30	out of water	electrical engineer on board
178/ 6:45	178/ 22:15	out of water	shallow depths
184/ 18:45	185/ 3:06	out of water	reparations

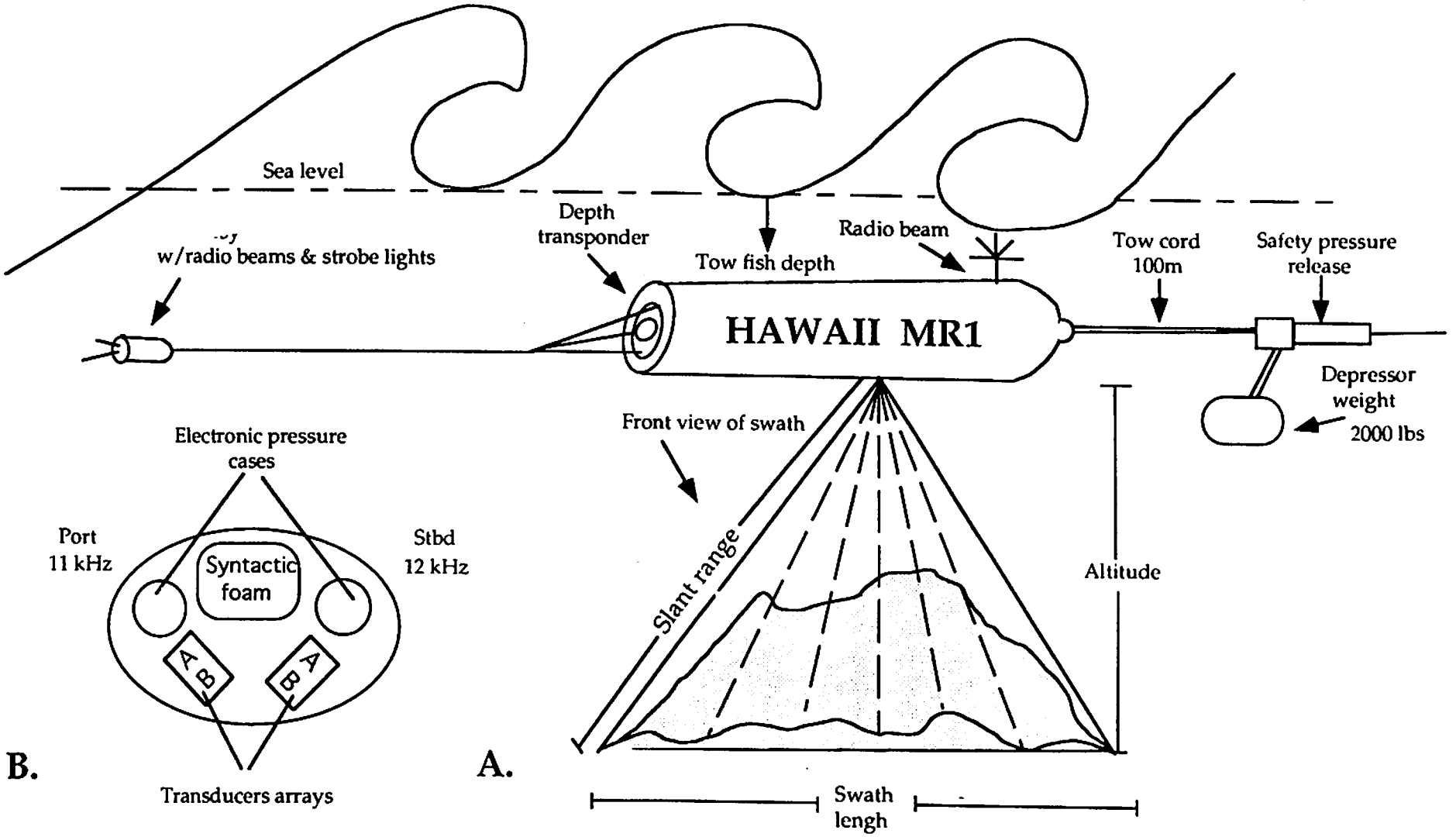

Figure 9.1: A. The MR1 towing configuration, safety devices and swath specifications.
B. Hawaii Mr1 cross section.

CHAPTER 10. MR1 DATA PROCESSING

by Frances Delano

Although processing for sonar data and bathymetry differs in methodology, both are dependent of the same raw data. The equilibration of the sidescan system is extremely important for the calculation of a flat bottom table this known value will result in the data processing parameter. Sidescan amplitudes are placed in swath range using a "flat bottom assumption. The information acquired during the cruise will be process using this known datum. The needle depth is the first received signal from bottom backscatter which is interpreted by the system as to be the general water depth. Editing graphically errors as needle depth, is crucial. Due to this fact it is possible to have spots which do not follow the surrounding features in the image. To correct these errors it is necessary to expand the surrounding data to fill the gap. During this procedure some degradation occurs. However, usually the extent of degradation does not affects the interpretations. Also, striped gaps may result due to the tow fish attitude, for example; if it goes too fast or if it is moving side ways it may not record all the sent signals.

To correct the angle varying gain the system uses beam configuration, water velocity, water column (sound velocity), and change in the gain. These allow the software to read the data. Finally, imaging enhancement is needed to maximize the gray levels and image relief.

Bathymetry processing also uses the flat bottom tables for calibration. The sound waves are received as electrical angles, the received angles have to be converted into acoustic angles. For example, using the equilibration data and the known electric angle then the acoustic angle can be calculated (e.g. 100° ea = 90° aa). The rest of the angles can be calculated using this datum. Assuming the water velocity is 1500 m/sec and using the time (sec) that the signal returned are use for simple sine and cosine calculations for the resultant slant range (meters). The slant range is the distance within amplitude imaginary line which is perpendicular to the fish and the acoustic angle. The sum of the amplitude (the distance between the MR1 and the sea floor) and the fish towing depth equal total the water depth. The navigation position of the ship is used to calculate the navigation position of the fish, which is approximately 100 meters from the ship. The bathymetry image is based on navigation position, slant range and water depth pairs.

CHAPTER 11. 3.5 kHz SONAR SYSTEM AND SODAR PROGRAM

by Araceli Munoz

The 3.5 kHz sonar system

The 3.5 kHz sonar system is an echosounder used to obtain bathymetric information and at the same time subbottom structures in shallow waters. It consists of a transceiver, a transducer, a chart recorder and the SODAR real time display computer (Fig. 11.1). It works as follow: the chart recorder triggers the transmitter, which send a tone burst into the water through the transducer. The echo from the sea floor is received by the transducer, amplified by the receiver, displayed in real time by SODAR program and on a thermal graphic recorder.

Transceiver. The transceiver determines the frequency, power and length of the sounding pulse, and amplifies the echoes received. The transceiver consists of a transmitter controlling the sending signals and a receiver which amplifies the echo.

- The transmitter also controls the signal's pulse. The selection has four channels:
  - Short: 3.5 kHz = 0.15 ms; 12 kHz = 0.25 ms.
  - Medium: 3.5 kHz = 0.8 ms; 12 kHz = 0.8 ms.
  - Long: 3.5 kHz = 3.5 ms; 12 kHz = 3.5 ms.
  - External.

- The receiver usually control the gain for amplification of signals in a operational mode called time varying gain (TVG). Immediately after transmitting the signal, the gain of amplifier attains a minimum value of 40 dB. The gain is increased in a rate proportional to the loss of sound in the water. The TVG is not activated until a prescribed delay time after the signal is transmitted. After the delay time passes, the TVG activates and the gain is increased to 60 dB. This function is used for subbottom profiling. On arrival the bottom echo, the gain is increased to normalize the weaker echo from the deeper subbottom layers.

Transducer. The transducer performs two functions:

- Converts the high power electrical output of the transmitter part of the transceiver into a high power acoustic wave.
- Converts the returning low power acoustic echoes into a electrical signal for amplification and processing by the receiver section of the transceiver.

Recorder. The recorder is a thermal graphic recorder from EPC Laboratories. The trigger time interval is controlled and determines the interval at which signals are sent from the transducer. A one (1) second interval time was used and also automatic delay changes during EW 96-05.

SODAR system

The R/V EWING's Sonar Digitizing And Recording system (SODAR) was developed to give a real time display of acoustic signals the ship monitors and recorders. There are the 3.5 kHz and 12 kHz sonar signals via transceivers; and also SODAR records the returns from sonobuoys via two radio receiver. In EW 96-05, SODAR is used for recording and displaying 3.5 kHz bathymetry, and writing sampled data to a thermal graphic printer.

The sonar digitizing and recording system (SODAR) consists of a PC housed analog to digital converted, a standard PC, a VGA display and an external wall mounted BNC panel. There are also three colored RG59 cables that have to be moved for any of the three modes of operation. The program does not have to be monitored and unless it looses depth information for Hydrosweep system should be trouble free.

The SODAR program should be run in DOS mode and when is started the A/D board will automatically be configured and data acquisition will begin. In the bathymetry mode , the transceiver should be set up to transmit/receive at the desire frequency and the power on. If this is all set then the program should be running and the current depth, obtained from Hydrosweep system, appear on the screen. Then it is parsed from the logging computer, and the must be running to get accurate bathymetry. At this point the program should continue to run without user intervention.

The PC display and the EPC recorder annotate automatically every 15 minutes with time and navigation information.

CHAPTER 12. SEA WATER TEMPERATURE

by John Charles, III

The sea water temperature was recorded by an Omega DP 10 series thermometer and an Expendable Bathythermograph (XBT). The Omega DP 10, which is mounted on the ship, collected data from the start of the cruse to the end. There is no checking or smoothing done to the data. The data that is merged with navigation is stored at L-DEO. The format of the data is:

ct.nddd
yy+ddd:hh:mm:ss:mmm N 12 12.1234 E 123.1234 26.3
yr day time lat long sea temperature (°C)

The XBT, XT-7 series measures the temperature of the upper 800 meters of the water column by launching an expendable probe into the water. The temperature is derived from the difference in voltage between two matched current sources. Once the probe is launched into the water it starts to send a signal to an analog to digital converter and the data in put into a form that can be read on a personal computer .

A profile of temperature versus depth is recorded that is used to help determine the velocity of sound in water (Figure 12.1, 12.2, 12.3, 12.4, 12.5). Five XBTs were done over the course of the survey. The XBT data were used to create a velocity profile for a one degree by one degree area. The data were stored on a computer disk.

The XBTs where done at the following locations :

XBT	Lat	Long
1	18° 49.298N	065° 20.329W
2	19° 34.12N	066° 10.29W
3	19° 58.96N	066° 08.75W
4	19° 55.97N	067° 16.05W
5	18° 25.07N	067° 49.58W

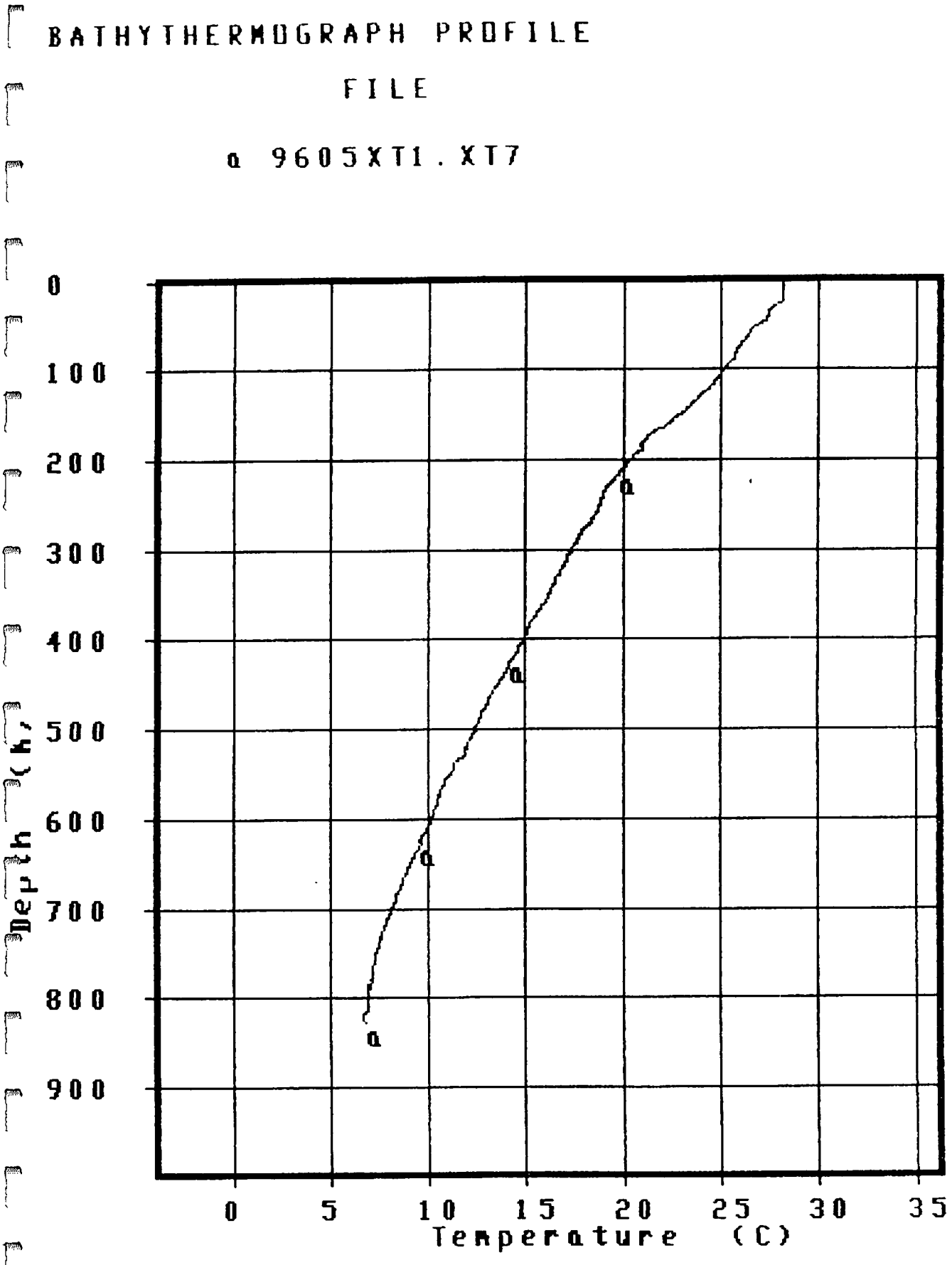

Figure 12.1 First XBT

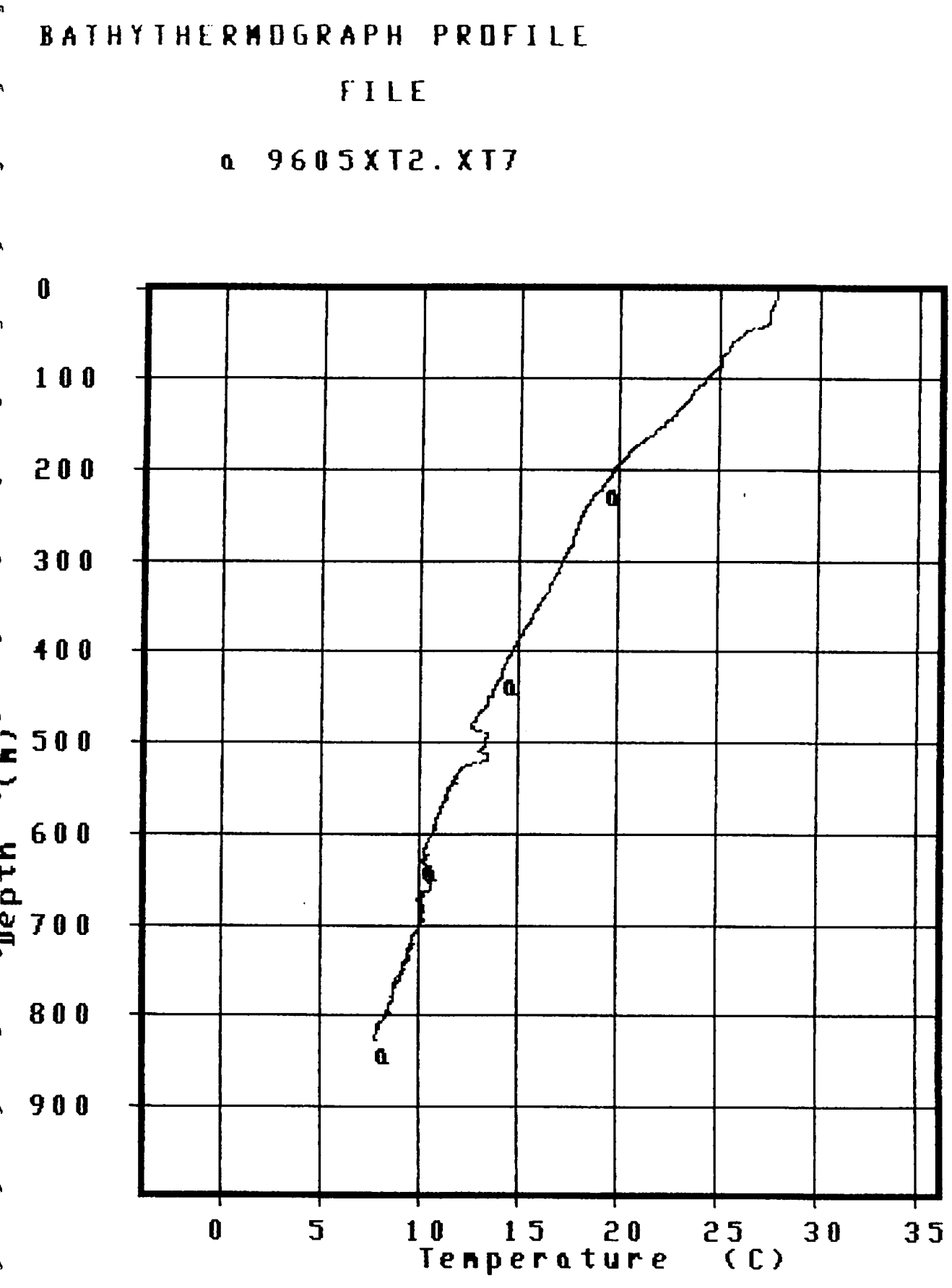

Figure 12.2 Second XBT

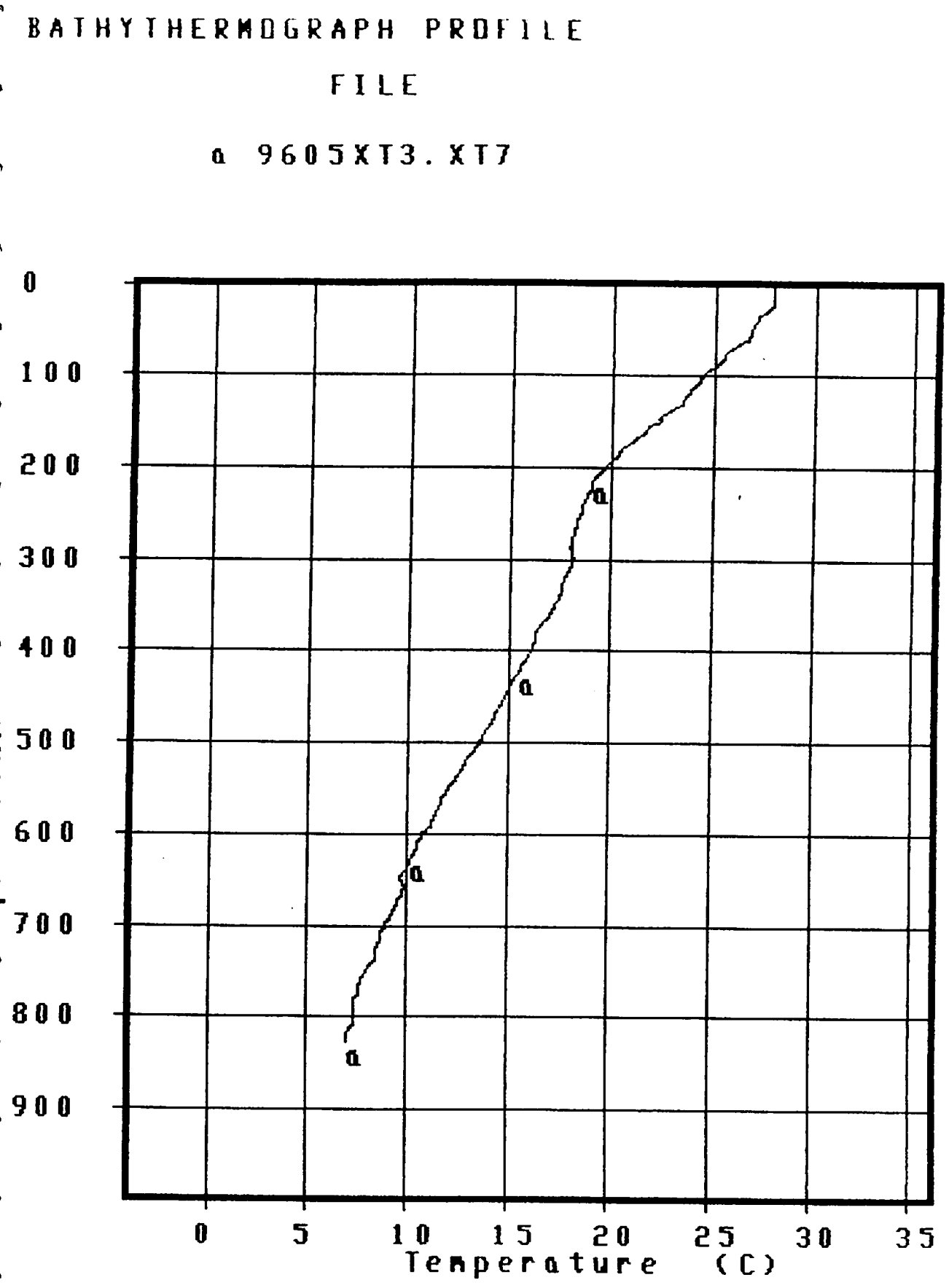

Figure 12.3 Third XBT

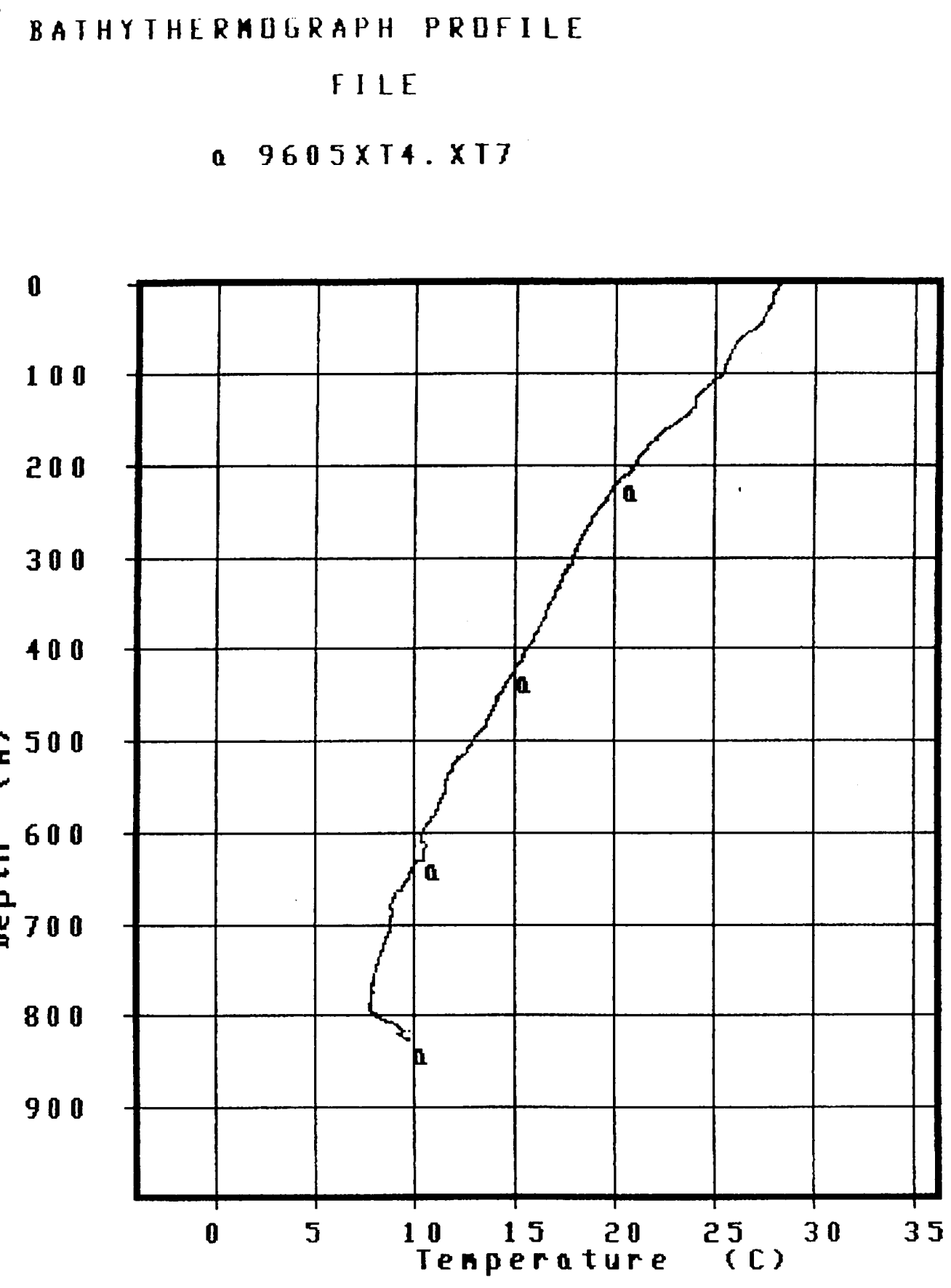

Figure 12.4 Fourth XBT

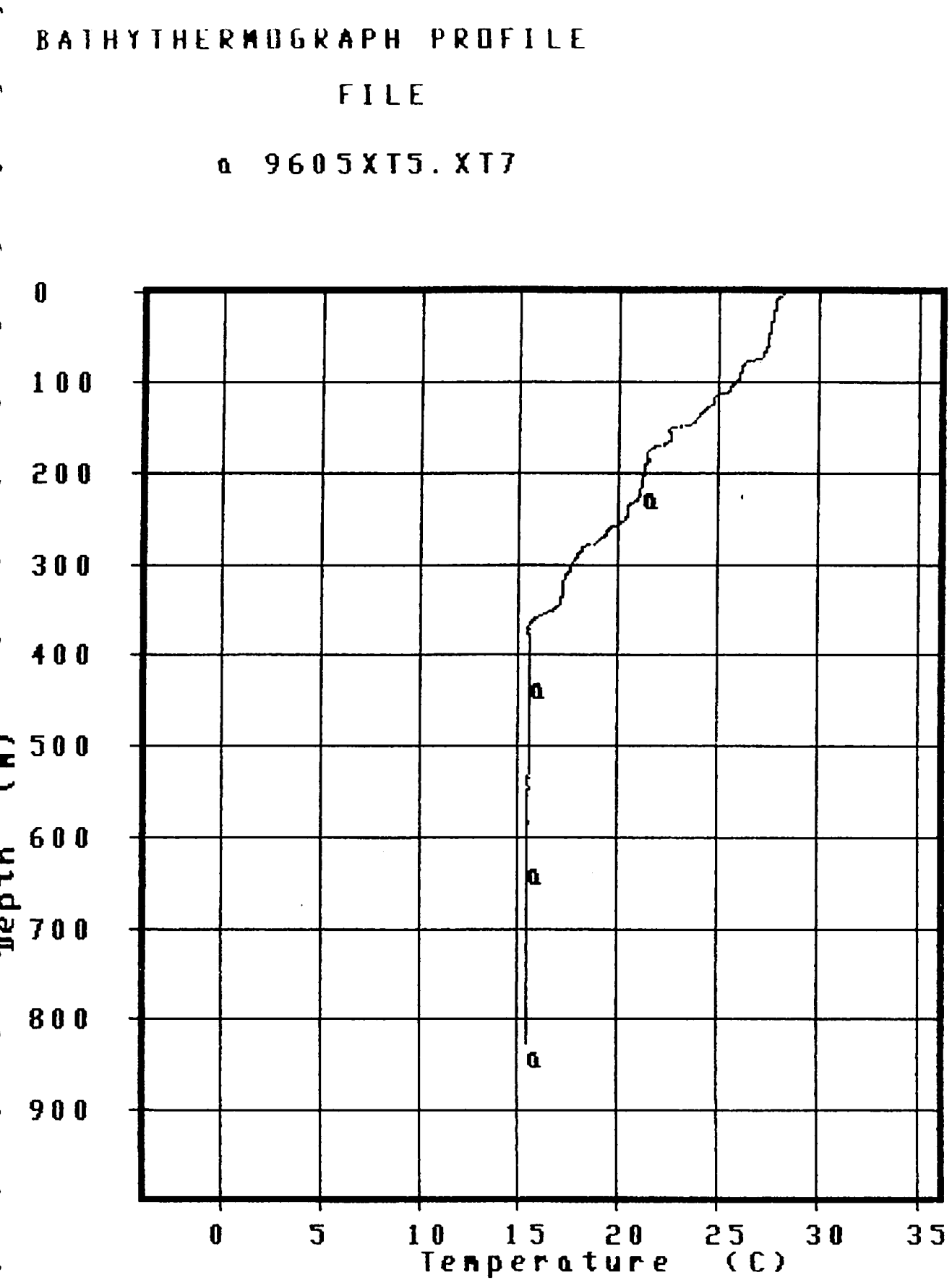

Figure 12.5 Fifth XBT

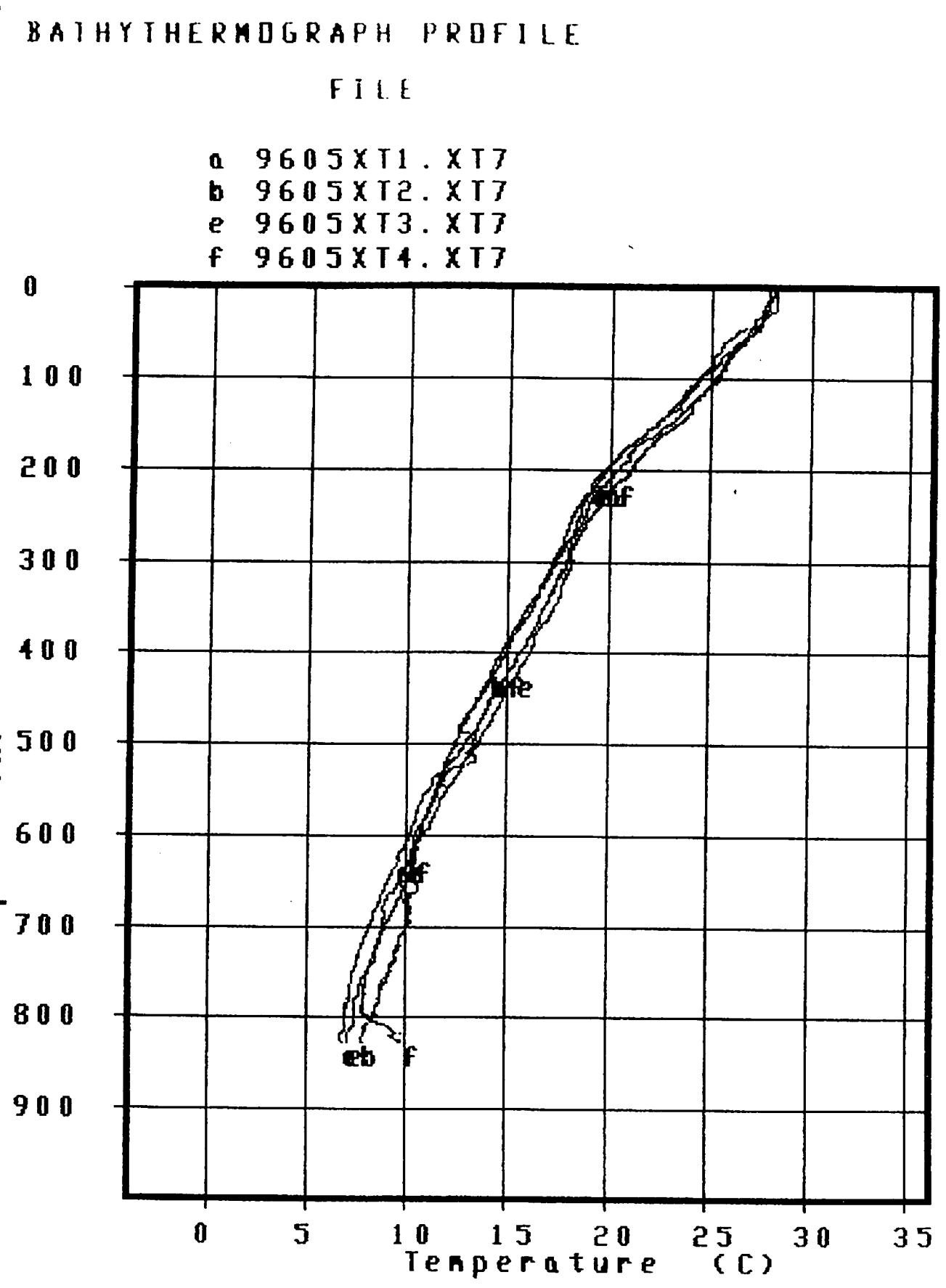

Figure 12.6 Plot of XBTs 1-4

CHAPTER 13. WEATHER STATION
by John Charles, III

The weather was logged at one minute intervals by a R.M./ Young Precision Meteorological Instruments (26700 Series). The data are not checked and reside at L-DEO. The true speed and true wind direction are calculated as data is collected. The format of the data is:

```
wx.rddd
Port bird is bird #1; starboard bird is bird #2.

96+002:00:00:00.244  3.4 231 9.3   15.4  13.2  21.1  271  261
date     time          tspd tdir wsi1 wss1 wsm1 wsx1 wdc1 wds1

 6    12.6  15.9  15.6  20.7  261  253     6    66.7  66.7
wdm1 wsi2 wss2 wsm2 wsx2 wdc2 wds2 wdm2 tcur tavg

66.5 67.0  66  58  68  1016.8
tmin tmax rh  rhn rhx  baro
```

The abbreviations represent:

tspd	true speed
tdir	true wind direction
wsi1/2	wind speed, instantaneous, birds #1 and #2
wss1/2	wind speed, 60 second average, #1 and #2
wsm1/2	wind speed, 60 minute average, birds #1 and #2
wsx1/2	wind speed, 60 minute maximum, birds #1 and #2
wdc1/2	wind direction, current, birds #1 and #2
wds1/2	wind direction, 60 second average, birds #1 and #2
wdm1/2	wind direction, 60 minute average, birds #1 and #2
tcur	temperature, current
tavg	temperature, 60 minute average
tmin	temperature, 60 minute minimum
tmax	temperature, 60 minute maximum
rh	relative humidity
rhn	relative humidity, 60 minute minimum
rhx	relative humidity, 60 minute maximum
baro	barometric pressure

The data were logged from Julian day 167, June 15, 1996 GMT 16:00 to Julian day 190 , July 8, 1996 GMT 16:00.

CHAPTER 14. COMPUTER SYSTEM

by Steve Muszala

The computer system that was on board the R/V EWING during cruise EW96-05 can be seen in schematic 14.1 (schematic modified from S. Budhypramono). There were no network related crashes throughout the entire cruise, hence no SCS data were lost due to downtime of the system.

There were, however, problems with two of the tape drives. The 3480 drive that collected the SCS data in the real-time portion of the lab had mechanical problems, it was printing duplicate labels for tapes that did not exist. This did not create any major data gaps, although one shot number and file number were sometimes lost at the end of the tape preceding the duplicate label. The drive was switched, but the problem persisted and could not be remedied.

In the non real-time portion of the lab a 3480 tape drive that was being used in processing the SCS data had mechanical problems in that it wouldn't always eject the tape. This didn't result in any data loss. Furthermore, the exabyte tape used in the SCS processing would not read to the high density tapes that were brought by UTIG. This problem resulted in no lost data.

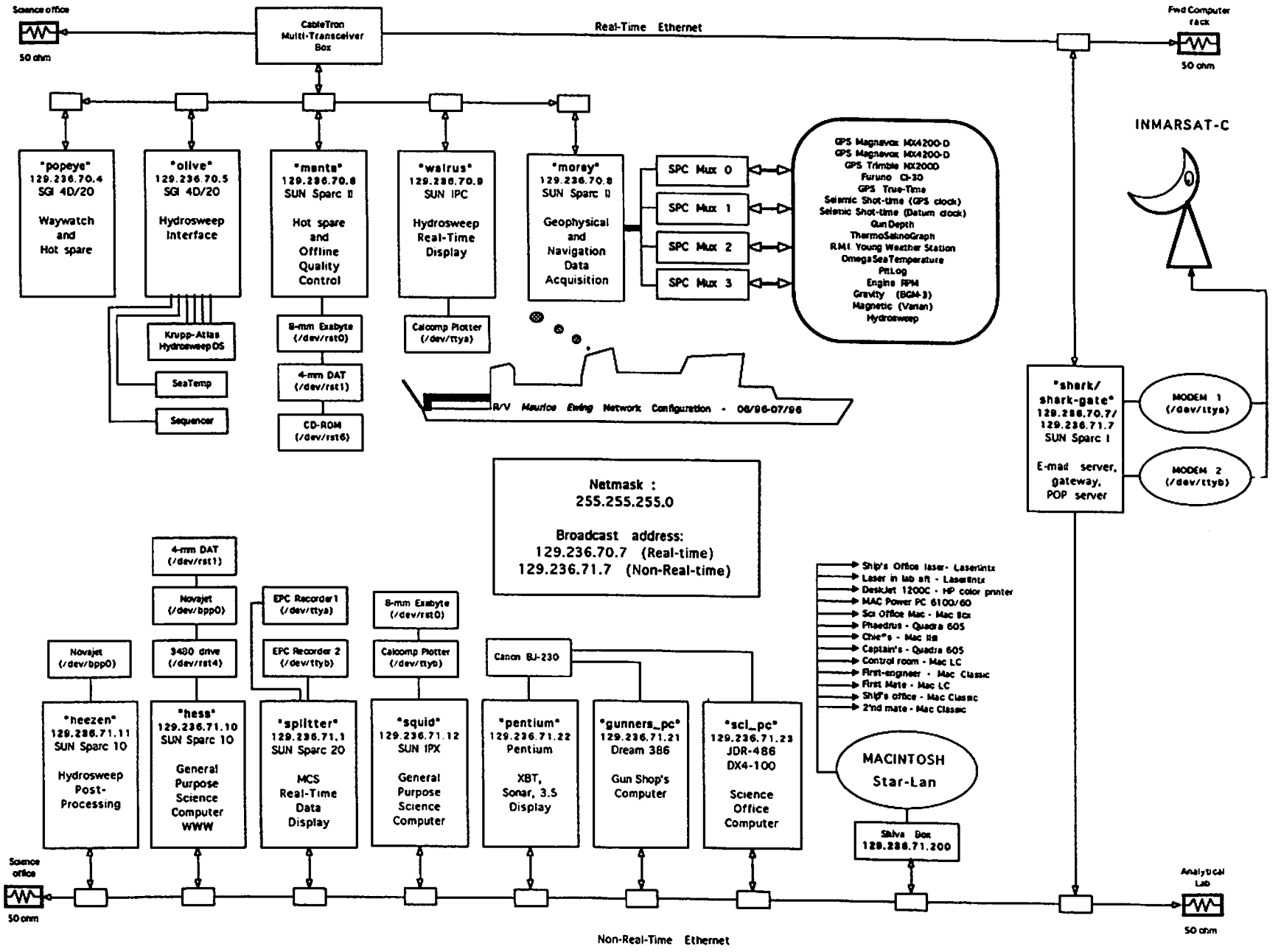

Figure 14.1 -Computer system in use for cruise EW96-05
(modified from S. Budhypramono)

CHAPTER 15. NAVIGATION

by Frances Delano and Stefan Muszala

Time Logging

Time was logged at one minute intervals throughout the EW96-05 cruise using a Kinemetric/True Time Division Model GPS-DC GPS Synchronized Clock. The True Time clock was used to calibrated the CPU clock of the logging computer. The logging computer in turn sends the True Time clock signal to the other computers on the on-board network via a UDP broadcast. Once this has been done, all of the CPU's adjust their times to UTC time.

Time logging information for cruise EW96-05		
Day	Time	Notes
167	2242	start of cruise/began logging & processing
189	1530	end of cruise/ceased logging & processing

Logging of Speed and Heading Information

The Furuno CI-30 2-axis Doppler speed log mounted on a Sperry MK-27 gyro provided speed and heading information. The information was logged at three second intervals and was checked visually using data plots. The data were smoothed in order to provide a mean value of all good data within a one minute interval.

Time logging information for cruise EW96-05		
Day	Time	Notes
167	2242	start of cruise/began logging & processing
189	1530	end of cruise/ceased logging & processing

Navigation Using GPS

The United States Government has developed a satellite-based, radio navigation aid that provides global, all-weather, precise navigation and timing capabilities 24 hours a day. This navigation system is known as the Global Positioning System, or GPS. The build-up of the GPS satellite system has occurred in two phases so far, with the third phase scheduled for completion somewhere in the very near future. Phase one, or Block I (1978-1989), built and tested a ground support network, experimental user equipment and production user equipment.

Phase 2, known as Block II, was completed in 1992. By 1992, the satellite constellation consisted of 18 satellites with 3 active on-orbit spares. The Block II satellites are collectively termed NAVSTAR satellites (Navigation System with Time and Ranging). The NAVSTAR satellites are sent into certain orbits so that full GPS coverage of the earth can be achieved during any period during 24 hours. By the end of Block III, the government hopes to have 21 satellites in orbit including 3 spares. In a few years, the government has planned to turnoff selective availability, allowing even greater accuracy's in GPS measurements.

The GPS system is divided into three segments, the space segment, the control segment and the user segment. The space segment consists of the satellites that are currently in orbit and it receives it information from the control segment and transmits it to the user segment. The space segment transmits the following data; Health data, Ephemerides, Satellite constellation almanac, Time, Ranging signals and Atmospheric correction data. Health data indicate the quality of the signal. A good signal will provide reliable time and position data, while a poor signal will not. The ephemerides describes the detailed orbital characteristics of the particular satellite that is being tracked, while the satellite constellation almanac describes the coarse orbital information for all of the satellites in the constellation. The constellation almanac is primarily used to predict the visibility of the satellites. Time deals with the synchronization of the time between satellites, and ensures that individual satellite

positions are accurately known. Ranging signals are used to calculate the position of a GPS receiver on a moving platform (e.g. a ship) from the known position of a satellite. The last segment transmitted by the space segment is Atmospheric data. This corrects for delays in signal time related to atmospheric conditions and local weather patterns.

The control segment of the GPS system, in a nutshell, monitors and tracks the NAVSTAR satellites, synchronizes their operation, performs satellite position computations, and transmits orbital and corrected time data to the satellites. This is accomplished at five monitor stations, one Master Control station, and three load-up stations. The monitor stations are in Ascension Island, Hawaii, Diego Garcia, Kwajalein, and Colorado. The Master station and one-load up station are in Colorado. The other two data load-up locations are in Hawaii and Ascension Island.

Finally, the user segment is made up of equipment that tracks the NAVSTAR satellites, receives the signals and uses the signals in a manner dependent on the users application. Such applications include, but are not limited to navigation and geodetic positioning. The common denominator among all of the applications is that they all use the satellite signals to update their positions in respect to the surface of the earth. Positioning accuracy can range from a few millimeters to 100 meters. This accuracy is dependent on the equipment in use (i.e. a base station), the equipment design and the environment in which the equipment is being used.

For the military and certain users, an accuracy known as Precise Positioning Service (PPS) is allowed, while all other users are provided with Standard Positioning Service (SPS). The accuracy of SPS is intentionally degraded by the government through Selective Availability (SA). Other factors that affect accuracy while using SPS are the receiver design and whether differential corrections are being used or not.

The five most common GPS error sources and their errors are as follows:

1) SA errors: $\pm$ 30 meters
2) Ionospheric delays: $\pm$ 20 to 30 meters (day) /$\pm$ 3 to 6 meters (night)
3) Tropospheric delays: up to 30 meters
4) Ephemerides errors: < 3 meters (w/out SA)
5) Satellite clock errors: < 3 meters (w/out SA)

Differential GPS (DGPS) is a method that is employed that virtually eliminates the error imposed by Selective Availability. The method employs at least two GPS receivers, one of which is placed at a known location. This location is then referred to as a base, or reference station. The other receiver(s) at either an unknown location or a mobile platform is the Differential Navigator, and is labeled the MX 4200D. The purpose of the base station is to measure relative errors in location and to remove these errors. The corrections are then sent in real time to the Differential navigator, which has the effect of improving the signal, and hence the position coordinates. As the Differential Navigator gets farther from the base station, the error corrections become increasingly unreliable. Therefore, Differential GPS is usually used only relatively close to the base station.

CHAPTER 16. GRAVITY MEASUREMENTS

By Wilfredo Rosado Chaparro

Bell Aerospace BGM-3 Gravimeter

A Bell Aerospace BGM-3 Marine Gravity Meter System was used to measure accelerations related to variations in mass distribution of the sea floor beneath the ship during cruise EW96-05.

The Bell Aerospace BGM-3 sea gravity system consists of a navigation-grade force feedback accelerometer mounted on a gyrostabilized platform, with sensors that don not require cross-coupling correction. the sensor is a Model XI accelerometer; a schematic model is shown in Figure 16.1. The model consists of a proof mass wrapped around by a coil. The mass is constrained from moving vertically by two permanent magnets. The system works by keeping a balance between the gravitational force acting on the proof mass and the electromagnetic force produced by the electric current in the coil. The balance of this two forces will maintain the proof mass in a constant position. If a change in the vertical acceleration occurs, the current passing through the coil will vary accordingly to compensate for the change in the gravitational force acting on the proof mass. In sea-going surveys these acceleration are the sum of the Earth's gravitational acceleration and the vertical acceleration acting upon the ship. Any change in the position of the proof mass is detected by a second order servo loop which regulates the current going through the coil, driving the mass back to its constant position.

The accelerometer's output is a current proportional to vertical accelerations in the order of 0-200 Gals. By adding the output with the 880 Gal of the reference bias, the system is capable of responding to the range of accelerations that can be encountered in the sea. The current will then be filtered by an RC filter to prevent leakage of high frequencies. Finally, the analog signal is converted into a digital pulse rate for an output of counts every one seconds to the data handling system. The BGM-3 gravity meter (with adequate navigation) is capable of submGal accuracy and resolution of wavelengths of 1 to 2 km.

Data Reduction , Observations and Preliminary Interpretations

Reduction of the gravity data consisted of:

1. **filtering**: an observed gravity value in mGal is calculated by filtering the 1 second readings with a 360 second Gaussian filter, scaling the result and adding a bias. A value in mGal is calculated at 6 second intervals.

2. **smoothing**: mean gravity values at 00 seconds of each minute are calculated from the milligal values +-30 seconds of this time.

3. **merging with navigation and calculating the Eotvos correction and Free Air Anomaly (FAA).** The ship's speed and course, from the navigation, used in the Eotvos correction are smoothed with a 5 point running average from all days.

To compute the Eotvos correction the formula below was applied:

$$\text{Eotvos Corr.} = (7.487 * \text{speed} * \sin(\text{course}) * \cos(\text{lat})) + (\text{speed}^2 / 240.8)$$

where speed = ship's speed in kts, course = ship's heading in degrees and lat = ship's latitudinal position in degrees.

The 1980 theoretical gravity formula was used to calculate the reference gravity value:

$$\text{Ref gravity} = 978049.0 * (1.0 + 0.0052884 * \sin^2(\text{lat}) - 0.0000059 * \sin^2(2 * \text{lat})$$

where lat = ship's latitudinal position in degrees

The FAA was obtained by adding the Eotvos correction and then subtracting the reference gravity value.

To obtain estimates of the drift during the cruise, gravity measurements were taken at a base station in San Juan, PR before and after the cruise (See Lamont Gravity Tie Report). A DC shift of 23.1 mGal from the pre-cruise tie at San Juan Puerto Rico is applied.

4. **visual check** of plot of data to determine satisfactory Eotvos corrections and delete spikes of data at turns.

The FAA is plotted along track the ship's course and in contours in Figures 16.2 and 16.3, respectively. Both figures show a large negative anomaly associated with the axis of the Puerto Rico trench. To the eastern side of the survey area the main negative anomaly seems to divide into two directions when reaching the area of the Main Ridge. One heads to the southeast, south of the Main Ridge, and the other heads to the northeast, north of the Main Ridge. This may be due to the Main Ridge producing a slight positive anomaly which cancels the main negative anomaly in the Puerto Rico trench. To the west of the survey area, patterns are present that do not follow the general signatures of the rest of the Puerto Rico Trench. This is produced by the presence of the Mona Canyon and the intensive faulting in the area.

A. BGM-3 Accelerometer

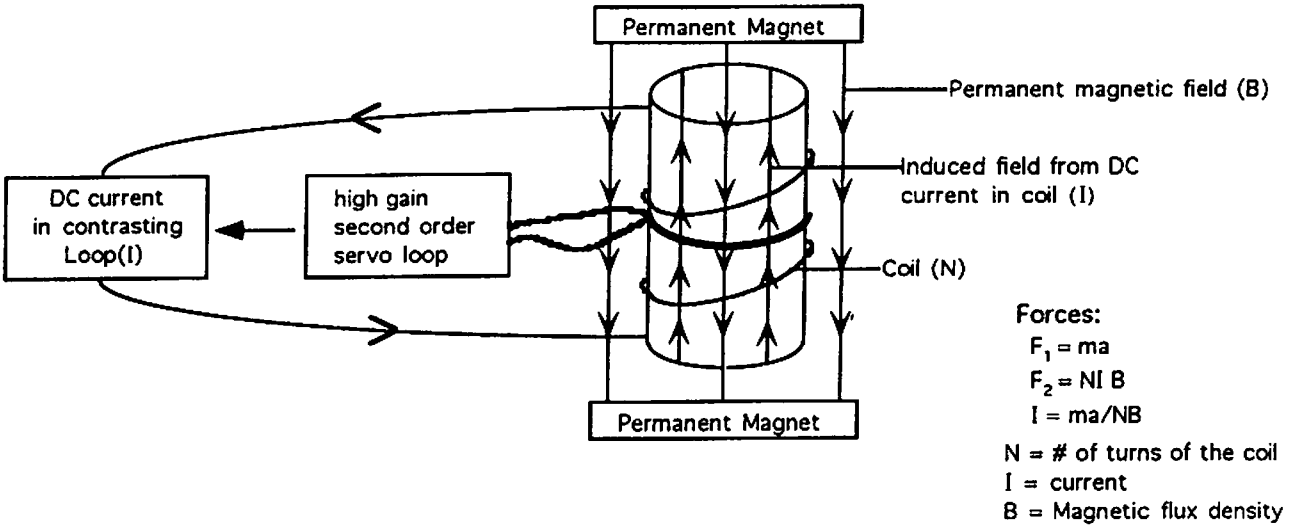

B. Sensor system

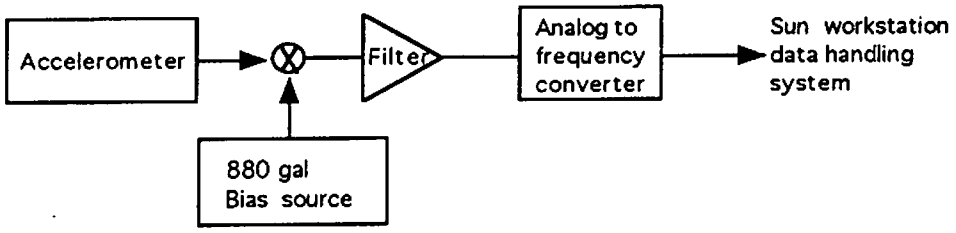

Figure 1. Schematic sketch of the BGM-3 sensor subsystem. (A) BGM-3 Accelerometer configuration with the proof mass, the coil wrapped around it and the two permanent magnets. The balance of the forces are: F1= local gravitational force; F2= electromagnetic force induced by the current in coils where m = mass of proof mass; a = local vertical acceleration; N = the # of turns on the coil around the proof mass; and B = magnetic flux density. (B) Configuration of the sensor system showing how the output signal from the accelerometer is summed with the reference bias source, then filtered by the RC filter. Then the signal is changed from an analog to a digital signal, that has an output to the on board Sun workstation data handling system at 1 second interval. (modified from Bell and Watts, 1986).

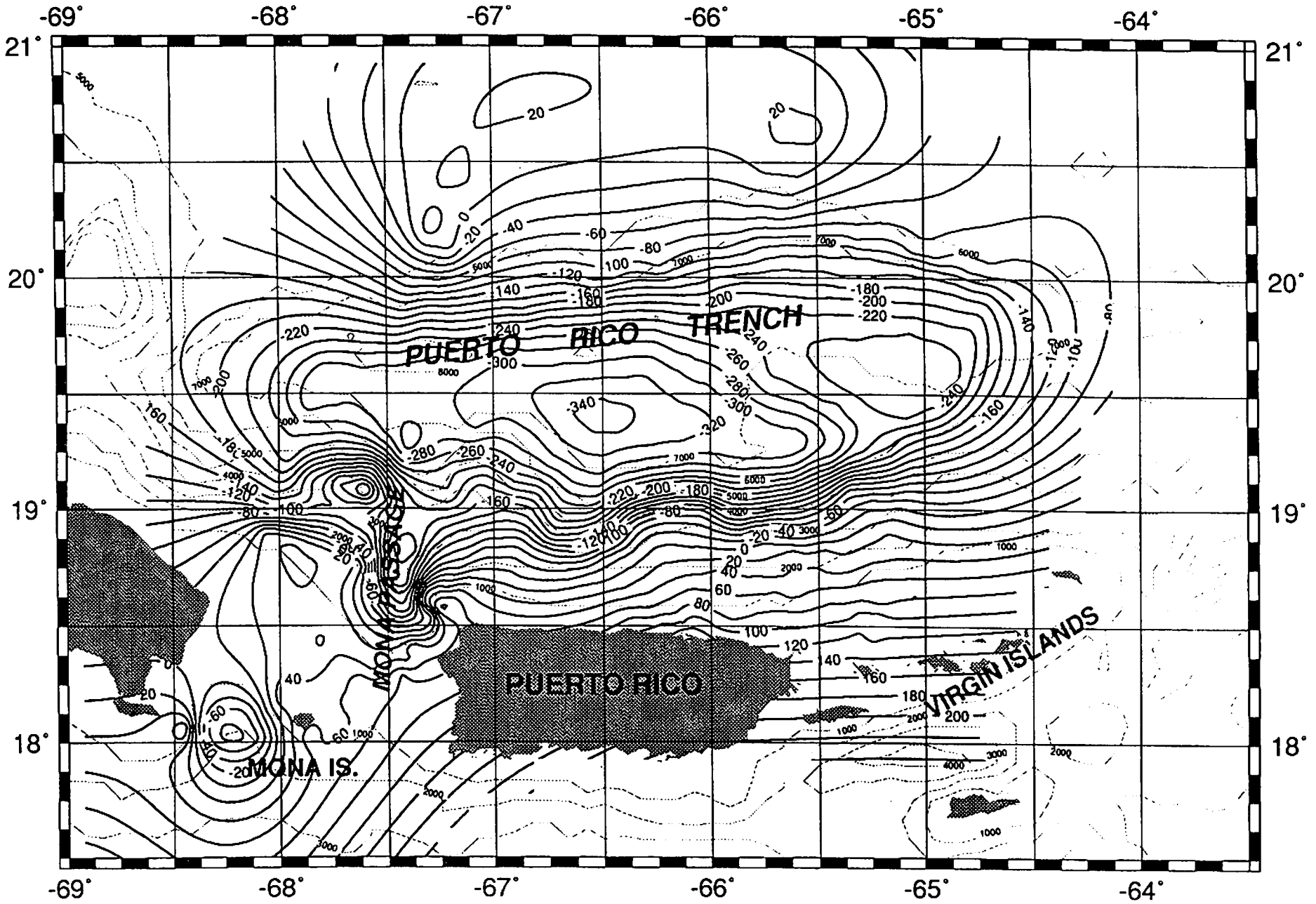

Figure 16.2 Gridded Free-Air Anomaly, grid interval = 1nm

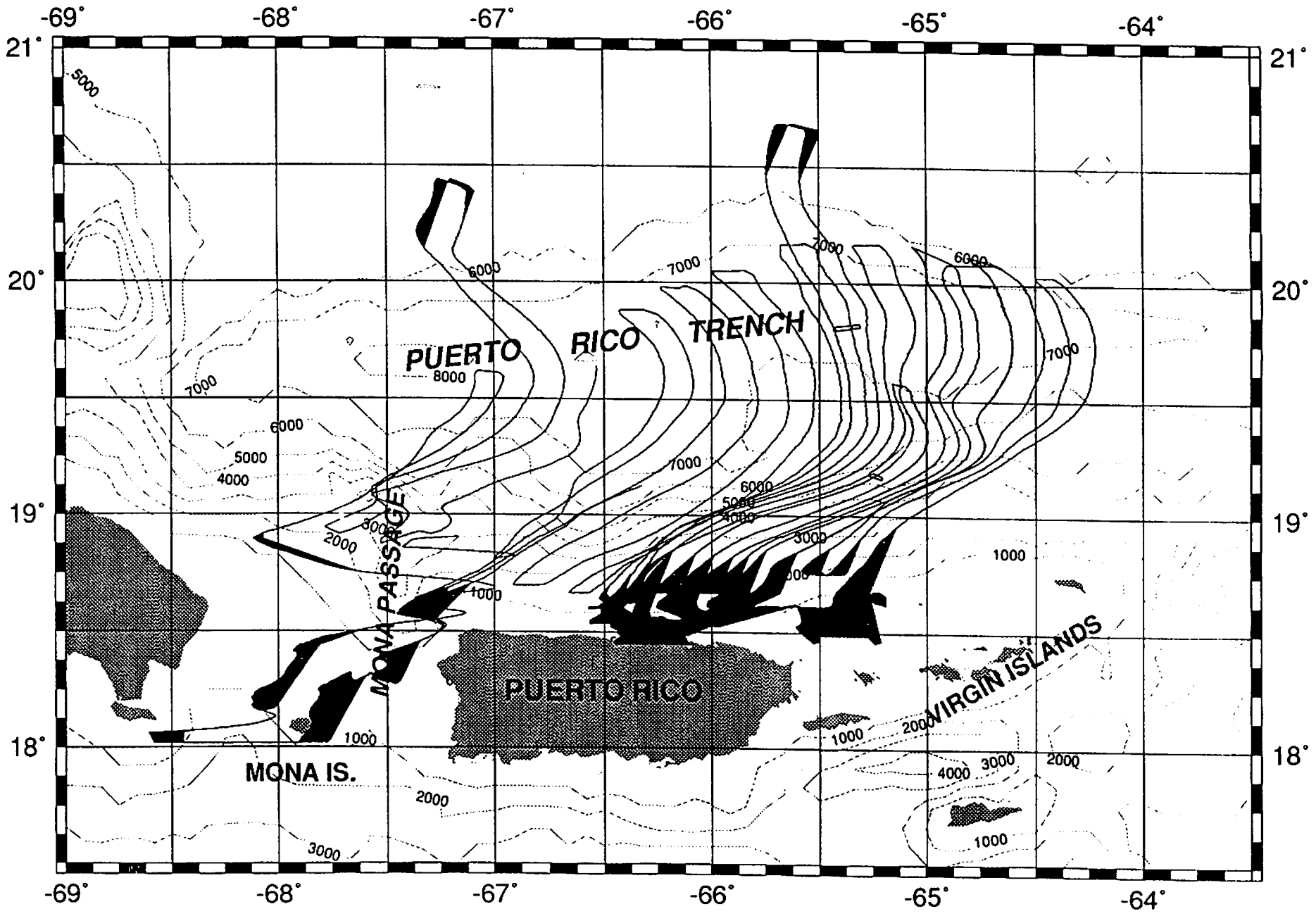

Figure 16.3 Free-Air Anomaly plotted along track.

Lamont Gravity Tie Report

R/V Ewing gravity meters:
Bell Aerospace BGM-3 marine gravity meter
bias = 852680.0;
scale = 5.0940744;

Port: San Juan, Puerto Rico

Date: June 13, 1996

Operator: Chris Leidhold

Reference Station:
Berth B tie point on San Antonio Channel

Reference Value: 978680.7

Pier/Ship's position:
The Ewing is docked at pier 15

Portable Gravity meter: L & R meter G-237
meter temperture 49 deg C

Readings and calculations:

Time	Location	L-R reading	
1250 L	pier 15	2341.51	1650 Z
1355 L	Berth B	2337.49	1755 Z
1408 L	pier 15	2341.46	1808 Z

Lacoste difference in LR units:
delta_LR = pier_LR - ref_LR
delta_LR = 2341.48 - 2337.49
delta_LR = 3.99

Difference in mgal:
note: 1 LR unit = 1.06 mGals
delta_mgal = delta_LR * constant
delta_mgal = 3.99 * 1.06
delta_mgal = 4.2294

Pier gravity value:
pier_grv_val = ref_val + delta_mgal
pier_grv_val = 978680.7 + 4.23
pier_grv_val = 978684.93

Height correction:
At 1535 L / 1935 Z (when data logging computer was on)
C deck is 1.0 m below the pier at time of reading.
Difference between pier and gravity lab = 6.5 meters

note: free-air constant of +0.31 mgal per meter going towards
the center of earth; -0.31 mgal per meter going away.

hgt_corr = hgt * constant
hgt_corr = 6.5 m * 0.31 mGal/m
hgt_corr = 2.01 mGal

Gravity at BGM level:
grv_at_BGM_level = pier_grv_val + hgt_corr
grv_at_BGM_level = 978684.93 + 2.01
grv_at_BGM_level = 978686.94

BGM-3 reading:

On June 13, 1996 (day 165) at 1935 Z
BGM_grv_val = 978710.0 mgal

BGM-3 Mistie:
BGM_mistie = BGM_grv_val - grv_at_BGM_level
BGM_mistie = 978710.0 - 978586.94
BGM_mistie = 23.1 mgal

BGM-3 DC shift:
BGM_dc_shift = 23.1 mgal

CHAPTER 17. MAGNETIC DATA ACQUISITION

by Stefan Muszala

Introduction

The purpose of the cruise EW96-05 was to gather data that would characterize the nature of the Puerto Rico Trench and consequently the nature of the northeastern North American Caribbean plate boundary. Part of this data set included magnetic measurements, which were useful in determining the crustal nature of the Puerto Rico Trench and the surrounding area. The variability of the earth's magnetic field was measured using a Scintrex V-75 proton precession magnetometer between the dates of June 15, 1996 and July 7, 1996.

Theory

Magnetic poles, force and field strength. The first principle of magnetism deals with the concept of magnetic poles. The easiest way to visualize them is through a bar magnet on a table with iron filings sprinkled on it. The sprinkles will align themselves along the lines of force. These lines of force connect the two poles of the magnet. Essentially, the two ends of the bar magnet act as two distinct magnetics, one positive and one negative (Fig . 17.1).

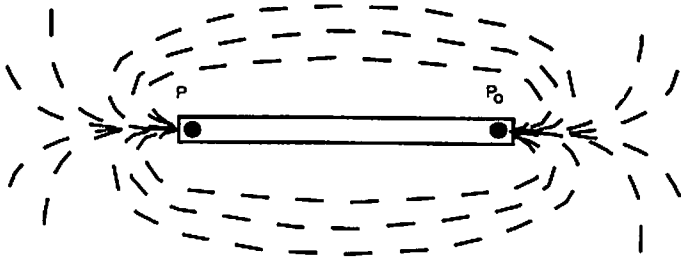

Fig. 17.1-the lines of force around a bar magnet with poles P & P_o.
(modified from Dobrin & Savit, 1988)

The force associate with two poles P and P_o that are separated by a distance r is given by:

$$F = \frac{P_o P}{\mu r^2} \qquad \text{(eq. 1)}$$

where μ is the permeability constant. The permeability is a function of the material in which the poles are found. In a vacuum or air, the permeability constant equals 1. If the poles are alike, the force is repulsive and if the poles are unlike, the force is attractive.

From the magnetic force, F, we can obtain the magnetic field strength, H. This is simply the force per unit pole strength or the flux representing the field at a point. The flux is given by:

$$H = \frac{F}{P_o} = \frac{P}{\mu r^2} \qquad \text{(eq. 2)}$$

where F is the force given in equation 1, P_o, and P are pole strengths, μ is the permeability constant and r is the distance between the poles. The units of H are N/cm^2, 1 dyne/unit pole in the cgs system and 1 tesla in SI units (1 tesla=10^{14} Oersted).

Magnetic moment, polarization and susceptibility In reality, poles are never found by themselves, but as pairs, or dipoles. The distance that the poles are separated, L, can be

multiplied by the pole strength P, to give the magnetic moment M. The moment is along the line connecting the poles and is usually pointing toward the north-seeking pole.

The magnetic moment then brings us to the polarization I, or induced magnetization, of a magnetic material. The polarization occurs when an external field is applied to a magnetic material with randomly oriented dipoles. The dipoles in the magnetic material then line up in the direction of the applied field. Once the polarization I is known, one can calculate the susceptibility, k. It is given by the following equation:

$$I = kH\cos\theta \quad \text{(eq. 3)}$$

where H is an external field, and I is the magnetic polarization.

Ferromagnetic materials typically have large susceptibilities and the susceptibility in a vacuum is zero. Paramagnetic magnetic materials with small positive susceptibilities are weakly magnetic, while diamagnetic materials have negative susceptibilities and are essentially magnetically inert. In the case of ferromagnetic materials, the alignment of atomic magnetic moments occur in groups, referred to as domains, with their long axes parallel to the induced field. Paramagnetic and diamagnetic materials, which constitute the majority of all rocks, align their domains perpendicular to the induced magnetic field.

Magnetic Induction, permeability and remanent magnetism. If a magnetic material is placed in a external field, H, the field that is induced in the material is referred to as H'. H' is given by:

$$H' = 4\pi I \qquad \text{(eq. 4)}$$

where I is the polarization or magnetic intensity and π is a well known constant.

Once H' is known, the magnetic induction B can be calculated. B is simply the total magnetic flux inside the material of a fixed volume or the sum of the internal and external magnetic fields. B found through the relation:

$$B = H + H' \quad \text{(eq. 5)}$$

after substituting equation 4 for H' and manipulations, equation 5 can be rewritten as:

$$\begin{aligned} B &= (1 + 4\pi k)H \\ &= \mu H \end{aligned} \qquad \text{(eq. 6)}$$

From equation 6, we see that $\mu = B/H = (1 + 4\pi k)$ (eq. 7). This shows how the permeability, μ, first defined in equation 1, is derived.

A very important aspect of magnetic theory is that of remanent magnetism. It is best described by the hystersis loop (fig. 17.2). The loop can be seen in experimental setting where a magnetic material is placed between the poles of an electromagnet. If a material with no existing field is magnetized, B increases in response to H, by the relation $B = \mu H$ (I). At this point, H is reversed and brought back to zero, leaving a remanent magnetization, B' (II). If H is further reversed(III), B will approach a negative saturation. From here, if we increase H (IV) we can see another remanent magnetization B'' on the negative B axis. On increasing H further

(V), B once again reaches a positive saturation and the loop repeats itself offset by an amount H'.

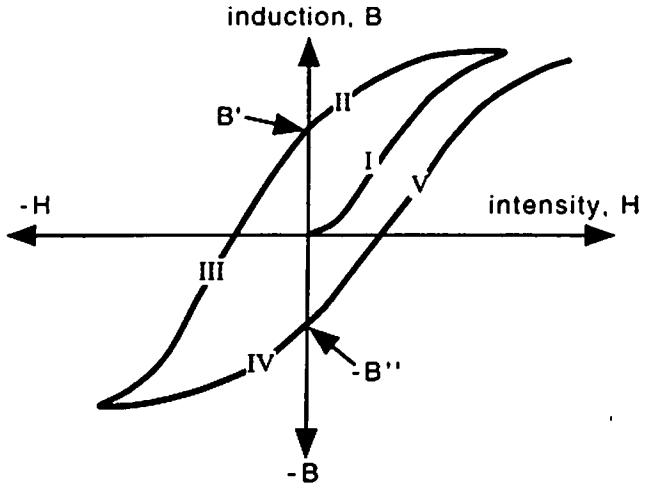

Fig. 17.2-Hystersis loop for remanent magnetism. Steps I-V described in text. (modified from Dobrin & Savit, 1988)

This component of remanent magnetism can be seen in magnetic rocks well after the external field has been removed, and it is this remanent magnetization that contributes to variations in the overall magnetic field of the earth. Other factors that produce variations in the earth's field are due to diurnal variations, secular variations and magnetic storms. External forces not included, the earth's field varies from the equator to the poles. These changes are due to variations in the number of field lines that surround the earth and a similarity exists between the earth's field and that shown in figure 17.1. At the equator, the regional field is approximately 30 to 40,000 gammas while at the poles, the field is upwards of 50,000 gammas. There also exist changes in the inclination of the earth's field. Currently, the inclination is positive in the northern hemisphere and negative in the southern hemisphere. This current alignment of the inclination is indicative of "normal" field. Quasi-periodically, the earth's field reverses itself and the inclinations reverse themselves. The magnetic field is produced in the earth' s outer core as a result of large convection cells. The reversals are then due to large scale changes in these convection cells. The timing of the reversals is of considerable debate, some saying it is non-random, while others believe the timing is related to chaos theory.

Equipment

During this cruise, EW96-05, magnetic data were recorded using a Scintrex V-75 proton precession magnetometer. A magnetometer measures the magnitude of the earth's total field vector F_t. There are two components to this, the earth's field vector, F_e and a local perturbation vector, denoted F' (fig. 17.3). A proton precession magnetometer measures the earth's total field by measuring the precession, or spin, of protons. The precession of the proton is related to the frequency ω(Hz) by the following relation:

$$|\overline{F}| = \omega\gamma \qquad \text{(eq. 8)}$$

where γ is an atomic proportionality constant equal to 23.4873826 gamma's/Hz. The error inherent in this constant is ± 4 ppm. A typical range for ω is 851.52 Hz to 4257.60 Hz, which corresponds to a magnetic field range of 20,000 to 100,000 gamma's (note: 1 gamma = 1 nanotesla [nT] / 100,000 gammas = 1 Oersted[Oe]=1 gauss).

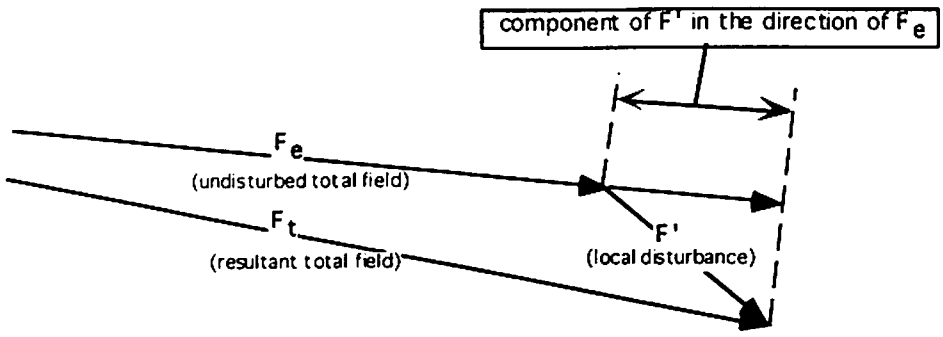

Fig. 17.3-Vector representation of a local disturbance added to the earth's total field. Not to scale. (modified from Dobrin & Savit, 1988)

The V-75 is packaged with an electronics console, and analog recorder with power supply mounted in a cabinet with anti-vibration mounts, a marine towing system and a winch to console cable. A direct readout is given on the front panel of the analog recorder. The V-75 can cover the worldwide field range of 20,000 to 100,000 nT in 10 ranges with a 50% overlap. The V-75 comes with automatic sampling rates of 3, 6, 30 and 60 seconds as well as a manual and external trigger mechanism, which allows synchronization with other geophysical equipment.

The error for a low sensitivity survey is ± 1 nT and the two channels record 100 and 1000 nT full scale. The high sensitivity range, use in this survey, is ± 0.1 nT and records the two channels at 10 and 100 nT full scale. The reference frequency accuracy is $\pm$ 1 ppm (25° C), the reference frequency stability is 5 ppm/year while the overall accuracy of the V-75 is $\pm$ 5 ppm.

The magnetometer sensor consists of a coil emersed in a proton rich fluid. The signal from the sensor emits a frequency, from equation 8. The signal is processed similarly as the processing flowchart that is shown in Figure 17.4. The major difference between the figure 17.4 and the processing that occurs in the Varian V-75 is that the V-75 counter and display are analog as opposed to digital. The analog signal is then converted via an ADC (analog to digital converter) to a digital signal, which is sent to the Sun computer system found on the R/V EWING Once the data are downloaded, the IGRF (International Geomagnetism Reference Field) field is removed using a program written in C+ (See Appendix II). The data were then plotted using GMT (Wessel and Smith, 1995) , a software mapping tool.

Data Reduction and Preliminary Interpretations

Data were acquired between JD167 2242 GMT and JD189 1530 GMT. Gaps in the magnetic field acquisition were insignificant to affect the data to any degree. The magnetometer was towed 200 meters behind the ship (Fig. 3.1) and data were collected every six seconds. The IGRF95 reference field was subtracted from the magnetic anomaly and merged with navigational data every minute.

At Longitude 66° W the data (Figs. 17. 5 & 17.6) show an area of high negative anomalies in the region between 18.70° and 18.8° N. There is a magnetically quiet zone with low positive anomalies from approximately 18.8° N to 19.6° N. North of this, there seem two distinct bands of high positive anomalies at 19.75°N and 20° N. In the eastern portion of the trench, at approximately 65.5° W, the anomalies merge and are found farther to the south, indicating that they trend approximately 330 to 340 (north-west to south-east). At 65.5° W, the area of large negative anomalies is found near 18.62° N, while the quiet zone has started to merge with the two bands of positive anomalies. This is occurring around 19.25° N. Between 65.5° W and 66° W there exists yet another area of high positive anomalies. This is found between 20.5° N and 20.6° N.

The magnetic trends found during the EW96-05 correspond to the orientations of Cretaceous trends on Puerto Rico and the Virgin Islands and are similar to trends found in the Dominican Republic as well as the main trends of the Bahama Islands (Alonso-Harris et. al. 1987). Bunce et. al. (1974) have also found this northeast-southwest trend. Alonso-Harris et al. (1987) have similar results to those found in this survey. They find a quiet zone of low amplitude anomalies lies north of Puerto Rico and they found a region of closely spaces high-amplitude anomalies close to Puerto Rico itself. North of the magnetic quiet zone, Alonso-Harris et. al (1987). also find the northeast-southwest trends that were found in this survey and in that by Bunce et al..(1974).

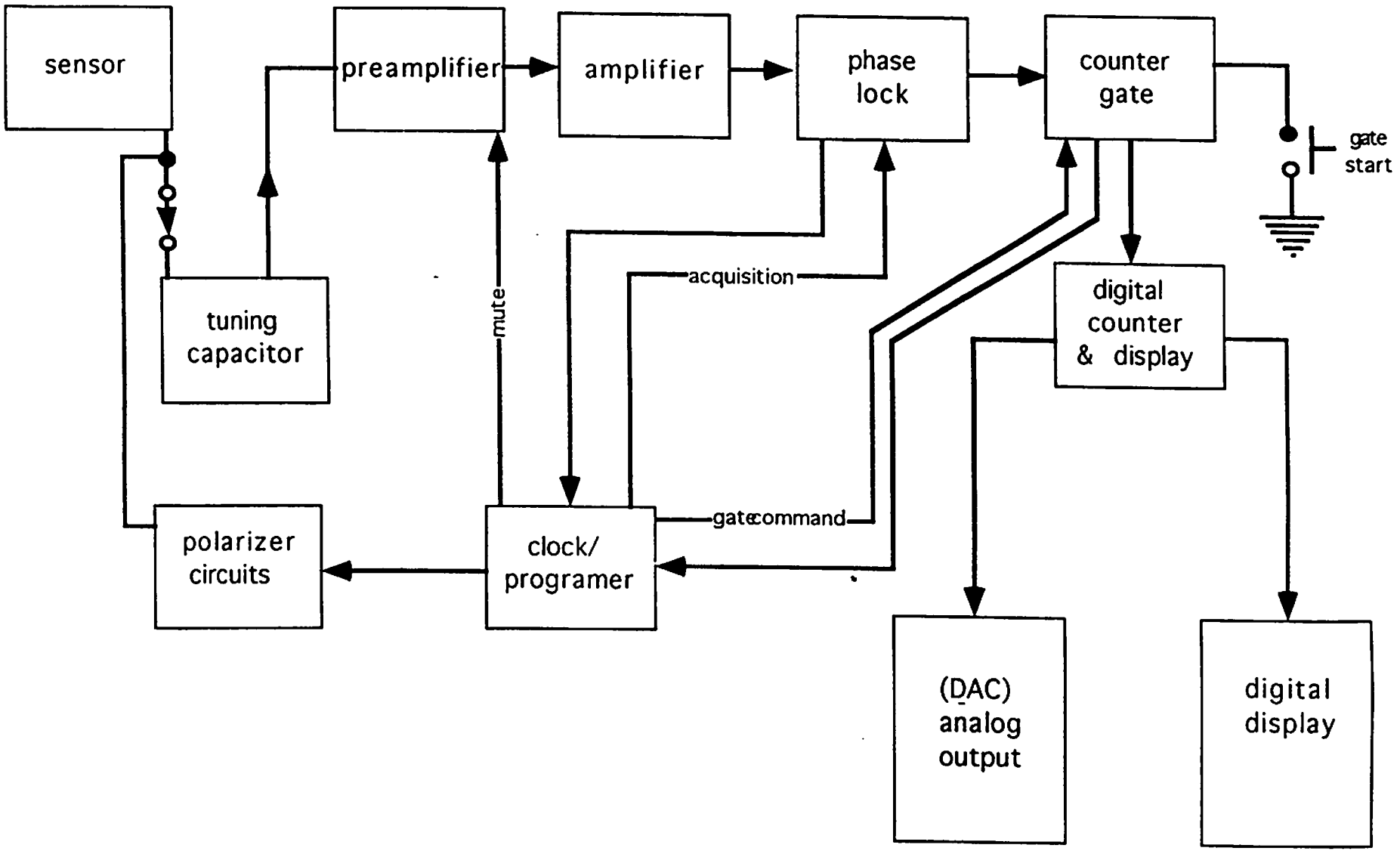

Figure 17.4 -Generalized flow chart of the steps involved in obtaining magnetic data with a proton-precession magnetometer. The major difference between this flow chart and the system used on the *Ewing* is that the Scintrex V-75 outputs analog data from the counter gate. This is then converted via an ADC to digital data (modified from Dobrin & Savit, 1988).

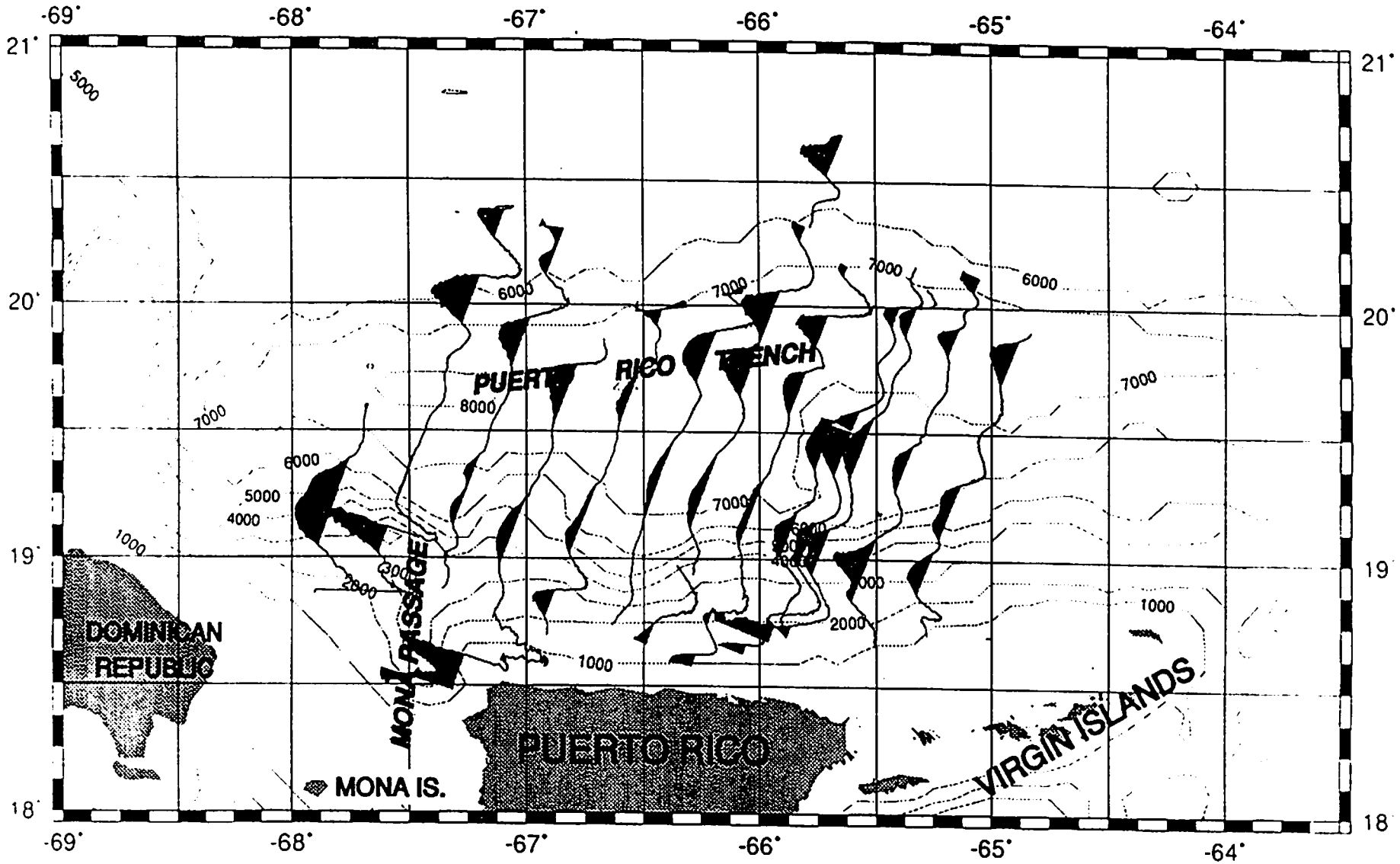

Figure 17.5 - Variable area display of along track magnetic data in the Puerto Rico Trench (EW96-05).

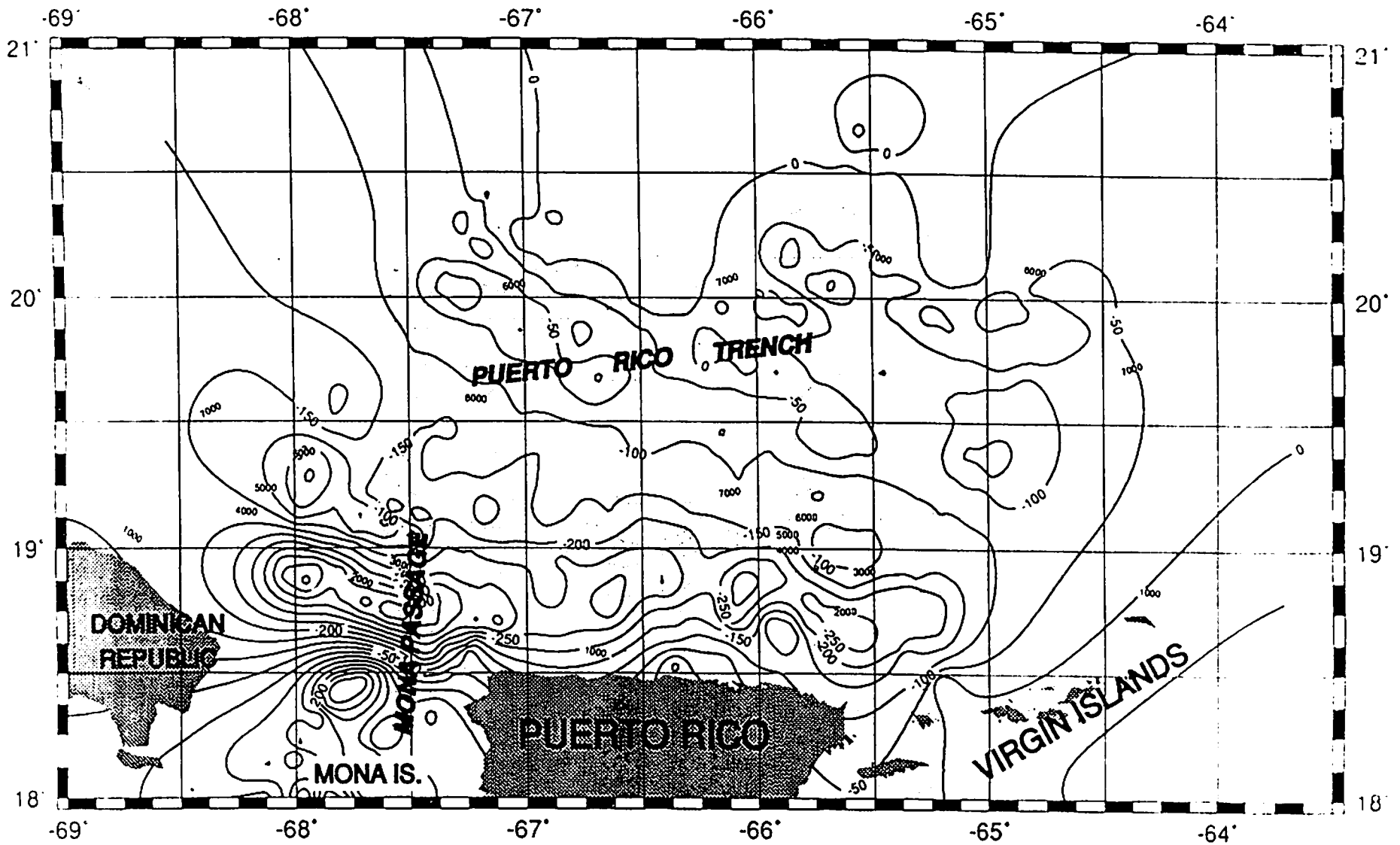

Figure 17.6 - Contoured magnetic data in the Puerto Rico Trench(EW96-05).

CHAPTER 18. REVIEW OF EXISTING LITERATURE

18.1. Review of Crustal Structure inStudy Area

By Nancy Grindlay, Steve Muszala and Wilfredo Rosado

Since the late 1950's a number of geophysical and geological surveys have been conducted in the general region of the Puerto Rico trench. These include marine seismic reflection/refraction studies, airborne and marine magnetic studies and marine gravity studies and seafloor sampling. In this chapter several of these studies will be reviewed giving special emphasis to those studies that pertain to the crustal structure of the Outer Rise and the Puerto Rico trench, including the Main Ridge and the northern Puerto Rico/Virgin Island margin.

Magnetic Studies of Puerto Rico Trench

Griscom and Geedes (1966) analyze aeromagnetic data collected by the US Naval Oceanographic Office over the Puerto Rico trench and outer rise in 1962. Numerous linear anomalies generally about 10-20 wide with pronounced northwest/southeast trends are observed on the outer rise (Fig. 18.1.1 a and b). They find a prominent magnetic anomaly north of the trench, a linear high trending roughly N50W with an amplitude of 500 gammas. The anomaly is believed to be caused by a bathymetric high more than 100 km long and 13 km wide. The magnetic anomaly extends approximately 220 further northwest of their survey area (Burton, 1965 ,unpub; Bracey 1968). The source of these anomalies is believed to be a susceptibility contrast (serpentinites juxtaposed basalts in the underlying Cretaceous oceanic basement.

Bunce et al., (1974) note an additional series of magnetic anomaly highs. These trend approximately N20E-N30E and are interpreted to be a seafloor spreading anomaly pattern, the Keithley sequence, an anomaly pattern identified by Vogt et al., (1971), which has a similar trend, wavelength and amplitude.

It appears that from these patterns that the outer rise has formed near the boundary between two magnetic provinces. On the north the magnetic anomalies trench north-northeast, whereas south of the ridge the trends are east-southeast. This boundary is believed to extend from the Bahama Platform to the Anegada Passage (Fig. 18.1.2). Bunce et al., 1974 reason that the two different magnetic provinces formed as the result of sea floor spreading s different plate pairs moved apart to form the equatorial Atlantic and Caribbean. The north-northeast-trench anomalies most likely were formed as a result of the separation of Africa from North American and the south-southeast trends formed as South America moved away from Africa.

The magnetic data collected during the EW96-05 cruise also identify a series of N50W trending highs (Figs. 17.5 and 17.6) over the outer rise. There is a high amplitude short-wavelength anomaly is associated with a bathymetric high, not identified by Bunce or Griscom and Geddes (1966), believed to be an aseismic ridge associated with a fracture zone (Fig 18.1.3a). This aseismic ridge may be an extension on the North American plate of the Main Ridge, presumably a ridge formed as the result of oblique collision of the aseismic ridge on the northern Puerto Rico/Virgin Island margin (McCann and Sykes, 1984). This aseismic ridge may extend as far southeast at the Barracuda ridge which is presently impinging on the Lesser Antilles forearc.

Griscom and Geedes (1966) observe an area of very flat constant gradient magnetic pattern with a few very wide low amplitude anomalies associated with the deepest parts of the trench and its south slope. They propose that the relatively flat anomaly patterns are associated with the most deeply buried portions of the Puerto Rico Trench. Three hypotheses are put forth to explain the relatively flat anomaly pattern: 1) rocks similar to those of the outer ride are found beneath the sediments of the Puerto Rico Trench but in the process of

subduction and burial their remanent magnetization has been partly destroyed by low-grade metamorphism, 2) the rocks beneath the trench more closely resemble the less magnetic rocks of the Puerto Rico Island arc than the more magnetic rocks of the outer ridge. 3) Some other kind of rocks exists at the base of trench. Some combination of 1 and 2 seem to be the most plausible explanation.

The EW96-05 magnetic data indicate a broad low amplitude positive anomaly is associated with the Main Ridge (Fig. 18.1.3b). This would support the idea that the Main Ridge is not highly magnetic oceanic crust obducted on the northern island slope. Rather it is more likely that less magnetic island arc material is being pushed upward as the Caribbean plate overrides the aseismic ridge on the North American plate.

A transverse aeromagnetic line of Mona Canyon shows no magnetic expression (Griscom and Geddes, 1966), therefore they hypothesize that sedimentary rocks are exposed on the canyon walls. Just west of the canyon a high amplitude anomaly is associated with a topographic high (Mona Block). Given the documented tectonic nature of the Mona Canyon, Griscom and Geddes,(1966) suggest that the Mona block is an upthrust piece of metamorphic and or igneous material.

Griscom and Geddes (1966) identify a large magnetic minimum is identified in the region between Puerto Rico and Anegada Island (Fig 18.1.1a and b). This is an area of low-amplitude and possible shallow depth anomalies. The northern limit of this area is abrupt and curvilinear indicating the possibility of a fault (Griscom and Geddes, 1966). The southern limit of this low amplitude area is also abrupt and perhaps indicates a sudden change in lithology (carbonate platform to island arc?) Depth determinations from the aeromagnetic data indicate that the magnetic rocks are located within 2 km of the surface.

Gravity Studies of the Puerto Rico Trench

The Puerto Rico Trench is associated with the world's largest free air-gravity anomaly. Vening Meinesz first measured the large negative anomaly during a submarine crossing of the trench (Vening Meinesz et al., 1934). Studies that have followed since this initial measurement have defined the extent and trend of the negative anomaly and also have identified a linear trench-parallel positive anomaly over the outer rise (Talwani et al., 1959; Bowin, 1971, 1972)(Fig 18.1.4). Treadgold (1985) reports that the peak amplitude of the gravity high on the outer rise lies 110 km seaward to the Puerto Rico Trench axis and appears to follow the basement topography.

On the basis of seismic refraction studies Talwani et al, (1959) explained the low negative anomaly as a thick accumulation of relatively low density sediments and crustal material with in an extension graben. Later as plate tectonic became an accepted paradigm, the anomaly was interpreted in context of a subducting lithospheric slab beneath the Caribbean plate. Until recently, however, the cause of the unique nature of the negative anomaly has not be addressed. Dillon and Coleman (in review) suggest that the large negative anomaly is caused by the interaction of the southward dipping North American plate with the northward dipping Caribbean plate beneath Puerto Rico. Loading of the North American plate and buoying up of the Caribbean generates a down to the north tilting of the substructure of the plate boundary zone beneath Puerto Rico which may account of the tilting of the Pliocene limestone beds on the north coast of Puerto Rico.

Bowin (1971, 1972) have identified a +20 free air gravity anomaly high 25-0 south of the outer rise and directly north of a gravity low in the Puerto Rico Trench. The closed positive anomaly is associated with a ridge near 21°N and lies directly north of the area of minimum value over the trench. This high is also observed in the EW96-05 free-air anomaly data set. Data plotted along track (Fig 18.1.3A) show that the positive anomaly occurs over a

bathymetric high on the North American plate which is presumed to be an aseismic ridge associated with a fracture zone. Gravity modeling of seismic ridges elsewhere in the Caribbean have shown that they are uncompensated, nonbuoyant features (Birch, 1970).

Seismic Refraction Studies in the Puerto Rico Trench

There are four important seismic refraction lines that bear mentioning in relation to the Puerto Rico Trench. They are found in Bunce et. al. (1974), Officer et. al. (1957) , Talwani et. al. (1959), and Treadgold (1985). All of the refraction lines contain similar cross-sections and compressional wave velocities.

Bunce et. al. (1959) using a Molnar and Sykes (1969) refraction line (Fig. 18.1.5a & 18.1.5b), found that the layers with compressional wave velocities of 2.0, 5.2 and 6.6 km/s are continuous from the Nares Basin to the north slope of the trench. The 4.2 km/s layer pinches out at 21° 30' N. The 2.0 km/s each correspond to transparent sediments while the 4.2 km/s indicates stratified sediments. Both the 5.2 and 6.6 km/s layers are indicative of oceanic basement. Below this, the mantle is seen with compressional wave velocities of approximately 8.0 km/s. Under the trench itself, a different velocity profile is found. Here, there is a sedimentary layer with higher than 3.8 km/s velocities that overlays a section of 6.0 km/s layer (oceanic basement) Under this there is a layer of 7.2 km/s that lies over a 7.9 km/s layer. The 7.2 km/s layer has been found in other active orogenic regions such as mid-ocean ridges and some Pacific troughs and trenches (Bunce and Fahlquist, 1962).

Talwani et. al. (1959) found a similar velocity to that found in the Bunce et. al. (1974) paper (Fig. 18.1.6a & 18.1.6b) Talwani et. al. (1959) find a 2.1 km/s layer (transparent sediments) that overlays a layer with 3.8 km/s compressional wave velocities. This could be interpreted as belonging to the layered sediments that Bunce et. al. had found. Below this, a 5.5 km/s layer is found. Although different from the 5.2 and 6.6 km/s layer found in Bunce et. al. (1974). this could be indicative of oceanic basement. Below these first three layers, there lie a 7.0 km/s layer and a 8.2 km/s layer. The 7.0 km/s layer is probably the intermediate layer found in Bunce et. al. (1974), while the 8.2 km/s layer is mantle material.

Officer et. al. (1957) conducted a series of seismic refraction lines that trended approximately east-west in the Puerto Rico Trench. Although the data had to be correlated to produce a north-south profile and data are therefore sparse, there exist certain similarities in the compressional wave velocities that Bunce et. al. (1974) and Talwani et. al. (1959) found. Officer et. al. (1957) finds a crustal velocity of 6.3 km/s and a mantle velocity of 8.0 km/s. Officer et. al. (1957) note that the crustal velocity in the Puerto Rico Trench is lower than the average 6.5 km/s compressional wave velocities of the Atlantic crust. A thickening of the crust from 4 km to 7 km was also found toward the deeper part of the trench.

Through the analysis of multichannel seismic (MCS) data, nineteen sonobuoys, and three expanding spread profiles (ESP's) Treadgold (1985), characterizes the crust found north of Puerto Rico. In his study of the Puerto Rico Trench, the Greater Antilles Outer Ridge and the Nares Abyssal Plain (Fig. 18.1.8a), Treadgold (1985) found that the NE-SW mantle ridge high is offset by a fracture zone (Fig. 18.1.8b). McCann and Sykes (1984) found an aseismic ridge trending northeast-southwest in their study of the Puerto Rico Trench (Fig. 18.1.9). Figure 18.1.10 shows that the aseismic ridge is parallel to the Treadgold (1985) fracture zone and both the aseismic ridge and the fracture zone are perpendicular to the mantle high.

The general stratigraphy that Treadgold (1985) found is as follows: The uppermost layer is acoustically transparent material made up of a brown homogeneous silty clay with minor biogenic material. Underlying this is a layer of strongly reflective stratified sediments deposited by turbidity currents. Underneath these first two layers is the oceanic crust, which is divided into three distinct layers. They are a 3.8 km/s layer, a 5.1 km/s layer and a 6.0 km/s

layer. The average thickness of the crust was calculated to be 1.8 - 2.0 km. Beneath this, there is a layer with a velocity of 6.6 km/s and 7.2 km/s. This layer is has an average thickness of 4.3 km and is composed of gabbro, metagabbro and some ultramafics. The last layer records velocities between 7.5 km/s and 8.2 km/s. This increase in velocity occurs at the Mohorovicic discontinuity and is thought to occur as the result of a petrologic change from serpentinized ultramafics to unaltered ultramafics (Clague and Straley, 1977).

Dredge Results for the Puerto Rico Trench

In this section three papers on coring and dredging within the Puerto Rico trench are discussed. The location of cores and dredges are shown in Figure 18.1.11. The geographic positions and a short description of the each core and dredge are present in Appendix III.

Conolly and Ewing, 1967, Sedimentation of the Puerto Rico Trench. In this paper the Puerto Rico trench is divided into five separate lithotectonic sections (Fig. 2.1):

1. Slope
2. South wall scarp
3. Main ridge, basin ridge and lower north wall
4. North wall scarp and outer ridge
5. Trench floor

Holocene through Upper Cretaceous sediments are present in the Puerto Rico trench area. All samples described by this paper come from cores taken in the above mentioned areas (Fig. 18.1.12).

Slope. The term slope is used to name the upper part of the slope that makes up the southern part of the Puerto Rico trench. It is covered by 400-500 m of sediments with bedding conforming to the slope of the area. These beds are cut by numerous canyons coming from Puerto Rico and the Virgin Islands. The sediments that are present in this sections are:

-brownish gray to greenish gray lutite (lutite refers to homogeneous silty clays or clayey silts).
-yellow calcareous sands composed mainly of shallow warm water organisms, serpentine and quartz.
-foraminiferal ooze

All of these sediments are mostly Holocene in age. Some upper Miocene fossils were found in the greenish-gray lutite.

South Wall Scarp. The scarp is devoid of stratified sediments. Cores from this area consist of:

-Pleistocene-age brown lutite, silts and sands.
-Upper to lower Miocene-age olive-green lutite
-serpentinized peridotite
-tertiary-age limestone

Main ridge, basin ridge and lower north wall. The sediments in this area are mostly composed of Miocene abyssal brown lutites with minor amounts of calcareous sands. Of the six cores taken at this area, four contained slumped or faulted zones, while the other two contained gray and green lutites and thin layers of calcareous sands.

North wall scarp and outer ridge. Seismic reflection studies of the outer ridge (Bunce and Fahlquist, 1962) imaged three different layers of rocks, with velocities of 2.2, 5.3, and 6.6 km/s. Dredge results (Hersey, 1962) of the north wall at this site indicate that the middle layer (5.3 km/s) whose top is 6 km deep, is made out of Cenomian andesitic volcanics, interbedded with cherts, and that the lower layer (6.6 km/s) whose top is 8 km deep, is probably altered ultrabasic rocks.

The cores taken at this site are mostly composed of burrowed brown lutite. The bottom currents with speeds of 5-10 cm/s consistently move fine suspended sediments in this area.

Trench floor. There are two abyssal plains that make up the floor of the trench shown in Figure 2.1; an elevated plain which dips northwestward into the main plain. Cores taken at both areas consist of sediments deposited by turbidity currents. They consist of graded beds made out of calcareous sands, silts, and gray and brown clays. Three different types of graded beds are present. This variation is based on the difference in color of the upper clay layer. The sand layers are fairly similar in composition throughout the abyssal plains. They are made mostly of sediments derived from the Puerto Rico-Virgin Islands shelf. However, there are some amounts of slope and wall material scraped off while being transported down to the trench by tubidity flows.

The chief process for the erosion and the transportation of sediments into the Puerto Rico trench are turbidity currents. These turbidity currents originate at the Puerto Rico-Virgin Islands shelf, and move down slope through the canyons in the southern slope of the Puerto Rico trench. These currents converge at the entrance into the elevated basin south of the main trench basin; then move southwestward into the main abyssal plain where they spread laterally all over the main plain.

Nalwalk, 1969, Geology of a Portion of the North Wall of the Puerto Rico Trench. Dredge results from the north wall of the Puerto Rico trench indicate the presence of a thick accumulation of rock types consisting of siliceous mudstones, cherts, basalts, serpentinites, volcanic wackes and limestone.

A tentative stratigraphic sequence for the north wall according to their results in descending order is:

-Recent unconsolidated sediments
-Pliocene basalts
-Pre-Pliocene volcanic wackes
-Eocene-Pliocene siliceous mudstones and cherts
-Upper Cretaceous-Eocene serpentinites
-Upper Cretaceous-Eocene limestones
-Upper Cretaceous siliceous mudstones and cherts
-Cenomian limestones

This stratigraphic sequence is based on fossil dating in the sedimentary rocks and chemical analysis of the volcanic rocks.

Nalwalk concludes that the rocks in the north wall were formed in an ocean environment. This is based on the fossil content of the sedimentary rocks and limestones dredged from the wall. Theses sedimentary rocks were deposited in deep ocean environments and contain numerous planktonic radiolarian and foraminifera. The basalts underlying are similar to MORB type basalts.

The basalts in the north wall have low magnetic susceptibilities and a high remanent magnetism. The suggests that the basalts were quickly quenched and have small magnetite crystals with small magnetic domains. It is likely that this remanent magnetism is the main type of magnetism measure by previous magnetic surveys in the area.

The basalts in the north wall are Pliocene in age. However, they are different from the basalts of equivalent age extruded along the inner island arc in that their K_2O and MgO contents are lower and higher, respectively. The reaffirms the above statement, that these basalts are of oceanic origin and differ from the basalts in the Lesser and Greater Antilles. Moreover, the basalts from the north wall are ocean type tholeiitic in composition.

Perfit, Heezen and others, 1980, Chemistry, origin, and tectonic significance of metamorphic rocks from the Puerto Rico Trench. Three sections in and around the Puerto Rico trench were chosen for dredging during the extent of this survey. There three regions were the south wall of the Puerto Rico trench, the north wall of the Puerto Rico trench and the Mona Canyon. The results from the study of the dredge hauls reveals three different lithologic groups, one at each of the regions surveyed.

South Wall: Marble, calc-schist, mica-schist, greenschist, amphibolite, magnesian schist and serpentinite. At shallower depths, limestones, cherts and other sedimentary rocks.
North Wall: Tholeiitic basalts, serpentinite and deep sea sediments characteristic of Atlantic oceanic crust.
Mona Canyon: Mainly igneous rocks, volcanic breccias, limestones and calcilithite that have been slightly metamorphosed. The above rocks are overlain by middle Eocene to Miocene and younger limestones.

The metamorphic rocks are similar to those exposed in subaerially exposed melanges that are believed to be subduction complexes. This is based on the mineral assemblages and phase relations observed in the metamorphic rocks of the south wall of the Puerto Rico trench. Conditions of 400°C to 500°C and 3 to 7 kbar are estimated for the metamorphic rock in the Puerto Rico trench.

Chemical analyses of the metamorphic rocks in the south wall suggest that these metamorphic rocks were island arc igneous rocks. The protoliths of the marbles and calc-schists were carbonates and arc-derived pelagic sediments.

Other results suggest that:
-the basalts and the serpentinites dredged from the north wall are geochemcially similar to oceanic tholeiites (MORBs) and ultramafics.
-only two greenschist collected in the south wall are geochemically similar to MORBs.
-the magnesian-schist and serpentinte collected at the south wall have either been severely metasomatized or represent metamorphosed ultrabasic rocks from under the Greater Antilles.
-a great amount of material derived from the volcanic arc has been accreted on the south wall, while the amount of oceanic crust incorporated in the subduction wedge has been minor.

Hispaniola - Puerto Rico trench Metamorphic belt. West of the south inner trench wall limestones and marbles, identical to the ones dredged a the Puerto Rico trench south wall, crop out in the blueschist belt in the Samana Peninsula in northern Hispaniola. South of the Puerto Rico trench, low-grade metavolcanics in Puerto Rico seem to be continuous across the Mona Canyon to Central Hispaniola. This belt is parallel to the blueschist complex in the inner trench. This constitutes a paired belt, a blueschist belt in the inner trench and a greenschist belt south of the Puerto Rico trench (Fig. 18.1.13). These paired metamorphic belts extend more than 500 km along the northern Caribbean plate boundary.

The development of these belts is most likely due to the inception of the Puerto Rico trench during the middle to late Cretaceous with the southerly subduction of the Atlantic plate under the Caribbean plate. Then an eastward movement of the Caribbean plate relative to the North American plate in the late Cretaceous to early Tertiary started transcurrent and tension faulting which increased the uplift of the metamorphosed subduction wedge. During the late Eocene local tectonic readjustment started to produce the graben-like (?) trench observed at present.

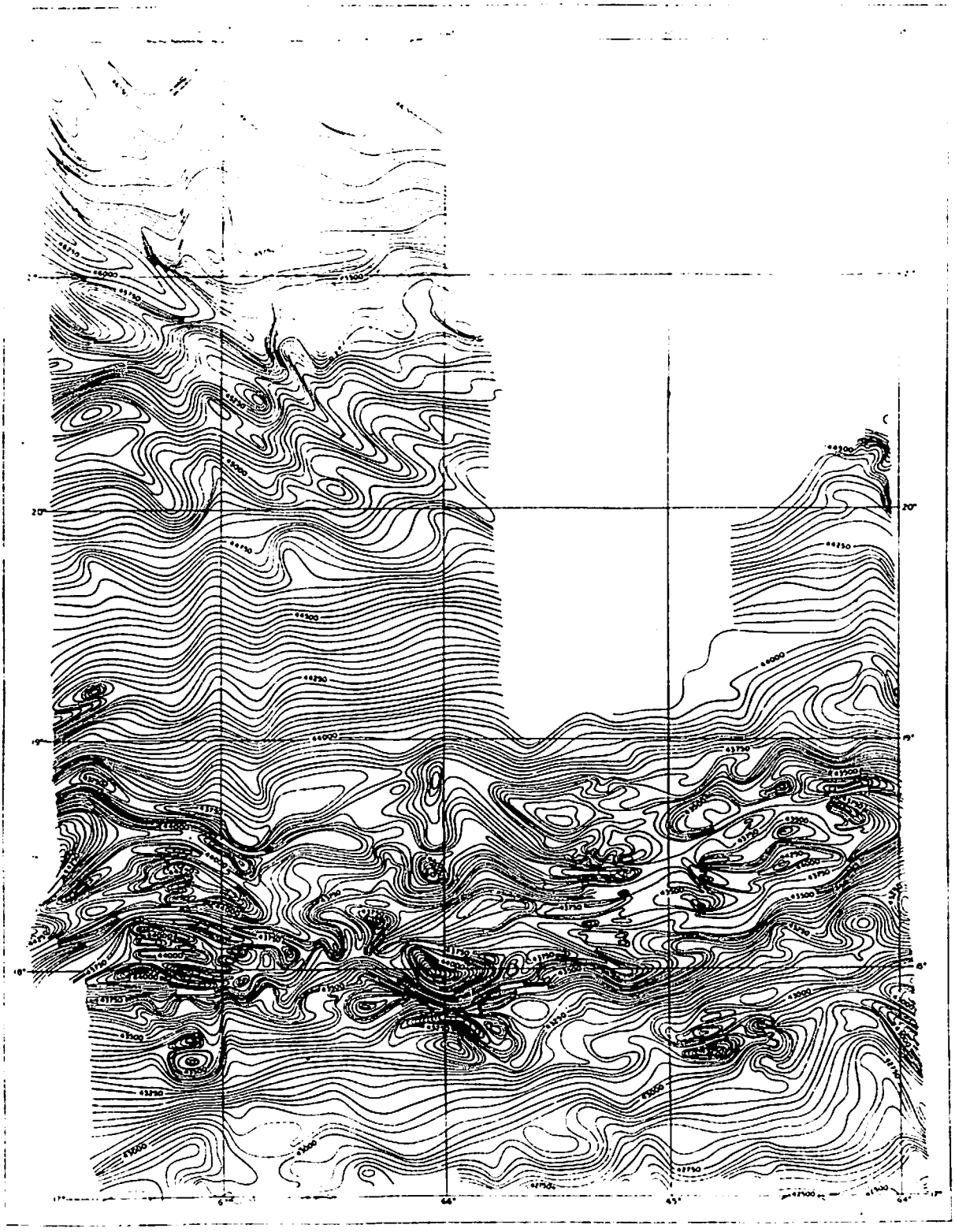

Figure 18.1.1A Magnetic Anomaly Data from Griscom and Geddes (1966).

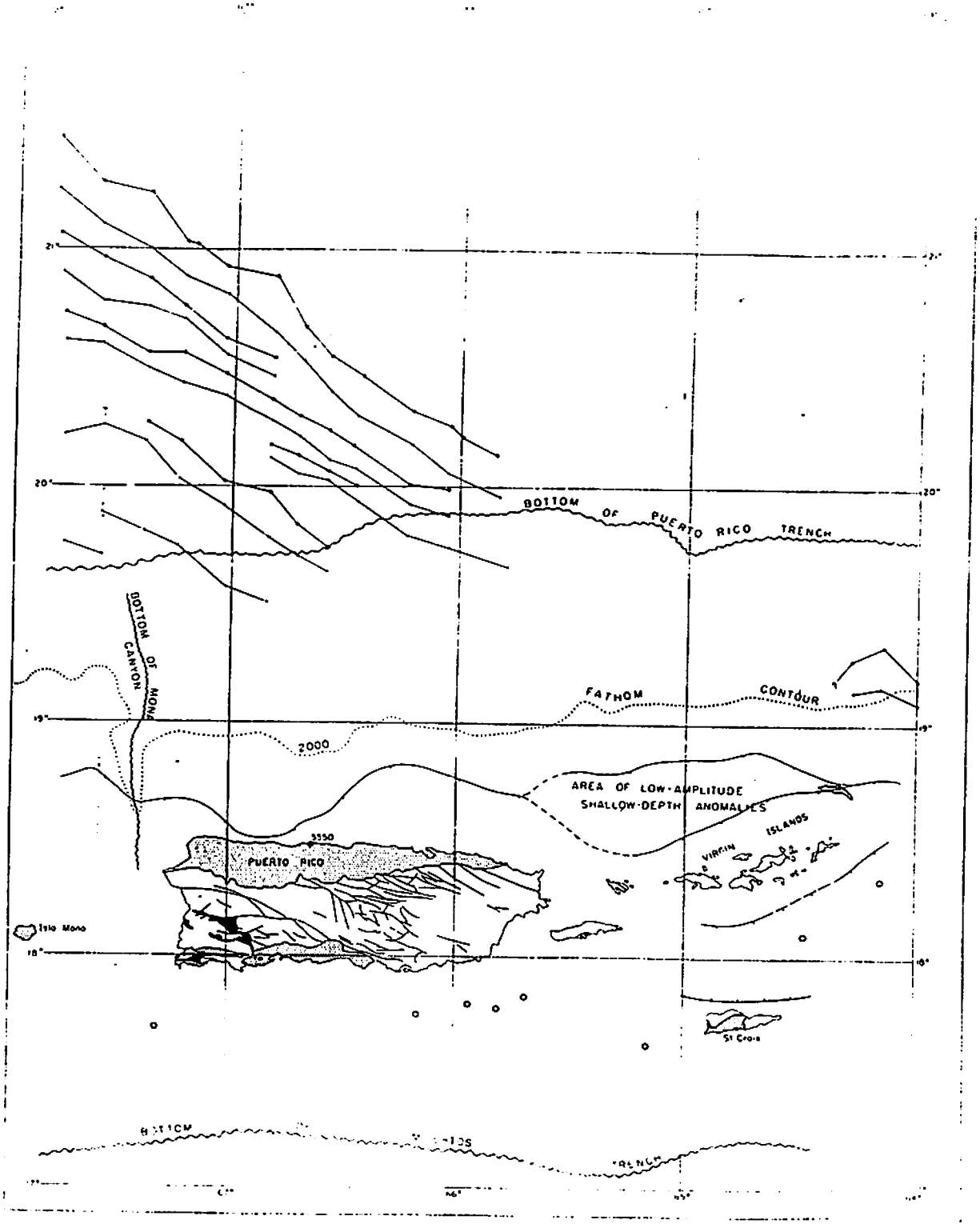

Figure 18.1.1B Interpretation of magnetic anomaly data from Griscom and Geddes (1966).

Table 5.1

Single Channel Seismic data table

Line 1

start-point	JD 167	22.41'58"	18 40' 635 N	66 03' 118 W		SP 100
CC-point1	JD 168	08.19'	19 33' 957 N	65 42' 164 W		SP 2194
CC-point2	JD 168	09.18'	19 34' 08 N	65 48' 55 W		SP 2429
CC-point3	JD 168	18.15'	18 58' 240 N	66 02' 910 W		SP 3631
CC-point4	JD 168	21.32'	18 55' N	66 17' W	WP 59A	SP 4475
end-point	JD 168	23.02'59"	18 37' N	66 22' 0 W	WP 59	SP 4865
reelnumber	100	SP 100	SP 1002	902	10 sec.	prline1
reelnumber	101	SP 1003	SP 2002	999	10 sec.	prline1
reelnumber	102	SP 2003	SP 3003	1000	10 sec.	prline1
reelnumber	103	SP 3004	SP 3261	257	10 sec.	prline1
reelnumber	104	SP 3263	SP 4118	855	12 sec.	prlin1a
reelnumber	105	SP 4119	SP 4865	746	12 sec.	prlin1a

In this line we made a several course changes.
CC 1 from 20 degrees to 285 degrees. CC 3 from 200 degrees to 227 degrees.
CC 2 from 285 degrees to 200 degrees. CC 4 from 227 degrees to 285 degrees.
During recording of line 1 we made a turn in the line. This was between 12 hrs. 55 min. and 16 hrs. 49 min.

Line 3

start-point	JD 168	23.21'22"	18 37' 957 N	66 25' 724 W		SP 4871
fin. turn-point	JD 169	00.32'	18 41' 192 N	66 28' 772 W	WP 56	SP 6689
end-point	JD 170	04.03'22"	20 41' 271 N	65 37' 748 W	WP 57B	SP 10698
reelnumber	106	SP 4871	SP 5727	856	12 sec.	prline3
reelnumber	107	no SP recorded on this reel				
reelnumber	108	SP 5729	SP 6586	857	12 sec.	prline3
reelnumber	109	SP 6587	SP 6683	96	12 sec.	prline3
reelnumber	110	SP 6689	SP 7544	855	14 sec.	prlin3a
reelnumber	111	SP 7545	SP 8275	730	14 sec.	prlin3a
reelnumber	112	SP 8278	SP 9133	855	14 sec.	prlin3a
reelnumber	113	no SP recorded on this reel				
reelnumber	114	SP 9135	SP 9990	855	14 sec.	prlin3b
reelnumber	115	SP 9991	SP 10698	707	14 sec.	prlin3b

Between line 3 or SP 6683 and line 3a or SP 6689 9 min. 25 sec. not recorded.
During recording of line 3 we made 2 turns in the line. The first turn was between SP 5870 and SP 6234.
The second turn was between SP 8276 and SP 8514.
Missing SP on line 3 : 5728, 6684-6688, 9134

Line 4

start-point	JD 170	04.14'01"	20 41' 271 N	65 37' 748 W		SP 10700
fin. turn-point	JD 170	05.21'	20 39' 31 N	65 29' 92 W	WP 60B	SP 10952
end-point	JD 171	04.29'13"	18 31' 09 N	66 21' 54 W		SP 16157
reelnumber	116	SP 10700	SP 11557	857	14 sec.	prline4
reelnumber	117	SP 11558	SP 12415	857	14 sec.	prline4
reelnumber	118	SP 12416	SP 13275	859	14 sec.	prline4
reelnumber	119	SP 13276	SP 14132	856	14 sec.	prline4
reelnumber	120	SP 14133	SP 14989	856	14 sec.	prline4
reelnumber	121	SP 14990	SP 15846	856	14 sec.	prline4
reelnumber	122	SP 15849	SP 16157	308	14 sec.	prline4

Missing SP on line 4 : 15847,15848

Line 5

start-point	JD 171	06.19'28"	18 32' 171 N	66 08' 524 W		SP 16160
fin. turn-point	JD 171	08.15'	18 34' 989 N	66 17' 454 W	WP 100	SP 16655
end-point	JD 172	01.43'34"	20 10' 003 N	65 33' 334 W	WP 101	SP 20736

reelnumber	123	SP 16160	SP 17015	855	12 sec.	prline5
reelnumber	124	SP 17016	SP 17872	856	12 sec.	prline5
reelnumber	125	SP 17873	SP 17973	100	12 sec.	prline5
reelnumber	126	SP 17975	SP 18832	857	14 sec.	prline5a
reelnumber	127	SP 18833	SP 19690	857	14 sec.	prline5a
reelnumber	128	SP 19691	SP 20548	857	14 sec.	prline5a
reelnumber	129	SP 20549	SP 20736	187	14 sec.	prline5a

Between line 5 or SP 17973 and line 5a or SP 17975 4 min. 30 sec. not recorded.
Missing SP on line 5 : 17974

Line 6

start-point	JD 172	01.50'43"	20 09' 986 N	65 32' 432 W	WP 101	SP 20738
fin. turn-point	JD 172	02.42'	20 09' 994 N	65 29' 45 W	WP 102	SP 20931
end-point	JD 172	18.54'03"	18 39' 993 N	66 07' 670 W	WP 103	SP 24544

reelnumber	130	SP 20738	SP 21594	856	14 sec.	prline6
reelnumber	131	no SP recorded on this reel				
reelnumber	132	SP 21596	SP 22451	855	14 sec.	prline6
reelnumber	133	SP 22452	SP 23308	856	14 sec.	prline6
reelnumber	134	SP 23309	SP 23624	315	14 sec.	prline6
reelnumber	135	SP 23626	SP 24482	856	12 sec.	prlin6a
reelnumber	136	no SP recorded on this reel				
reelnumber	137	SP 24484	SP 24544	60	12 sec.	prlin6a

Between line 6 or SP 23624 and line6a or SP 23626 8 min. 56 sec. not recorded
Missing SP on line 6 : 21595, 23645, 24483

In this line is a little shift	SP 22367	19 34' 572 N	65 43' 742 W
to the West between	SP 22600	19 29' 658 N	65 47' 604 W

Line 7

start-point	JD 172	19.04'59"	18 39' 993 N	66 07' 670 W	WP 103	SP 24546
fin. turn-point	JD 172	20.42'	18 40' 66 N	65 57' 78 W	WP 104	SP 24910
end-point	JD 173	12.37'47"	20 09' 526 N	65 19' 722 W	WP 105	SP 28470

reelnumber	138	SP 24546	SP 25403	857	12 sec.	prline7
reelnumber	139	no SP recorded on this reel				
reelnumber	140	SP 25405	SP 25641	236	12 sec.	prline7
reelnumber	141	SP 25643	SP 26500	857	14 sec.	prlin7a
reelnumber	142	SP 26501	SP 27357	856	14 sec.	prlin7a
reelnumber	143	SP 27358	SP 28214	856	14 sec.	prlin7a
reelnumber	144	SP 28215	SP 28470	255	14 sec.	prlin7a

Between line 7 or SP 25641 and line7a or SP 25643 6 min. 56 sec. not recorded
Missing SP on line 7 : 25404, 25642

Line 8

start-point	JD 173	12.45'47"	20 04' 649 N	65 18' 918 W	WP 105	SP 28472
fin. turn-point	JD 173	14.07'	20 04' 798 N	65 12' 798 W	WP 106	SP 28779
end-point	JD 174	05.21'52"	18 39' 837 N	65 49' 693 W	WP 107	SP 32334

reelnumber	145	SP 28472	SP 29327	855	14 sec.	prline8
reelnumber	146	no SP recorded on this reel				
reelnumber	147	SP 29329	SP 30184	855	14 sec.	prline8

reelnumber	148	SP 30185	SP 31042	857	14 sec.	prlin8a
reelnumber	149	SP 31043	SP 31190	147	14 sec.	prlin8a
reelnumber	150	SP 31191	SP 32047	856	12 sec.	prlin8a
reelnumber	151	no SP recorded on this reel				
reelnumber	152	SP 32049	SP 32334	285	12 sec.	prlin8a

Between line 8 or SP 28472 and line8a or SP 32334 4 min. 35 sec. not recorded
Missing SP on line 8 : 29328, 30225, 32048
SP with wrong numbers: 6477-6480 should be 29115-29118 and 7070-7078 should be 29708-29716

Line 9

start-point	JD 174	15.41'45"	18 45' 227 N	65 38' 606 W	WP 108	SP 32336
end-point	JD 175	06.04'41"	20 05'399 N	65 03' 753 W	WP 109	SP 35572

reelnumber	153	SP 32336	SP 33191	855	14 sec.	prline9
reelnumber	154	no SP recorded on this reel				
reelnumber	155	SP 33193	SP 34049	856	14 sec.	prline9
reelnumber	156	SP 34050	SP 34908	858	14 sec.	prline9
reelnumber	157	SP 34909	SP 35572	663	14 sec.	prline9

Missing SP on line 9 : 33192
SP with wrong numbers: 9863-9882 should be 32502-32522 and 9698-9699 should be 32337-32338

Line 10 and 11 only recorded MR 1 data.

Line 12

start-point	JD 176	08.54'55'	20 05' 01 N	64 58' 83 W		SP 35573
fin. turn-point	JD 176	09.34'	20 04' 001 N	64 55' 744 W	WP 112	SP 35722
end-point	JD 176	23.41'52"	18 45' 586 N	65 29' 730 W	WP 113	SP 38974

reelnumber	158	SP 35573	SP 36430	857	14 sec.	prline12
reelnumber	159	no SP recorded on this reel				
reelnumber	160	SP 36432	SP 37287	855	14 sec.	prline12
reelnumber	161	SP 37288	SP 37992	704	14 sec.	prline12
reelnumber	162	SP 37994	SP 38852	858	12 sec.	prlin12a
reelnumber	163	SP 37994	SP 38974	980	12 sec.	prlin12a

Missing SP on line 12 : 36431, 37993
Between line 12 or SP 37992 and line12a or SP 37994 11 min. 36 sec. not recorded
In the beginning of this line there is a lot of low-frequent noise in channel 4.

Line 13

start-point	JD 176	23.53'54"	18 44' 975 N	65 28' 937 W	WP 113	SP 38979
fin. turn-point	JD 177	00.57'	18 45' 492 N	65 22' 351 W	WP 114	SP 39250
end-point	JD 177	14.48'25"	20 01' 997 N	64 45' 016 W	WP 115	SP 42473

reelnumber	164	no SP recorded on this reel				
reelnumber	165	SP 38979	SP 39835	856	12 sec.	prline13
reelnumber	166	SP 39836	SP 40286	450	12 sec.	prline13
reelnumber	167	SP 40287	SP 41144	857	14 sec.	prline13
reelnumber	168	no SP recorded on this reel				
reelnumber	169	SP 41146	SP 42001	855	14 sec.	prlin13a
reelnumber	170	SP 42002	SP 42473	471	14 sec.	prlin13a

Missing SP on line 13 :41145
Between line 13 or SP 40286 and line13a or SP 40287 6 min. 37 sec. not recorded.
Reel 167, 169 and 170 give a "string is not a number" error when raeding out.

Line 14

start-point	JD 177	14.53'56"	20 02' 017 N	64 47' 374 W	WP 115	SP 42476
fin. turn-point	JD 177	16.30'	19 59' 590 N	64 40' 573 W	WP 116	SP 42835

end-point	JD 178	06.54'05"	18 39' 949 N	65 15' 894 W	WP 117	SP 1675
reelnumber	171	SP 42476	SP 43331	855	14 sec.	prline14
reelnumber	172	SP 43332	SP 44190	858	14 sec.	prline14
reelnumber	173	SP 44191	SP 44651	460	14 sec.	prline14
reelnumber	174	SP 100	SP 113	13	12 sec.	prlin14a
reelnumber	175	SP 114	SP 970	856	12 sec.	prlin14b
reelnumber	176	SP 971	SP 1675	704	12 sec.	prlin14b

Between line 14 or SP 44651 and line14a or SP 100 7 min. 34 sec. not recorded.
Reel 171, 172, 173 and 174 give a "string is not a number" error when raeding out.

Line 15

start-point	JD 178	07.01'01"	18 39' 191 N	65 15' 663 W		SP 1676
end-point	JD 178	07.06'37"	18 38' 747 N	65 15' 554 W		SP 1700
reelnumber	177	SP 1676	SP 1700	24	12 sec.	prline15
reelnumber	178	no SP recorded on this reel				

This line was cancelled right after the start because the people of the MR 1 were still busy.

Line 16

start-point	JD 178	08.40'30"	18 40' 82 N	65 13' 18 W	WP 117	SP 1705
CC-point	JD 178	11.39'	18 26' 955 N	65 14' 162 W	WP 118	SP 2471
end-point	JD 178	13.06'02"	18 33' 29 N	65 21' 01 W	WP 118A	SP 2843
reelnumber	179	SP 1705	SP 2560	855	12 sec.	prline16
reelnumber	180	SP 2561	SP 2843	282	12 sec.	prline16

In this line we made a course change from 170 degrees to 310 degrees.

Line 17 and 18 only recorded MR 1 data.

Line 19

start-point	JD 179	22.25'14"	18 39' 989 N	66 35' 938 W	WP 123	SP 2845
end-point	JD 180	14.11'29"	20 03' 270 N	66 08' 016 W	WP 124	SP 6485
reelnumber	181	SP 2845	SP 3678	833	12 sec.	prline19
reelnumber	182	SP 3680	SP 4535	855	14 sec.	prlin19a
reelnumber	183	no SP recorded on this reel				
reelnumber	184	SP 4537	SP 5392	855	14 sec.	prlin19a
reelnumber	185	SP 5393	SP 6249	856	14 sec.	prlin19a
reelnumber	186	SP 6250	SP 6485	235	14 sec.	prlin19a

Between line 19 or SP 3678 and line19a or SP 3680 3 min. 35 sec. not recorded.
Missing SP on line 19 :3679, 4536

Line 20

start-point	JD 180	14.40'41"	20 03' 010 N	66 10' 801 W	WP 124	SP 6490
fin. turn-point	JD 180	15.21'	20 02' 522 N	66 15' 193 W	WP 125	SP 6642
end-point	JD 181	06.09'29"	18 42' 012 N	66 50' 774 W	WP 126	SP 10050
reelnumber	187	SP 6490	SP 7347	857	14 sec.	prlin20a
reelnumber	188	SP 7348	SP 8204	856	14 sec.	prlin20a
reelnumber	189	SP 8205	SP 9061	856	14 sec.	prlin20a
reelnumber	190	SP 9062	SP 9303	241	14 sec.	prlin20a
reelnumber	191	SP 9304	SP 10050	746	12 sec.	prlin20b

Between line 20a or SP 9303 and line20b or SP 6642 4 min. 36 sec. not recorded.

Line 21

start-point	JD 181	06.16'02"	18 41' 991 N	66 51' 051 W	WP 126	SP 10053
fin. turn-point	JD 181	07.14'	18 42' 371 N	66 56' 750 W	WP 127	SP 10305

end-point	JD 181	20.48'29"	19 59' 038 N	66 25' 571 W	WP 128	SP 13440
reelnumber	192	SP 10053	SP 10909	856	12 sec.	prline21
reelnumber	193	SP 10910	SP 11208	298	12 sec.	prline21
reelnumber	194	SP 11211	SP 12068	857	14 sec.	prlin21a
reelnumber	195	SP 12069	SP 12926	857	14 sec.	prlin21a
reelnumber	196	SP 12927	SP 13439	512	14 sec.	prlin21a

Between line 21 or SP 11209 and line21a or SP 11210 8 min. 49 sec. not recorded.
Missing SP on line 21: 12070, 11209, 11210.

Line 22

start-point	JD 181	20.56'16"	19 59' 038 N	66 25' 571 W	WP 128	SP 13443
fin. turn-point	JD 181	22.08'	19 58' 344 N	66 33' 210 W	WP 129	SP 13716
CC-point	JD 182	11.40'	18 43' 978 N	67 04' 983 W	WP 130	SP 16802
end-point	JD 182	15.53'22"	18 28' 368 N	67 19' 494 W	WP 131	SP 17887
reelnumber	198	no SP recorded on this reel				
reelnumber	199	SP 13443	SP 14299	856	14 sec.	prline22
reelnumber	200	no SP recorded on this reel				
reelnumber	201	SP 14301	SP 15156	855	14 sec.	prline22
reelnumber	202	SP 15157	SP 15943	786	14 sec.	prline22
reelnumber	203	SP 15944	SP 16800	856	12 sec.	prlin22b
reelnumber	204	SP 16801	SP 17658	857	12 sec.	prlin22b
reelnumber	205	SP 17659	SP 17887	228	12 sec.	prlin22b

Between line 22 or SP 15943 and line22b or SP 15944 17 min. 4 sec. not recorded.
Missing SP on line 22 :13441, 13442, 14300
In this line we made a course change from 220 degrees to 230 degrees.

Line 23

start-point	JD 182	16.30'10"	18 30' 199 N	67 18' 721 W	WP 131	SP 17885
end-point	JD 183	07.11'56"	19 52' 979 N	66 44' 973 W	WP 132	SP 21516
reelnumber	206	SP 17888	SP 18744	856	12 sec.	prlin23a
reelnumber	207	SP 18745	SP 19601	856	12 sec.	prlin23a
reelnumber	208	SP 19602	SP 19843	241	12 sec.	prlin23a
reelnumber	209	SP 19844	SP 20701	857	14 sec.	prlin23b
reelnumber	210	SP 20702	SP 21516	814	14 sec.	prlin23b

Between line 23a or SP 19601 and line23b or SP 19602 6 min. 44 sec. not recorded.

Line 24

start-point	JD 183	07.16'11"	19 52' 912 N	66 45' 625 W	WP 132	SP 21517
fin. turn-point	JD 183	08.24'	19 52' 330 N	66 52' 217 W	WP 133	SP 21772
CC-point	JD 183	19.54'	18 48' 809 N	66 18' 759 W	WP 134	SP 24487
end-point	JD 183	22.45'26"	18 52' 549 N	66 44' 973 W	WP 135B	SP 25223
reelnumber	211	SP 21517	SP 22375	858	14 sec.	prlin24a
reelnumber	212	no SP recorded on this reel				
reelnumber	213	SP 22377	SP 23233	856	14 sec.	prlin24a
reelnumber	214	SP 23234	SP 23316	82	14 sec.	prlin24a
reelnumber	215	SP 23319	SP 24175	856	12 sec.	prlin24b
reelnumber	216	no SP recorded on this reel				
reelnumber	217	SP 24177	SP 25032	855	12 sec.	prlin24b
reelnumber	218	SP 25033	SP 25223	190	12 sec.	prlin24b

Between line 24 or SP 23317 and line 24b or SP 23318 5 min. 17 sec. not recorded.
Missing SP on line 24 : 22376, 23317, 23318, 24176.
In this line we made a course change from 220 degrees to 280 degrees.

Line 25

start-point	JD 183	22.51'30"	18 51'925 N	67 36' 486 W	WP 135B	SP 25224
fin. turn-point	JD 183	23.10'	18 53' 392 N	67 35' 696 W	WP 135C	SP 25304
CC-point	JD 183	01.07'	18 55' 725 N	67 23' 725 W	WP 135D	SP 25809
end-point	JD 184	16.09'16"	20 19'852 N	66 53' 216 W	WP 136	SP 29216

reelnumber	219	SP 25224	SP 26080	856	12 sec.	prline25
reelnumber	220	SP 26081	SP 26179	98	12 sec.	prline25
reelnumber	221	SP 26180	SP 27039	859	14 sec.	prlin25b
reelnumber	222	no SP recorded on this reel				
reelnumber	223	SP 27041	SP 27897	856	14 sec.	prlin25b
reelnumber	224	SP 27898	SP 28754	856	14 sec.	prlin25b
reelnumber	225	SP 28755	SP 29215	460	14 sec.	prlin25b

In this line we made a course change from 80 degrees to 20 degrees.
Between line 25 or SP 26179 and line 25b or SP 26180 5 min. 36 sec. not recorded.,
Missing SP on line 25 : 26181, 26182, 27040.
In this line we did a noise test. This was between SP 29147 and SP 29182.

Line 26

start-point	JD 184	16.14'40"	20 20' 053 N	66 53' 776 W	WP 136	SP 29218
fin. turn-point	JD 184	16.56'	20 21' 063 N	66 57' 973 W	WP 137	SP 29374
end-point	JD 185	07.41'27"	18 54' 990 N	67 33' 541 W	WP 138	SP 32213

reelnumber	226	no SP recorded on this reel				
reelnumber	227	SP 29218	SP 29725	507	14 sec.	prline26
reelnumber	228	SP 29734	SP 30590	856	14 sec.	prlin26b
reelnumber	229	SP 30591	SP 31178	587	14 sec.	prlin26b
reelnumber	230	SP 31180	SP 32035	855	14 sec.	prlin26c
reelnumber	231	no SP recorded on this reel				
reelnumber	232	SP 32037	SP 32213	176	14 sec.	prlin26c

Missing SP on line 26 : 29726-29733, 31179, 32036.
Between line 26 or SP 29725 and line 26b or SP 29726 1 hrs. 08 min. not recorded.
Between line 26b or SP 31178 and line 26c or SP 31179 1 hrs. 02 min. not recorded.

Line 27

start-point	JD 185	07.48'01"	18 55' 223 N	67 34' 186 W	WP 138	SP 32214
fin. turn-point	JD 185	9.09'	18 53' 021 N	67 41' 054 W	WP 139	SP 32520
end-point	JD 186	00.55'12"	20 24' 280 N	67 05' 306 W	WP 140	SP 35530

reelnumber	233	SP 32214	SP 33070	856	14 sec.	prlin27a
reelnumber	234	no SP recorded on this reel				
reelnumber	235	SP 33072	SP 33652	580	14 sec.	prlin27a
reelnumber	236	no SP recorded on this reel				
reelnumber	237	no SP recorded on this reel				
reelnumber	238	SP 33663	SP 33686	23	18 sec.	prlin27d
reelnumber	239	SP 33690	SP 34440	750	18 sec.	prlin27e
reelnumber	240	SP 34441	SP 35191	750	18 sec.	prlin27e
reelnumber	241	SP 35192	SP 35530	338	18 sec.	prlin27e

Missing SP on line 27 : 33071, 33653-3362, 33667,33668.
Between line 27a or SP 33652 and line 27d or SP 33663 17 min. 51 sec. not recorded.
Between line 27d or SP 33686 and line 27c or SP 33690 6 min. not recorded.
In the beginning of this line we made an extra turn south.
In SP 32290 at 8.08' we changed course to 290 grs and in SP 32520 at 9.19' we came on line 27 in WP 139.

Line 28

start-point	JD 186	00.58'33"	20 24' 380 N	67 05' 630 W	WP 140	SP 35531
fin. turn-point	JD 186	9.09'	20 26' 148 N	67 12' 488 W	WP 141	SP 35787
end-point	JD 186	17.55'05"	18 55' 001 N	67 48' 870 W	WP 142	SP 39343

reelnumber	242	SP 35531	SP 36388	857	14 sec.	prline28
reelnumber	243	SP 36389	SP 37245	856	14 sec.	prline28
reelnumber	244	SP 37246	SP 38102	856	14 sec.	prline28
reelnumber	245	SP 38103	SP 38959	856	14 sec.	prline28
reelnumber	246	SP 38960	SP 39343	383	14 sec.	prline28

Line 29

start-point	JD 186	18.01'36"	18 55'176 N	67 49' 580 W	WP 142	SP 39346
fin. turn-point	JD 186	18.01'	18 57' 561 N	67 55' 367 W	WP 143	SP 39585
end-point	JD 187	01.45'20"	19 35' 938 N	67 40' 375 W	WP 144	SP 41085

reelnumber	247	no SP recorded on this reel				
reelnumber	248	SP 39346	SP 40202	856	14 sec.	prline29
reelnumber	249	no SP recorded on this reel				
reelnumber	250	SP 40204	SP 41059	855	14 sec.	prline29
reelnumber	251	SP 41060	SP 41085	25	14 sec.	prline29

Missing SP on line 29 : 40203.

Line 30

start-point	JD 187	02.01'32"	19 36' 782 N	67 42' 171 W	WP 144	SP 39346
fin. turn-point	JD 187	03.00'	19 36' 674 N	67 48' 251 W	WP 145	SP 39585
end-point	JD 187	09.52'28"	18 54' 538 N	68 04' 433 W	WP 146	SP 41085

reelnumber	252	no SP recorded on this reel				
reelnumber	253	SP 41088	SP 41943	855	14 sec.	prline30
reelnumber	254	SP 41944	SP 42800	856	14 sec.	prline30
reelnumber	255	SP 42801	SP 42854	53	14 sec.	prline30

Missing SP on line 29 : 40203.
Speed up to 6.6 knots.

Line 31

start-point	JD 187	10.01'23"	18 53' 753 N	68 03' 791 W	WP 146	SP 42858
end-point	JD 187	17.29'56"	18 37' 265 N	67 15' 061 W	WP 147	SP 44517

reelnumber	256	no SP recorded on this reel				
reelnumber	257	SP 42858	SP 42889	31	12 sec.	prline31
reelnumber	258	SP 42889	SP 43745	856	12 sec.	prlin31a
reelnumber	259	SP 43746	SP 44517	771	12 sec.	prlin31a

The pop rate was 16 sec. in stead of 14. sec.
Between line 21 or SP 42889 and line 31a or SP 42889 7 min. 11 sec. not recorded.

Line 32

start-point	JD 187	17.33'59"	18 37' 043 N	67 15' 444 W	WP 147	SP 44518
end-point	JD 187	21.22'15"	18 16' 571 N	67 28' 777 W	WP 148	SP 45377

reelnumber	260	SP 44518	SP 45377	859	12 sec.	prline32

The pop rate was 16 sec. in stead of 14. sec.

Line 33

start-point	JD 188	00.07'36"	18 10' 210 N	67 40' 681 W		SP 45389
end-point	JD 188	01.41'52"	18 01' 229 N	67 45' 883 W	WP 150	SP 45741
reelnumber	261	no SP recorded on this reel				
reelnumber	262	no SP recorded on this reel				
reelnumber	263	SP 45389	SP 45741	352	14 sec.	prline33

Line 34

start-point	JD 188	01.45'34"	18 00' 955 N	67 46' 226 W	WP 150	SP 45744
end-point	JD 188	08.09'56"	18 01' 870 N	68 27' 086 W	WP 151	SP 47185
reelnumber	263	SP 45744	SP 46600	856	14 sec.	prline34
reelnumber	264	no SP recorded on this reel				
reelnumber	265	SP 46602	SP 47185	583	14 sec.	prline34

Missing SP on line 34 : 46601.

Line 35

start-point	JD 188	08.20'48"	18 02' 791 N	68 27' 086 W	WP 151	SP 47186
fin. turn-point	JD 188	8.33'	18 03' 71 N	68 26' 59 W	WP 152	SP 47243
CC-point	JD 188	13.20'	18 15' 402 N	67 56' 176 W	WP 153	SP 48472
CC-point	JD 188	15.20'	18 26' 299 N	67 48' 705 W	WP 154	SP 49000
end-point	JD 188	20.00'48"	18 38' 015 N	67 15' 240 W	WP 155	SP 50186
reelnumber	266	SP 47186	SP 48043	857	12 sec.	prlin35b
reelnumber	267	SP 48044	SP 48900	856	12 sec.	prlin35b
reelnumber	268	SP 48901	SP 49758	857	12 sec.	prlin35b
reelnumber	269	SP 49759	SP 50186	427	12 sec.	prlin35b

CHAPTER 6. PROCESSING PLAN AT UTIG FOR THE SCS DATA

by Jean Paul van Gestal and Paul Mann

The processing plan of the seismic data at UTIG will consist of two parts:

1. Additional Processing. Process all the lines with the above described processing sequence including migration. With the use of better previewing tools not available on EW96-05, it will be easier to carry out deconvolution and AGC. It was also not possible to make a frequency spectrum of the data on the cruise. This will be done at UTIG using Matlab to improve the filter settings.

2. Interpretation of the seismic lines. We will use the GeoQuest software package. This software allows interactive onscreen digitization of reflective horizons, creation of interpretive cross-sections and various map projections. In addition to the state-of-art processing facilities, UTIG is considered the ideal location for data analysis because of the accessibility of existing MCS data sets of the Caribbean region, including several lines over the Puerto Rico trench study area.

The following data seismic reflection data sets will be merged with the one collected during EW96-06:

- We plan to migrate about 1400 km of existing 48 channel data collected in 1981 in the area of the Main Ridge as part of the North Atlantic transect (NAT) study (Treadgold, 1985) and described by Larue (in press). These data are archived at UTIG.

- We plan to migrate an extensive 24 channel, stacked Western Geophysical MCS data collected in 1975 along the north coast and in the Mona Passage area. These tapes are stored at the Department of Geology of the University of Puerto Rico and are described by Larue (1987) and Meyerhoff et al. (1987). One tape will be examined to insure that the tapes are still readable.

- We plan to migrate onland and offshore multichannel data collected during the drilling of the Toa Baja well (Larue, 1993). These data are housed at the University of Puerto Rico.

- We plan to migrate older MCS data housed at UTIG that include the VB lines (need more info).

CHAPTER 7. HYDROSWEEP SYSTEM
by Araceli Munoz

The Atlas Hydrosweep echosounder was developed by the German company Krupp Atlas Elektronik. Derives its name from the expression: "HYDROgraphic multibeam SWEEPing survey echosounder". Hydrosweep belongs to the family of multibeam sweeping survey systems with a broad coverage of 90° perpendicular to the ship's longitudinal axis (Fig. 7.1). The equipment is used for the hydrographic surveying of areas in both shallow and deep water. In order to be able to measure bathymetry optimally in all depth ranges without an operator having to intervene in the process, the equipment automatically adapts the necessary transmitting and receiving modes to the depth in a range from 10 to over 10,000 m.

Hydrosweep works by transmitting beams with a frequency of 15.5 kHz. The centerlines of adjacent beams are about 1.53°. Table 7.1 shows the different operational modes on the transmitting side used by the system, in both calibration and surveys. The beam width varies depending on the operational mode. In shallow water it is 4.3° and in the deep sea it is 2.3°. When the ocean bottom is reached the signal is returned and received by the reception beams. It is possible to measure 59 depth values with an accuracy of 1% +- 1 m, and covering a width of double the vertical depth, if the bottom is level. This means there is a smaller coverage in shallow than in deep water, and so working in shallow water is more time-consuming.

MODE	ARRAY CONFIGURATION	DEPTH (m) VERTICAL	
SHALLOW WATER	ODT	10 -100	4.3° ; 1 Sounding Transducer beam width reduced because of near field
MEDIUM WATER	ODT	100 - 1000	2.3° ; 1 Sounding Large beam width of transducer
DEEP SEA	RDT	1000 - 10000	2.3° ; 3 Sounding -36° ->0° ->+36°

Table 7.1. Hydrosweep transmission modes.

ODT: Omni-Directional-Transmission = Only one pulse at the instant of transmission.
RDT: Rotational-Directional-Transmission = Three overlaying beams.

Transmission takes place in three directions and the three transmission pulses take place immediately after one another (Fig. 7.2).

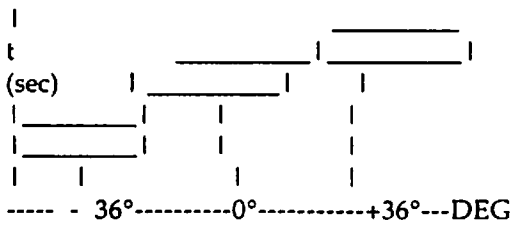

Figure. 7.2. Timing of the beams in the RDT mode

There are two important items in a multibeam echosounder. The sound velocity profile and the calibration of the echosounder for roll, pitch, heading, etc. In order to determine a Sound Velocity Profile, the Hydrosweep can measure the 59 depth values parallel to the ship's longitudinal axis. This is called "Calibration mode". With this special calibration method the mean velocity of sound is determined over the water column and the system compensated for sound refraction effects in the slanting beams. Stabilization for both roll and pitch takes place on the transmission side, and on the receiving side for roll only, because the stabilization for pitch is unnecessary as the beam width in the pitch direction is about 22°.

Structure of the equipment

The Hydrosweep equipment consist mainly of the following (Fig. 7.3):

- Two Hydroacoustic transducer arrays, installed in a T-shaped configuration on the hull of the ship
- The Transmission/Reception electronics, installed in three electronics cabinets
- The Control/Display Console, on which the measured values are displayed
- The Bottom mapping recorder, which is a printer or a plotter
- Magnetic Tape Drive, where parameters such as measured depth values, position values, heading from the Gyro, etc. are recorded.

The exchange of data and signals between the Hydrosweep system and the other equipment takes place via the external interfaces. These data and signals are as follow: position, time, speed, heading, roll, pitch, heave, sound velocity profile. Together with the measured depth values these data are stored on a magnetic tape, or processed computationally for on-line calculation of the isoline presentation on the plotter.

Transducer Arrays. The transducer arrays are mounted flush with the bottom of the vessel and the signal of these arrays is electronically compensated against rolling, pitching, etc. The two transducer arrays are arranged perpendicular to one another, one of them having its longer axis parallel to the ship's longitudinal axis, and the other arranged transversely to it at 90°. Both arrays can both transmit and receive. Each transducer array consists of three identical subarrays, installed together, with their narrower sides adjacent to each other. These forming an array about 3 m long and 30 cm wide. Each subarray is constructed as an arrangement of 96 transducers, each of which can be driven individually. In the normal survey operational mode, the array installed parallel to the longitudinal axis of the vessel acts as the transmission array and the reception array is arranged perpendicular to that axis.

Electronic Cabinets. There are three types of electronic cabinets. Distribution cabinets: These control the transducer adaptation to transmission/reception function, in addition to the following other functions:

- Power-matching to the transmitter
- Compensation of the vessel's roll and pitch

Another cabinet contains the reception unit and the signal evaluation circuit for computation of the digital depth information. This cabinet controls:

- Bottom detection by echo processing
- Computation of the digital depth in each of the 59 preformed beams
- Generation of telegrams with depth, position, heading, etc.

The last type of cabinet acts as the central data processing unit, and monitors the control commands for the Control/Display console, and controls the data output. This cabinet controls:

- Computation of the relative position of the depth measured in each beam
- Computation of the mean sound velocity profile
- Preparation of the data for recording and control the transfer process.

Control/Display Console. This console is the central control and display unit. During a normal survey this unit generally works automatically. It is composed of the graphic display unit and data display monitor.

The graphic display unit, which it is used for colored graphic display of depth values, either as a cross profile presentation or as an areal scrolling display of the sea bed.

• Cross profile presentation: This display provides the best overview of the operational status of the Hydrosweep unit. The following information is presented:
- Start of measuring range
- End of measuring range
- Depth information of each preformed beam
- Position within the depth window
- Measured of echo level (grouped into 8 groups)
- Position and number of the preformed beam
- Gain corresponding to the echo reception channels
- Receiving level of central beam
- Receiving level of the beams is dB
- General evaluation window (longitude, latitude, speed, course, roll, pitch, etc.) both for port and starboard

• Areal depth presentation: In this type of display the received depths are broken down into colored increment. An impression of a scrolling map is obtained moving downwards in proportion to the distance traveled. The displayed depth values are shown in white characters to the left of the central line.

The data display monitor acts as the alpha-numeric display system for operating procedures and for display. It can show:
• Measured velocity of sound in water
•Computed mean velocity of sound in the water
• Depth of the middle beam
• Mode of survey: shallow, deep, or calibration
• Status of tape and plotter

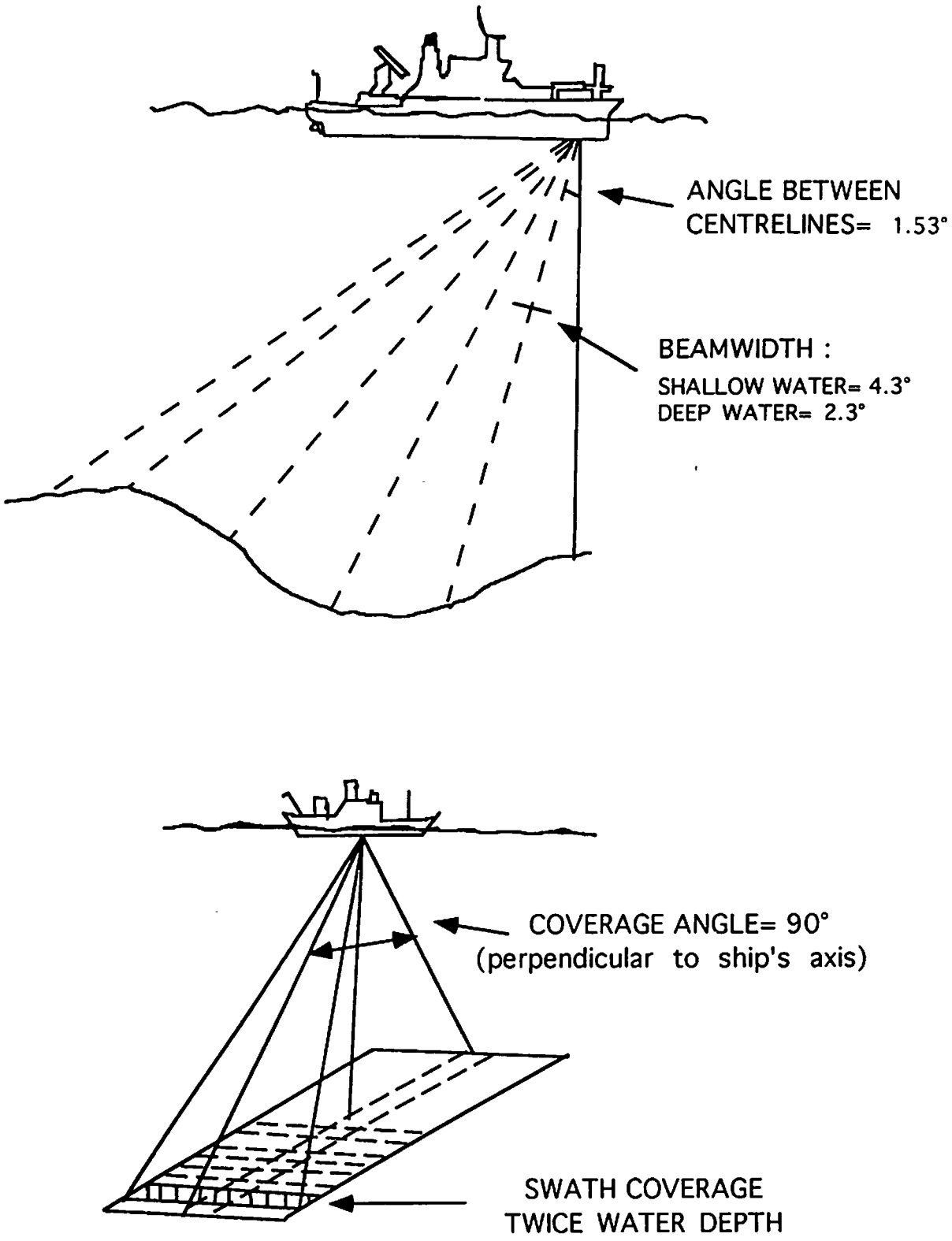

Figure 7.1 Hydrosweep configuration of the transmission/reception beams

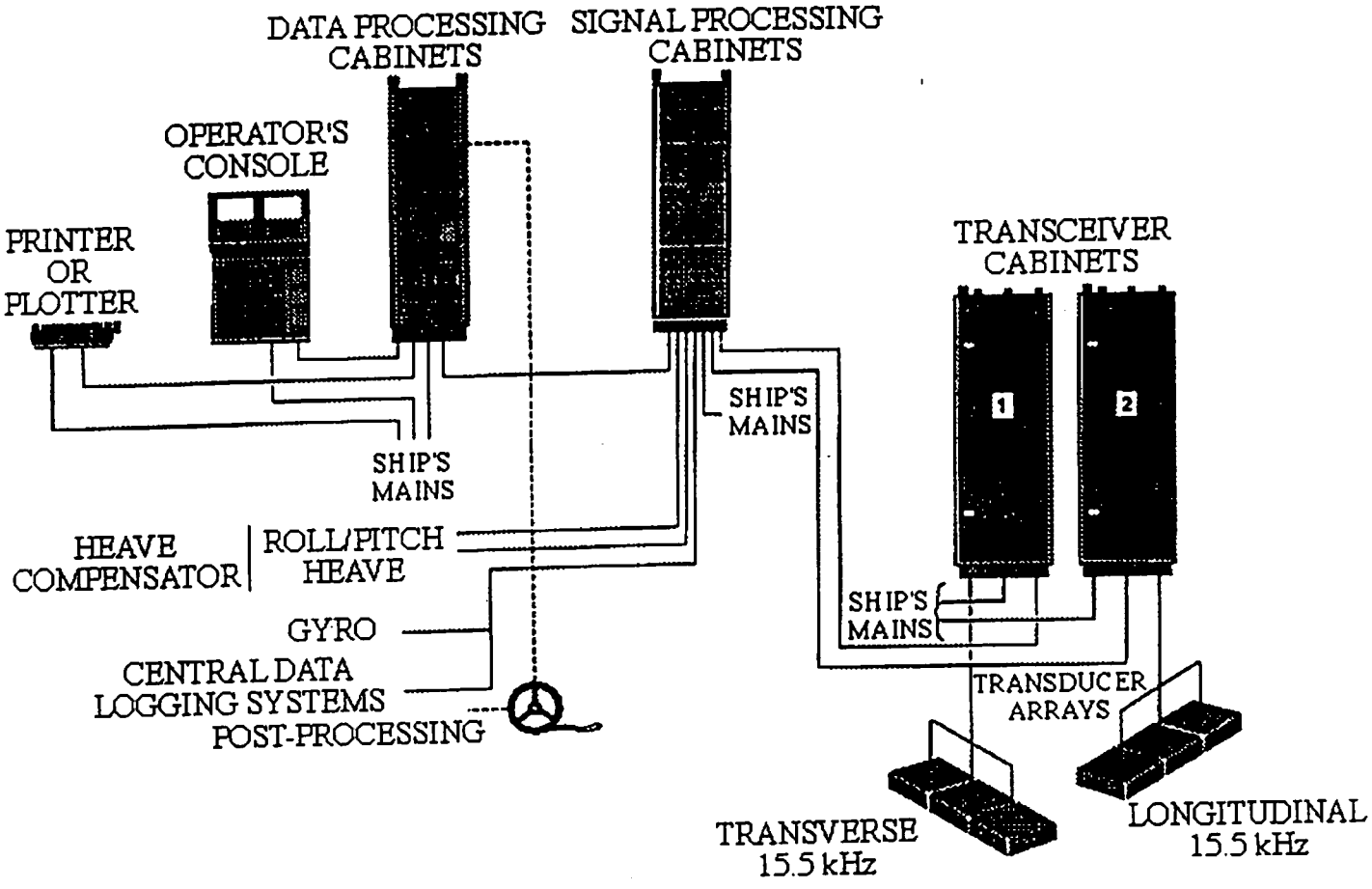

Figure 7.2 Hydrosweep Equipment

CHAPTER 8. HYDROSWEEP DATA PROCESSING

The initial processing of the Hydrosweep bathymetric data (JD167-175) was performed using the software package MBSYSTEMS version 4.3.B, developed by Dale Chayes and David Caress. MBSYSTEMS software is freeware and is available over the Internet. The compressed tarfile of the directory structure containing the source code can be obtain via anonymous ftp at lamont.ldgo.columbia.edu in pub/swath_data.

```
++ DONE ONCE AT THE BEGGINNING OF THE CRUISE ++
New Cruise setup:
-----------------
 - Create a directory in ~hs with the cruise ID. eg. ~hs/ew9504.
        % mkdir ~hs/ew9504
 - Copy the example cruise pedigree file into the new dir:
        % cp ~hs/examples/ew9309.pedigree ~hs/ew9504/ew9504.pedigree
        % chmod 644 ~hs/ew9504/ew9504.pedigree
 - Edit the pedigree file to fit your leg.
        % nedit ~hs/ew9504/ew9504.pedigree
 - Edit ~hs/macros/mbm_env_variables.csh to reflect the cruise
   specific variables.
        % nedit ~hs/macros/mbm_env_variables.csh

Environment variables:
----------------------
        Set your C-shell environment variables by sourcing:

        % source ~hs/macros/mbm_env_variables.csh

which is also linked to ~hs/bin/mbm_env_variables). You can either
include it in your .cshrc file or source the file before you run any
of the programs.
        This file is (automatically) sourced in the .cshrc file of the
user "hs".  Processing of hydrosweep data should be done by the user
"hs". The password for the "hs" account is "hydrosweep"

++ END OF DONE ONCE AT THE BEGGINNING OF THE CRUISE ++


Processing XBT and Levitus data and the importance of sound velocity profile:
-----------------------------------------------------------------------------
Hydrosweep survey sometimes covers more than one degree square area.
It is recommended that an XBT probe is taken for each sqared degree area,
especially if there is a large change in water temperature, or on survey
area near the Gulf Coast, for example.

NOTE:
The purpose of this exercise is to create a new velocity profile suitable
for the specified survey area.

Steps to be taken:
------------------
Create a sub-directory under your specified cruise directory to process this
XBT data, and to create a velocity profile.
```

```
        % mkdir ~hs/ew9504/sound_vel     (done only once at the beginning of
                the cruise)
```

1. Raw hydrosweep data.

Raw hydrosweep data is located in the directory specified in your mbm_env_variables.csh under the variable name of:

```
        $HS_RAW_DATA_DIR=/net/manta/data/hs
```

To find out what that is, simply execute the command:

```
        % env
```

This will produce an output similar to this:

```
        .... stuff deleted ....
        USER=hs
        WINDOW_PARENT=/dev/win0
        WINDOW_TTYPARMS=
        WMGR_ENV_PLACEHOLDER=/dev/win3
        XFILESEARCHPATH=/usr/openwin/lib/%T/%N%S
        WINDOWID=14680077
        LDEO_CRUISE_ID=9504
        HS_RAW_DATA_DIR=/net/manta/data/hs
        HS_DATA_DIR=/net/heezen/staff/hs/ew9504
        HS_PUBLIC_DIR=/net/hess/science/data
        PEDIGREE_FILE=/net/heezen/staff/hs/ew9504/ew9504.pedigree
        HS_FINAL_DIR=/net/hess/science/data
        HS_LONFLIP=0
        LDEO_NAV_FILE_PRFX=n
        MMHOME=/net/heezen/packages/mapmaker/MapMaker_sun
        .... stuff deleted ....
```

Simply search for a line that begins with HS_RAW_DATA_DIR and the directory name should be to the right of the equal sign.

You need to copy the hydrosweep data corresponding to the survey area to your sub-directory where you process your sound velocity profile (~hs/ew9504/sound_vel).

Example:

```
        % cp /net/manta/data/hs/9504hs.d173 ~hs/ew9504/sound_vel
```

Note that the raw HS format is format 5.

2. XBT Data processing:

XBT data is acquired on a PC located aft of the main-lab watch-desk. This data needs to be transferred to the SUN, and stored in the above sub-directory. The following steps can be taken to transfer the data:

On the PC side:

```
        C> CD A_DIRECTORY_WHERE_XBT_DATA_IS_STORED (ask)
        C> TELNET HEEZEN
```

A login prompt should come up on the screen:

```
        heezen login:
```

Log in as you would if you are in the SUN

Now you are in the SUN side:

```
        % cd ~hs/ew9504/sound_vel
        (this being the directory where you want to store your XBT file)
```

Type the following: <ALT> F
This access the FTP prompt. Hit return when asked about your username and password.

You are now back on PC side:
ftp> put 9504-1.xt7 (that being the name of the XBT file)

Type <CTRL> D to get out of ftp mode. Check if the file is succesfully transfered by typing:
% lt

After you are sure the data is there, log out from telnet by typing <CTRL> D. You are now done with that PC, so mosey on back to heezen.

An XBT data produced by Sparton is an X-Y value pair of depth and temperature. This needs to be converted to an XY value pair of depth and sound velocity.
To do this, execute the following:
% cd ~hs/ew9504/sound_vel
(you want to make sure that you are in XBT dir.)
% mbm_xbt -I9504-1.xt7

This will produce a file with a ".sv" extension at the end of your input file name.
e.g. if your input file is 9504-1.xt7 then your output file is 9504-1.xt7.sv

3. Levitus data file:

MBLEVITUS(1) USER COMMANDS MBLEVITUS(1)

NAME
mblevitus - Create a water velocity profile which is representative of the mean annual water column for a specified 1 degree by 1 degree region.

VERSION
Version 3.00

SYNOPSIS
mblevitus [-Rlon/lat -Ooutfile -V -H]

DESCRIPTION
MBLEVITUS generates a mean water velocity profile for a specified location from the Levitus temperature and salinity database. The water velocity profile is representative of the mean annual water column structure for a specified 1 degree by 1 degree region. The profile is output to a specified file which can be read and used by programs (e.g. HSBATH) which calculate multibeam sonar bathymetry from travel times by raytracing through a water velocity model.

For each XBT data you acquire, we will need to accompany that with a levitus data. To acquire the correct levitus data, you need to make sure that you choose the correct lon/lat pair. This pair should indicate the left bottom part of the one degree square of survey area.

To find out where the survey area is, you can execute the following command:
% mbinfo -F5 -I9504hs.d149
Note carefully on the "-F" option and the "-I" option. Look at the manual page for more info on mbinfo. Hmm... that rhyms..

So, if you have a survey area from -118 to -117 W and 12 to 13 N, you want to do this:
NOTE: make sure you are in ~hs/ew9504/sound_vel directory

```
        % mblevitus -R-118/12 -Oew9504.levitus.118.12

and the ouput filename would be: ew9504.levitus.118.12

MB
HSVELOCITYTOOL:
--------------
Now you are ready to use hsvelocitytool. hsvelocitytool is a
windowing program. So, typing
        % cd ~hs/ew9504/sound_vel
        (make sure you are in sound_vel directory)
        % hsvelocitytool
will get you a new window where you can load up on the data as
neccessary.

MB HSVELOCITYTOOL(1)        USER COMMANDS        MBHSVELOCITYTOOL(1)

NAME
     MB
     HSVELOCITYTOOL - Interactive water velocity profile editor.

VERSION
     Version 3.00

SYNOPSIS
  MB Hsvelocitytool [-V -H]

DESCRIPTION
  MB HSVELOCITYTOOL is an interactive water velocity profile edi-
     tor  used to examine multiple water velocity profiles and to
     create new water velocity profiles which can be used for the
     processing  of hydrosweep multibeam sonar data.  In general,
     this  tool  is  used  to  examine  water  velocity  profiles
     obtained from XBTs, CTDs, or databases, and to construct new
     profiles consistent with these various sources  of  informa-
     tion..

Or, basically you need three files to use this tool properly:
        *. Two display profile :
                1. XBT data file that has been converted using mbm_xbt.
                2. Levitus data.
        *. One Hydrosweep data file:
                3. Raw Hydrosweep data.

Steps to take: (no reverse order, por favor)
        1. Open the two display profile first( XBT, then levitus.
        2. Open new editable profile.
        3. Open hydrosweep data.
           (note: make sure of the format type e.g. 5 for raw, 8 for
                processed)

IMPORTANT:
        Once you are satisfied with your velocity profile (your
        residual curve falls below 1/2 of 1% of max depth), it is very
        important to save the file into some logical name, e.g. ew9504.svp.1
        for the first velocity profile, and so on.

        Also, it is necessary for you to copy that file into your cruise
        working directory:
                % cd ~hs/ew9504/sound_vel
                (make sure you are in sound_vel directory)
                % cp ew9504.svp.1 ~hs/ew9504/ew9504.svp.1

        As always, when in doubt, do that friendly "lt" command to check
        and make sure everything is kosher.
```

```
-------------
DAILY ROUTINE:
-------------

Three simple steps to daily processing routine:
        % cd ~hs/ew9504
(step1) % mbm_process1 173 ew9504.svp.1 -P
        where 173 should be your previous julian day
              ew9504.svp.1 is your sound velocity profile created by
              MB-velocitytool
          and -P if you want people to be able to access your final HS
              data.

        File it looks for (expects to be there):
              *. Raw hydrosweep swath data in HS_RAW_DATA dir:
                    /net/manta/data/hs/9504hs.d173
              *. Velocity profile in hs cruise directory:
                    ~hs/ew9504.svp.1

        File created:

-rw-r--r--  1 hs          14914 Jun 24 02:33 hs173.log
-r--r-----  1 hs        4688368 Jun 23 23:11 hs_ew9504_173_bc.mb8
-rwxr-xr-x  1 hs           3535 Jun 23 22:36 mbm_process2_173.csh
-rwxr-xr-x  1 hs            954 Jun 23 22:36 mbm_edit_173.csh
-rwxr-xr-x  1 hs           3002 Jun 23 22:36 mbm_process2_noedits_173.csh
-r--r-----  1 hs        2536181 Jun 23 22:29 hs_ew9504_173.mb5.Z
    |       |             |         |           |
permission   owner       size    date created file name

Description:
hs173.log                          - log file, history of processing
hs_ew9504_173_bc.mb8               - hs file, format 8, merged with sound
                                     vel. profile, and cleaned
mbm_process2_173.csh               - shell script for step 3
mbm_edit_173.csh                   - shell script for step 2
mbm_process2_noedits_173.csh       - use this script if you don't want to
                                     edit the data.
hs_ew9504_173.mb5.Z                - raw format 8 hs data, copied straight from
                                     HS_RAW_DATA_DIR

::::NOTE::::
If you only want to process a portion of the day, you need to use the
'mbcopy' utility to cut and paste, so to speak, the data. You will need to
do the following:
        1. Always use the final data from mbm_process1, which in this
           case is: hs_ew9504_173_bc.mb8
        2. Say you want to process data from 0000 to 0400, you will then
            do following:
                % mbcopy -F8/8 -B1995/06/22/00/00/00 -E1995/06/22/04/00/00 -Ihs_ew9504_173
_bc.mb8 -Otemp.file
           NOTE: make sure you know what each option does!
                -F8/8   - it says that you want to copy a format 8 data to a
                          format 8 data
                -B...   - begin time
                -E...   - end time
                -I...   - input file
                -O...   - output file
        3. Now you want to save the original (full day) data to some
           other file
                % mv hs_ew9504_173_bc.mb8 hs_ew9504_173_bc.mb8.complete
        4. Now move the output file of mbcopy (the cut up version) to the
           "bc" file
```

Due to the file permission, this will produce a response as follows:
rm: override protection 444 for hs_ew9504_173_bc.mb8?
Type "y" to override.

** NOTE INSIDE NOTE **
What happened if you want to process from 0000-0400 and then from 0800-1200 ???
Then you want to do this:

```
% mbcopy -F8/8 -B1995/06/22/00/00/00 -E1995/06/22/04/00/00 -Ihs_ew9504_173
_bc.mb8 -Otemp.file1
(copy the first chunk, note the output filename)
% mbcopy -F8/8 -B1995/06/22/08/00/00 -E1995/06/22/12/00/00 -Ihs_ew9504_173
_bc.mb8 -Otemp.file2
(copy the second chunk, note the output filename)
% mv hs_ew9504_173_bc.mb8 hs_ew9504_173_bc.mb8.complete
(move the original to a save place)
% cat temp.file1 temp.file2 > hs_ew9504_173_bc.mb8
(combine chunk1 and chunk2, and make a new cut up version
$ rm temp.file1 temp.file2
(remove the temporary file)
```

You are now ready to proceed to step 2.

(step2) % mbm_edit_173.csh
this will open up a window where you can edit your file.

File it looks for:
*. hydrosweep swath data, format 8, ran thru hsbathy, and cleaned:
~hs/ew9504/hs_ew9504_173_bc.mb8

File created:

```
-rw-r--r--  1 hs        4688368 Jun 23 23:11 hs_ew9504_173_bce.mb8
```

Description:
hs_ew9504_173_bce.mb8 - hs file, format 8, merged with sound vel. profile, and cleaned, and edited.

::::NOTE::::
What happened if you got tired, and couldn't finish editing all in one swoop? Well, first, note the time (how far along) you have finished editing, then you would want to click "Done" button, which will save the file, then "Quit" which will quit the window all together. Doing an 'lt' command at this point, you will see a new file created:

```
-rw-r--r--  1 hs        4688368 Jun 23 23:11 hs_ew9504_173_bce.mb8
```

When you are ready to do some more editing, type the following:
% cd ~hs/ew9504 (make sure you are in the cruise directory)
% mbedit

IMPORTANT HERE: You will need to select this file: hs_ew9504_173_bce.mb8, which is the new file created from your last edit. This in turn will create a new file:

```
-rw-r--r--  1 hs        4688368 Jun 23 23:11 hs_ew9504_173_bcee.mb8
```

Note the"bcee" as compared to "bce" from the previous file.
You can repeat this process as many times as necessary. Just make sure that you don't loose sight of how many "eee"s is your most recent edit. A good check for this is by typing 'lt' and choose one that has the most recent time stamp on.

NOTE: Before you can proceed to step3, you will need to copy your most recent edit, to the original "bce" file. So, you need to do the following:

```
% mv hs_ew9504_173_bceeeee.mb8 hs_ew9504_173_bce.mb8
```

Now you are ready for step3.

```
        % rlogin hess
        % cd ~hs/ew9504
(step3) % mbm_process2_173.csh
```

File it looks for:

*. hydrosweep swath data, format 8, ran thru hsbathy (merged with sound vel. profile), cleaned, and edited:
~hs/ew9504/hs_ew9504_173_bce.mb8

File created:

```
-rw-r--r--  1 hs         4688368 Jun 23 23:11 hs_ew9504_173_bcen.mb8
```

Description:

hs_ew9504_173_bcen.mb8 - hs file, format 8, merged with sound vel. profile, and cleaned, and edited, and merged with final nav.

A little bit about the name covention:

Notice the ".bcen" extension on the file name? Well, this is what it means:

- "b" - ran thru hsbath (tarvel times, need velocity profile)
- "c" - cleaned, ran thru rudimentary automatic cleaning.
- "e" - edited. ran thru mbedit.
- "n" - merged with final navigation, final product.

Note: the last extension,

- "mb8" means that it is format 8
- "mb5" means that it is format 5

... and so on

==========
GENERAL NOTE:
==========

>>>> Every steps you take, every moves you make... each daily process keeps a log file in your cruise directory (~hs/ew9504):
hs173.log
If you encounter any problem, look in that file, you might see something, then again, you might not. It is quite descriptive and somewhat gibberish, but plod thru it regardless.

>>>> Wondering what day is what???

```
        % conv_date 174 1995
          day of year: 174              Fri Jun 23 00:00:00 1995

        % conv_date 06 23 1995
          day of year: 174              Fri Jun 23 00:00:00 1995
```

>>>> To view the plot on the screen:
Unless you modify the mbm_process2 script to make it not remove the postscript file, you have to be pretty sneaky to be able to this.
The only time you can do this is when your mbm_process2 start outputting the following comment:

```
        Saving image.....
```

At that point, type lt, and pick the file that ends with a ".ps" extension.
Then type the following:

```
        % gs  hs_ew9504_173_bcen.mb8.ps
```

Type <CTRL> C when you are done.

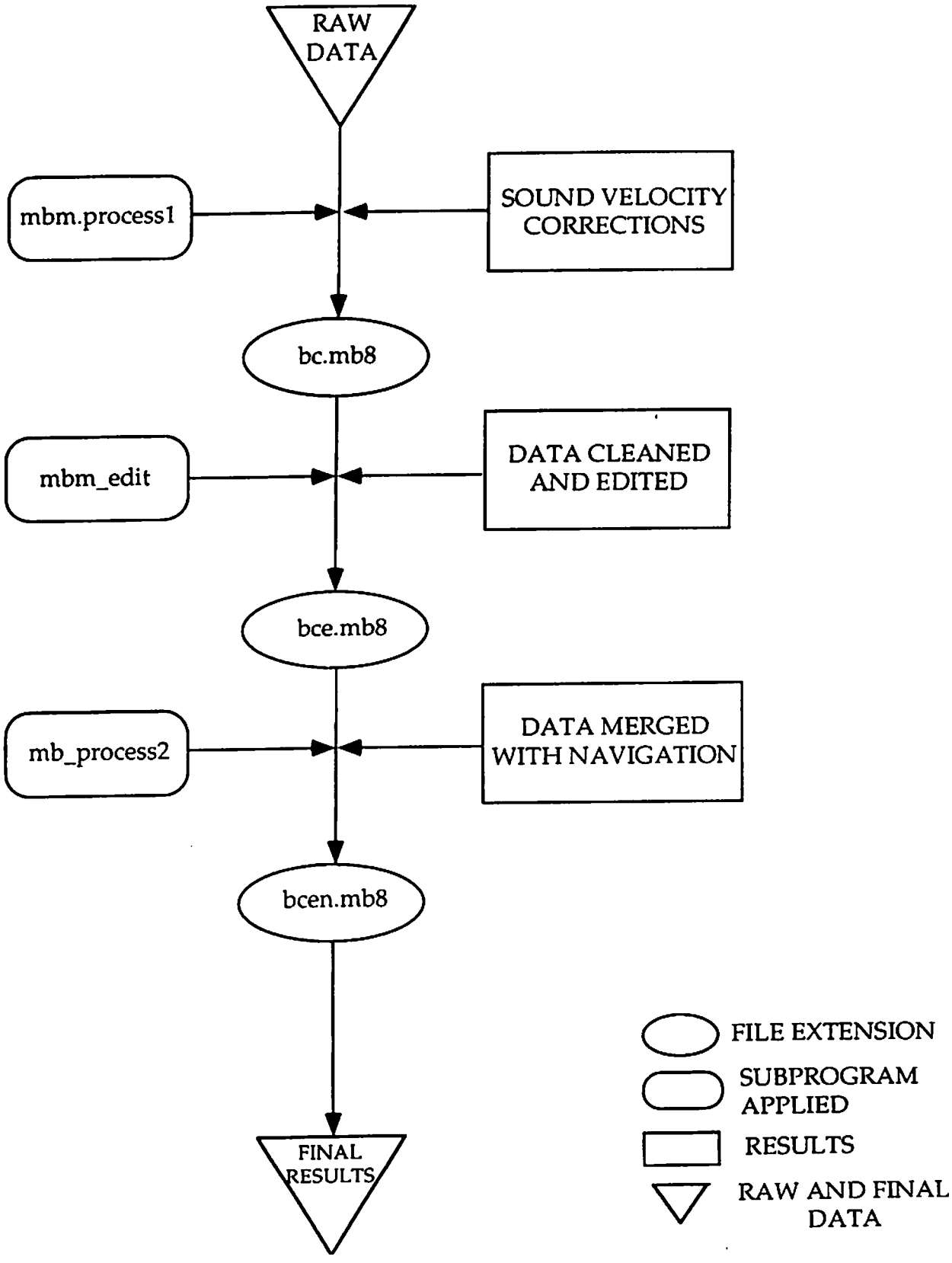

Data processing flow chart

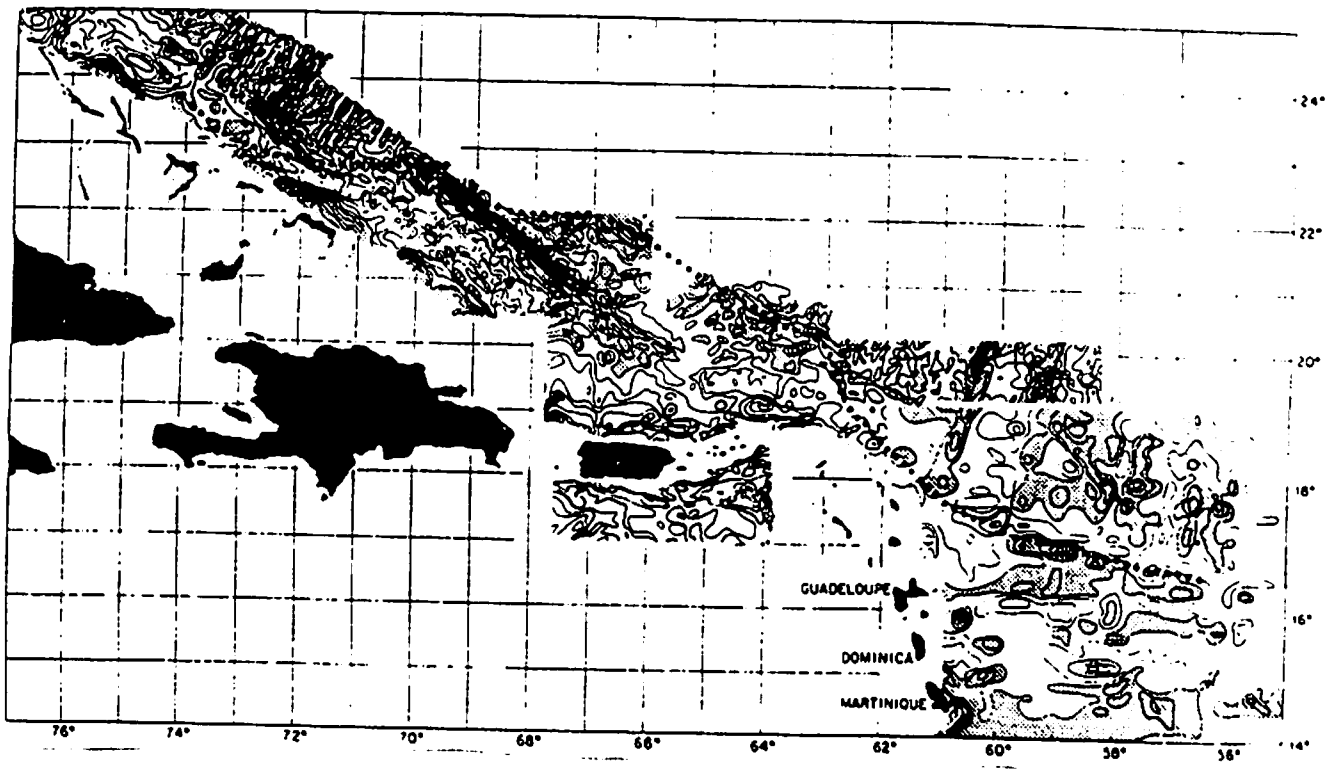

Figure 18.1.2 Regional magnetic anomalies after Bracey (1968) and Phillips (unpub. data). Solid circles mark line of postulated magnetic boundaries. From Bunce et al., (1974)

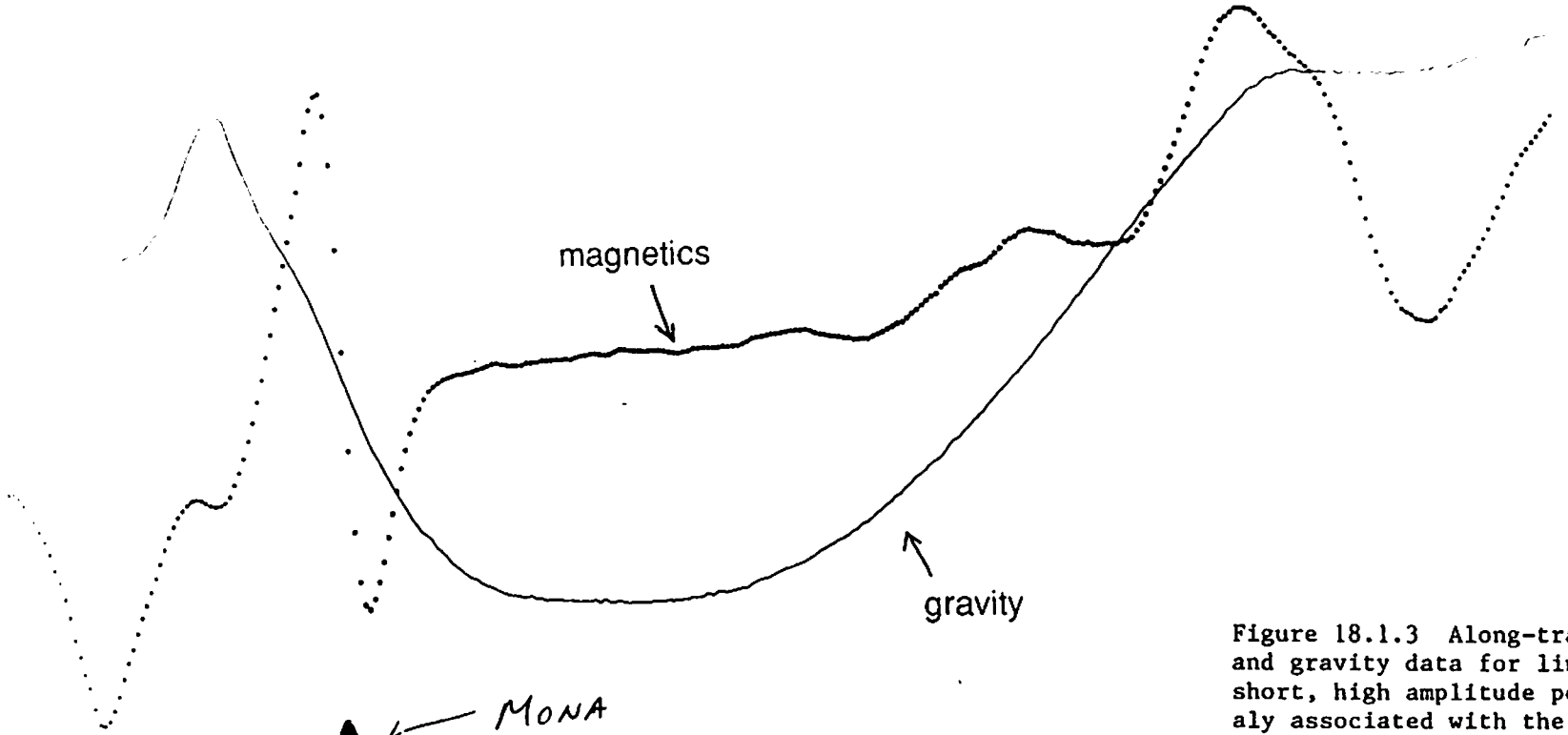

Figure 18.1.3 Along-track magnetic and gravity data for line 27. Note short, high amplitude positive anomaly associated with the Fourth of July Ridge.

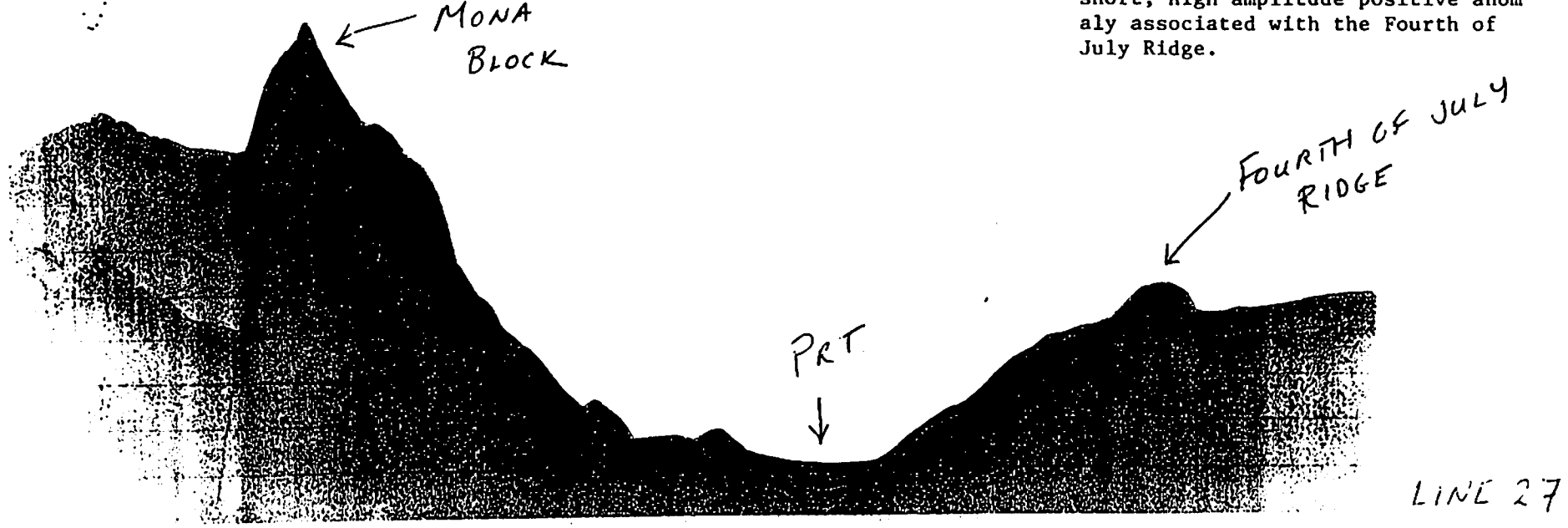

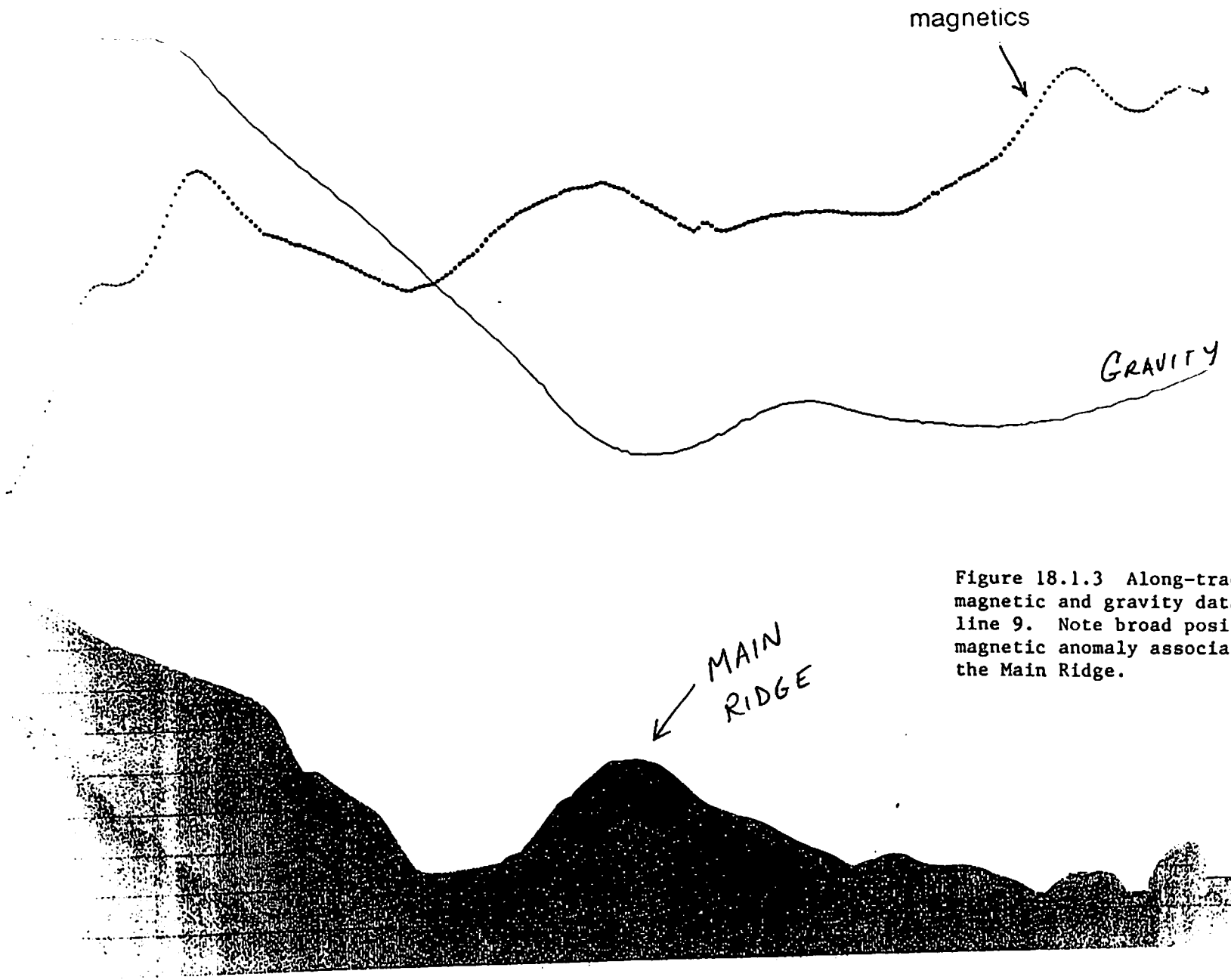

Figure 18.1.3 Along-track magnetic and gravity data for line 9. Note broad positive magnetic anomaly associated with the Main Ridge.

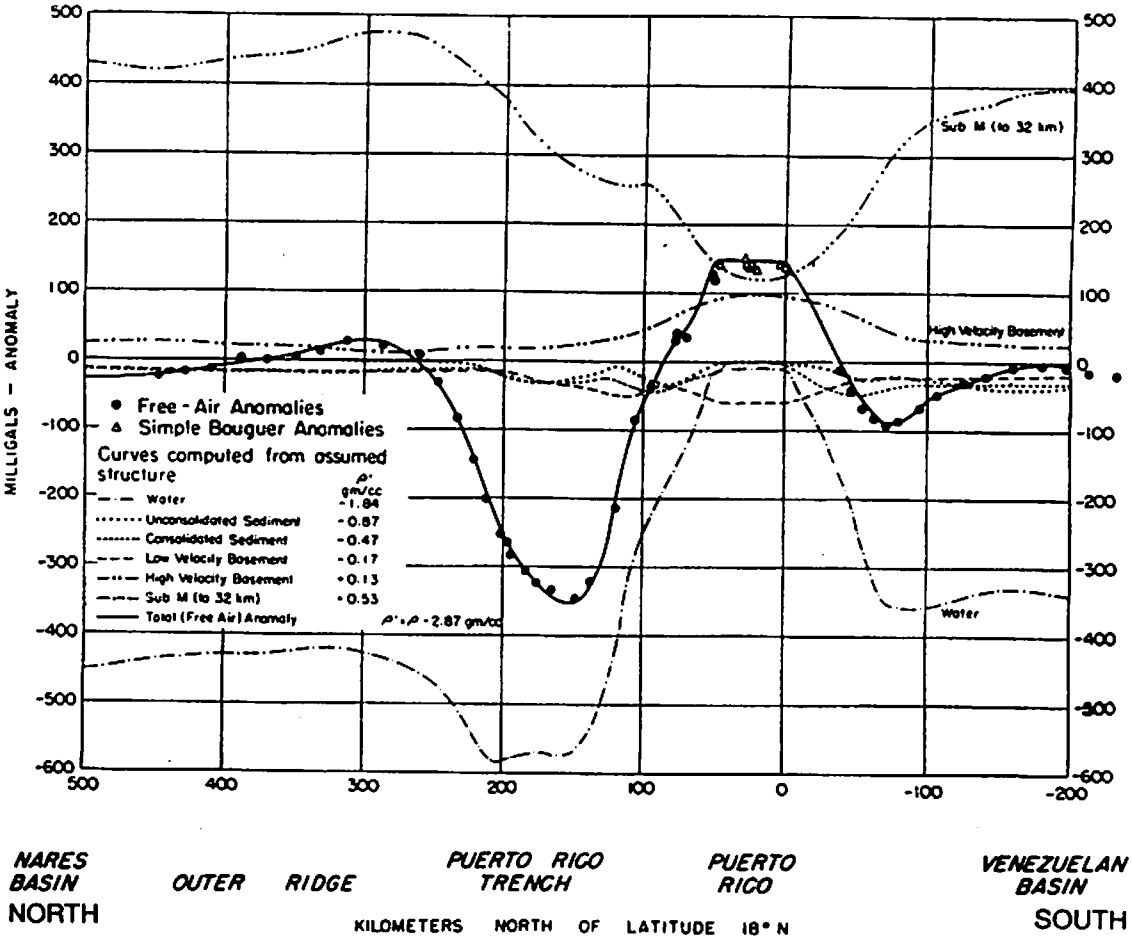

Figure 18.1.4 Across-trench gravity profile after Talwani et al.(1959).

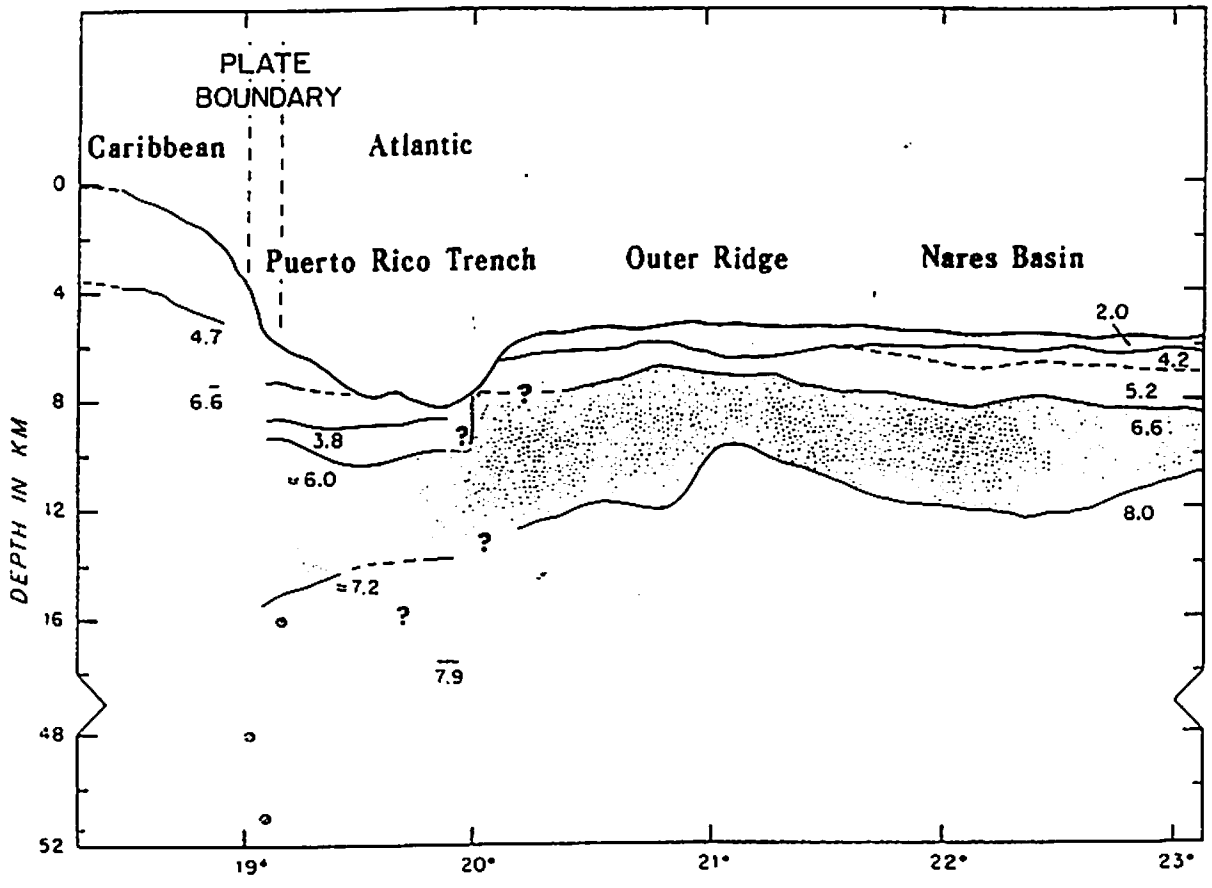

Fig. 18.1.5A .- Crustal cross section of the Puerto Rico Trench. Dashed lines indicate the Caribbean- Atlantic plate boundary (Modified from Molnar & Sykes, 1969, cited in Bunce et. al., 1974).

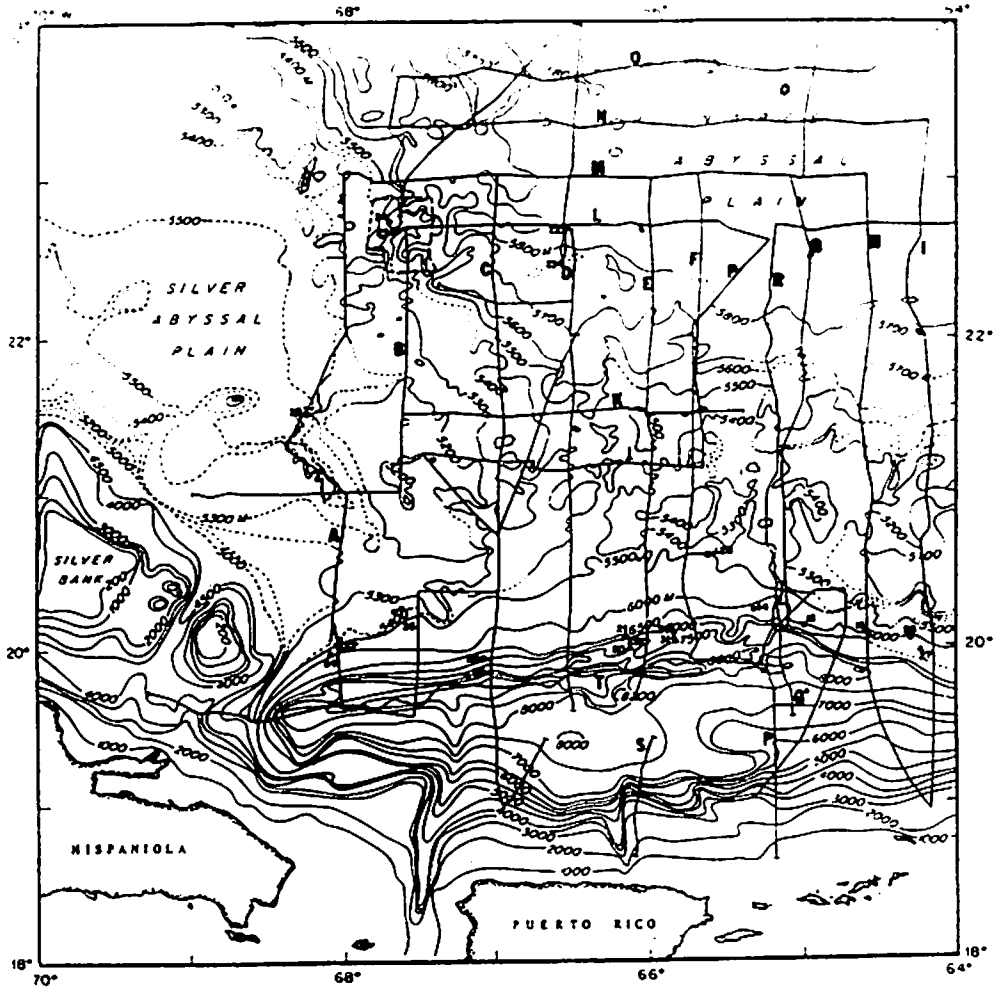

Fig. 18.1.5B - Location of the Molnar & Sykes (1969) refraction line.

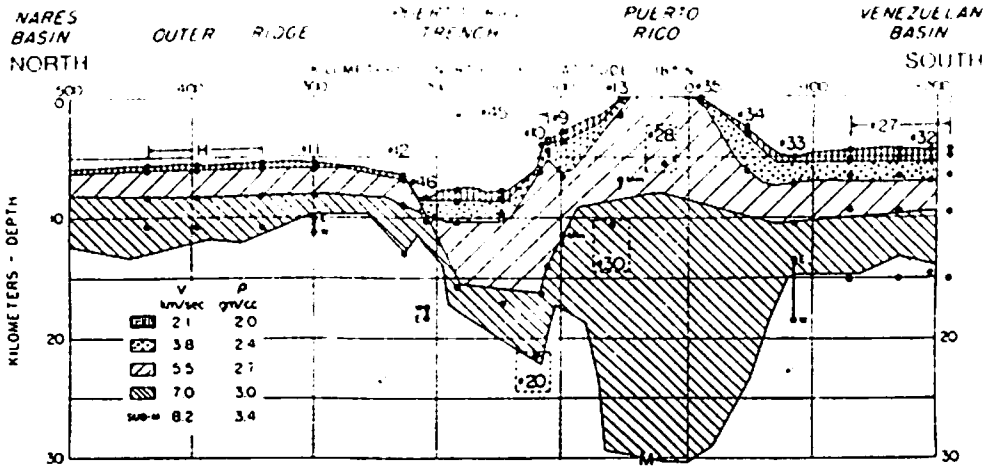

Fig. 18.1.6A - Crustal cross section of the Puerto Rico Trench and nearby areas. Points indicate an inferred boundary (Modified from Talwani et. al. 1959).

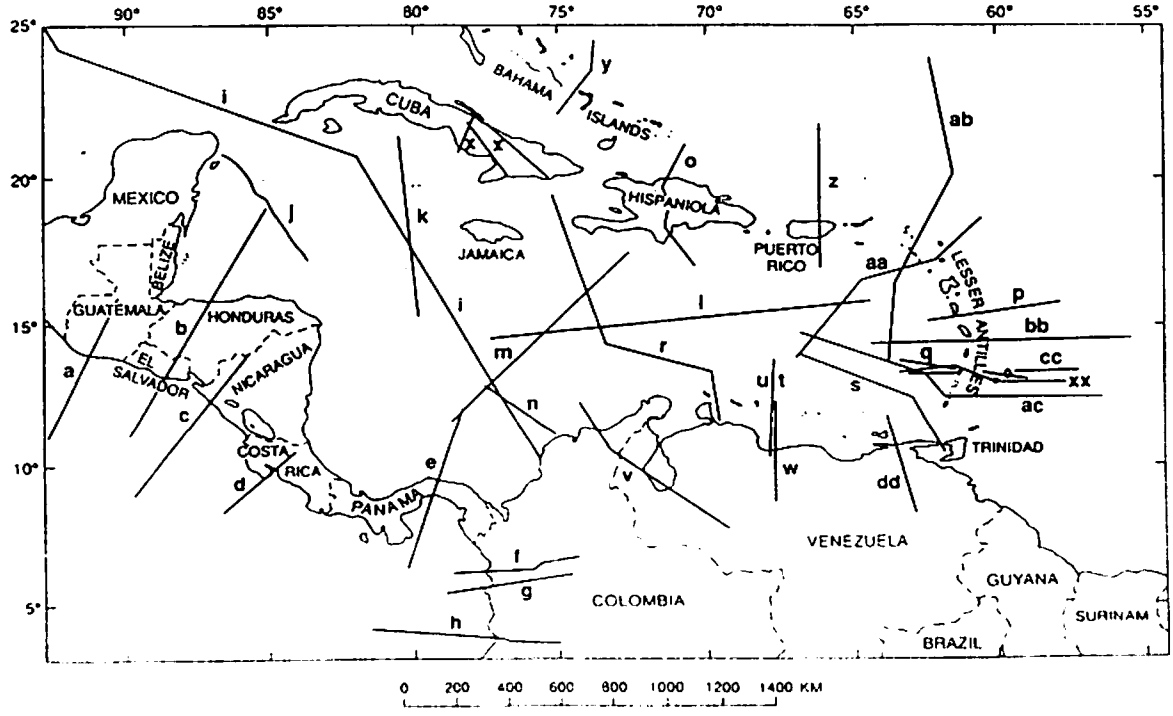

Fig. 18.1.6B - Location of the Talwani et. al. (1959) refraction line. It is line 'z' on the map.

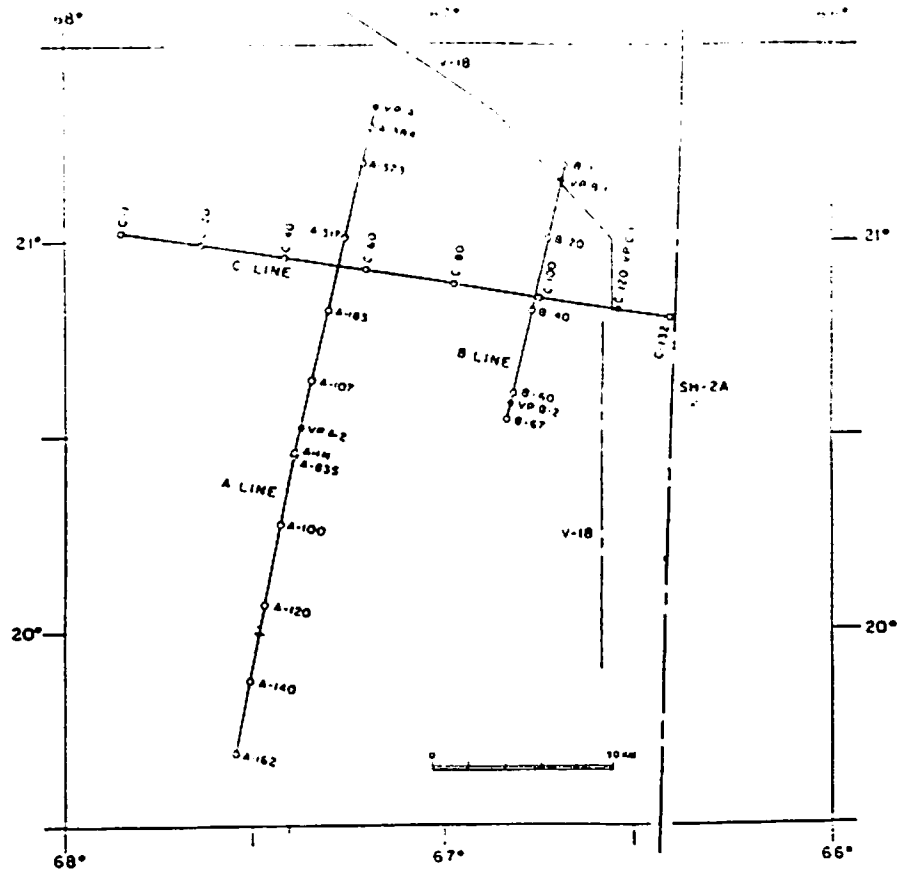

Fig. 18.1.7A - Map showing the location reflection lines from Savit et. al. (1964). Line 'A' was superimposed on Figure 18.1.10.

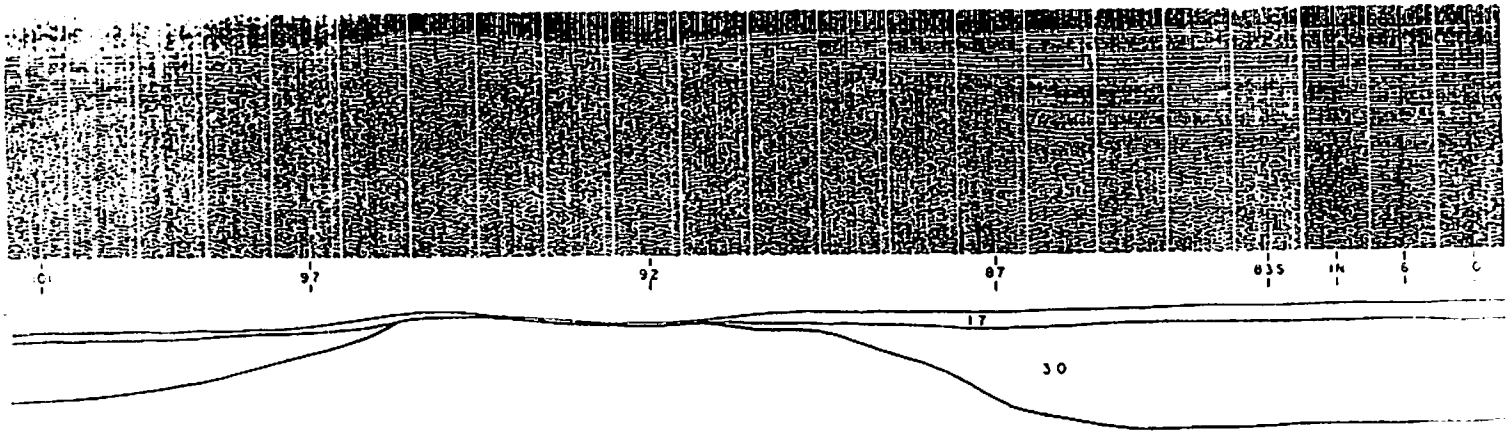

Fig. 18.1.7B - Portion of Savit et. al. reflection line 'A' that shows the crustal high in the same trend as the Main Ridge projection of McCann and Sykes (1984).

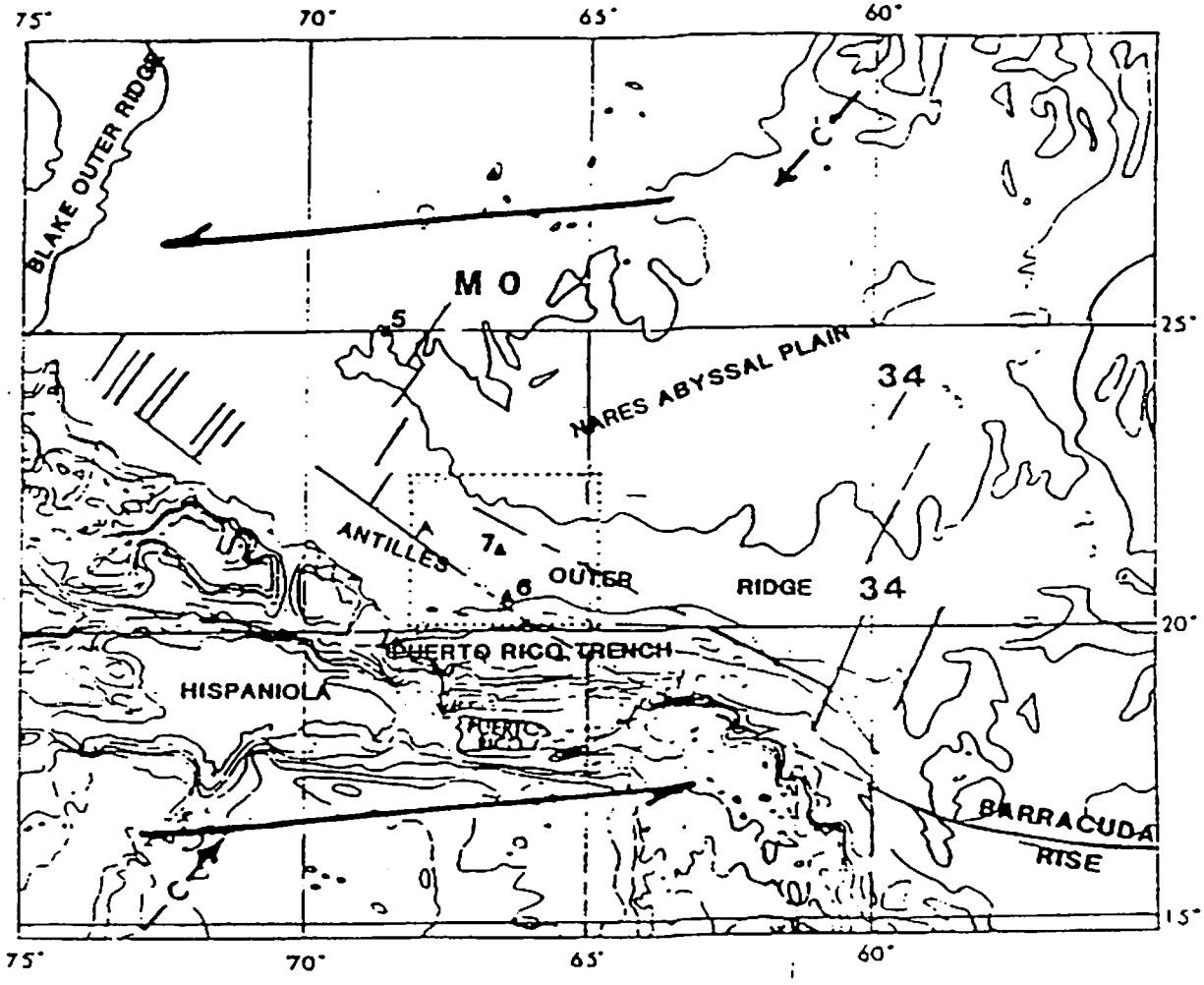

Fig. 18.1.84 - Location map showing the Puerto Rico Trench, the Greater Antilles Outer Ridge and the Nares Abyssal Plain(Threadgold, 1985).

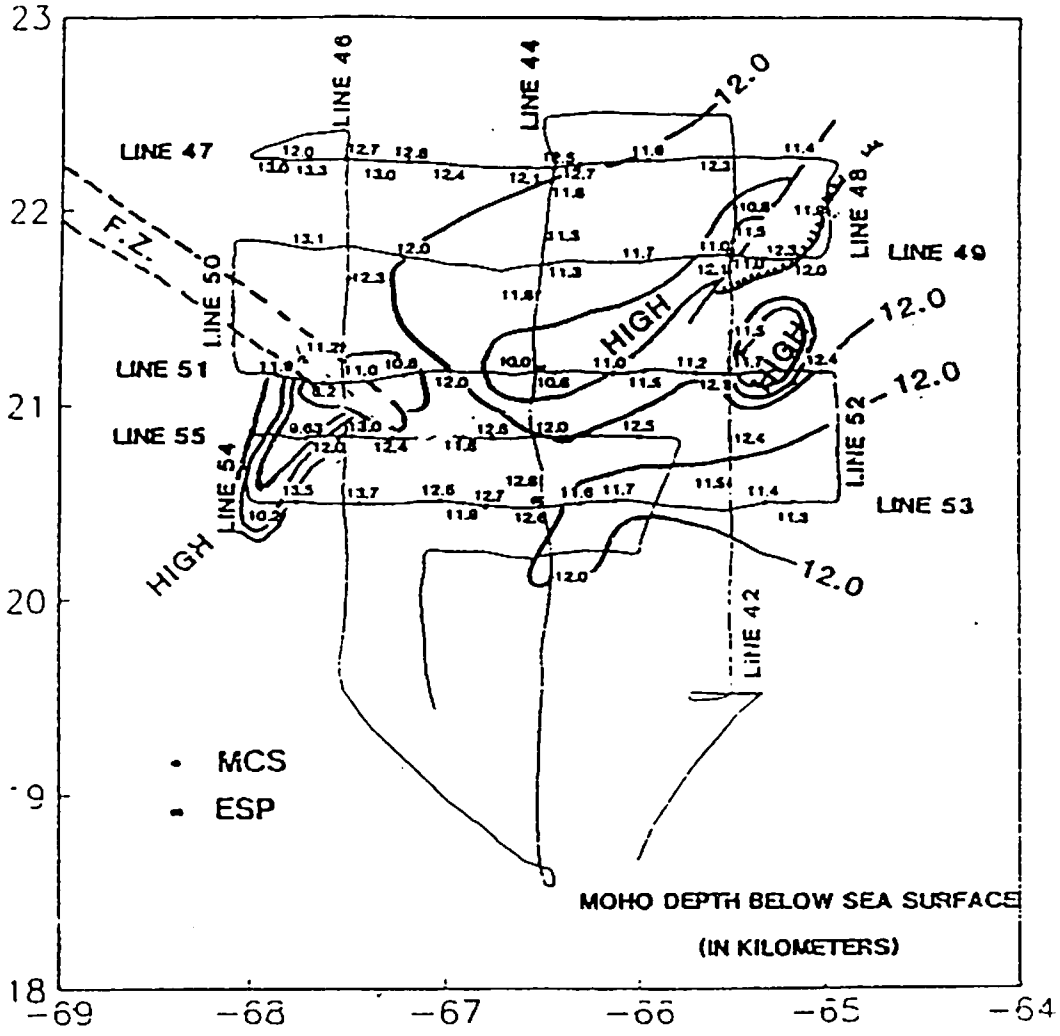

Fig. 18.1 *B* - Depth to the Moho showing NE-SW mantle ridge (contoured Moho high) offset by the fracture zone (dashed lines) and including the eastern mantle high (Threadgold, 1985).

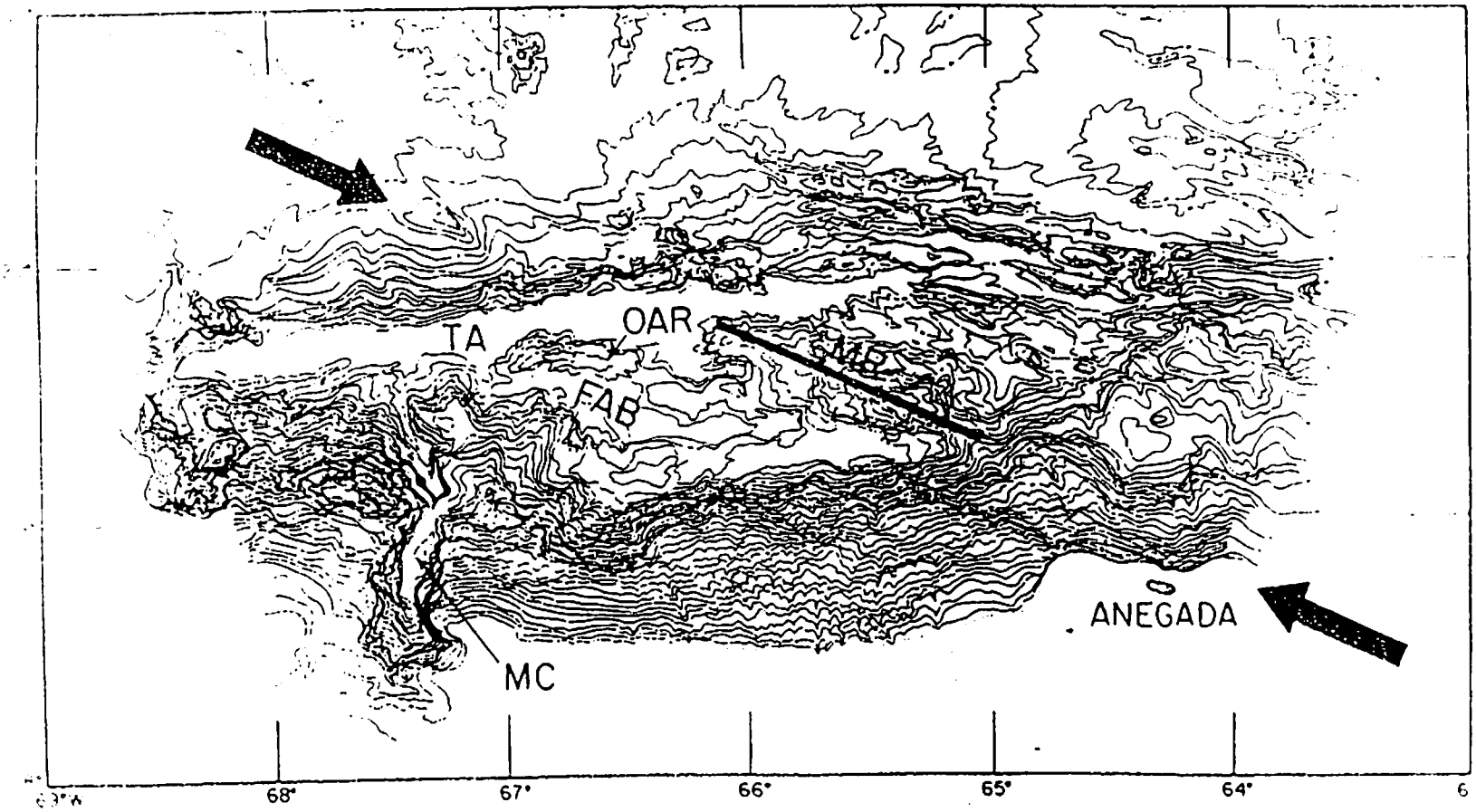

Fig. 18.1.9 - Map showing the location of the aseismic ridge found by McCann and Sykes (1984).

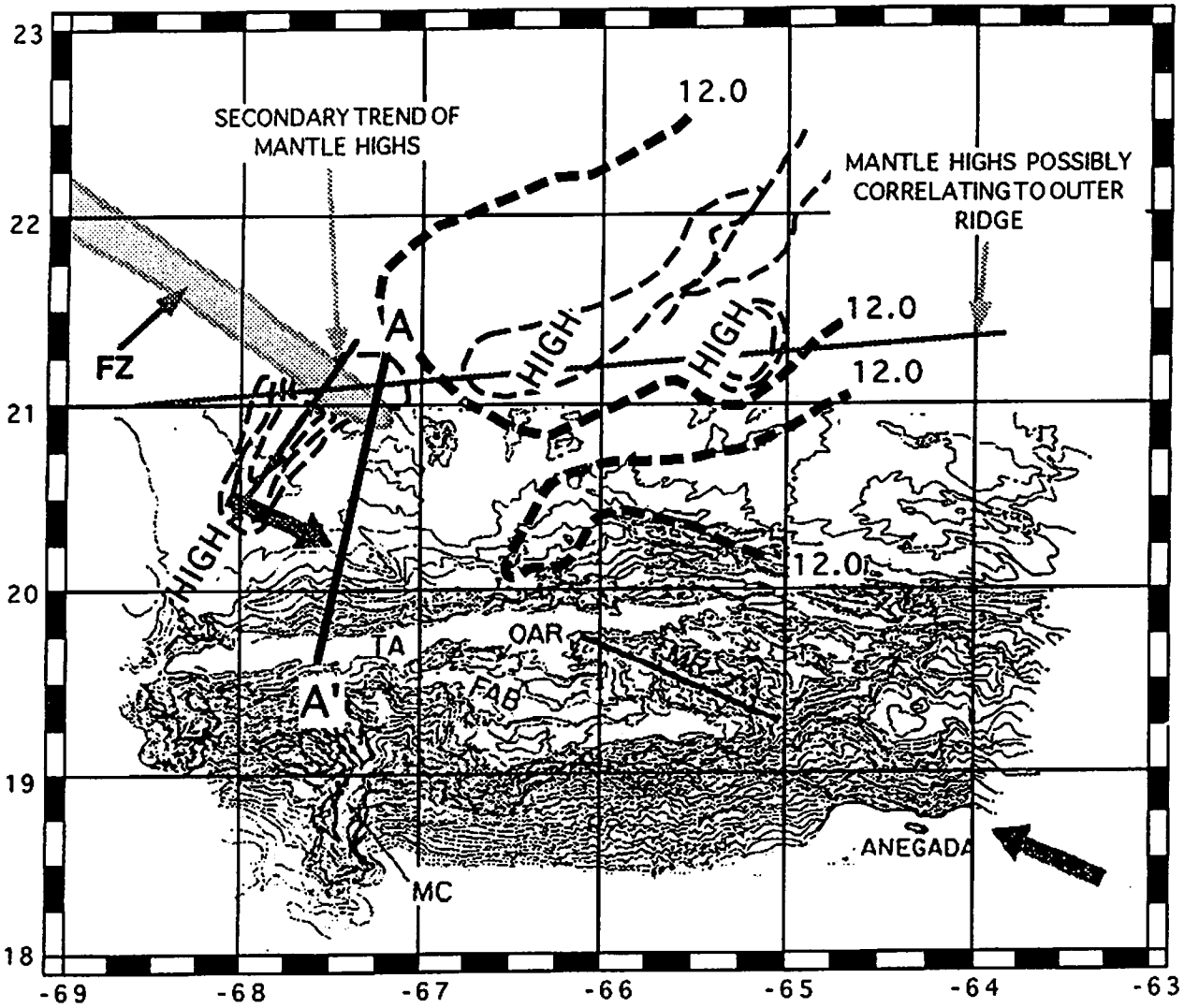

Figure 18.1.10 - Bathymetry (A. Leonardi, unpublished data, 1981; published in McCann and Syke, 1984) and of the Puerto Rico trench north of Puerto Rico and the Virgin Islands (1 contour interval = 1 fathom = 1.829m. Depth to the MOHO is shown by the bold hashed lines. MR = Main ridge; TA = trench axis; OAR = outer arc ridge; FAB = forearc basin; FZ = fracture zone; MC = Mona Canyon. The reflection line from Savit et. al. (1964) that shows a crustal high that corresponds to the projection (dark arrows) of the Main Ridge by McCann and Sykes, 1984 is shown by line A-A' (fig. 18.1.7A & 18.1.7B). The main ridge and the fracture zone are oblique to the other tectonic structures in the trench. The depth to the Moho shows a mantle ridge that is orthogonal to the fracture zone and the Main Ridge (figure modified from McCann and Sykes, 1984 and from Treadgold, 1985).

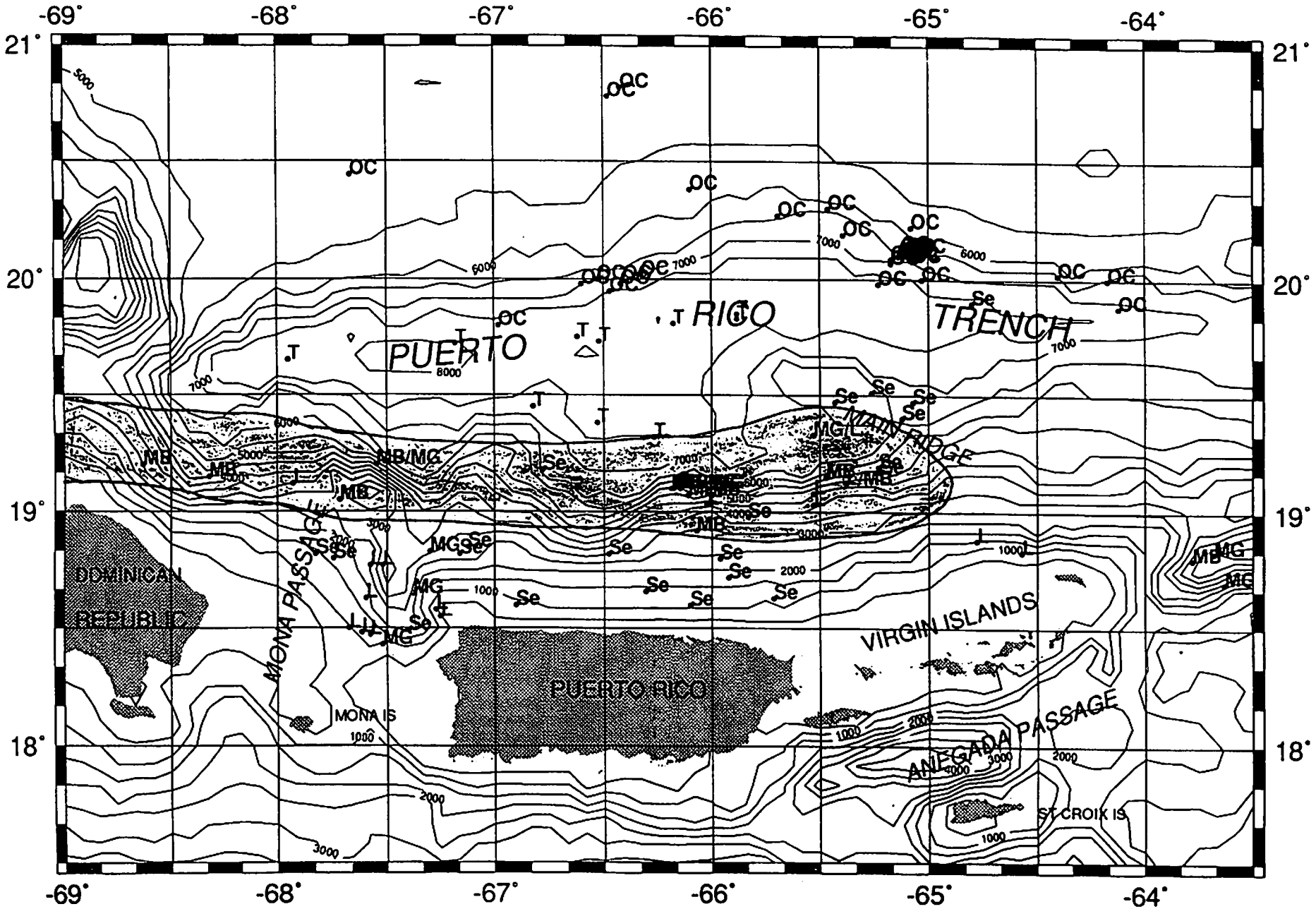

Figure 18.1.11. Core and dredge location in and around the PRT. The exact location of the cores and dredges is listed in Table 18.4.2. Each dredge and core is classified according to the rock type present: L-limestone, T-turbidite, Se-other sedimentary rocks and layers, MG-metamorphic rocks, Green Schist facie, MB-metamorphic rocks, Blue Schist facie, and OC-ocenic crust type rock. The shaded zone indicates the location were all the Blueschist facie metamorphic rocks dredge hauls. This zone indicates the location of the Blueschist belt complex; that extends more than 500 km , from northern Hispaniola to the northeastern Caribbean (Perfit and others, 1980).

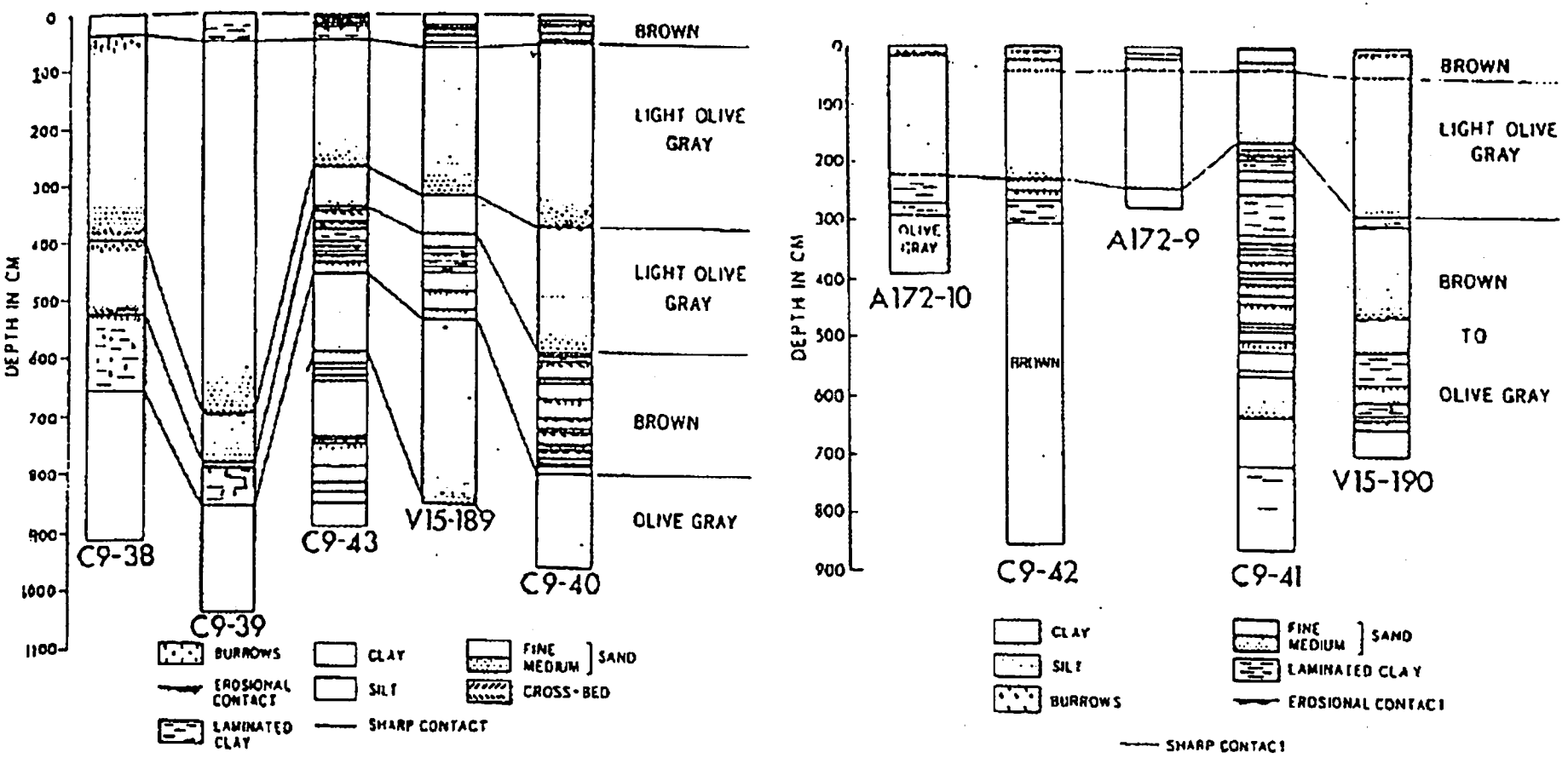

Figure 18.1.12 Cores from the northern, southern, western, eastern parts of the PRT. In the first five cores five distinct zones can be correlated, this belong to the southern and western parts of the PRT. On the other hand, in the last five cores only two zones can be correlated, this belonging to the northern and eastern parts of the PRT (Modified from Conolly and Ewing, 1967).

18.2 Review of Shallow Structures in Study Area

by Stefan Muszala and Paul Mann

Structures related to relative motion of Caribbean and North American plates

Many different theories have been proposed to explain the relative motions of the Caribbean and North American plates in the vicinity of the Puerto Rico Trench. Multi-Channel Seismic reflection data (Larue and Ryan, in press; Fig. 18.2.1) and GLORIA side-scan sonar and single-channel seismic reflection data (Masson and Scanlon, 1991) help constrain these theories.

Larue and Ryan (in press) characterize the trench as a broad, flat-floored basin consisting of up to two seconds of sediment. They characterize the relative plate motion differently along the eastern and western portions of the Puerto Rico slope. In the west the lower slope exhibits abundant evidence of contractional deformation, whereas in the west it exhibits a combination of contractional and transcurrent motion. Due to the lack of a well developed accretionary prism, Larue and Ryan (1990) believe that the deformation along the trench is either very recent or occurring very slowly.

To the north of the trench, the seafloor is broken by numerous normal faults, while to the south of the trench there exist a series of terraces also broken by normal faults. The topography on the southern slope is due mainly to the 19° left-lateral strike-slip fault that in some regions makes up the boundary of the North American and Caribbean plates (Larue & Ryan, in press). In the eastern portion of the trench, there is an overall lack of sediment fill and the trench is narrower than elsewhere (MCS line LS 126 57; Fig 18.2.2). In this region, a small accretionary sedimentary prism overlies undeformed sedimentary strata that are truncated along the top of a packet of gently south-dipping reflectors that are interpreted as the uppermost layers of underthrust oceanic crust (Larue and Ryan, in press). The truncated reflectors along this interface indicate that it is a fault contact with underlying strata.

The western portion of the trench can best be characterized by MCS line NAT 42 (Fig. 18.2.3) Immediately south of the Puerto Rico Trench, Larue and Ryan (1990), find a layer of diffuse south-dipping reflectors that are interpreted as the boundary between the Atlantic oceanic crust and the rocks that underlie the south wall of the trench. It is in this portion of the trench that the valley of the south wall is in alignment with the 19° strike-slip fault that was found in the GLORIA side-scan study (Masson and Scanlon, 1991; described below).

West of MCS line NAT 42, Larue and Ryan (in press) describe the Puerto Rico Trench as strike-slip dominated. This is best shown on MCS line NAT 58 (Fig 18.2.4). Here the north wall of the slope is smooth and discontinuously layered (Larue and Ryan, in press). The evidence for strike-slip motion in this portion of the trench is given by steeply dipping fault complexes against which trench reflectors are deformed. Such structures are known as a contractional flower structure s, and they are common features in areas where strike-slip motion is combined with some contraction (Larue and Ryan, in press).

GLORIA data presented by Masson and Scanlon (1991) show that the floor of the Puerto Rico Trench is easily recognized by a band of low back scattering due to recent turbidite sedimentation. On the lower Puerto Rico slope, a zone of ridges and sediment filled basins occurs between 19°N and 19.5°N. In deeper portions of the trench, the deeper strata are seen to tilt gently southward (Fig. 18.2.5), suggesting that subduction in the trench has either stopped or is occurring extremely slowly (Masson and Scanlon, 1991). The ridges and basins trend 095°-105°, oblique to the axis of the 085° Puerto Rico Trench.

Several 085° to 105° trending lineaments extend for 250 km across the entire Puerto Rico slope. In the west, a similar lineament is found paralleling the main ridge and occurring just

south of the Puerto Rico Trench. These lineaments are thought to be part of a large strike-slip fault system and are seen in figure 18.2.6 (Masson and Scanlon, 1991). Although no offset could be determined from the GLORIA data, the overall left-lateral nature of the North America and Caribbean plate boundary suggests that motion on the Puerto Rico slope fault complex is also left-lateral (Masson and Scanlon, 1991). In light of this, Masson and Scanlon (1991) suggest that the Main Ridge could have formed as the result of a right-step in of the left-lateral strike-slip fault system (Masson and Scanlon, 1991). In contrast, McCann and Sykes (1984) propose that the Main Ridge is a high-standing aseismic ridge that developed along the Atlantic oceanic fracture zone during seafloor spreading.

In the western-most portion of the GLORIA survey, some evidence of recent tectonic activity was found on the northern continental slope of Puerto Rico (McCann, 1985). Here Masson and Scanlon (1991) find numerous faults trending northwest-southeast. It has also been assumed that the Mona canyon, a box shaped canyon with extremely steep walls, is fault controlled. These faults have a north-south trend and are offset by the northeast-southwest-trending faults (Masson and Scanlon, 1991).

Stratigraphy of the Oligocene-early Pliocene shelf and underlying Eocene arc rocks

There are two previous MCS lines that provide synoptic views of the stratigraphy of the Oligocene-early Pliocene shelf and underlying Eocene arc rocks. The purpose of this section is to compare these previous two dimensional attempts to image the margin with a more three dimensional view provided by the EW96-05 SCS lines across the margin of the carbonate margin.

Moussa et al. (1987) seismic stratigraphy of the Puerto Rico margin and CPR4 well stratigraphy. Moussa et al. (1987) interpreted a long MCS line collected by Western Geophysical in the early 1970's and tied to the CPR4 wildcat well (Fig. 2.6A). They divided the line into three parts based on the seismic reflection character and continuity of reflectors:

1) Unit 1 is interpreted as basement rocks of Late Jurassic to mid Eocene age (age based on onshore rocks and dredge hauls). There are no continuous reflections are apparent in this unit. Its upper surface is apparently offset by some large normal faults.

2) Unit 2, a middle unit, has somewhat regular internal reflectors and some reflectors have apparent landward dips suggesting listric faulting. Ages and compositions are poorly constrained but by a process of elimination they suggest an age of late Middle Eocene to Middle Oligocene.

3) Unit 3, the upper unit, has continuous parallel reflectors, a constant thickness, and a constant dip. Unit 3 crops out in karst terrain across northern Puerto Rico and is completely penetrated by well CPR4. Reef or very shallow water limestone and terrestrial clastics of the San Sebastian Fm. are present at the base of the section. Unit 3 ranges in age from mid-Oligocene to early Pliocene.

Larue and Berong (1991) seismic stratigraphy and Toa Baja well stratigraphy. Larue and Berong (1991) collected a 55 km long MCS line (Line 2) that intersects and strikes north of the Toa Baja wildcat well along the north coast of Puerto Rico (Fig. 2.6B). As seen by Moussa et al. (1987) and Birch (1986), they observed deformed Cretaceous and Eocene rocks overlain with angular unconformity by Late Oligocene to Miocene rocks that dip northward by 5° because of late Miocene-Pliocene tectonism.

Three major seismic stratigraphic packages are observed in the well and on Line 2 (Fig. 2.6B):

1) The **uppermost unit** is a north-dipping, planar laminated reflectors, that are Oligocene to Miocene in age according to Montgomery (1991). Larue and Berrong (1991) divide this uppermost unit into two subunits: the upper subunit occurs south of the shelf break is in angular unconformity with the lower subunit. Tilting of upper unit occurred during Late Miocene to Pliocene time. The post-tilt unit can be observed as a northward prograding series of clinoforms from SP 480-400 on line 2 (Fig. 2.6B).

2) The **middle unit** exhibits an anticlinal structure that was originally interpreted as a shelf break reefal buildup. The middle unit shown by drilling to be of Eocene age (volcanic sandstone and rare marly limestone). This section appears to contain bedding-parallel thrust faults. An angular unconformity separates the upper and middle units. There is no obvious discordance between the middle and lower unit in the northern part of the line and only a modest and local unconformity in the southern part of the line. Reflectors in the middle unit apparently downlap the lower unit.

3) The **lowermost unit** is not penetrated by the Toa Baja well and may be of Cretaceous age. The lowermost unit is separated from the middle unit by several high amplitude reflectors. Drilling shows that these reflectors are related to changes in rock type that are possibly associated with bedding parallel thrust faulting and possibly associated with the flow of water into the borehole as indicated by a thermal anomaly. These reflectors are similar to a series of offshore reflectors called reflector R.

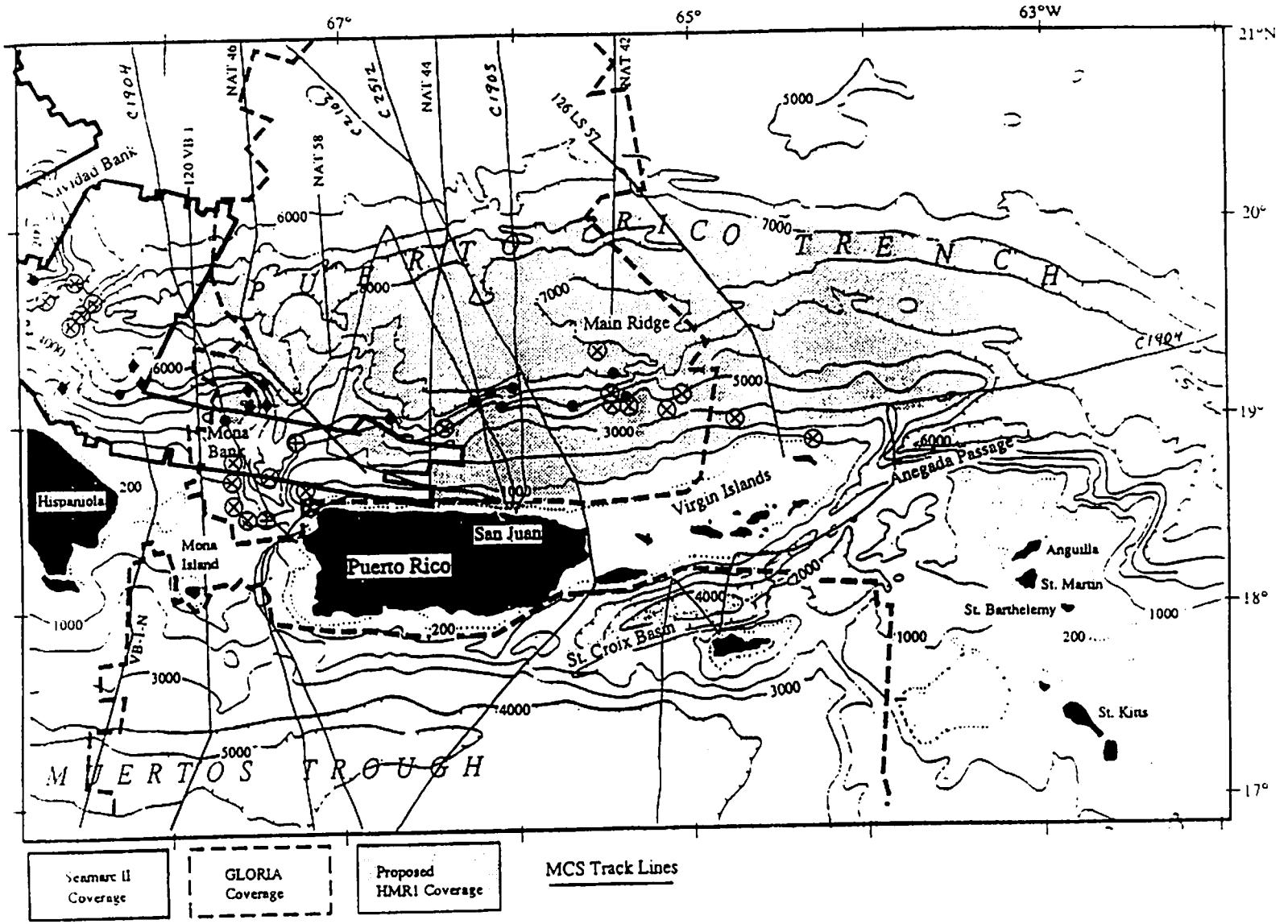

Figure 18.2.1 - Map showing the locations of Larue and Ryan's (1991) MCS reflection lines in the Puerto Rico Trench area.

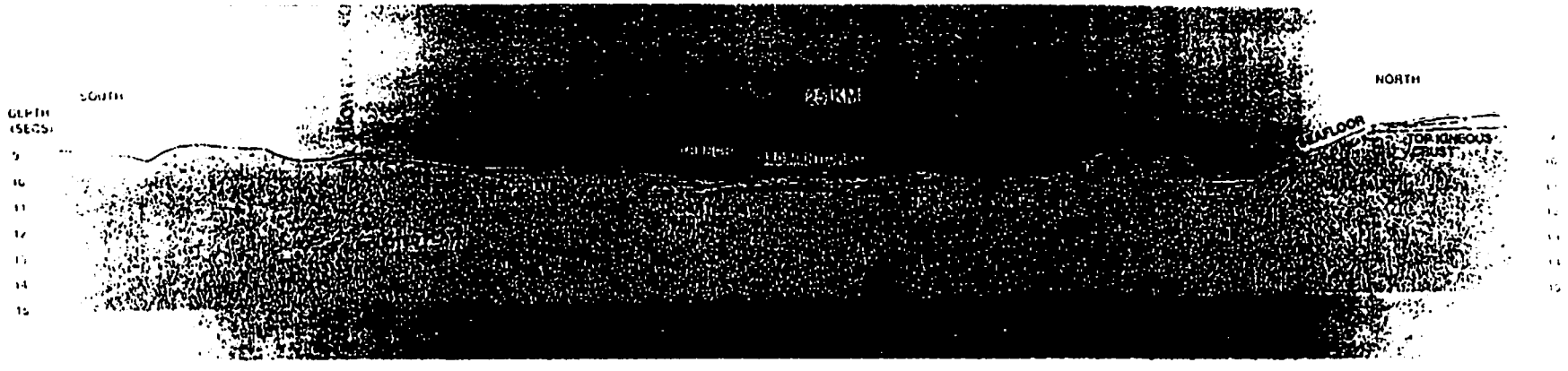

Figure 182.2 - MCS line LS 126 57 (from Larue and Ryan, 1991).

Figure 18.2.3 - MCS line NAT 42 (from Larue and Ryan, 1991).

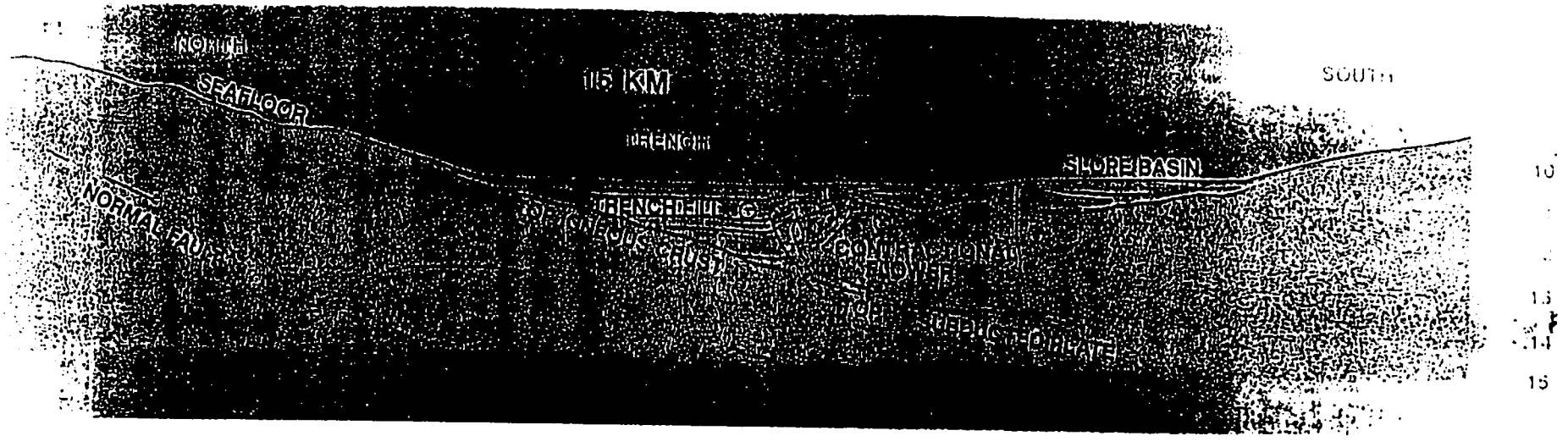

Figure 18.2.4 - MCS line NAT 58 (from Larue and Ryan, 1991).

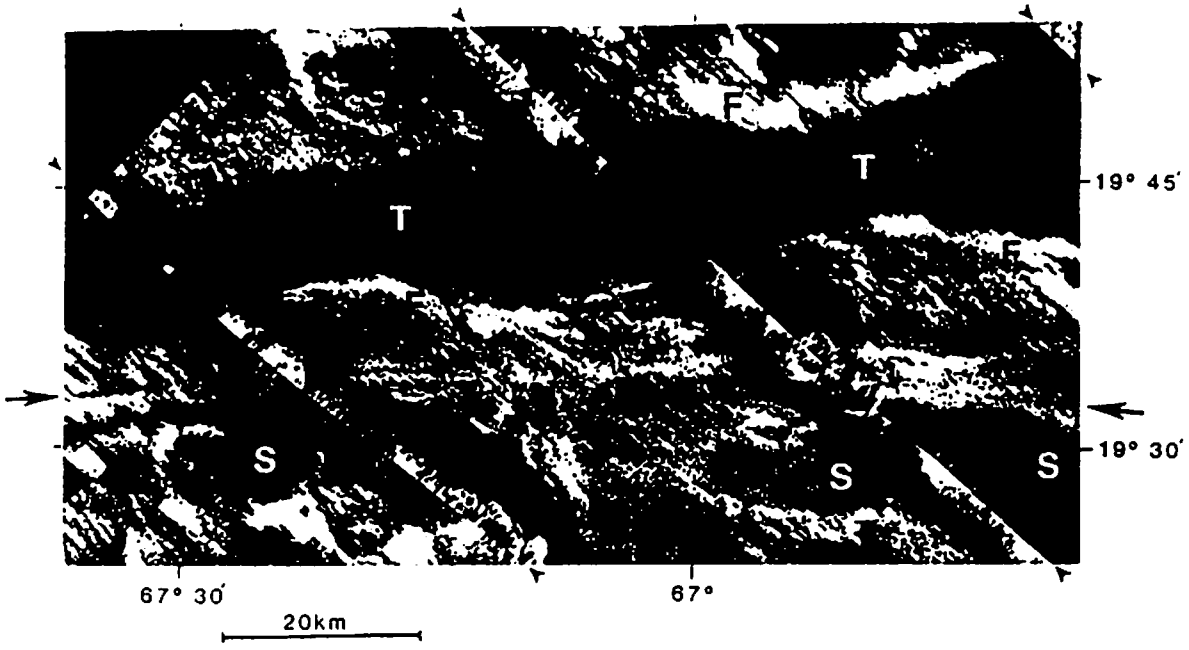

Figure 18.2.5 - GLORIA mosaic of the western portion of the Puerto Rico Trench. Lighter shades indicate areas of high back scattering, small arrowheads indicate the ship's tracks and the large arrowheads are indicative of the strike-slip fault that is found south of, and sub-parallel to the trench.

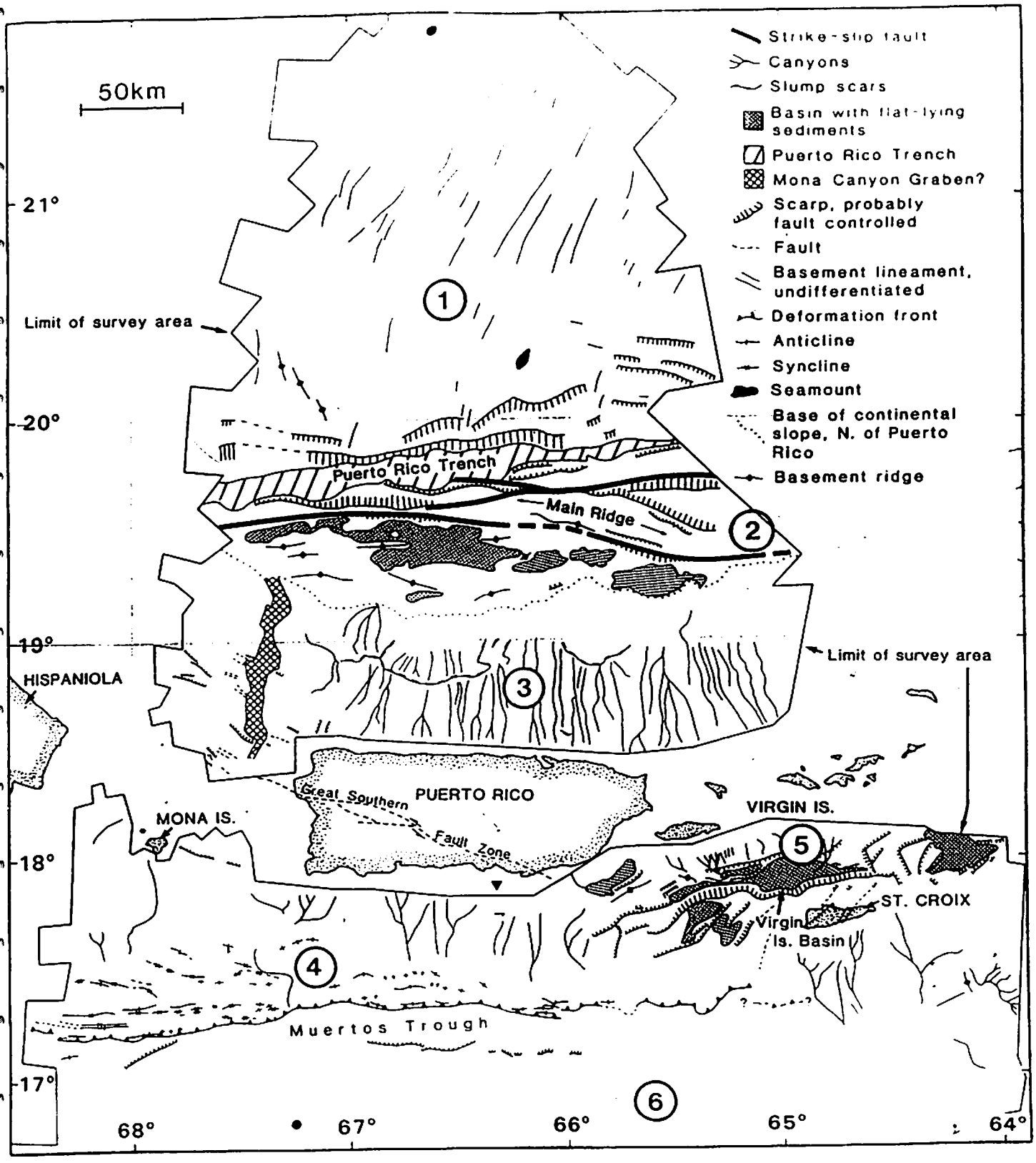

Figure 18.2.6 - Generalized interpretation of tectonic elements mapped in the GLORIA side scan survey (From Masson and Scanlon, 1991).

18.3 Review of Currents and Deposition in Study Area
by John Charles III

The Puerto Rico Trench is a nutrient poor environment with a below average amount of biomass in the sediment. One reason for this is that the island of Puerto Rico has not had a significant role in depositing organic material in the Puerto Rico Trench (Richardson, 1993). This may be because there are only two main entry points for turbidity currents into the trench from Puerto Rico. These two openings are the abyssal plain to the north of the trench and by the Mona Canyon. The flow of organic material is obstructed by the median ridge.

An other source of organic material is biogenic particles. Biogenic particles are only found in the ocean surface waters. The particles consist of microscopic and macroscopic skeletal remains of plankton. Examples of these particles are, plankton foraminifera shells, pteropod shells, radiolarian test and diatom frustules (Honjo, 1986). Since the Puerto Rico Trench is a nutrient poor environment the amount of these creatures is low and therefor their are less amounts of biogenic particles in the trench. The only shells and test that make it to the bottom to form sediment are the larger particles, because as the shells sink to the bottom they start to decompose leaving some of there matter suspended in the water. According to Richardson (1993) the low biomass communities have little effect on the sediment structure.

The Puerto Rico Trench bottom water is affected by the Antarctic Bottom Water Flow (Fig, 18.3.1). It would seem according to McCave and Tucholke (1986) data that the water that flows up from the Antarctic ocean, deposits most of its sediment in the Hatteras abyssal plane because of the Gulf Stream grabs the sediment in the water and traps the sediment (Fig. 18. 3.2).

The currents associated with these bottom waters have potentially redistributed sedimentary layers on the down going North American Plate, depositing sediment on the Greater Antilles Outer Ridge (Bunce et. al, 1974). This current carrying the sediment in the nephloid layer is traveling past the Puerto Rico Trench. Potentially the outer rise is acting as a barricade preventing sedimentation, and/or the trench itself acts as a funnel shooting the water through the trench and eroding the sediments.

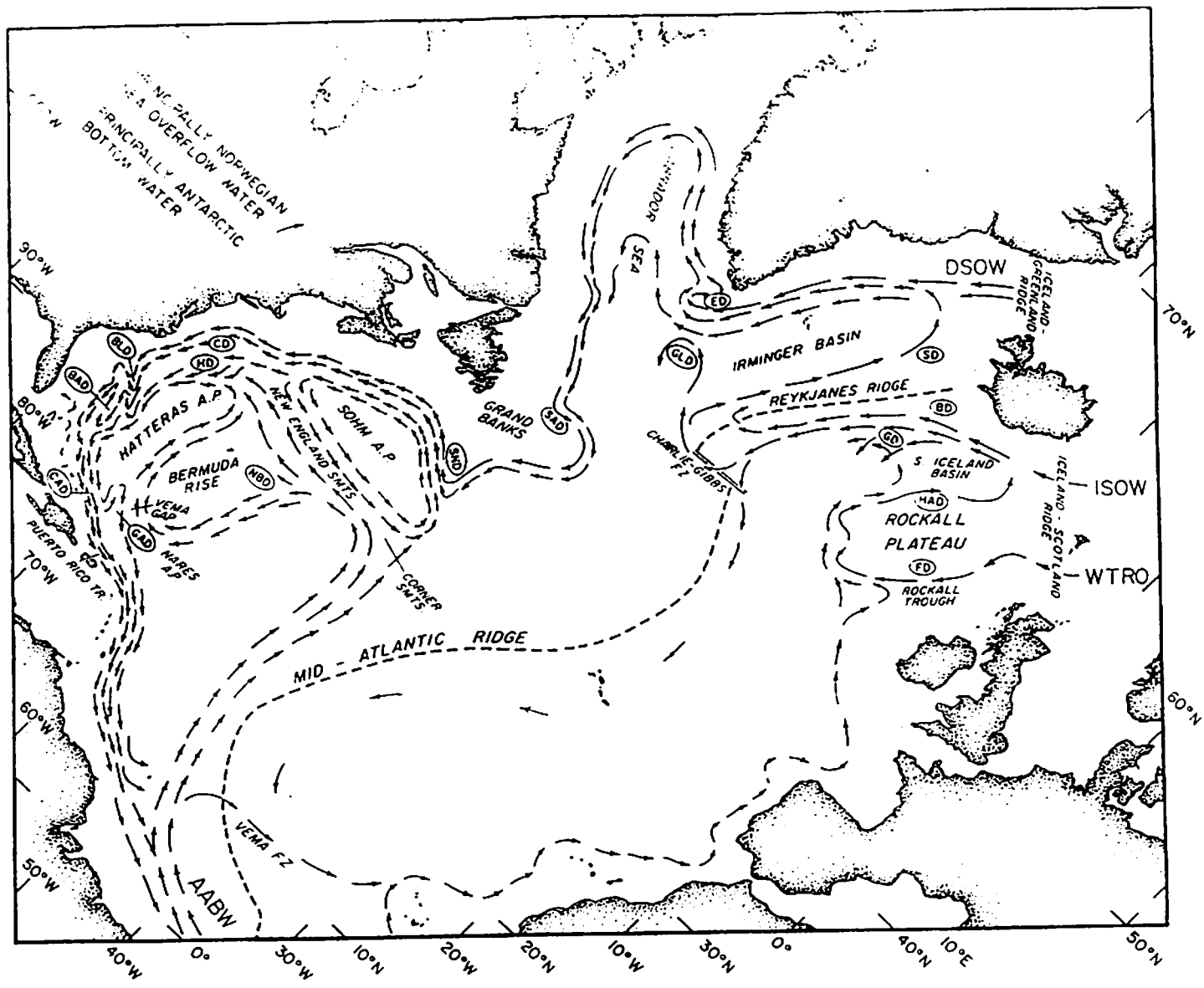

Figure 18,3a. Generalized Circulation of bottom water in the North Atlantic Ocean. DSOW - Denmark Strait overflow water, ISOW - Iceland - Scotland overflow water, WTRO - Wyville - Thomson Ridge overflow, AABW - Antarctic Bottom Water.

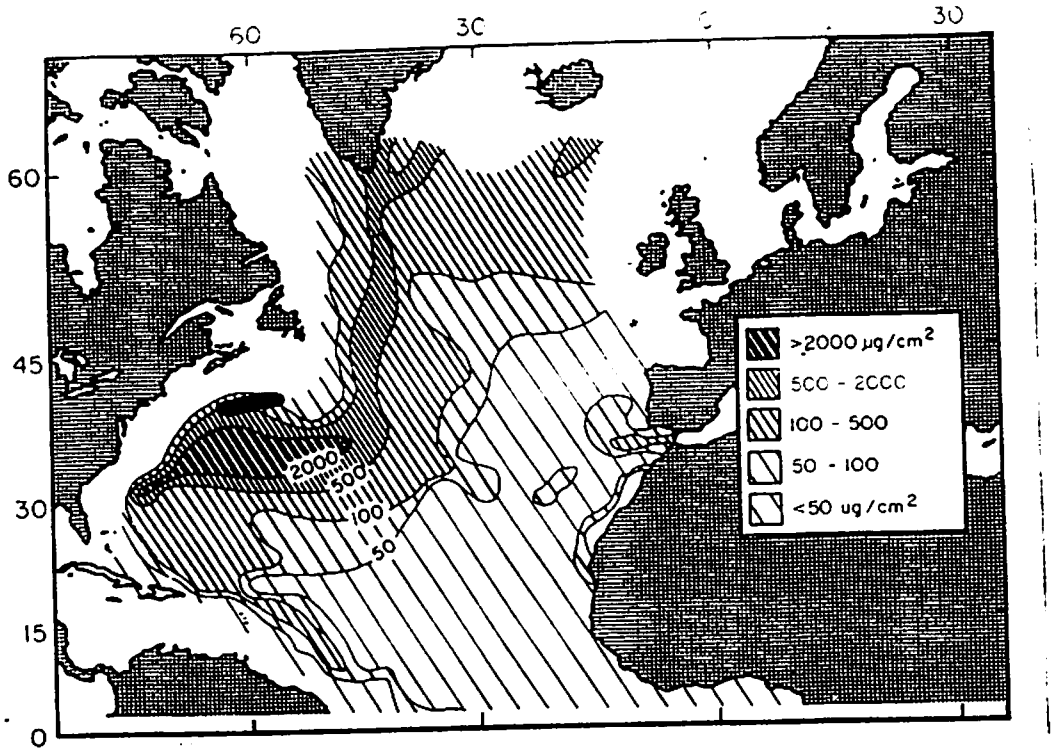

Figure 18, 3b. Map of the net load (mass per unit area) of suspended sediment in the bottom nepheloid layer.

BIBLIOGRAPHY

Alonso-Harris, R.M., Kreig, E.A., and Meyerhoff, A.A., 1987, Post-early Piocene age of the Puerto Rico Trench, in H. Duque-Caro (eds.), *Transactions of the 10th Caribbean Geological Conf.*, 82-103, Cartagena, Columbia.

Austin, J.A., 1983, Overthrusting in a deep-water carbonate terrane. In: A.W. Bally Editor, Seismic Expression of Structural Styles, *Am. Assoc. Petrol. Geol. Stud. Geol.* 15: 3.4.2-167-3.4.2-172.

Ave, L.H., 1990, The Caribbean-South American plate boundary, Araya Peninsula, Eastern Venezuela, In: D.K. Larue and G. Draper (eds)., *Trans. 12th Caribbean Geological Conference*, 461-471.

Ballance, P. School, D., Vallier, T., Stevenson, A., Ryan, H., Herzer, R., 1989, Subduction of a late Cretaceous seamount of the Louisville Ridge at the Tonga trench: A model of normal and accelerated tecontic erosion, Tectonics, 8, 953-962.

Beach, D.K. and Trumbull, J.V.A., 1981, Marine geologic map of Puerto Rico insular shelf, Isla Caja de los Muertos area, *United States Geological Survey. map.*

Byrne, D. B., G. Suarez, and W. R. McCann, 1985, Muertos Trough subduction--Microplate tectonics in the northern Caribbean: *Nature*, v. 317, p. 420-421.

Birch, F.S., 1986, Isostatic, thermal and flexural models of the subsidence of the north coast of Puerto Rico, *Geology*, v. 14, p. 427-429.

Birch, F.S., 1970, The Barracuda fault zone in the western North Atlatnic: Geological and geophysical studies, *Deep Sea Res.*, 17, 847-859.

Bowin, C.O., Nalwalk, A.J. and Hersey, J.B., 1966, Serpentinized peridotite from the North wall of the Puerto Rico Trench, *GSA Bull.*, 77, 257-270.

Bowin, C., 1972, Puerto Rico trench negative anomaly belt, GSA Mem. 132, 339-350.

Bowin, C., 1976, Caribbean gravity field and plate tectonics, GSA Special paper 169, 79.

Bunce, E.T. and Fahlquist, D.A., 1962, Geophysical Investigations of the Puerto Rico Trench and Outer Ridge. *Jourr. Geoph. Res.*, 67, 3955-3972.

Bunce,E.T. and Hersey, J.B. 1966, Continuous seismic profiles of the Outer Ridge and Nares Basin North of Puerto Rico., *Geol. Soc. Am. Bull.*, v.77, 803-812.

Bunce,E.T., Phillips, J.D., and Chase, R.L. 1974, Geophysical study of Antilles Outer Ridge, Puerto Rico Trench, and Northeast Margin of Caribbean Sea. *Am.Assoc.Petrol.Geol, Bull*, v.58(1), 106-123.

Calais, E., Béthoux, N., and Mercier de Lépinay, B., 1991. From transtension to traspression along the northern Caribbean plate boundary off Cuba: implications for the Recent motion of the Caribbean plate. *Tectonophysics*, 186, 329-350.

Calais, E., Béthoux, N., and Mercier de Lépinay, B., 1992, From transcurrent faulting to frontal subduction: A seismotectonic study of the northern Caribbean plate boundary from Cuba to Puerto Rico: *Tectonics*, v. 11, p. 114-123.

Calais, E. and Mercier de Lepinary, B., 1993, Semiquantitative modeling of strain and kinematics along the Caribbean/North America strike-slip plate boundary zone, *Jour. Geophys. Res.*, v.98, p. 8293-8308.

Calais, E. and Mercier de Lepinay, B., 1995. Strike-slip tectonic processes in the northern Caribbean between Cuba and Hispaniola (Windward Passage): *Mar. Geophys. Res.*, 63-95.

Clague, D. A., and Straley, P. F., 1977, Petrologic nature of the oceanic Moho: Geology, v. 5, p.133-136.

Connolly, F. and Ewing. M., 1967, Sedimentation in the Puerto Rico Trench, *J.our. Sed. Petrology*, 37, 44-59.

Crook, K. A. W., 1989, Suturing history of an allochthonous terrane at a modern plate boundary traced by flysch-to-molasse facies transitions: *Sedimentary Geology*, v. 61, p. 49-79.

Dehlinger, P. and Antonie, J.W. 1962, Seismic refraction profiles on the Outer Ridge north of Puerto Rico. *The A&M College of Texas.*

Denning, W.H., 1995, Preliminary results of the geophysical investigations for gas and oil on the south coast of Puerto Rico., *Puerto Rico Division of Mineralogy and Geology Bulletin*, 2, 17.

Dillon, W.P., Austin, J., Scanlon, K., Edgar, N. and Parson, L., 1992, Accretionary margin of north-western Hispaniola: Morphology structure and development as part of the northern Caribbean plate boundary: *Marine and Petroleum Geology*, v. 9, p. 70-88.

Dillon, W.P. and Coleman D.F., 1996, Plate responses to the transition from subduction to strike-slip motion in the northeastern Caribbean- hypothesis on the origin of the Puerto Rico Trench., *Geology*, submitted.

Dobrin and Savit, 1988, Introduction to Geophysical Prospecting: McGraw-Hill Book Company, New York, New York, p. 631-666.

Dolan, J., Mann, P., de Zoeten, R., Heubeck, C., Shiroma, J. and Monechi, S., 1991, Sedimentologic, stratigraphic and tectonic synthesis of Eocene-Miocene sedimentary basins, Hispaniola and Puerto Rico. In: P. Mann, G. Draper and J.F. Lewis (eds.) Geologic and Tectonic Development of the North America-Caribbean Plate boundary in Hispaniola, *Geological Society of America Special Paper*, 262, 217-264.

Dolan, J. and Wald, D., Localization of large thrust earthquakes at the Hispaniola-Bahamas collision zone, in prep.

EEZ SCAN 85 Scientific Staff, 1987, Atlas of the US Exclusive Economic Zone, eastern Caribbean: *US Geologic Survey Miscellaneous Investigation* Series I-1864-B, 58 p.

Erikson, J.P., Pindell, J.L. and Laure, D.K., 1990, Mid-Eocene-early Oligocene sinistral transcurrent faulting in Puerto Rico associated with the formation of the northern Caribbean Plate Boundary zone. *Journal of Geology*, 98 (3): 365-384.

Ewing, J.I. and Heezen, B.C. 1955, Puerto Rico Trench topographic and geophysical data. In: A. Poldervaart (eds), Crust of the Earth (A symposium): *Geological Society of America Special Paper*, 62, 255-267.

Ewing, J., Talwani, M. amd Ewing, M. 1966, Sediment distribution in the Caribbean Sea. *Trans, 4th Caribb. Geol. Conf.*, p. 317-323.

Ewing, M., Lonardi A., and Ewing, J., 1966, The sediments and topography of the Puerto Rico trench and outer ridge, *Trans, 4th Caribb. Geol. Conf.*, p. 325-334.

Fink, L. K. and Harrison, C. G. A., 1972, Paleomagnetic investigations of selected lava units on Puerto Rico: *Transactions 6th Caribbean Geological Conference Proceedings*, 379 p.

Fischer, K. M. and W. R. McCann, 1984, Velocity modeling and earthquake relocation in the North East Caribbean: *Seismological Society of America Bulletin*, v. 74, p. 1249-1262.

Fox, J. and Heezen, B., 1975, Geology of the Caribbean crust, in *The Ocean Basins and Margins*, vol. 3 edited by A. Nairn and F. Stehli, pp.421-466, New York, NY.

Gardner, W.D., Glover, L.K., and Hollister, C.D., 1980, Canyons off northwest Puerto Rico: Studies of their origin and maintenance with the nuclear research submarine NR-1, *Marine Geology*, 37, 41-70.

Garrison, L.E., 1969, Structural Geology of the Muertos Insular shelf, Puerto Rico., *U.S. Geological Survey, Open File Report*,

Geddes, W. and Dennis, L., 1964, Preliminary report on a special aeromaganetic survey of the Puerto Rico Trench. *A study of the Serpentinite the AMSOC core hole near Mayaguez, Puerto Rico*, 188: 175.

Glover, L., 1971, Geology of the Coamo area, Puerto Rico, and its relation to the volcanic arc-trench association. *U.S. Proffesional Paper*, 636, 102 p.

Griscon, A. and Geddes, W., Island-arc structure interpreted from aeromagnetic data near Puerto Rico and the Virgin islands, 1966, *Geol. Soc. Am Bull.*, v.77, 153-162.

Hersey, J.B., Findgs made during the June 1961 Cruise of the R/V Chain to the Puerto Rico Trench and the Outer Ridge, J. Geophys. Res., 67, 498-511, 1962.

Honjo, S., 1986. "Oceanic Particles And Pelagic Sedimentation In The Western North Atlantic Ocean," The Geology of The North America Volume M. The Geological Society of America, Boulder, Colorado

Iiyama, J., Bourgois, J., Mercier de Lepinay, B., Tournon, J. Muller, C., Butterlin, J., and Glacon, G. 1985., Premiers resultats de la campagne d'essai du submersible francais <<Nautile>> dans la fosse de porto-Rico (Grandes Antilles). *C.R.acad.Sc.Paris.*, 301 (II) 10, 743-749.

Ito, M., and Matsuda, F., 1986, Evolution of clastic piles in an arc-arc collisions zone: Late Cenozoic depositional history around the Tanzawa Mountains, central Honshu, Japan: *Sedimentary Geology*, v. 49, p. 223-259.

Heezen, B.C., Nesteroff, V., Rawson, M., Freeman-Lynde, R.P., 1985, Visual evidence for subduction in the western Puerto Rico Trench, Geodynamiques des Caribes, Symposium Paris, Editions Technip.

Heubeck, C., Mann, P., Dolan, J., and Monechi, S., 1991, Diachronous uplift and recycling of sedimentary basins during Cenozoic tectonic transpression, northeastern Caribbean plate margin: *Sedimentary Geology*, v. 70, p. 1-32.

Heubeck, C. and Mann, P., 1991, Geologic evaluation of plate kinematic models for the North American-Caribbean plate boundary zone, *Tectonophys.*, v. 191, p.1-26.

Jany, I., Mauffret, A., Bouysse, P., Mascle, A., Mercier de Lepinay, B., Renard, V., and Stephan, F., 1987. Releve bathymetrique Seabeam et tectonique en decrochements au sud des Iles Vierges (Nord-Est Caraibes). *C.R.Acad.Sc.Paris*, 304 (II) 10, 527-532.

Jordan, T., 1975, The present-day motions of the Caribbean plate, *J. Geophys. Res.*, 80, p. 4433-4439.

Kelleher, J., Sykes, L., and Oliver, J., 1973, Possible criteria for prediction earthquake locations and their application to major plate boundaries of the Pacific and the Caribbean: *Jour. Geophys. Res.*, v. 78, p. 2547-2585.

Klitgord, K.d. and Schoute, H. 1986. Plate kinematics of the Central Atlantic. In: The Geology of North America. vol. The Western North Atlantic Region. Eds. Vogt, P.R. and Tucholke, B.E. .*Geol Soc. Am. Bull.*,351-378.

Ladd, J.W., Holcombe, T.L., Westbrook, G.K., and Edgar, N.T. 1990. Caribbean marine geology; Active margins of the plate boundary. In: The Geology of North America. vol. The Caribbean Region. Eds. Dengo, G and Case, E.J. *Geol Soc. Am. Bull.*, 261-285.

Larue, D.K. 1994. Puerto Rico and the Virgin Islands. In: Caribbean Geology: An Introduction. U.W.I. Publishers' Association, Kingston. 151-165.

Larue, D.K. and Berrong, B., 1991, Cross-SEction through the Toa Baja drillsite: Evidence for northward change in Late Eocene deformatin intensity, *Geophys. Res. Lett*, 18,561-564.

Larue, D.K. and Ryan, H.F. 1989, Extensional Tectonism in the Mona Passage, Puerto Rico and Hispaniola: A Preliminary Study. *Trans. 12th Caribbean Geological Conference.*, 223-230.

Larue, D.K. and Ryan, H.F. 1996, Seismic Reflection Profiles of the Puerto Rico Trench: Bearing on motion between the North American and Caribbean Plates. submitted.

Larue, D. K. , Joyce, J. and Ryan, H., 1989, Neotectonics of the Puerto Rico Trench: Extensional tectonism and forearc subsidence, *Trans. 12th Caribbean Geological Conference*, p. 231-247.

Lundgren P.R., and Russo, R.M. 199. Finite element Modeling of crustal deformation in the North America-Caribbean Plate Boundary Zone. submitted

Maley, T.S., Sieber, F.D. Johnson, G.L. , 1974, Topography and Structure of the Western Puerto Rico Trech. *Geol. Soc. Am. Bull.*, v.85, 513-518.

Mann, P. and K. Burke, 1984, Neotectonics of the Caribbean: *Reviews of Geophysics and Space Physics*, v. 22, p. 309-362.

Mann, P., Schubert, C. and Burke, K., 1990, Review of Caribbean neotectonics. In: G. Dengo and J.E. Case (editors), The Geology of North American, vol. H, The Caribbean Region. *Geol. Soc. Am.*, Boulder, CO, p. 307-337.

Mann, P, Tyburski, S., and Rosencrantz, E., 1991, Neogene development of the Swan Islands restraining-bend complex, Caribbean Sea, *Geology*, v. 19,p. 823-826.

Mann, P., Taylor, F.W., Edwards, R.L. and Ku, T.L., 1995, Actively evolving microplate formation by oblique collision and sideways motion along strike-slip faults: An example from the northeastern Caribbean plate margin. *Tectonophysics*, 246, 1-69.

Mann, P., Draper, G., and Lewis, J.F., 1991, Overview of the geologic and tectonic development of Hispaniola, in Mann, P., Draper, G., and Lewis, J.F., eds., Geologic and tectonic development of the North America-Caribbean plate boundary in Hispaniola: *GSA Special Paper* 262, p. 1-28.

Masson, D. G. and K. M. Scanlon, 1991, The neotectonic setting of Puerto Rico: *Geological Society of America Bulletin*, v. 103, p. 144-154.

Mattson, P., Draper, G. and Lewis, J.F. 19 , Puerto Rico and the Virgin Islands., In: Eds. Lewis, J.F. and Draper, G. 112-120.

Mauffret, A., and Jany I., 1990, Collision et tectonique d'expulsion le long de la frontiere Nord-Caraibe. *Oceanologica Acta*, v.10, 97-116.

McCann, W. R., 1985, On the earthquake hazards of Puerto Rico and the Virgin Islands: *Seismological Society of America Bulletin*, v. 75, p. 251-262.

McCann, W. and Sykes, L., 1984, Subduction of aseismic ridges beneath the Caribbean plate: Implications for the tectonics and seismic potential of the Northeastern Caribbean, *Jour. Geophys. Res.*, v. 89, p. 4493-4519.

McCann, W. R., and Habermann, R. E., 1989, Morphologic and geologic effects of the subduction of bathymetric highs: *Pure and Applied Geophysics*, v. 129, p. 41-68.

McCann, W.R., and Pennington, W.C., 1990, Seismicity, large earthquakes, and the margin of the Caribbean plate. In: G. Dengo and J.D. Case (editors), The Geology of North America, v. H, The Caribbean Region, *Geol. Soc. Am.*, Boulder, CO, pp. 291-305.

McCave, I. N. and B. E. Tucholke, 1986. "Deep Current-Controlled Esdimentation In The Western North Atlantic," The Geology OF The North America Volume M. The Geological Society of America, Boulder, Colorado

Meyerhoff, H.A., 1975., Stratigraphy and Petroleum possibilities of Middle Tertiary rocks in Puerto Rico: Discussion. *Am.Assoc.Petrol Geol.Bull.*, 169-175.

Molnar, P., and L. R. Sykes, 1969, Tectonics of the Caribbean and Middle America regions from focal mechanisms and seismicity: Geol. Soc. America Bull., v. 80, p. 1639-1684.

Monroe, W.H., 1968, The Age of the Puerto Rico Trench. *Geol. Soc. Am. Bull.*, v.79, 487-494.

Monroe,W.H., 1973, Stratigraphy and Petroleum possibilities of Middle Tertiary rocks in Puerto Rico. *Am. Assoc. Petrol Geol. Bull.*, v.57 (6). 1086-1099.

Moussa, M.T., 1977, Bioclastic sediment gravity flow and submarine sliding in the Juana Diez Formation, southwestern Puerto Rico, *Jour. Sedment. Petrol.*, 47(2), 593-599.

Moussa, M.T., and Seiglie, G.A.,1975, Stratigraphy and Petroleum possibilities of Middle Tertiary rocks in Puerto Rico: Discussion. *Am.Assoc.Petrol.Geol.Bull.*, 163-168.

Moussa, M.T., Seiglie, G.A., Meyerhoff, A.A. and Taner, I. ,1987, The Quebradillas Limestone (Miocen-Pliocene), northern Puerto Rico, and tectonics of the northeastern Caribbean margin. *Geol. Soc. Am. Bull.*, v.99, 427-439.

Mullins, H.T., Breen, N., Dolan, J., Wellner, R., Petruccione, J., Gaylord, M., Andersen, B., Mellillo, A., Jurgens, A. and Orange, D., 1992, Carbonate platforms along the Southeast Bahamas-Hispaniola collision zone, *Marine Geology*, v. 105, 169-209.

Officer, C.B., Ewing, J.I., Edwards, R.S. and Johnson, H.R. 1957, Geophysical investigations in the Eastern Caribbean: Venezuelan Basin, Antilles Islands arc and Puerto Rico Trench. *Geol. Soc. Am. Bull.*, v. 68, 359-378.

Perfit, M.R., Heezen, B.C., Rawson, M . and Donnelly, T., 1980, Chemistry, origin and tectonic significance of metamorphic rocks from the Puerto Rico Trench, *Marine Geology*, v. 34, p. 125-156.

Prentice, C.S., Mann, P., Taylor, R.W., Burr, G., and Valastro. S., Jr., 1993, Paleoseismicity of the North American-Caribbean plate boundary (Septentrional fault), Dominican Republic: *Geology*, v. 21, p. 49-52.

Prentice, C.S., Mann, P., and Burr, G., Long-term rates of plate offset and paleoseismicity of the North America-Caribbean boundary, in preparation.

Richardson,M.D., Briggs, K.B., Bowles, F.A. and Tietjen,J.H., 1995, A depauperate benthic assemblage from nutrient-poor sediments of the Puerto Rico Trench. *Deep-Sea Research I*, v. 42, 351-364.

Rosencrantz, E. and P. Mann, 1991, SeaMARC II mapping of transform faults in the Cayman Trough, Caribbean Sea: *Geology*, v. 19, p. 690-693.

Russo,R.M. and Speed,R.C., 1992, Oblique collision and tectonic wedging of the South American continent and Caribbean terranes. *Geology*, v.20, 447-450.

Savit,C.H., Knox,W.A., Blue,D.M., and Paitson,L., 1964, Reflection and Velocity profiles at the Outer Ridge, Puerto Rico., *Jour. Geoph.Res.*, v. 69, 701-719.

Scanlon,K.M., Masson,D.G. and Rodriguez,R.W., 1988, Gloria sidescan-sonar survey of the EEZ of Puerto Rico and the U.S. Virgin Islands. *Trans. 11Th. Caribbean Geological Conference*. 31, 1-32:9

Schell,B.A. and Tarr,A.C., 1978, Plate tectonics of the Northeastern Caribbean sea Region. *Geologie en Mijbouw*, v.57 (2) 319-324.

Schwab, W. C., Danforth, W. W., Scanlon, K. M., and Masson, D. G., 1991, A giant submarine slope failure on the northern insular slope of Puerto Rico: *Marine Geology*, v. 96, p. 237-246.

Seiders, V.M., Briggs, R.P. and Glover, L., 1972, Geology of Isla Desecho, Puerto Rico, with notes on the Great Southern Puerto Rico Fault Zone and Quaternary stillstands of the sea., *U.S. Geological Survey Professional Paper*, 739, 22p.

Seiglie, G.A., and Moussa,M.T., 1984, Late Oligocene-Pliocene Transgressive-Regressive Cycles of sedimentation in Northwestern Puerto Rico. In: J. Schlee (eds), Interregional unconformities and hydrocarbon accumulation, *Am. Ass. Petrol. Geol.* Mem., 36.

Shurbet, G.L. and Ewing, M., 1956, Gravity reconnaissance survey of Puerto Rico, *Geol. Soc. Am. Bull* 67, 511-534.

Speed, R. and Larue, D., 1991, Extension and transtension in the splate boundary zone of the northeastern Caribbean, *Geophys. Res. Lett.*, 13, 573-576.

Stein, S., C. DeMets, R. G. Gordon, J. Brodholt, D. Argus, J. F. Engeln, P. Lundgren, C. Stein, D. S. Weins, and D. F. Woods, 1988, A test of alternative Caribbean plate relative motion models: *Jour. of Geophys. Res.*, v. 93, p. 3041-3050.

Stephan, J.F. Blanchet, R. and Mercier de Lepinay, B., 1986, Northern and Southern Caribbean festoons (Panama, Colombia- Venezuela and Hispaniola - Puerto Rico), interpreted as pseudosubductions induced by the east-west shortening of the pericaribbean continental frame., In: F.C. Wezel (eds), The origin of the arcs. *Developments in Geotectonics*, 21, 401-422.

Sykes, L. R., W. R. McCann, and A. L. Kafka, 1982, Motion of Caribbean plate during last 7 million years and implications for earlier Cenozoic movements: *Jour. Geophys. Res.*, v. 87, p. 10656-10676.

Taggart, B.E. and Joyce, J. 1991, Radiometrically dated marine terraces on northwestern Puerto Rico, In: D.K. Laure and G. Draper (Eds), *Transc. 12th Caribbean Geological Conference*, 248-258.

Talwani, M., Sutton, G.H., and Worzel, J.L. A crustal section across the Puerto Rico Trench., *Joour. Geoph. Res.*, 65, 1545-1555.

Threadgold, G. E., 1985, Modelling and interpretation of the oceanic crustal structure north of the Puerto Rico Trench: Masters Thesis, The University of Texas at Austin.

Tucholke,B.E. and Ewing,J.I., 1974, Bathymetry and sediment Geometry of the Greater Antilles Outer Ridge and Vicinity. *Geol. Soc. Am. Bull.*, v. 85, 1789-1802.

Valyashko,G.M., Yel'tsina, G.N. Litvin, V.M., Rudenko, M.V., Ryabukhin, A.G., Savostin, L.A. and Khain, V.Y., 1976, New data on structure of deep-water trenches, Puerto Rico y Cayman, *Vest. Mosk. Univ.., Ser. Geol.* 1, 34-43.

Van Voorhis, G.D. and Davis, T.M., 1964, Magnetic Anomalies North of Puerto Rico: Trend removal with orthogonal polynomials. *Jour. Geoph. Res.*, v. 69, 5363-5371.

Vening Meinesz, F.A., Umbgrove, J.H.F., and Kuenen, P.H., 1934, Gravity expeditions at sea 1923-1932, Delft, 2d Netherlands Geod. Comm., 139p.

Vila,J.M., Jany, I., Lepvrier, C., Feinberg H. and Mauffret, A., 1990, Mise en evidence de l'age post-pliocene inferieur de la collision entre la ride de Beata et l'orogene nord-caraibe (Grandes Antilles). *C.R.Acad.Sci.Paris*, v. 311(II), 1359-1366.

Vogt, P.R., 1986, Magnetic anomalies and crustal magnetization, in Vogt, P.R., and Tucholke, B.E., eds., The Geology of North America, v. M., The Western North Atlantic Region: *Geol Soc Am.*, Boulder, CO 229-256.

Vogt. P.R., Anderson, C.N. and Bracey, D.R., 1971, Mesozoic magnetic anomalies. sea-floor spreding and geomagnetic research in the southwestern North Atlantic, *J. Geophys. Res.*, 76, 4796-4823.

von Huene, R. and Lallemand, S., 1990, Tectonic erosion along the Japan and Peru convergent margins, GSA Bull., 102,704-720.

von Huene, R. and 16 others, 1995, Morphotectonics of the convergent margin of Costa Rica, in Mann, P., eds. *Geologic and Tectonic Development of the Caribbean Plate Boundary in Southern Central America*, GSA special paper 295.

Weaver, J.D., A.L. Smith and G. Sieglie, 1975, Geology and Tectonics of the Mona Passage, *Eos, Trans. Amer. Geophys. Union*, v.56, p.45.

Wessel, P., and W. H. F. Smith, New version of the Generic Mapping Tools Released: *EOS Trans. Amer. Geophys. U.*, v. 76, p. 329, 1995.

Westbrook, G.K. and McCann, W.R., 1986, Subduction of Atlantic lithosphere beneath the Caribbean., In: G. Dengo and J.E. Case (editors), The Geology of North American, v. M, The Western North Atlantic Region. *Geol. Soc. Am.* .Boulder CO, 341-350.

APPENDICES

APPENDIX I - CRUISE EW96-05 DAILY JOURNAL
SAN JUAN-SAN JUAN, PR JUNE 15 - JULY 8, 1996

by Nancy Grindlay

JD167, Saturday June 15
Departed San Juan, PR Saturday 12:00 PM Local Time, 16:00 GMT

Cleared San Juan harbor in about an hour, once we reached depths of 500 m began deployment of MR1 system. Fully deployed by 1900 GMT

JD168, Sunday June 16
Began recording seismics at 0048 GMT. Started with a 10 sec sampling interval but by the end of the first run realized for the deeper waters a 12 sec sampling interval would be more appropriate as we were clipping the deep bottom signal with the shorter interval. Pop rates for the guns ranged from 12 sec to 16 sec. With the sampling interval, pop rates must be at least 2 sec greater to allow for data recording. Planned profile spacing of 14 km ~7.55nm, profile length, approx. N21E orientation. Profile nomenclature PRLINE#

MR1 data initially looked good. Starboard bathymetry was rough on the outer portions of the swath, but we had been forewarned about this problem. When we passed over the shelf and into water depths >5000m about six hours into the first deployment we became aware of a severe problem with both starboard sidescan and bathymetry. The majority of the starboard side-scan swath became uniformly gray, showing little to no evidence that we were actually collecting data in this region. We decided to cut the line short passing over the Marginal Basin and coming to the apex of the Main Ridge at approximately 19°35'N and turning west to run a line southward into shallow waters. MR1 data did not improve so the decision was made to recover at approximately 1300 GMT half way down the return profile. After recovering the MR1 we redeployed the guns and continued seismic profiling with PRLIN1A.

Began new seismic line PRLINE3 at approximately 2322 GMT

JD169, Monday June 17
End of seismic line PRLINE3 at 0314 GMT, begin deployment of MR1. No obvious reason why MR1 was malfunctioning. Found some wet connectors on fish? Ran multiple tests on various components. MR1 fully deployed by 0348 GMT. New seismic line PRLIN3A begun at 0458 GMT. Once again sidescan data initially looked good in shallow water but soon after deployment began to get telemetry errors indicating lack of communication between ship and fish, as well as overall background noise interference. First telemetry error occurred at 1008 GMT within the next few hours rate of telemetry errors increased. Decision was made to recover fish once again. End of seismic line PRLIN3A at 1520 GMT. MR1 recovered at approximately 1700 GMT. Begin new seismic line PRLIN3B at 1717 GMT.

While recovering tow fish it was discovered that the coaxial cable to the fish had been damaged and would need to be reterminated (6-7 hr job). Upon opening the fish onboard it became apparent that several pieces of hardware had been damaged (including an array of transducers on starboard side) and would need to be replaced and tested. Discussed possibility of flying in engineer from Hawaii to meet ship in San Juan. Would take 24 hrs to get him here. Several calls were made by the MR1 group to engineer in Hawaii to discuss possible cause of problems and means to test. Decision was made to replace parts, reterminate cable, run tests, redeploy and see results before flying in engineer.

JD170 Tuesday June 18

Meanwhile finished seismic line PRLIN3B turned eastward to PRLINE4 southward, begin time 0400 GMT. We extended these profiles further north than originally planned to the outer ridge on the down going North American plate. Wanted to image the trench parallel normal faults which seem to lack the typical horst and graben relation seen at other subduction zones. More like the inner wall of a mid-ocean ridge, a series of down-stepping normal faults. We also extended the line close to PR shore to water depths ~500 m to potentially image any near shore deformation.

Finally got Dominican Republic Clearance.

JD171 Wednesday June 19
End of PRLINE4 at approximately 0400 GMT, begin deployment of MR1. Begin seismic line PRLINE5 at 0619 GMT. MR1 data looked good initially, we were in shallow water, as depth increased to >4500m the same problems on the starboard side began to appear. Initially this gray shadow as attributed to problems with the timing of the gain step toward the outer edges of the swath and it was thought by increasing the widths of the gain step to essentially a half swath the gray shadow problem would disappear. This was not the case. Bathymetry on starboard side is totally bogus. Both seismic and Hydrosweep systems all through the ordeal with the MR1 have been working beautifully. We decided to increase the sampling rate of the seismic system to 7000 samples or 14 sec in the deep waters of the trench and that seems to give us fair penetration (also requires that we stop and start a new line thus the nomenclature 5, 5A in line numbering). Seismic data to this point show little evidence of deformation (compressional or otherwise) in trench. Paul speculates that the trench is a dead or relict feature comparable to the trenches near the Macquire Ridge. End seismic line PRLINE5 at 1322 GMT, begin seismic PRLIN5A 1327 GMT. We observe our first solid evidence of compressional deformation in trench at 2130 GMT in basin of turbidites, high angle thrust fault s (80°)with monoclinal fold.

JD172 Thursday June 20
Start turn to east at 0113 GMT, end of seismic line PRLIN5A at 0140 GMT beginning of line PRLINE6 at 0150 GMT. After over 16 hours of analysis MR1 group decides that the starboard sidescan and bathymetry has a series problem. Transducer array has blown again for unknown reasons. This means that there is not enough signal to generate bathymetry data at any depth, and sidescan at depths greater than 4500-5000m. Thus far the decision is to have the Hawaii engineer fly out arriving tomorrow sometime and possibly grabbing a launch out to the R/V EWING. What we have to negotiate is getting an extra day or more from NSF to cover the time it will take him to fix the system. Finished PRLINE6 at 1440 GMT begin PRLIN6A at 1446 GMT, changing recording interval to 12s and pop interval to 14 s. End of PRLIN6A at 1838 GMT, turn eastward on to new line PRLINE7 at 1904 GMT. Finished PRLINE7 at 2358 GMT

Been having problems with tape drive number 2 for recording seismic data. When we start a new line the system will first go to drive 3, gets a message that its not ready, then back to drive 2, has some kind of write problem, will try to write a couple of shots, fail, print out a label, then go back to drive 3 and start a new reel.

JD173 Friday June 21
Started PRLIN7A at 0003 GMT. This change over from 12s to 14s sampling interval at 5000 m happens, depending on the orientation of the profile, just before or after a break in the slope, limestone platform, at about 4000 m which seems to mark a giant headwall for mass wasting slumps. We have seen this break in slope on every line. We continue to get complete sidescan coverage in water depths <4500m, only port side in water depths >4500m. Bathymetry is okay on port throughout, bogus on starboard throughout. Channels incised into the limestone shelf are clearly visible in the sidescan data and can be traced as continuous lineaments across the shelf from to the shelf break. Beyond the slope break the sidescan data show a dark (higher

reflectivity) incoherent returns, presumably the debris displaced during the mass wasting event.

Looks like there are at least two distinctive faults that run perpendicular to the profiles, one associated with the south side of "trench" and one south of the Main Ridge. It is not clear if these are the same ones identified by Masson and Scanlon (1991) as strike-slip faults. Difficult to make definitive identifications without complete mosaic.

Will rendez-vous with a launch at ~0700 local time Saturday morning at the sea buoy outside PR harbor to pick up Hawaii engineer, Mark Rognstadt. Meanwhile we steam north on PRLINE7, will turn east then south on PRLINE8. At the end of PRLINE8A we will pull gear and head for the San Juan.

End of PRLIN7A at 1236 GMT, begin PRLINE8 at 1245 GMT.

JD174 Saturday June 22
Began editing Hydrosweep data. Processing is a little more complicated than on the KNORR SeaBeam 2100 system as the processor has to incorporate the sound velocity data as well as navigation and rudimentary cleaning before getting to the mbedit stage. This takes approximately 30 - 45 min. The data are surprisingly good. Initial processing of day file 167 showed few pings that actually needed to be edited, however, when plotted with scripts generated by the processing, only a little editing seemed to show up in the data a lot more readily than with the Sea Beam 2100 systems (probably due to the fact that the Sea Beam 2100 system as 121 beams as compared to the 59 beams of the Hydrosweep system). Will have to play with this to determine how prudent the editing has to be. Finished JD 167 and 168.

End of PRLINE8 0050 GMT, begin PRLIN8A 0100 GMT. End PRLIN8A 0522 GMT

Picked-up Hawaii engineer, Mark Rognstadt at ~0730 local time at sea buoy outside harbor. Turned eastward and steamed at 10.5 knots to way point for start of next profile. Made it to way point by 1030 local time. Began to deploy guns and magnetometer. Begin PRLINE9 1541 GMT. Ran PRLINE9 with guns only while the MR1 group worked on the fish. By lunch time they had found two problems, both apparently fixable. The first, and the cause for the starboard transmitter to be damaged on both previous deployments, was a shorted tuning inductor. This was repaired and the starboard receive hardware checked out to make sure it was operating properly. The second problem was time varying gain. The instruments ability to correctly do the varying in the gain on the outer part of the swath seem to be impaired. The problem was also linked to the tuning inductor and disappeared once the inductor was fixed. The MR1 group worked for the remainder of day and the fish was ready for deployment by the end of PRLINE9 at 0604 GMT on JD 175

JD175 Sunday June 23
MR1 fully deployed by 0710 GMT. Start of profile PRLINE10 at 0805 GMT, line run without seismics, exact repeat of PRLINE9. Found that on the repeat run the overlapping Hydrosweep data was off by up to 200 m on the outer 1/3 beams. Two possible problems: sound velocity profile incorrect; hippie (vertical referencing) was whacked out due to turn while deploying MR1. Had Robert Hagg, OS that has worked with SeaBeam 2100 data on the Palmer, look at the day files to determine if Hippie problem, but he didn't see the usual indicators (ramping up of beams on one side of the swath). MR1 looked pretty good, certainly much better than before. We were getting full sidescan coverage on both starboard and port, and bathymetry seemed OK, but noisier than what was desirable. We ran both PRLINE10 and PRLINE11 at 9 kts without the guns, basically filling in between lines where we had a data gap.

End of profile PRLINE10 at 1920 GMT, began profile PRLINE11 at 2100 GMT . On the turn between profiles put the fish on receive only to get a handle on noise interference. Also throttled the engines back to zero, i.e. reducing the screw turns to zero, to assess engine noise in the MR1 signal.

Emailed weekly science report #1 to Rawson.
Emailed Dave Epp and/or Connie Sancetta requesting extra ship time to make up for time lost due to MR1 problems, which are directly related to lack of time to complete dockside testing in port.

JD176 Monday June 24
Sent Fax to NSF showing HMR1 coverage as of JD175 relative to proposed survey coverage.

End of profile PRLINE11 at 0821 GMT. Ship slowed to 6 kts to start shooting seismics. Began profile PRLINE12 at 0934 GMT. It became apparent during these runs and more so during PRLINE12 when slowing the ship caused the tow fish to come closer to the ship that the system was picking up a strong component of 60 cycle noise. This was attributed to the diesel electric motors. EWING is diesel electric engine which produces AC power. It has a single fixed prop. To speed up/slow down the amount of AC wave that is sampled is change. The noise is introduced when the converts change AC power to DC power? Tried to tow fish at deeper depths, 200m rather than 100m, so the fish was further away fro the ship. Didn't see any improvement in signal. It was proposed that we bring the fish in and attempt to shield the electronics on the starboard side might reduce this noise problem. Also saw the introduction of noise in the seismic data that was possibly linked to starting the lubrication purifier, in addition to an overall low frequency (5 Hz) noise. End of PRLINE12 at 1941 GMT, began PRLIN12A at 1951 GMT. End of PRLIN12A at 2341 GMT, began PRLINE13 at 2354 GMT.

JD177 Tuesday June 25
End of PRLINE13 at 0458 GMT, began PRLIN13A at 0506 GMT. End of PRLIN13A at 1447 GMT. Start of PRLINE14 at 1454 GMT. Will replace unshielded cable of starboard side with shielded cable when we recover the MR1. Apparently this shielded cable was removed after the last cruise due to a short? and heat damage to the connector. Mark has brought a new used shielded cable with him and will replace the deck connector.

JD178 Wednesday June 26
End of PRLINE14 at 0034 GMT. Initiation of PRLIN14A caused the system to hang. Had to reboot system. Began PRLIN14B at 0049 GMT. MR1 cable rubbed through air hose of one of the guns and got tangled with the gun line. At to make a sharp turn to port to free up lines and retrieve gun at 0228 GMT. At the end of line 14B, 0654 GMT, we pulled in MR1 to shield electronics and check grounds. PRLINE15 aborted to due to miscommunication, guns needed to be recovered during MR1 recovery. Start of PRLINE16 at 0840 GMT. During the MR1 repair we steamed part way up the Virgin Island platform to get a look at the limestone cap. Looks like the same sequence of Pliocene Quebradillas Limestone, underlain Late - Middle Miocene Aymamon Limestone, Los Puertos Limestone, Early Miocene Cibao Formation, Lower Montebello Limestone Mbr. (best aquifer in northern Puerto Rico due to exposure during a time of low sea-level stand. This increased the possibilities of solution and therefore of porosity and permeability) and Oligocene Lares Limestone, San Sebastian Formation observed on the northern Puerto Rico slope. We get strong reflective signal, swamped the returns, possible too much reverberation. Will be interesting to see how this is processes out. We were considering steaming through the shallow Virgin Island Passage across the cap and presumably anticline to try and identify areas of faulting, but decided didn't have enough time. End of PRLINE16 1306 GMT.

Dropped Mark off outside San Juan Harbor around 1900 GMT. Actually used the life boat aboard the EWING to shuttle him to the cruise dock in Old San Juan. Took about an hour? Underway by 1930 GMT and MR1 fully deployed and on PRLINE17 by 2300 GMT. For the first time on the cruise the data both bathymetric and side scan are of high quality. Will run to profiles over areas where we had collected seismic data only. Will run at 9 kts without seismics.

JD179 Thursday June 27
Finished PRLINE17 at 1012 GMT. Start PRLINE18 at 1114 GMT, end of PRLINE18 at 2203 GMT. Both lines run at 9 kts, no seismics. Sidescan data looks fairly decent, still some noise in starboard side but significantly better than before. Received request from Rawson cruise scenarios, 1) area covered with remaining time, 2) area covered with 1.5-2.0 additional days. Start of PRLINE19 at 2224 GMT

Main Ridge just doesn't show up in the sidescan data. It is apparently draped with pelagic sediments with low reflectivity. We continue to see a featureless mass when we cross this feature with little evidence for deformation. The fault scarps on the down going North American plate are very pronounced as are the canyons on the northern Puerto Rico shelf. Hard pressed to identify any major lineaments in trench area. Sediments definitely decrease eastward in the "trench" proper which makes it difficult to say anything about the style of deformation (e.g. LINE12). Apparently the Main Ridge blocks the flow of turbidites from the Mona Canyon and the northern Puerto Rico Virgin Island platform/shelf. In those crossing that have sediment we are seeing evidence of rollover folds and thrust faults in sediments in marginal basin south of Main Ridge (e.g. PRLINE7) and strike-slip faulting in trench area (e.g. PRLINE4). We can also see top of downing North American plate on a few profiles (e.g. with similar seismic layers to those described by Bunce et al., transparent layer) draping horst and graben structures. Regularly penetrating to 12 secs in deepest portions of the trench. Found on PRLINE3 and 4 trench is greater than 8400 m, deeper than was is predicted by the Etopo5 bathymetric data set, although Ewing et al., 1966? seems show a fairly complete and accurate morphologic and bathymetric map based on Navy soundings.

JD180 Friday June 28
End of PRLINE19 at 0139 GMT, begin PRLIN19A at 0143 GMT

Sent in morning at 0830 local time fax of area cover, area to be covered with remaining days and area covered given an extra two days. Repeat my request for two additional days. Found out approximately 1800 local time via fax from Rawson at that we got approval to extend our cruise an additional 2 days. New ETA to San Juan is now Monday July 8 at 0800 local time.

Still trying to track down low frequency noise in streamer. Chris has an email into John Diebold and Joe Stennent to see if they have any ideas. The noise, however, is also appearing in the 3.5 kHz and the MR1 data which leads me to believe that is not related to the streamer electronics, rather may be a mechanical, acoustic signal, associated with the ship. They did have problems with the prop at low Rpm, doing station work and trying to maintain speeds of 1 kt. We did see a dramatic difference in the amount and type of noise in the MR1 data with varying Rpms. We have been keeping a careful watch on the data since asking the bridge to call down any Rpm changes. We are varying between 88 and 93 Rpm to maintain our 6 kt SMG.

End profile PRLIN19A 1411. System hung at PRLINE20, had to restart profile. Start of PRLIN20A at 1439 GMT.

JD181 Saturday June 29

End of PRLIN20A at 0311 GMT, start of PRLIN20B 0315 GMT. End of PRLIN20B at 0609 GMT, start of PRLINE21 at 0616 GMT. Still keeping careful track of Rpms. End of PRLINE21 at 1045 GMT, start of PRLIN21A at 1055 GMT. End of PRLIN21A at 2056 GMT, of PRLINE22 at 2056 GMT. MR1 cable tangled with air gun hoses. Turn at 2144 GMT to untangle. Response from J. Diebold is that low frequency noise <6 Hz is typically filtered out, so noise problem on SCS is really not a problem. This low frequency noise is most likely due to cable and ship moving through water.

JD182 Sunday June 30

End of PRLINE22 at 0803 GMT. System hung at start of PRLIN22A, had to reboot. Start of PRLIN22B at 0819 GMT. End of PRLIN22B at 1552 GMT. Went very close to North Puerto Rico close into water depths as shallow as 295 m. We pulled up the MR1 closer to the ship so that it would be towed at a shallower depth. We traversed diagonally over limestone cap avoiding the extremely shallow promontory extending from Aguadilla, Punta Aguadilla. For the most part the limestone is undeformed and tilting northward toward the trench right up to the Mona Canyon. As we crossed Mona canyon we imaged a spectacular normal fault scarp bounding the canyon. Very impressive down dropped block, depths increased rapidly to 1100 km in less than 3 km. Turbidites fill canyon floor. Turned in middle of canyon and headed back up over the carbonate cap. PRLIN22B extends northward to the North American plate on the north side of the trench. The North Puerto Rico Slope Fault, presumably a strike-slip fault, appears to be associated with a elongate and trench-parallel high (8000m above trench floor, 6 nm wide). This high is also observed on trench crossing of PRLIN21.

End of PRLIN22B at 15:52, start of PRLIN23A at 1603 GMT. System hung at start of PRLINE23. End of PRLIN23A at 2340 GMT, start of PRLIN23B at 2346 GMT.

Sent weekly science report #2 to Rawson

JD183, Monday July 1

Composed and sent letter to Margo Edwards about what we expect from the MR1 group in terms of compensation for the down time with the system and the marginal data collected during the first half (at least) of the survey.

End of PRLIN23B at 0718 GMT, start of PRLIN24A at 0718 GMT. End of PRLIN24A at 1516 GMT, start of PRLIN24B at 1521 GMT. End of PRLIN24B at 2244 GMT, start of PRLINE25 at 2251 GMT.

PRLINE23 extended to the of the North American plate across the trench. As on the previous two profiles the North Puerto Rico slope fault is seen as an elongate trench-parallel high just south of the deepest part of the trench. Turbidites are ponded to the north (largest relative accumulation) and south of this high. Beginning to see a suggestion of frontal deformation(?) small accretionary prism type deformation, folds/disruption in turbidites adjacent to north side of high within trench.

PRLIN24A and B ran southward back to the Mona Canyon. It was decided to extend the trackline at the southernmost turn several nm westward to get a complete track across the Mona Canyon, perpendicular to the bounding walls. It was also decided that we extend the next four profiles at least 25 nm northward on to the Outer Rise to try and image the possible bathymetric expression of the Main Ridge on the North American plate.

Got our first definite crossing of the Septentrional Fault Zone at about 1740 GMT.

JD184, Tuesday July 2

Got an email back from Margo addressing our requests. Need to talk with Bruce Appelgate about details of deal. MR1 failed at approximately 1730 GMT.
End of PRLINE25 at 1609 GMT, start of PRLINE26 at 1614 GMT. End of PRLINE26 due to MR1 failure at 1830 GMT. Start of PRLIN26B at 1938 GMT, without seismics.

The extended line PRLINE26 did image a narrow (~9nm wide, ~600 m high) ridge trending roughly N30E. This high was also shown on an unpublished map of PRT bathymetry by Leonardi, 1981 in McCann and Sykes (1984) and hypothesized to be an extension of the subducted Main Ridge. Next two profiles to the west will most likely give more complete coverage of this feature.

JD185, Wednesday July 3
End of PRLIN26B at 0203 GMT, start of PRLIN26C at 0300 GMT, with MR1 operational. End of PRLIN26C at 0741 GMT, start of PRLIN27A at 0748 GMT
End of PRLIN27A at 1406 GMT, start of PRLIN27B, C, D and E at 1442 GMT.

Fumble code with tape change. Thought we could put the recording interval up to 18 s and shot interval at 20s, but maximum value is 16 s for recording interval and 18s for shot interval. Want to make the swath of the MR1 as wide as possible to get maximum coverage along portion of adjacent swath were no data were collected. With a 19s ping interval for the MR1 we were able to get a 20-24 km swath width and cover at least half of the lost data. The real time data looked good, although it without processing it is difficult to say if we sacrificed along-track resolution with the longer ping interval.

Extended the start of PRLIN27A further south to ensure imaging the entire width of the Septentrional Fault Zone.

JD186, Thursday July 4
Panic about time remaining, i.e. not enough given all the things that we want to do, about 8 hours over. Increased speeds to 6.5 kts , cut line up Dominican shelf, shorten northward extent of eastern two profiles and spaced them further apart assuming a 20 km swath with at the longer ping intervals. All this got us to within one hour of desired time, 0700 local time at San Juan Harbor including two hours for recovery of equipment. Made alternative plans for Mona Passage survey and set time limit for this survey at 1730 Saturday local time.

Bruce Appelgate, as a spokesperson for the HMRG, said the thinking at this point was to buy us some portion of the Hydrosweep data, deep waters, and would process and merge these with the shallow water MR1 data. We were reluctant to agree to this without seeing how well these data merged. Bruce will process a combined MR1 and Hydrosweep swath. We discussed a September 1 delivery date for the finalized sidescan mosaic and general dates around December, i.e. before AGU for delivery of processed bathymetry data.

Crossed the Septentrional Fault Zone heading northward on PRLIN27E. Northern extensions of PRLIN27E and PRLIN28 crossed over a very prominent basement high (~15 km wide, 600 m high) following same trend of high imaged on PRLINE26. Confirmation of fracture zone/transverse ridge hypothesis of McCann and Sykes?

Close to 2 sec of sediments in Puerto Rico trench. See evidence of deformational front, folds and thrust faults of sediments on south wall of trench in seismic lines 27, 28 and 29. Extended PRLINE29 to ensure imaging this deformation front.

End of PRLIN27E at 0055 GMT, start of PRLINE28 at 0059 GMT. End of PRLINE28 at 1755 GMT, start of PRLINE29 at 1905 GMT.

JD187, Friday July 5
End of PRLINE29 at 0145 GMT, start of PRLINE30 at 0202 GMT. End of PRLINE30 at 0953 GMT, start of PRLINE31a at 1001 GMT, end of PRLIN31A at 1730 GMT. Start of PRLINE32 at 1734 GMT, end of PRLINE32 at 2122 GMT.

Traveled across the Mona Canyon once again. Large normal fault dip to the east was imaged several nm to the west of the canyon. Lineament identified by Dolan in SeaMARCII data but interpreted to be a jointing pattern in limestone. Passed through seaway between Desecheo Island and Mainland PR, over Desecho Ridge at about 1930 GMT. At the apex of the ridge seafloor shallowed to depths of ~400 m. On the south side of the ridge the seafloor dropped to 2000m along a steep normal fault. Made a sharp turn westward to avoid shallow water platform/shelf and then turned southward without guns to ensure if indeed we did run into uncharted shallow waters <300m, it would be fairly easy to pull up the fish to a shallower tow depth. A third engine was on stand-by in case we needed burst of speed to pull up the fish.

Passed over shallow area reaching depths of 311m. Hydrosweep system went down soon after crossing shallow area at around 0000 GMT. Crashed when tape change was initiated. Once we passed the shallow area, brought guns back on line. There was about an hour delay due to gun misfiring.

After processing MR1 bathymetry data, Bruce Appelgate, felt that although there was retrievable data the amount of processing time required to get these data to a reasonable condition would be too great and certainly not doable give our time constraints. Thus the MR1 group has agreed to buy the unprocessed Hydrosweep data for the cruise.

First notice of tropical storm Bertha located approximately 1000 km east of Lesser Antilles

JD188, Saturday July 6
Start of PRLINE33 at 0007 GMT, end of PRLINE33 at 0141 GMT. Start of PRLINE34 at 0145 GMT, end of PRLINE34 at 0810 GMT

Continued PRLINE33 southward past Mona Island to latitude 18°02. Cross several northeast dipping faults just east of Mona Island. PRLINE34 is an east-west line south of Mona Island over shallow shelf waters of the island and across Yuma Basin. Large normal faults dipping east and west are imagine on this line. The carbonate cap has been faulted and down dropped more than a 1 km in several places. Beautiful horst in the center of the basin bounded by half graben structures.

Start of PRLIN35B at 0820 at turn to the east back across Yuma Basin. Will keep same line for the remainder of the survey in the Mona passage to avoid break in data collection. On the second pass further north across the Yuma Basin, again imaged large normal faults delineating bordering the basin and horst and graben structures in the center and deepest part of the basin. As we approach Mona and Monita Islands we turn northeastward at 1223 GMT. Depths in passage shallow and we image a series of normal faults are dipping to the northeast and southwest creating classic NW-SE trending horsts and grabens. We pass over the shallowest portion of the Mona Passage at the same point the SeaMARCII survey 1987 survey cross and made another course change to the northeast at 1519 GMT. Cross over the Mona Canyon once again and reach the end of PRLIN35B at 2001 GMT. Pull in guns and begin to follow trace of Septentrional Fault across the slope of the northern Puerto Rico margin at 2355 GMT

Tropical storm Bertha continues to grow in intensity and is moving westward heading directly for Puerto Rico.

Hydrosweep system still down.

JD189, Sunday July 7
As of 0200 Tropical Storm Bertha is located at 15°5' N, 54°3'W, heading west to northwest at 23 m.p.h. with winds up to 70 m.p.h.

Imaged the trace of Septentrional fault near western end of large mass wasting scarp on northern shelf of Puerto Island. Followed the trace down the slope maintaining a course of roughly 070. The fault trace changes it's overall trend from ENE to EW back to ENE changing from highly oblique-slip normal faults, to pure strike-slip, back to oblique-slip normal faults. The trace of the fault crosses the southern portion of the Main Ridge and was imaged as a small saddle in the ridge. At 1346 GMT we turned southward to begin the remaining two planned trench-crossing profiles.

Mike Rawson called the ship and requested that we head into San Juan port before the port is closed. At 1507 GMT turned into wind to begin recovery of all instrumentation. Recovery complete at 1600 GMT, transit at 11-12 kts to San Juan port.

Hydrosweep system still down.

JD190, Monday July 8
Arrive outside port (which has been officially closed, but ship's agent has arrange to get us in) at approximately 0030 GMT, 2030 local time, approximately 12 hours before the scheduled end of cruise. Had to turn into wind and wait outside port for two hours before getting clearance to proceed in. Docked at approximately 0330 GMT, 2330 local time.

APPENDIX II - GEOMAG PROGRAM

```
      SUBROUTINE GEOMAG(RLAT,ELON,DATE,FIELD)
c*
c* mod 7jan84 j.hildebrand,smsmith - adapt for f77 vax.
c* mod 14jan84 m.keeler - convert to subroutine and streamlined
c* mod 4apr85 smsmith - delete ref to unit 2, replace with call
c*                      to subr fnunit.
c* mod 9may85 smsmith - set path of igrf80A.coeff file to
c*                      /usr/local/src/lib/MAGFLD/igrf80A.coeff
c* mod 6jan87 smsmith sio - install 4th generation 5 yr interval
c*             igrfs to replace igrf80a.coeff.
c*      Reference: International Geomagnetic Reference Field
c*                 Revision 1985, IAGA Div. 1, Working Group 1,
c*                 N.W. Peddie, et al., Geophysics, V. 51, No. 4,
c*                 pp 1020 - 1023. (1986)
c* Mod 20Oct88  r.bartholomew for C compatibllity
c*
c* UPDATE NOTE: When next igrf update becomes available, after 1990,
c*              modify if-then-else statement (stat 5) and see README
c*              in MAGFLD library source directory.
c*
c*
c* mod 05July89 budhy - change 'DATE' to double to accomodate m_mag2
c*                      change path for igrf80A.coeff file to
c*                      /opus/reduction/lib
c*
c*
      REAL *8 DATE
      CHARACTER SCCSID*50
      COMMON  / XYZVAL / X, Y, Z, DX, DY, DZ
      common / FTNUNT / igunit
      character coefil*80, coedir*80, cfile*80
      CHARACTER*8  MODELC
      CHARACTER*1  GEO
      LOGICAL  LREAD
      INTEGER  OUCHAN
C      DIMENSION  MAX(3), ISP(3), EPOCH,
C     +           YRMIN, YRMAX, ALTMIN, ALTMAX
      DIMENSION  MAX(3), ISP(3)
C      REAL EPOCH, YRMIN, YRMAX, ALTMIN, ALTMAX
c*
c*    The size of the MFC, SVC, and AC arrays might be too large for some
c*    machines.  To calculate how large the arrays have to be for each model:
c*    Let N$ be the maximum degree and order of a set of coefficients.  Then the
c*    number of coefficients (array positions) needed is equal to
c*    ( N$ ) * ( N$ + 2 ).  Add the totals needed for each model.  For the SVC
c*    and AC arrays, add one to that total (keeps computer from signalling an
c*    error).
c*
c*    For WC80, N$ = 12 for main field coefficients, so MFC can be dimensioned
c*    at 168.  N$ = 8 for secular variation coefficients, so SVC can be
c*    dimensioned at 81.  N$ = 0 for acceleration coefficients, so AC can be
c*    dimensioned at 1.
c*
c*    If you change the size of the arrays, change the value of MAXCO1, MAXCO2,
c*    MAXCO3, and the DATA statement that initializes the arrays.
c*
c*    To save more memory, if you do not have IGRF80A, do not include SUBROUTINE
c*    IRF80A and delete all lines in this program referencing it.
c*
      DIMENSION  SVC(6240), AC(6240)
      REAL  MFC(6240)
c*
c*    ***** ABOVE DIMENSIONS MUST BE AT LEAST ONE! *****
c*
```

```
c*
c*    If you have a model with maximum degree and order of a set of coefficients
c*    greater than 30, change the value of MAXDO and edit SUBROUTINE MAGSYN as
c*    explained in the subroutine.
c*

      DATA SCCSID /"@(#) geomag.f 1.2 8/28/89 reduction"/
      SCCSID(1:1)=SCCSID(1:1)

      DATA  MAXMOD, MAXDO, MAXCO1, MAXCO2, MAXCO3 / 10, 30, 3 * 6240 /,
     +      MFC, SVC, AC / 18720 * 0.0 /,
     +      INCHAN, OUCHAN / 5, 6 /
      DATA ALT/0./
      DATA IFIRST/0/
      DATA GEO,MODELC,MOD/' ','IGRF80A',1/
c*
c*    directory path for igrf coefficient files
      coedir = '/home/wjr/redtools/lib/'
c*
c*
      if (ifirst.eq.0) then
      ifirst=1
c*
c       check date for appropriate field to load
 5      if (date .gt. 1995.0) then
 7       WRITE  ( OUCHAN, 250 )
 250      FORMAT ( /1X,'WARNING!! The most recent IGRF field'/
     +    ' available is 1990-1995. It is not strictly valid'/
     +    ' beyond 1995...Use with caution. '/)
         end if
         if (date .gt. 1995.0) then
          WRITE  ( OUCHAN, 260 )
 260      FORMAT ( /1X,'The IGRF95 should be available in early 1995.'/
     +    ' Contact Norm Peddie at the USGS in Denver for the'/
     +    'new coefficient file.' /)
         end if


         if (date .ge. 1990.0) then
           cfile = 'igrf90.95'
         else if (date .ge. 1985.0) then
           cfile = 'dgrf85.90'
         else if (date .ge. 1980.0) then
           cfile = 'dgrf80.85'
         else if (date .ge. 1975.0) then
           cfile = 'dgrf75.80'
         else if (date .ge. 1970.0) then
           cfile = 'dgrf70.75'
         else if (date .ge. 1965.0) then
           cfile = 'dgrf65.70'
         else if (date .ge. 1960.0) then
           cfile = 'igrf60.65'
         else if (date .ge. 1955.0) then
           cfile = 'igrf55.60'
         else if (date .ge. 1950.0) then
           cfile = 'igrf50.55'
         else if (date .ge. 1945.0) then
           cfile = 'igrf45.50'
c        else
c          go to 7
         endif

         coefil = coedir(1:lnblnk(coedir))//cfile(1:lnblnk(cfile))
```

```
c       TEST###
c       write(*,*) "coedir =", coedir
c       write(*,*) "cfile =", cfile
c       write(*,*) "coefil =", coefil

c*      find an available unit
c       call fnunit(igunit)
        igunit=9


C       OPEN(igunit, FILE=coefil, STATUS = 'OLD',
C      +    ACCESS ='SEQUENTIAL',FORM='FORMATTED',BLANK='ZERO')
c*
       OPEN(igunit, FILE=coefil, STATUS = 'OLD',
      +    ACCESS ='SEQUENTIAL',FORM='FORMATTED')
c*
c*     Initialize position counters.
c*     Begin model reading section.
c*
10     LREAD = .TRUE.
       I = 1
       I1 = 1
       I2 = 1
       I3 = 1
c*
c*     Read model header card.
c*
c*


c       READ  ( igunit, 20, ERR=1020, END=100 )
c      +      M, N, MODEL, EPOCH, (MAX(J),J=1,3), YRMIN,
c      +      YRMAX, ALTMIN, ALTMAX
c20    FORMAT  ( 2I2, A8, F8.2, 3I3, 2F8.2, 2F7.1 )

C       ABOVE LINES COMMENTED OUT AND REPLACED WITH THE FOLLOWING


        READ  ( igunit, 20, END=100 ) EPOCH, MAX(1), MAX(2), MAX(3),
      +      YRMIN, YRMAX, ALTMIN, ALTMAX
20     FORMAT  (12x, F8.2, I3, I3, I3, F8.2, F8.2, F7.1, F7.1 )


          print *, EPOCH, MAX(1), MAX(2), MAX(3), YRMIN, YRMAX,ALTMIN, ALTMAX
          m=0
          n=0

C       END OF ADDED CODE

c*
       IF  ( ( M .NE. 0 ) .OR. ( N .NE. 0 ) )  GO TO  1020
       IF  ( MAX(1) .GT. MAXDO )  GO TO  1040
c*
c*     Assign positions for this model and calculate initial positions for next
c*     model.
c*
       ISP( 1 ) = I1
       ISP( 2 ) = I2
       ISP( 3 ) = I3
       I10 = I1
       I20 = I2
       I30 = I3
       I1 = I1 + MAX( 1 ) * ( MAX( 1 ) + 2 )
       IF  ( (I1-1) .GT. MAXCO1 )  GO TO  1060
```

```
      IF  ( (I2-1) .GT. MAXCO2 )  GO TO  1061
      I3 = I3 + MAX( 3 ) * ( MAX( 3 ) + 2 )
      IF  ( (I3-1) .GT. MAXCO3 )  GO TO  1062
c*
c*    Calculate number of cards for this model.
c*
      NCARDS = ( MAX( 1 ) + 1 ) * ( MAX( 1 ) + 2 ) / 2
      DO  50  JCARD = 2, NCARDS
          ICARD = JCARD
c*
c*      comment out
c*    If model is IGRF80A, call IRF80A to read model data card:
c*
c         IF  ( MODEL .EQ. 'IGRF80A ' )
c    +        CALL  IRF80A( *1080, LREAD, MFC( ISP( 1 ) ),
c    +        SVC( ISP ( 2 ) ), 0.0, EPCH, ICARD )
c         IF  ( MODEL .EQ. 'IGRF80A ' )  GO TO  50
c*
c*    Read model data card.
c*
c*
C
C       Commented out and replaced below
C
C          READ  ( igunit, 30, ERR=1080, END=1080 ) M,N,GNM,HNM,SVCGNM,
C     +          SVCHNM, ACGNM, ACHNM, MODELC
C30        FORMAT  ( 2I2, 2F8.1, 2F8.2, 2F8.3, 16X, A8 )

C
C               Start of new code
C
         READ  ( igunit, 30,ERR=1080, END=1080 ) M,N,GNM,HNM,SVCGNM,
     +          SVCHNM, ACGNM, ACHNM, MODELC
30       FORMAT  ( 2I2, 2F8.1, 2F8.2, 2F8.3, 33X, A8 )
c*
c*
c*    Store coefficients.
c*
C35        IF  ( MODELC .NE. MODEL )  GO TO  1080
35       continue
         MFC( I10 ) = GNM
         I10 = I10 + 1
         IF  ( M .NE. 0 )  MFC( I10 ) = HNM
         IF  ( M .NE. 0 )  I10 = I10 + 1
         IF  ( N .GT. MAX(2) )  GO TO  40
         SVC( I20 ) = SVCGNM
         I20 = I20 + 1
         IF  ( M .NE. 0 )  SVC( I20 ) = SVCHNM
         IF  ( M .NE. 0 )  I20 = I20 + 1
40       IF  ( N .GT. MAX(3) )  GO TO  50
         AC( I30 ) = ACGNM
         I30 = I30 + 1
         IF  ( M .NE. 0 )  AC( I30 ) = ACHNM
         IF  ( M .NE. 0 )  I30 = I30 + 1
50       CONTINUE
c*
c*    Model read and stored o.k., so increase model count.
c*
c*
c*
c*
c*
100   LREAD = .FALSE.
```

```
c*
c*
c*    Get model header information, coefficient array positions.
c*
180   I10 = ISP( 1 )
      I20 = ISP( 2 )
      I30 = ISP( 3 )
      YRMINI = YRMIN
      YRMAXI = YRMAX
      ALTMNI = ALTMIN
      ALTMXI = ALTMAX
      MAXMFC = MAX( 1 )
      MAXSVC = MAX( 2 )
      MAXAC = MAX( 3 )
      EPCH = EPOCH
c
c*
c*      close temp unit used for igrf coeff.
        close(igunit)
       end if

c*    Check latitude.
c*
      IF  ( ABS( RLAT ) .LE. 90.0 )  GO TO  220
c*
      WRITE  ( OUCHAN, 210 ) RLAT
210   FORMAT  ( / 1X, 'ERROR:  LAT ', F7.3, ' IS IMPOSSIBLE' / )
c*
      GO TO  1180
c*
c*    Check east longitude.
c*
220   IF  ( ( ELON .GE. 0.0 ) .AND. ( ELON .LE. 360.0 ) )  GO TO  240
c*
      WRITE  ( OUCHAN, 230 ) ELON
230   FORMAT  ( / 1X, '**ERROR:  LON ', F7.3, ' IS IMPOSSIBLE' / )
c*
      GO TO  1180
c*
c*    Check date against model minimum and maximum.
c*
240   IF ( DATE .LT. YRMINI )  go to 5
c*
c*
c*
      COLAT = 90.0 - RLAT
c*
c*    If model is IGRF80A, call IRF80A to get correct main field coefficients
c*    and secular variation coefficients.
c*
c       comment out
c     IF  ( MODELC .EQ. 'IGRF80A ' )
c    +    CALL  IRF80A( *1120, LREAD, MFC( I10 ), SVC( I20 ), DATE,
c    +    EPCH, ICARD )
c*
c*    Call MAGSYN with ITYPE set according to GEO to calculate values in
c*    XYZVAL.
c*
      CALL  MAGSYN
     +    ( 1, DATE, EPCH, ALT, COLAT, ELON, MFC( I10 ), SVC( I20 ),
     +    AC( I30 ), MAXMFC, MAXSVC, MAXAC )
c*
```

```
c*
      return
c*    Fatal error section.
c*
c*
c*
1000  WRITE  ( OUCHAN, 1010 ) MAXMOD
1010  FORMAT  ( '1' / 1X, 'FATAL ERROR:  MORE THAN ', I3, ' MODELS'
     +        /// )
c*
      GO TO  10000
c*
1020  WRITE  ( OUCHAN, 1030 ) I
1030  FORMAT  ( '1' / 1X, 'FATAL ERROR IN HEADER FOR MODEL ', I2 /// )
c*
      GO TO  10000
c*
1040  WRITE  ( OUCHAN, 1050 ) MAXDO
1050  FORMAT  ( '1' / 1X, 'FATAL ERROR:  MAXIMUM DEGREE AND ORDER ',
     +        'FOR MAGSYN, ', I3, ' EXCEEDED' /// )
c*
      GO TO  10000
c*
1060  WRITE  ( OUCHAN, 1070 ) I, 'MFC', MAXCO1
1070  FORMAT  ( '1' / 1X, 'FATAL ERROR:  MODEL ', I2, ' OVERFLOWS ',
     +        'ARRAY ', A3, ' - SIZE:  ', I5 /// )
c*
      GO TO  10000
c*
1061  WRITE  ( OUCHAN, 1070 ) I, 'SVC', MAXCO2
      GO TO  10000
c*
1062  WRITE  ( OUCHAN, 1070 ) I, 'AC ', MAXCO3
      GO TO  10000
c*
1080  WRITE  ( OUCHAN, 1090 ) ICARD, I
1090  FORMAT  ( '1' / 1X, 'FATAL ERROR IN CARD ', I4, ' OF MODEL ',
     +        I2 /// )
c*
      GO TO  10000
c*
1100  WRITE  ( OUCHAN, 1110 )
1110  FORMAT  ( '1' / 1X, 'FATAL ERROR:  NO MODELS' /// )
c*
      GO TO  10000
c*      comment out
c 1120  WRITE  ( OUCHAN, 1130 )
c 1130  FORMAT  ( '1' / 1X, 'FATAL ERROR:  IRF80A' /// )
c*
c     GO TO  10000
c*
1140  WRITE  ( OUCHAN, 1150 )
1150  FORMAT  ( '1' / 1X, 'FATAL ERROR IN BATCH:  READING MODEL NAME'
     +        /// )
c*
      GO TO  10000
c*
1160  WRITE  ( OUCHAN, 1170 )
1170  FORMAT  ( '1' / 1X, 'FATAL ERROR IN BATCH:  READING PARAMETERS'
     +        /// )
c*
      GO TO  10000
c*
```

```
1190  FORMAT  ( '1' / 1X, 'FATAL ERROR IN BATCH:  INCORRECT'
     +        ' INPUT PARAMETERS' /// )
c*
      GO TO  10000
c*
1200  WRITE  ( OUCHAN, 1210 )
1210  FORMAT  ( '1' / 1X, 'EOF ENCOUNTERED READING PARAMETERS IN BATCH'
     +        /// )
c*
c*
c*
10000 STOP 'GEOMAG'
      END
```

APPENDIX III - CORE AND DREDGE LOCATIONS

Lat (N)	Lon (W)	Dec. Lat	Dec. Lon	Rock Type	Core/Dredge	Core/Dredge No.
18 48.00	67 45.00	18.80	67.75	Se	Core	R5-13
18 36.00	66 6.00	18.60	66.10	Se	Core	V3-1
18 49.00	67 9.50	18.82	67.16	Se	Core	V3-2
18 51.00	67 7.00	18.85	67.12	Se	Core	V3-3
18 29.50	67 24.00	18.49	67.40	Se	Core	A172-8
18 49.00	66 29.00	18.82	66.48	Se	Core	SP12-10
18 37.60	65 42.50	18.63	65.71	Se	Core	SP12-11
18 47.70	65 57.80	18.80	65.96	Se	Core	SP12-12
18 49.00	67 50.00	18.82	67.83	Se	Core	V6-1
18 36.00	66 54.00	18.60	66.90	Se	Core	V6-2
18 43.00	65 55.00	18.72	65.92	Se	Core	V6-3
18 39.50	66 18.50	18.66	66.31	Se	Core	V6-4
18 59.00	65 50.00	18.98	65.83	Se	Core	C8-114
19 10.50	66 46.70	19.18	66.78	Se	Core	C8-115
19 11.00	66 46.50	19.18	66.78	Se	Core	C8-116
19 10.00	65 13.00	19.17	65.22	Se	Core	C8-117
19 11.50	65 14.00	19.19	65.23	Se	Core	C8-118
19 6.50	66 9.30	19.11	66.16	Se	Core	C8-121
19 5.90	66 11.40	19.10	66.19	MB	Core	C8-122
19 4.00	66 6.50	19.07	66.11	MB	Core	V20-1
18 55.00	66 4.00	18.92	66.07	MB	Core	V20-2
19 30.50	65 15.80	19.51	65.26	Se	Core	C8-127
19 28.00	65 25.70	19.47	65.43	Se	Core	C8-128
19 28.00	65 4.00	19.47	65.07	Se	Core	A172-12
19 24.00	65 7.00	19.40	65.12	Se	Core	A172-13
19 54.00	64 48.00	19.90	64.80	Se	Core	A172-14

Key

L-Limestones
T-Turbidites
Se-Other sedimentary rocks and layers
MG-Metamorphic rocks, Greenschist facie
MB-Metamorphic rocks, Blueschist facie
OC-Oceanic crust type rocks

Lat (N)	Lon (W)	Dec. Lat	Dec. Lon	Rock Type	Core/Dredge	Core/Dredge No.
19 39.00	67 57.00	19.65	67.95	T	Core	C9-38
19 43.00	67 11.00	19.72	67.18	T	Core	C9-39
19 19.00	66 16.00	19.32	66.27	T	Core	C9-40
19 51.00	65 53.00	19.85	65.88	T	Core	C9-41
19 44.00	66 31.00	19.73	66.52	T	Core	C9-42
19 27.00	66 49.00	19.45	66.82	T	Core	C9-43
19 22.50	66 31.50	19.38	66.53	T	Core	V15-189
19 49.50	65 53.00	19.83	65.88	T	Core	V15-190
19 48.50	66 11.00	19.81	66.18	T	Core	A172-9
19 45.00	66 37.00	19.75	66.62	T	Core	A172-10
20 18.20	65 27.70	20.30	65.46	OC	Core	C8-119
20 11.50	65 23.50	20.19	65.39	OC	Core	C8-120
20 7.10	65 7.90	20.12	65.13	OC	Core	C8-123
20 5.80	65 6.60	20.10	65.11	OC	Core	C8-124
20 7.50	65 7.00	20.13	65.12	OC	Core	C8-125
20 7.00	65 6.00	20.12	65.10	OC	Core	C8-126
20 5.10	65 10.00	20.09	65.17	OC	Core	C8-130
20 1.00	66 20.00	20.02	66.33	OC	Core	A172-11
20 13.00	64 65.00	20.22	65.08	OC	Core	A172-15
20 49.00	66 25.00	20.82	66.42	OC	Core	V15-181
20 26.50	67 40.00	20.44	67.67	OC	Core	V15-186
20 23.00	66 6.00	20.38	66.10	OC	Core	V15-188
20 46.50	66 29.00	20.78	66.48	OC	Core	V18-7
20 6.80	65 6.50	20.11	65.11	OC	Core	D1
20 5.30	65 4.80	20.09	65.08	OC	Core	D2
20 5.00	65 4.00	20.08	65.07	OC	Core	D4

Key

L-Limestones
T-Turbidites
Se-Other sedimentary rocks and layers
MG-Metamorphic rocks, Greenschist facie
MB-Metamorphic rocks, Blueschist facie
OC-Oceanic crust type rocks

Lat (N)	Lon (W)	Dec. Lat	Dec. Lon	Rock Type	Core/Dredge	Core/Dredge No.
20 0.00	66 24.55	20.00	66.41	OC	Dredge	Ch 19:D2
19 58.92	66 25.00	19.98	66.42	OC	Dredge	Ch 19:D3
20 0.00	66 31.95	20.00	66.53	OC	Dredge	Ch 19:D10
19 57.00	66 28.00	19.95	66.47	OC	Dredge	Ch 34:D2
20 15.97	65 41.40	20.27	65.69	OC	Dredge	Ch 34:D3
20 16.00	65 41.25	20.27	65.69	OC	Dredge	Ch 34:D4
20 5.70	65 8.52	20.10	65.14	OC	Dredge	All-11:D1
20 7.03	65 3.00	20.12	65.05	OC	Dredge	All-11:D2
20 5.93	65 7.47	20.10	65.12	OC	Dredge	All-11:D3
20 3.90	65 10.15	20.07	65.17	OC	Dredge	All-11:D4
19 58.85	65 14.00	19.98	65.23	OC	Dredge	All-11:D5
20 0.25	65 1.65	20.00	65.03	OC	Dredge	All-11:D6
20 6.10	65 5.45	20.10	65.09	OC	Dredge	All-11:D8
18 42.00	63 38.00	18.70	63.63	MG	Dredge	E-1392
18 50.00	63 41.00	18.83	63.68	MG	Dredge	E-1393
18 48.00	63 47.00	18.80	63.78	MB	Dredge	E-1394
18 50.00	64 34.00	18.83	64.57	L	Dredge	E-1599
18 53.00	64 47.00	18.88	64.78	L	Dredge	E-1601
19 20.00	65 32.00	19.33	65.53	MG/L	Dredge	E-1431
19 9.00	65 28.00	19.15	65.47	MB	Dredge	E-1432
19 2.00	65 32.00	19.03	65.53	L	Dredge	E-1433
19 7.00	65 23.00	19.12	65.38	L/MB	Dredge	E-1434
19 5.00	65 32.00	19.08	65.53	L	Dredge	E-1435
19 4.00	66 0.00	19.07	66.00	MB	Dredge	E-1436
19 2.00	66 1.00	19.03	66.02	L	Dredge	E-1437
19 6.00	66 9.00	19.10	66.15	MB/MG	Dredge	Core/Dredge No.

Key

L-Limestones

T-Turbidites

Se-Other sedimentary rocks and layers

MG-Metamorphic rocks, Greenschist facie

MB-Metamorphic rocks, Blueschist facie

OC-Oceanic crust type rocks

sec lon	sec lat	dec sec lon	dec sec lat
33	0	0.55	0.00
0	55	0.00	0.92
57	0	0.95	0.00
0	0	0.00	0.00
24	58	0.40	0.97
15	0	0.25	0.00
31	42	0.52	0.70
0	2	0.00	0.03
28	56	0.47	0.93
9	54	0.15	0.90
0	51	0.00	0.85
39	15	0.65	0.25
27	6	0.45	0.10

Lat (N)	Lon (W)	Dec. Lat	Dec. Lon	Rock Type	Core/Dredge	E-1438
19 6.00	66 11.00	19.10	66.18	MB/MG	Dredge	E-1602
18 50.00	67 18.00	18.83	67.30	MG	Dredge	E-1424
18 39.00	67 23.00	18.65	67.38	MG	Dredge	E-1423
18 35.00	67 16.00	18.58	67.27	L	Dredge	E-1422
18 33.00	67 15.00	18.55	67.25	L	Dredge	E-1421
18 26.00	67 31.00	18.43	67.52	MG	Dredge	E-1420
18 28.00	67 35.00	18.47	67.58	L	Dredge	E-1562
18 29.00	67 37.00	18.48	67.62	L	Dredge	E-1563
18 30.00	67 41.00	18.50	67.68	L	Dredge	E-1564
18 38.00	67 36.00	18.63	67.60	L	Dredge	E-1565
18 46.00	67 35.00	18.77	67.58	L	Dredge	E-1566
18 46.00	67 31.00	18.77	67.52	L	Dredge	E-1567
19 3.00	67 43.00	19.05	67.72	MB	Dredge	E-1568
19 12.00	67 33.00	19.20	67.55	MB/MG	Dredge	E-1426
19 7.00	67 56.00	19.12	67.93	L	Dredge	E-1569
19 9.00	68 19.00	19.15	68.32	MB	Dredge	E-1570
19 12.00	68 38.00	19.20	68.63	MB	Dredge	E-1571
19 53.00	64 7.00	19.88	64.12	OC	Dredge	E-1596
20 0.00	64 10.00	20.00	64.17	OC	Dredge	E-1595
20 1.00	64 24.00	20.02	64.40	OC	Dredge	E-1594
19 59.00	66 25.00	19.98	66.42	OC	Dredge	E-1430
19 59.00	66 36.00	19.98	66.60	OC	Dredge	E-1429
19 48.00	66 59.00	19.80	66.98	OC	Dredge	E-1428

Key

L-Limestones

T-Turbidites

Se-Other sedimentary rocks and layers

MG-Metamorphic rocks, Greenschist facie

MB-Metamorphic rocks, Blueschist facie

OC-Oceanic crust type rocks

APPENDIX IV - EW96-05 LOGGED DATA FORMAT

EW9605.README

Files:

Daily files:

The logged and reduced data are organized as sets of daily files. A filename is composed of 3 parts:

(1) cruise id "ew9605" or NULL
(2) data id "gp3.r"
(3) dayofyear "365"

example:

gp3.r365

Note: The cruise id is NULL for the data files for ew9605.

".Z" files:

files that end with a ".Z" have been compressed with the UNIX "compress" command. Use the "uncompress" command to make them readable

Directories:

LOGGER - contains the data files logged during the cruise with some minor editing or cleaning. These are referred to as the ".d" files.

SCCS - the directory holds the reduced files in the "sccs" format. The Source Code Control System (SCCS) that is used for program source files is also used for maintaining the data files. The SCCS facility serves as a backup and history mechanism for the data reduction process. Most files in SCCS are compressed, use the uncompress command and then issue the sccs command

```
sccs get filename
```

to get a copy of the file.

REPORT - cruise report files and PostScript plot files

shells - shell scripts that drive the data reduction

tmp - a temporary working directory

Time tagging:

During the logging process each record is tagged with the CPU's time. This tag usually appears at the beginning of the record as

yy+ddd:hh:mm:ss:mmm

where "yy" is the year, "ddd" is the day of year, "hh" is the hour, "mm" is the minute, "ss" is the second and "mmm" is the millisecond of the CPU time.

Note the variation in the positioning of these times as noted below in the Hydrosweep,

nav block (seismic) data use shot times instead of CPU times.

One of the processes on the logging computer logs the GPS TrueTime clock once a minute and continuously sets the CPU clock to UTC time from the TrueTime clock.

The following data sets use this CPU time tag as their "offical" time: Furuno, BGM-3 gravity, magnetics, sea temperature, meterological data, thermosalinograph.

The logged GPS data are also time tagged with this CPU stamp but all navigation derived from GPS uses the GPS position times.

Flag field:

The third column is used as a flag field to indicate a bad or rejected record.

"+" = initial field
"-" = rejected record

GPS MX-4200 (gp):
---

gp3 = GPS MX-4200D "3"
gp4 = GPS MX-4200D "4"

gp3.d - logged data (multiple records)

```
   93+258:00:22:12.282 $PMVXG,000,NAV,9,6,0000,0*02
   yy day  cpu_time               status

   93+258:00:22:20.834 $PMVXG,001,002220,1832.421,S,03837.602,W,00026.1,2*41
   yy day  cpu_time               time      lat         lon

   93+258:00:22:21.066 $PMVXG,011,233.5,012.3,,,,,,,,*4F
   yy day   cpu_time              course speed

   93+258:00:22:21.467 $PMVXG,022,260539.67,00.8,00.8,00.0,20,17,03,16,25,2
   yy day   cpu_time              fix time  EDOP NDOP VDOP PRN 1-6
```

gp3.r - gps 4200 after cleaning

   same as gp3.d

gp3.i - interpolated positions at 00,30 sec of each minute

```
   yy+ddd:hh:mm:ss.mmm N 12 12.1234 W 123 12.1234  gp3
   yy day   time          lat        lon           id
```

gp3.s - smoothed postions at 00,30 sec of each minute

```
   yy+ddd:hh:mm:ss.mmm N 12 12.1234 W 123 12.1234  gp3
   yy day   time          lat        lon           id
```

GPS Trimble NT200D (gp1):

gp1.d - logged data (multiple records)

GPS Position:

```
95+102:00:00:47.018 $GPGGA,000047,0929.387,N,08503.621,W,1,6,001,00030,M
yy day  cpu_time    position rec
```

GPS Position:
$GPGGA,XXXXXX,XXXX.XXX,N,XXXXX.XXX,W,X,X,XXX,uXX,M,uXX,M,XXXX,XXXX

Data Field:	Description
1	UTC of Position Fix
2	Latitude in Degrees, Minutes, and Decimal Minutes
3	N=North, S=South Latitude
4	Longitude in Degrees, Minutes, and Decimal Minutes
5	E=East, W=West Longitude
6	GPS Quality: 0=GPS Unavailable, 1=GPS Fix, 2=DGPS F
7	Number of satellites used
8	Horizontal Dilution of Precision (HDOP)
9,10	Antenna height in meters (u=+/-)
11,12	Geoidal height in meters (u=+/-)
13	Age of differential GPS data
14	DGPS reference station ID

NOTE: During Differential mode, it outputs the lat and lon with 4 d
digits accuracy in the minutes. But, when it is running on a
non-differential mode, it drops down to three decimal digits. Somet
to take into account when writing program for it.

Actual Track and Ground Speed:

```
95+102:00:00:47.053 $GPVTG,229,T,226,M,005.3,N,009.9,K
yy day  cpu_time    actual track and ground speed rec
```

Actual Track and Ground Speed:
$GPVTG,XXX,T,XXX,M,XXX.X,N,XXX.X,K

Data Field:	Description
1,2	COG; True
3,4	COG; Magnetic
5,6	SOG; Knots
7,8	SOG; Kilometer/hour

Heading and water speed: (this is an input from Furuno)

```
95+102:00:00:47.035 $GPVHW,249,T,246,M,05.30,N,09.82,K
yy day  cpu_time    heading and wayer speed rec
```

Heading and water speed:
$GPVTG,XXX,T,XXX,M,XXX.X,N,XXX.X,K

Data Field:	Description
1,2	Heading; True
3,4	heading; Magnetic
5,6	Speed; Knots
7,8	Speed; Kilometer/hour

Trimble Sample:

```
95+102:00:00:47.018 $GPGGA,000047,0929.387,N,08503.621,W,1,6,001,00030,M
95+102:00:00:47.035 $GPVHW,249,T,246,M,05.30,N,09.82,K
95+102:00:00:47.053 $GPVTG,229,T,226,M,005.3,N,009.9,K
95+102:00:00:56.969 $GPGGA,000056,0929.376,N,08503.626,W,1,6,001,00062,M
95+102:00:00:56.988 $GPVHW,252,T,249,M,05.20,N,09.63,K
95+102:00:00:57.114 $GPVTG,230,T,227,M,005.3,N,009.9,K
95+102:00:01:06.981 $GPGGA,000106,0929.366,N,08503.630,W,1,6,001,00103,M
95+102:00:01:06.999 $GPVHW,254,T,251,M,05.60,N,10.37,K
95+102:00:01:07.018 $GPVTG,231,T,228,M,005.3,N,009.8,K
```

gpl.r - Trimble GPS after cleaning

same as gpl.d

Furuno Speed and Heading (fu):

fu.d - speed & heading logged data (before cleaning stage)

```
yy+ddd:hh:mm:ss.mmm - 12.1 123.1 123.1
yr day   time      trk spd  hdg  gyro
```

trk: "-" = water track, "+" = bottom track

fu.r - speed & heading data after cleaning stage

same as fu.d

fu.s - smooth speed and heading data

```
yy+ddd:hh:mm:ss.mmm - 12.1 123.1 20
yr day   time      trk spd  hdg  number_pts
                                 in minute
```

Fix File (x):

x. - fix file

```
yy+ddd:hh:mm:ss.mmm N 12 12.1234 W 123 12.1234  id
yy day   time          lat        lon           id_string
```

id strings: "gp3" = GPS

One Minute Navigation (n):

n. - 1 minute navigation from the "x." file and "fu.s" file

```
yy+ddd:hh:mm:ss.mmm N 12 12.1234 E 123 12.1234   id 123.1 12.1
yr day   time          lat        lon           id  set  drift
```

id strings: "gp3" = GPS #1
"dr" = Dead Reckoned position corrected for set and drift error

Magnetics (mg):

mg.d - total intensity logged data

same as mg.r below

mg.r - total intensity magnetics after cleaning stage

```
yy+ddd:hh:mm:ss.mmm 41200.8
yr day   time       total_intensity
```

mg.m - median total intensity magnetics values at 00 seconds.
(median of values +-30 seconds)

```
yy+ddd:hh:mm:ss.mmm 41200.8
yr day   time       total_intensity
```

mg.n - median values merged with navigation; anomalies 1995 IGRF

```
yy+ddd:hh:mm:ss.mmm N 12 12.1234 E 123 12.1234 41200.8  -367.1
yr day   time          lat        lon          total    anomaly
                                                intensity
```

Hydrosweep center beam bathymetry (hb):

hb.d - center beam logged data

same as hb.r below

hb.r - center beam data after "cleaning" of hb.d file

```
yy+ddd:hh:mm:ss.mmm hh:mm:ss.mmm S 3445
yr day   time        2nd_time  mode depth_in_meters
          ^           ^
          |_ Ping time  |_ CPU time tag
```

mode: "S" for survey
note: 2nd time is CPU time tag

hb.i - interpolated center beam depth at 00 sec of each minute

```
yy+ddd:hh:mm:ss.mmm 3445
yr day  ping_time   depth_in_meters
```

hb.n - interpolated center beam merged with navigation

```
yy+ddd:hh:mm:ss:mmm N 12 12.1234 E 123.1234  2222.0
yr day  ping_time      lat         lon       depth_in_meters
```

BGM-3 Gravity (vt):
---

vc.d - BGM-3 "counts" logged data

same as vc.r below

vc.r - BGM-3 "counts" after "cleaning" of vc.d file

```
yy+ddd:hh:mm:ss.mmm 01:025069 00
yr day     time    int count  status
```

int - count interval; 01 = 1 second

vt.r - mGal gravity values calculated from the counts

```
yy+ddd:hh:mm:ss.mmm 979171.448000
yr day     time     grav
```

vt.s - smooth BGM-3 values at 00 secs of each minute.
(mean of values +-30 secs)

```
yy+ddd:hh:mm:ss.mmm 979171.448000
yr day     time     grav
```

vt.n - "vt.s" merged with nav with EOTVOS correction and FAA
Note: "vt30.n" is merged data using 1930 theoretical formula
80

```
yy+ddd:hh:mm:ss.mmm N 10 20.1234 W 120 23.1234 1980  77.1
yr day     time        lat          lon        theog  FAA

979317.5   64.1   1.5  10.2  -1.7  9.7  -1.6  9.8
raw_grav eotvos drift   dc    raw_vel   smo_vel
                       shift   N    E     N    E
```

Shot times (ts2):
---

ts2 = TrueTime Clock

ts2.d - shot times logged data

same as ts.r below

ts2.r - shot times after cleaning stage

```
        yy+ddd:hh:mm:ss.mmm 00:02:30.113 TrueTime
        yr day cpu_time     shot_time     clock
```

samples:

```
        ==> ts2.r098 <==
        95+098:00:01:28.645 00:01:28.266 TrueTime
        yr day cpu_time     shot_time     clock
```

Partial Nav Block data (nb2) - has realtime navigation:
---

nb2 = uses TrueTime Clock

nb2.d - nav block logged data

same as nb.r below

nb2.r - nav block after cleaning stage

```
yy+ddd:hh:mm:ss.mmm 15913 N 53 17.4460 W 166 59.4243 MCS1234c
yr day shot_time    shot #  latitude   longitude     line
```

Note: latitude and longitude are those values at shot time - a calculated realtime position

Samples:

```
==> nb2.r098 <==
95+098:00:01:28.266 14222 N 09 27.7300 W 085 05.1187 ex2-1
yr day shot_time    shot_#  latitude   longitude     line
```

Shot time/Nav Block data remerged with final nav (ts2.n):
---

ts2.n uses TrueTime Clock

ts2.n - shot time data merged with post processed navigation

```
94+195:00:02:50.371 15913 N 53 17.4459 W 166 59.4171 MCS1234c
yr day shot_time    shot #  latitude   longitude     line
```

latitude and longitude are from the post processed navigation

Sample:

```
==> ts2.n098 <==
95+098:00:01:28.266 14222 N 09 27.7288 W 085 05.0991 ex2-1
yr day shot_time    shot_#  latitude   longitude     line
```

Sea temperature (ct):
---

ct.d - sea temperature logged data

same as ct.r below

ct.r - sea temperature after cleaning stage

```
yy+ddd:hh:mm:ss.mmm 0007.6 00
yr day   time       temp (degrees C)
```

APPENDIX V - ADDRESSES OF SCIENCE PARTY

Dr. Araceli Munoz
Instituto Espanol de Oceanografia
Departamento de Geologia y Geofisica
C/Corazon de Maria, n8
28002 Madrid SPAIN
Tel: 34-1 3473617
Fax: 34-1 4135597
email: araceli.mrecio@md.ieo.es

Ms. Tina Mueller
Hawaii Mapping Research Group
SOEST-University of Hawaii
2525 Correa Road
Honlulu, HI 96822

Mr. Steve Muszala
Department of Geologic Sciences
University of Texas at Austin
Austin, TX 78713-7909
Tel: 512 471-5172
Fax: 512 471-9425

Mr. Wilfredo Rosado
Department of Geology
University of Puerto Rico
Mayaguez, PR 00681
tel: 787 265-3845
Fax: 787 265-3845

Ms Karen Sender
Hawaii Mapping Research Group
SOEST-University of Hawaii
2525 Correa Road
Honlulu, HI 96822

Mr. Steve Tottori
Hawaii Mapping Research Group
SOEST-University of Hawaii
2525 Correa Road
Honlulu, HI 96822

Mr. Jean-Paul van Gestel
Department of Geologic Sciences
University of Texas at Austin
Austin, TX 78713-7909
Tel: 512 471-5172
Fax: 512 471-9425